3-6-2020 2:30 PM

The Incorporation of Phosphorus into Polymer Networks for Drug Encapsulation and Release

Tristan D. Harrison, *The University of Western Ontario*

Supervisor: Ragogna, Paul J., *The University of Western Ontario*
: Gillies, Elizabeth R., *The University of Western Ontario*
A thesis submitted in partial fulfillment of the requirements for the Doctor of Philosophy degree in Chemistry
© Tristan D. Harrison 2020

Abstract

This thesis focuses on the incorporation of phosphonium salts into polymer networks for uses in drug delivery and antibacterial coatings. Compared to their ammonium analogues, which have been extensively investigated, phosphonium salts are of interest due to their different chemical properties and their higher chemical and thermal stabilities. The thesis describes the development of covalently crosslinked hydrogels, ionically crosslinked hydrogels and thin film materials to be utilized in the aforementioned applications.

Covalently crosslinked hydrogels were developed with the targeted application of drug delivery. The hydrogels were created by curing formulations with ultra-violet light. Then, anionic drug molecules were loaded, which would be contained in the hydrogels by electrostatic interactions. Release of the drug molecules was performed over 7 days in buffer and could be tuned based on the structure of the phosphonium salt and the pH and ionic strength of the release media. To lengthen the time to release these drugs, an alternative approach utilizing ionically crosslinked hydrogels was employed next. Four phosphonium polymers were produced and mixed with sodium hyaluronate to create ionic networks and their mechanical and rheological properties were studied to determine the differences in network properties. The ionic hydrogels showed sustained release of drug molecules over a period of 60 days and were also able to self-heal after damage in the presence of the release medium. Another ionic network was also synthesized using analogous ammonium and phosphonium polymers with alginate to compare network properties, release rates and self-healing abilities between ammonium and phosphonium polymers. This study proved that changing the polyanion does affect network properties and in this case, increased the release rate of drugs. It was also discovered that in analogous networks the identity of the cation (N or P) did not affect the release rate, but rather the substituents around the atoms did have an effect. Phosphonium salts were then incorporated onto self-immolative polymers for use as antibacterials. These polymers were then further functionalized with polymerizable allyl moieties to allow for crosslinking and thin film formation with the intended use of antibacterial surfaces that could degrade on command.

Keywords

Summary for Lay Audience

Modern medicine relies on the efficient delivery of drugs to treat infections and diseases. Ideally, these drugs should be administered at the exact concentration needed, target the affected area only and not harm healthy cells or tissues. Unfortunately, the delivery of drugs into the body is not so easy, as the rate of release, the area of release and stability of the drug need to be accounted for. To mediate these issues, drug delivery systems have been developed in hopes that relevant drugs can be administered in a safe and effective way. The need for these systems has increased dramatically over the years as new drugs, with different properties are continuously being developed. One of the most popular types of drug delivery system involves the use of hydrogels, which are materials that absorb large amounts of water. The high-water content can give them physical similarities to tissues which often makes them well tolerated in the body and gives them the ability to easily encapsulate drugs. There are many different ways to encapsulate drugs and release them in a controlled manner. For example, negatively charged drugs can be bound to positively charged polymers because opposite charges attract. In this thesis, phosphonium salts will be incorporated into hydrogels as the positive charges that can entrap negatively charged drugs. The drugs will then be released in media that has a similar salt concentration to the human body to mimic physiological conditions and a variety of different studies will be completed to compare hydrogel structure and drug release rate.

Positively charged phosphonium species also have inherent antibacterial properties as they can interact with negatively charged membranes of bacteria to cause cell death. This allows phosphonium salts to be incorporated into many different materials to help combat the spread of bacteria. For example, phosphonium containing coatings can be designed and applied to common surfaces such as door handles and tables to kill bacteria on contact, but over time these antibacterial coatings kill and accumulate dead bacteria and become inert. To deal with this issue, this thesis will also investigate phosphonium containing degradable antibacterial coatings. These coatings will be created to kill bacteria, but also be able to degrade upon command after high bacteria accumulation.

Co-Authorship Statement

Chapter One was written by Tristan D. Harrison and edited by Paul J. Ragogna and Elizabeth R. Gillies.

The work described in Chapter Two was co-authored by Tristan D. Harrison, Paul J. Ragogna and Elizabeth R. Gillies and was published in *Chemical Communications*, **2018**, *54*, 11164-11167. Tristan D. Harrison was the main experimentalist and Aneta Borecki, a research assistant, carried out the *in vitro* toxicity assays of the monomers and hydrogels along with cell growth on the hydrogels. Tristan D. Harrison wrote the first draft of the manuscript and all others contributed to the editing process of the published document.

The work described in Chapter Three was co-authored by Tristan D. Harrison, Olga Yunyaeva, Aneta Borecki, Cameron C. Hopkins, John R. De Bruyn, Paul J. Ragogna and Elizabeth R. Gillies and was published in *Biomacromolecules*, **2020**, *21*, 152–162. Tristan D. Harrison was the main experimentalist on the work. Olga Yunyaeva was an undergraduate student who Tristan D. Harrison mentored and contributed to the synthesis of poly[tris(hydroxypropyl)(4-vinylbenzyl)phosphonium chloride] and poly[triphenyl(4-vinylbenzyl)phosphonium chloride] along with initial studies of network formation and the swelling. Aneta Borecki carried out the *in vitro* toxicity assays of the polymers and networks and Cameron C. Hopkins aided in the initial rheometer setup. Tristan D. Harrison wrote the first draft of the manuscript and all others contributed to the editing process of the published document.

The work described in Chapter Four was co-authored by Tristan D. Harrison, Alexandre J. Salmon, Paul J. Ragogna and Elizabeth R. Gillies and will be submitted to the journal *Langmuir*. Tristan D. Harrison was the main experimentalist on the work. Alexandre J. Salmon was an undergraduate student Tristan D. Harrison mentored and contributed to the synthesis of poly[triethyl(4-vinylbenzyl)ammonium chloride and poly[tributyl(4-vinylbenzyl)ammonium chloride along with initial studies of network formation and the swelling studies. Aneta Borecki carried out the *in vitro* toxicity assays of the polymers and networks. Tristan D. Harrison wrote the first draft of the manuscript and all others contributed to the editing process of the published document.

The work described in Chapter Five was co-authored by Tristan D. Harrison, Amir Rabiee Kenaree, Paul J. Ragogna and Elizabeth R. Gillies. Tristan D. Harrison was the main experimentalist on the work. Amir Rabiee Kenaree synthesized the starting polymer, poly(ethyl glyoxylate).

Chapter Six was written by Tristan D. Harrison and edited by Paul J. Ragogna and Elizabeth R. Gillies.

Dedication

Dedicated to:

Francesco D'Angela and Audrey Harrison.

Acknowledgments

I would to first thank my supervisors Paul J. Ragogna and Elizabeth R. Gillies for their guidance and support throughout this entire degree. I very much appreciated your patience and willingness to help whenever I had needed it and I enjoyed working with both of you for the past five years.

I want to also thank all the past and present members of the Ragogna and Gillies groups for all of the chemistry discussions and conversations. I performed most of my work in the Ragogna Lab during my degree and would like to thank Vanessa, Tyler, Cam, Ben, Taylor, Matt, Soheil and Ava for the many great times we shared. Over the years new members have joined and I would also like to thank JW, Jeanette, Kelly, Ghazale, Likun, Monica and John as it has been a very fun time getting to know all of you and I'm very thankful for the office laughs. Completing a thesis is a very difficult task and I wouldn't have been able to do it without all of you. I can only hope that country music in the lab will live on without me.

The various staff in the chemistry department have also made it enjoyable to work here and I'm grateful for the help everyone has provided.

To my family: Marina, Phil, Jadon and Whistler, you have all helped me out more than words can describe, and I am very thankful that you have been with me on this journey. To my grandparents: Francesco D'Angela, Domenica D'Angela, David Harrison and Audrey Harrison, I am also grateful for the advice and support you have provided me over the years and will always cherish our memories.

Table of Contents

List of Tables

List of Figures

List of Schemes

List of Abbreviations

AIBN	Azobisisobutyronitrile
ATR-FTIR	Attenuated total reflectance Fourier transform infrared spectroscopy
Đ	Dispersity
°C	degrees Celsius
DAPI	4',6-diamidino-2-phenylindole
DI	De-Ionized
DSC	Differential Scanning Calorimetry
E. coli	*Escherichia coli*
EDX	Energy Dispersive X-Ray Spectroscopy
EE	Encapsulation Efficiency
ESI-MS	Electron Ionization Mass Spectrometry
g/mol	Grams per mole
GPC	Gel Permeation Chromatography
HA	Hyaluronic Acid
$\{^1H\}$	Proton decoupled
J	coupling constant (Hz)
kg/mol	Kilograms per mole
LC	Loading Capacity
LS	Light Scattering
mL	millilitre
M_i	Molar mass of polymer chain
mmol	millimole
M_n	Number Average Molecular Weight
mol	mole

MTT	(3-(4,5-dimethylthiazol-2-yl)-2,5-diphenyltetrazolium bromide)
M_w	Weight Average Molecular Weight
MWCO	Molecular Weigh Cut-off
N_i	Number of polymer chains with mass M_i
NMR	Nuclear Magnetic Resonance
PAA	Poly(acrylic acid)
PAH	Poly(allylamine hydrochloride)
PBS	Phosphate Buffered Saline
PEC	Polyelectrolyte complex
SEM	Scanning Electron Microscopy
PEG	Poly(ethylene glycol)
PEGDMA	Poly(ethylene glycol) dimethacrylate
PMMA	Poly(methyl methacrylate)
ppm	Parts per million
S. aureus	*Staphylococcus aureus*
SEC	Size-exclusion chromatography
S_N2	Bimolecular Nucleophilic Substitution
TBD	1,5,7-triazabicyclo[4.4.0]dec-5-ene
TGA	Thermogravimetric Analysis
VA-044	2,2'-Azobis[2-(2-imidazolin 2yl)propane]dihydrochloride
Wt %	Weight Percent
MH_Z	Megahertz
δ	chemical shift (ppm)
λ	Wavelength
UV	Ultraviolet

Chapter 1

1   Introduction

1.1   Introduction to Polymers

The word polymer is derived from the Greek words 'poly' meaning many and 'meros' meaning parts.[1] They are macromolecules made by connecting smaller molecules together, through a process called polymerization. Polymers can be classified into two types: natural or synthetic. Natural polymers date back to the beginning of life. Cellulose, for example, is a natural polymer and main constituent of plant cell walls.[2] Deoxyribonucleic acid (DNA) is also a natural polymer that carries genetic instructions for organisms.[3] Synthetic polymers are also important in everyday life. The grocery bags and water bottles we use are made from poly(ethylene), which has the highest production tonnage annually of any synthetic polymer.[4] Poly(tetrafluoroethylene), (i.e. Teflon®) has also found many uses as wire coatings and to coat non-stick cookware (Figure 1-1).[5]

Figure 1-1 A 1960s Dupont advertisement for a non-stick pan.[6]

1.2   Polymer Composition and Structure

Polymers were originally classified by Carothers in 1929 into either condensation or addition polymers. Condensation polymers are formed through a reaction where a small molecule by-product is lost when molecules join together.[7] A simple example of this is the formation of nylon, where a diamine reacts with a diacid, and a water molecule is produced (Scheme 1-1A). Addition polymers are formed by linking monomers without the loss of a small molecule.[1] The most common addition polymers are formed through the polymerization of molecules containing a carbon-carbon double bond. A simple example of an addition polymerization is the formation of polystyrene (Scheme 1-1B).
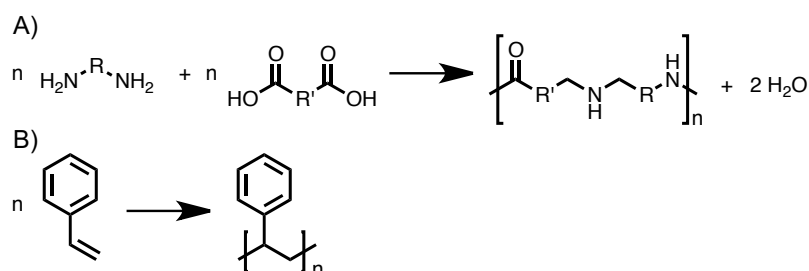
Scheme 1-1 A) A reaction of a diamine with diacid to produce nylon. B) Polymerization of styrene to produce Styrofoam.

1.3   Polymerization Mechanisms

Although Carothers coined the term condensation and addition polymerization, in 1953 Flory discussed the differences in their polymerization mechanisms.[7] He re-classified the polymerizations as either step or chain growth polymerizations, where the most important differences were how monomers that could react with one another, and how polymer molar mass depended on the extent of conversion. Step growth polymerizations proceed from monomer to dimer, trimer, tetramer, octamer and so on until large polymers are made (Figure 1-2A). Initially the molar mass and conversion of the polymers is low as dimers and tetramers are present, but as conversion increases polymers slowly gain mass until the final stages where high molar mass species are formed (Figure 1-2B).
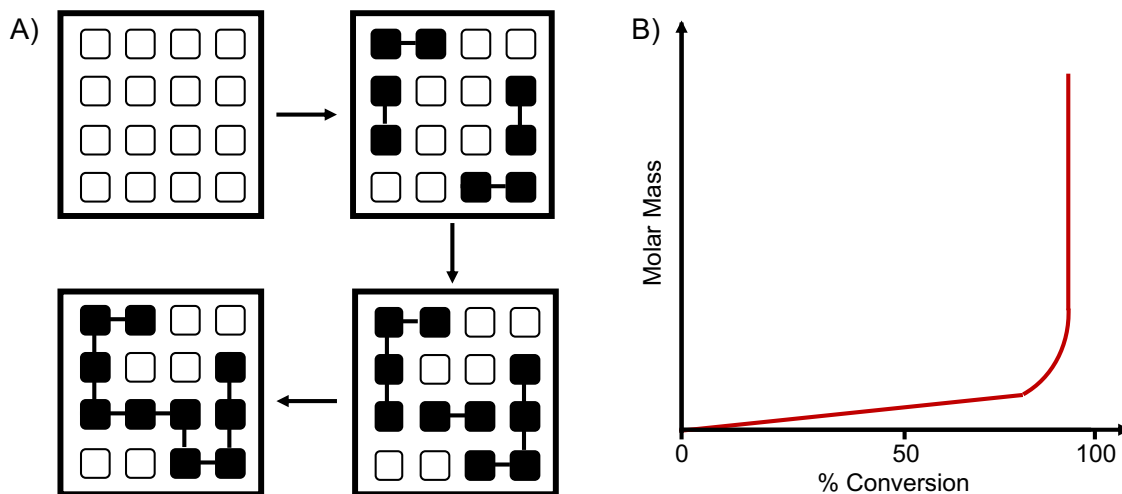
Figure 1-2 A) Representation of a step-growth polymerization showing dimer, tetramer, and decamer formation, leading to high molar mass polymers. B) A plot of molar mass versus conversion. Initially molar mass increases gradually until high conversions, where the molar mass increases more rapidly.

For living chain growth polymerization, an initiator is needed to produce a reactive initiating species, which can then react with a monomer to start polymerization. The reactive centre could be an anion, cation or free radical, for example. Polymerization then occurs by the propagation of the reactive species with other monomer units and only this reactive site can add monomers to it (Figure 1-3A). Living chain growth polymerization differs from step growth polymerization as higher-molar mass polymer molecules exist at low conversion percentages (Figure 1-3B).
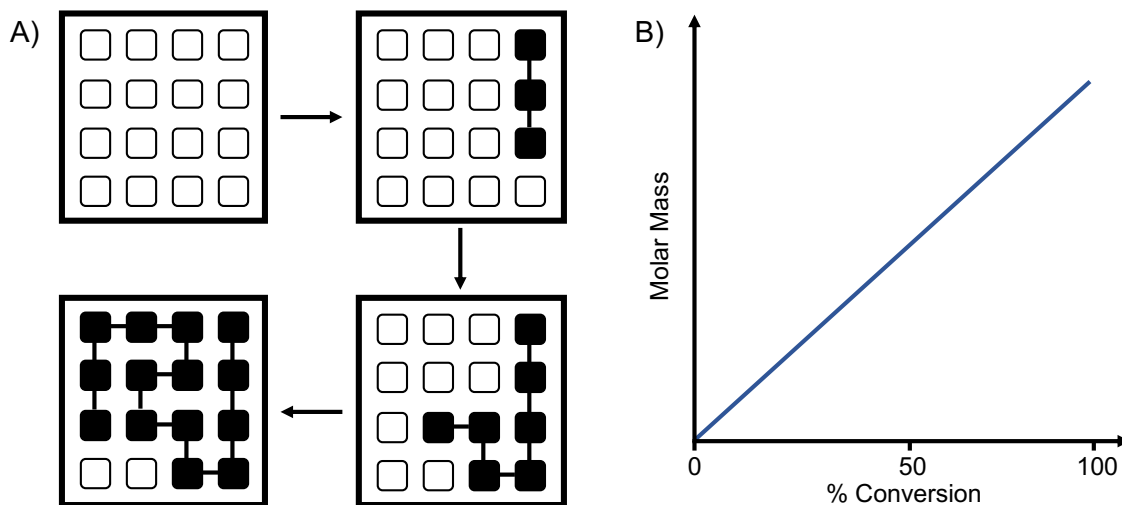
Figure 1-3 Representation of a living chain growth polymerization A) Showing addition of monomers units to one end of the polymer chain. B) A plot of molar mass versus conversion, showing that living chain growth polymerization results in higher molar mass polymers at low conversion percentages.

1.3.1 Chain Growth by Free Radical Polymerization

Free radical polymerization is a versatile technique because of the large range of polymerizable monomers available, the ability to polymerize in the presence of a variety of functional groups and the tolerance to a wide variety of reaction conditions. The first step is initiation, which generates a flux of radicals to start the reaction. The radicals are produced by homolytic cleavage through thermolysis or photolysis of the initiator, which then can add to the alkene tail of a monomer. Next, a radical is created at the head position of a polymerizable unit, which will propagate with more monomer until there are no more monomers left (Scheme 1-2). Along with the many benefits of free-radical polymerization there are limitations. Specifically, the loss of control can lead to termination events where the propagating radicals react by combination or disproportion giving a broad range of polymer chain lengths.

Initiation:
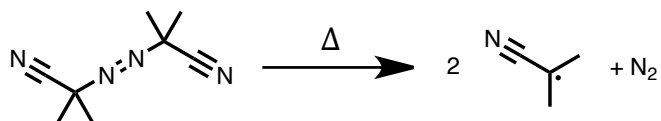
Propagation:
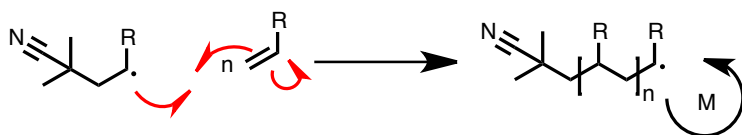
Termination:

Polymer Chain Coupling
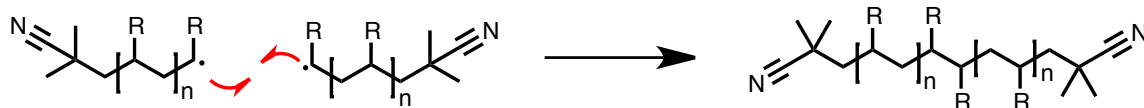
Disproportionation
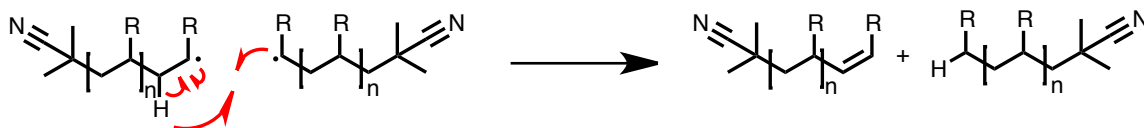
Scheme 1-2 Mechanism of initiation, propagation, and termination of polymer chains via free radical polymerization.

1.4   Molecular Weight Distribution

To determine the properties of a polymer, the size or molar mass plays a defining role. There are many different ways to represent the molar mass of a polymer, but the simplest is the *number average* molar mass, M_n, which is described as:

$$M_n = \frac{\Sigma N_i M_i}{\Sigma N_i}$$

Equation 1-1

In this equation, M_i is the molar mass of the molecular species i, and N_i is the number of molecules of i in the sample.

Alternatively, the *weight-average* molar mass is defined as:

$$M_w = \frac{\Sigma N_i M_i^2}{\Sigma N_i M_i}$$

Equation 1-2

The dispersity ($Đ$) of the sample can also be calculated from the ratio of M_w to M_n, as an indication of the range of molar masses in a polymer sample. The value of $Đ$ is greater than 1, but as the polymer chains approach the same length, the value becomes closer to 1.

$$Đ = \frac{M_w}{M_n}$$

Equation 1-3

1.5   Thermal Properties of Polymers

For most chemical species, molecules can be characterized into three different states of matter: solid, liquid or gas, however semi-crystalline polymers are characterized differently. They are characterized by their glass transition temperature (T_g) or crystalline melt transition temperature (T_m) (Figure 1-4).

Glassy and crystalline domains $\xrightleftharpoons{T_g}$ Rubbery and crystalline domains $\xrightleftharpoons{T_m}$ melt state
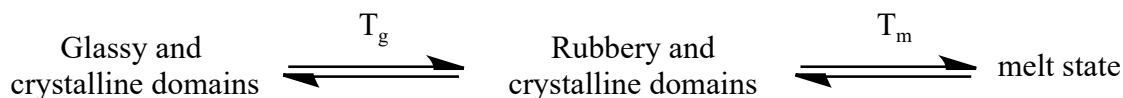
Figure 1-4 Thermal transitions of a semi-crystalline polymer between the glassy, amorphous, and melt states.

Below the glass transition temperature of a semi-crystalline polymer the chains exist both in ordered and disordered regions and are hard, brittle and frozen in place. When heated above the glass transition temperature, but below the crystalline melt transition temperature, the polymer chains in the ordered region remain locked into place with the chains in the disordered region become mobile causing the material to become soft. When the semi-crystalline polymer is heated above the crystalline melt transition temperature, the polymer chains in both the ordered and disordered regions become mobile and fluid-like. The thermal transition temperatures of polymers are very important to characterize, for example in 1986 the space shuttle Challenger disintegrated moments after lift-off resulting from a fluoroelastomer O-ring that was not in its rubbery state.[8]

1.6   Applications of Polymers

1.6.1   Polymer Networks

Polymer networks are materials composed of units that connect via 'junctions', that link one polymer to another.[9] Polymers can be linked together through covalent or intermolecular interactions (van der Waals, hydrophobic interactions or electrostatic interactions).

1.6.2   Covalent Polymer Networks

In covalent polymer networks, the network junctions are connected through covalent bonds and these materials are normally insoluble in all solvents. Two main methods for forming covalent networks involve chain growth polymerization and step growth polymerization. Polymer networks formed by chain growth involve one monomer adding to the growing end of a polymer chain, and in the presence of a multifunctional molecule, two or more of these propagating chains can link together forming a network. Polymer networks produced by step growth polymerization involve multifunctional monomers reacting to form dimers

then oligomers, and if one of the monomers has a functionality greater than two, branched polymers can form leading to network formation. For example, multi-functional thiol compounds can react with polymers containing pendent alkenes through thiol-ene chemistry to produce step-growth polymer networks (Scheme 1-3).[10]
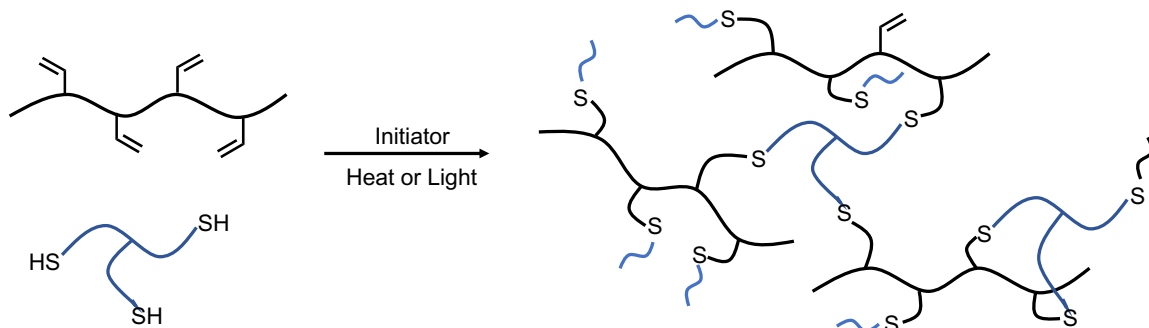
Scheme 1-3 Schematic diagram of network formation via the thiol-ene reaction.

1.6.2.1 Initiating Species in Crosslinked Polymer Networks

Species to initiate polymer networks can be activated thermally or by using light.[11] The use of UV initiators is advantageous because fast reaction times for network preparation and the overall energy footprint of the process is reduced when compared to thermal methods.[11] To generate photocured polymer networks, special photoinitiators are used which can undergo excitation upon absorption of a photon, cleave a bond and generate initiating species. Almost all radical photoinitiators contain the benzoyl structural element and there are two different types of radical photoinitiators: Type I and Type II.[12] Type I photoinitiators undergo unimolecular bond cleavage after absorption of light to generate initiating radicals to start polymerization. Type II photoinitiators undergo a bimolecular reaction, where after absorption of light the photoinitiator reacts with another molecule, usually a tertiary amine, to create the initiating species (Scheme 1-4).

A)

B)
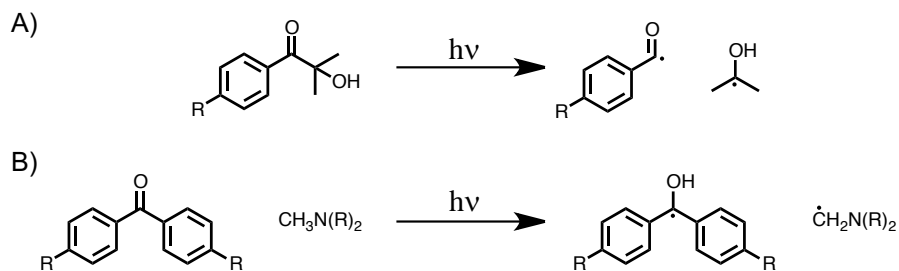
Scheme 1-4 A) Type I and B) Type II photoinitiator radical generation.

The light absorption and cleavage of the photo-initiator can be understood using a Jablonski diagram (Figure 1-5).[13] This process starts with the absorption of a photon, resulting in the excitation of a carbonyl electron on the photoinitiator, into a higher energy state ($S_2 \leftarrow S_0$). From this excited state, various processes can follow. The electron can vibrationally relax ($V_1 \leftarrow V_3$), then through internal conversion relax to the S_1 state ($S_1 \leftarrow S_2$). Subsequent transition to the ground state ($S_0 \leftarrow S_1$) can occur through fluorescence. Alternatively, the electron can relax to the ground state through internal conversion and the evolution of heat. Another path for dissipation of energy can occur through intersystem crossing. This occurs when an electron changes its spin form an excited singlet state to an excited triplet state. From the triplet state, the electron competes with further deactivation processes such as phosphorescence ($S_0 \leftarrow T_1$) or intramolecular scission of an α-bond can occur, producing radicals, which can then go on to initiate polymerization.
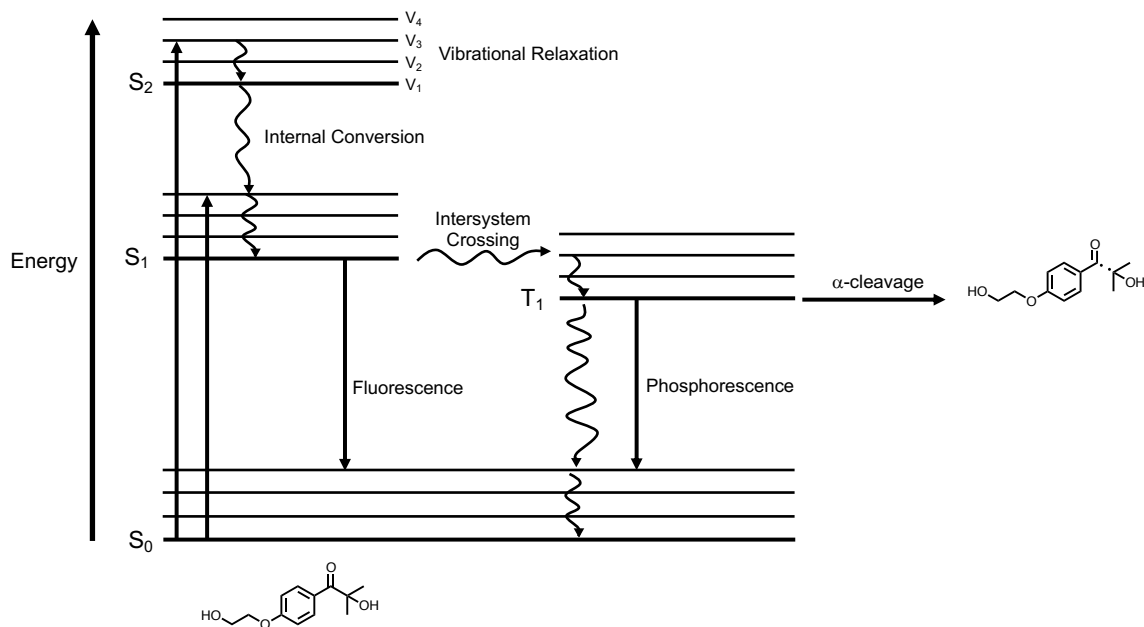
Figure 1-5 Jablonski diagram depicting photochemical processes with Igracure 2959, resulting in α-cleavage and radical formation.

1.6.3   Ionic Polymer Networks

Ionic polymer networks or polyelectrolyte complexes (PECs), are polymer networks formed through ionic crosslinks between polycations and polyanions.[14]   The driving force for these reactions is the entropically favourable release of counterions[15,16] and water molecules[17] (Equation 1-4):

$$Pol^+Cl^- \bullet xH_2O + Pol^-Na^+ \bullet yH_2O \rightarrow Pol^+Pol^- \bullet iH_2O + Na^+ + Cl^- + zH_2O \qquad \text{Equation 1-4}$$
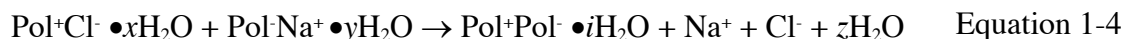
PECs have found many uses in self-healable materials,[18,19] drug and cell delivery,[20,21] and ion exchange membranes.[22,23] When creating PECs, it is very important to control the amount and rate of addition of each of the components, as different ratios can have drastic effects on network properties,[24] for example dilute solutions and a large excess of one polyelectrolyte can lead to semi-soluble nano- or micro-scale complexes.[25] Along with this, highly hydrated complexes can form coacervates that can be found in food science[26] and pharmaceutical industries.[27] To control the PEC properties, stoichiometry and network packing need to be carefully considered.

1.6.3.1   Controlling the Stoichiometry

The stoichiometry of PECs can be controlled based on the order and rate of addition which has a major effect on mechanical properties.[24] Extensive studies have been performed on the mixing rate and order of poly(allylamine) (PAH)/ poly(acrylic acid)(PAA) based systems.[14] For example, when a drop of PAA solution is added to a solution containing PAH, a network will form with an excess of PAH. This occurs because as PAA is slowly added, it complexes with a large excess of PAH and decrease of the concentration of unbound PAH in solution. As more PEC forms, all of the PAH become complexed and no further PAA can be added into the network.[14]

1.6.3.2   Importance of Compaction

Along with the rate and order of addition, compaction also has an effect on PEC mechanical properties.   As PECs form, they often manifest as transparent blobs resembling egg whites.[14] In this form the materials are hydrated with lots of water and the polymer chains are not completely associated with one another and compaction of the networks is beneficial. To remove much of the entrapped water, gravitational forces of *>*150 000 *g* are required by way of ultracentrifugation.[24] Loose particles become packed together into tougher, more mechanically robust materials (Figure 1-6).

$$>10^5\,g$$
$$2M\ NaCl$$
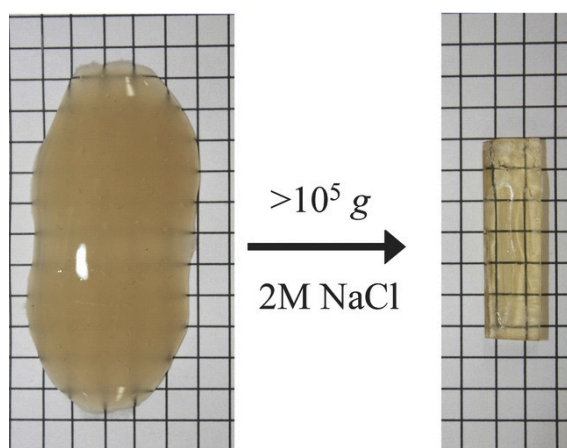
Figure 1-6 The effects of compaction of loosely packed ionic polymer networks. Reproduced with permission of the publisher (Appendix E).

1.7   Ionic Liquids and Their Applications

Ionic liquids are salts that that exhibit a melting point below 100 °C[28] and are very useful in synthesis as they normally have high thermal stabilities,[29] low vapor pressures[30] and high conductivities.[31] With these favorable properties, they have found uses in a wide range of applications including homogenous catalysis,[32] and electrolytic systems.[33] The most common compounds that exist as ionic liquids feature sulfonium, ammonium and phosphonium cations (Figure 1-7), where generally R = alkyl group; X = a variety of anions. If a polymerizable group is incorporated onto these ionic liquids, ionic polymers can also be created, opening up a wide variety of applications.
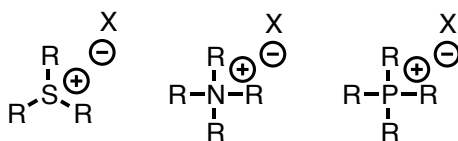
Figure 1-7 General structures of sulfonium, ammonium and phosphonium salts.

1.7.1   Ionic Polymers

Polymers bearing positive charges either on their backbones or side chains are considered to be ionic or more specifically, cationic polymers. Cationic polymers are used in many different applications with their usefulness arising from their charge, as this can be utilized in anion exchange membranes[34] and even in antibacterial applications. [35,36]

1.7.1.1   Polyammoniums

Quaternary ammonium compounds (QACs) are heavily used as antibacterials,[37] phase transfer catalysts,[38] fabric softeners,[39] detergents,[39] and in personal care products like shampoos.[39] Due to their extensive use in industry, they reach wastewater treatment plants in high levels and are released into the environment. QACs are generally degradable, but depending on the concentration and the counterion, this process could be hindered.[39] Their overall decomposition over time can occur via Hoffman elimination or nucleophilic substitution (Scheme 1-5).[40]
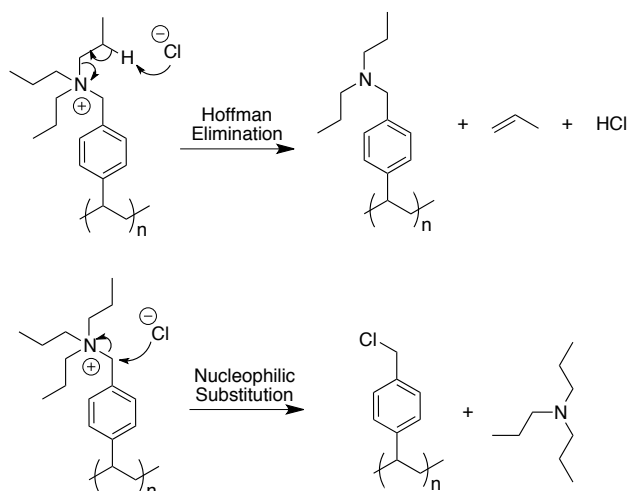
Scheme 1-5 Hoffman elimination and nucleophilic substitution of ammonium salts.

1.7.1.2   Polyphosphoniums

Polyphosphonium salts have emerged as attractive alternatives to their ammonium counterparts in many different applications, as they are generally less prone to undergo Hofmann elimination or nucleophilic substitution, leading to their higher thermal and chemical stability.[40] Phosphonium salts also have very different chemical and physical properties when compared to ammonium salts. For example they have longer C-P (~1.81 Å) bond lengths compared to C-N bond lengths (~ 1.53 Å) which allows them to be closer to their anionic counterions.[41] The cationic charge distribution is also more localized on the phosphorus centre while in ammonium salts the charge is distributed to adjacent carbons.[42,43]

1.7.2   Applications of Cationic Polymers

1.7.2.1   Antibacterials

In 1935, Domagk first published the development of a new type of surface disinfectant based on a quaternary ammonium compound,[44] making ammonium compounds the most popular ingredient in modern day household disinfectant products.[44] Despite the higher chemical and thermal stabilities,[40] and lower toxicities,[45] quaternary phosphonium compounds have been less extensively explored. Some of the initial phosphonium polymer

work was completed by Kanazawa *et. al.* and involved evaluating the antibacterial activities of a variety of phosphonium polymers on *S. aureus* and *E. coli*. The initial work involved synthesizing a wide variety of low molar mass styrenic-based phosphonium polymers with aryl or alkyl substituents around phosphorus. The results indicated that effect of substituents played a major role in antibacterial activity and increased with increasing hydrophobicity of the substituents.[46] Kanazwa *et. al.* also performed antibacterial studies of phosphonium polymers and tested the effects of molar mass and counter ion,[47] grafting to surfaces[20] and fibres,[49] and altering side chain lengths[50] and backbone structures.[51] More recently other phosphonium systems have included covalently crosslinked polymer films,[52] semi-interpenetrating polymer networks (SIPNs),[53] block copolymers[54] and sugar functionalized polyphosphoniums designed for targeted antibacterial applications.[55]

1.7.2.2 Delivery of Biologically Relevant Molecules

Cationic polymers have been used extensively over the past few decades in a wide range of biologically relevant applications. The field has been dominated by ammonium polymers, for example, poly(2-*N*,*N*-dimethylaminoethylmethacrylate) (PDMAEMA)[56–58] and poly(ethylenimine)[59,60] have been used extensively for drug delivery as they have high water solubility and the ability to become cationic when placed in physiological conditions. Molecules with a permanent charge on a specific atom (such as nitrogen or phosphorus) have also found uses in drug delivery, but to a lower degree. Nonetheless, expansive work surrounding phosphoniums polymers for nucleic acid and gene delivery have been reported noting the improved abilities of phosphonium over ammonium derivatives.[61–66]

1.8   Degradable Polymers

Development of biodegradable polymers has been increasing for the past several years as discussions of plastic pollution have received significant media attention. Biodegradable polymers are generally divided into two groups that include synthetic and natural polymers. Synthetic polymers offer advantages over natural polymers as they can be designed to be more tunable for the desired application. Degradable polymers find many uses in medicine and are used as drug delivery carriers,[67] sutures,[67] and in tissue regeneration.[67] Much

attention has focused on polysaccharides and polyesters as these materials typically undergo gradual degradation, either *in vivo* or in the environment[68] but more recently a newer class of polymers, termed self-immolative polymer have arisen.

1.8.1 Natural Polymers

Polysaccharides have been studied and used in a variety of different applications over the past century. The ability of these polymers to exhibit low toxicity and biodegradability adds to their usage. Natural polymers can have molar masses ranging from thousands to millions, with modifiable chemical groups to allow for applications. Some examples of common natural polymers are chitosan, cellulose, chondroitin sulfate, hyaluronic acid and alginic acid and have been reviewed in detail.[68] For the purpose of this thesis, hyaluronic acid and alginic acid will be discussed.

1.8.1.1 Hyaluronic Acid

Hyaluronic acid (HA) is a naturally occurring polymer found throughout the body in places such as the vitreous of the eye and the extracellular matrix of the cartilage tissues.[69] HA is composed of repeating disaccharide units composed of β-1,4-D-glucuronic acid and β-1,3-N-acetyl-D-glucosamide (Figure 1-8) and can have molar masses ranging from 100 kg mol^{-1} to 8000 kg mol^{-1}.[70]
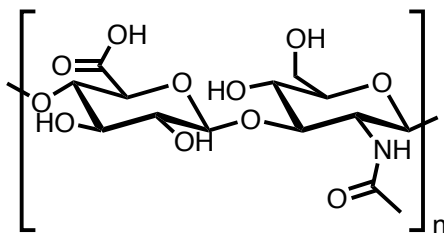
Figure 1-8 Structure of hyaluronic acid.

HA can also be degraded by enzymes such as hyaluronidase[71] and has been used in medical products for decades, with its structural properties mediating its activity in tasks such as cell signaling, wound repair and matrix organization.[72] Shoichet *et. al.* recently developed a thermogel consisting of hyaluronan and methylcellulose (HAMC) for cell and drug delivery,[73–75] where the hydrogel was used for the first demonstration of intravitreal protein

release of ciliary neurotrophic factor (CNTF) to treat degenerative diseases in the retina.[76] The protein (CNTF) was chemically conjugated to the hydrogel complex and then injected into the retina (Figure 1-9) and release was sustained for 7 days *in vitro*.[76]
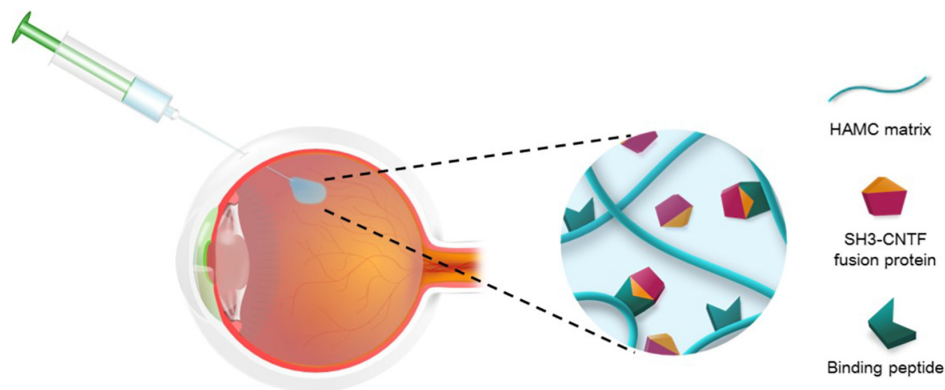
Figure 1-9 Graphic representation of the injection of HAMC hydrogel into the eye. Reproduced with permission of the publisher (Appendix E).

1.8.1.2   Alginic Acid

Alginic acid is a naturally occurring biopolymer obtained from brown sea algae[77] and its structure consists of copolymer α-L-guluronic acid (G) and β-D-mannuronic acid (M) residues, with the blocks composed of consecutive G residues, M residues, or alternating G and M residues (Figure 1-10).[78]

(M)   (G)
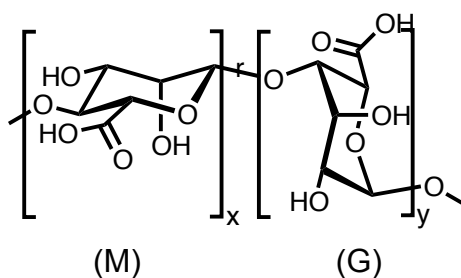
Figure 1-10 Alginic acid containing blocks of linked (1,4)-linked β-D-mannuronate (M) and α-L-guluronate (G) residues.

Alginate is typically used in gel form for a variety of applications including tissue engineering,[79] heavy metal scavenging,[80] and drug delivery.[81] The low toxicity and low

cost associated with alginate are its most valuable properties. Typically, the gels that form from alginates are achieved by ionic crosslinking with divalent cations such as Ca^{2+}. It is believed that only the G-blocks of alginate participate in ionic crosslinking with divalent cations, as they have the correct orientation.[77] In this form, the polymer chains of alginate are not degradable, but oxidation of backbone hydroxyl groups can lead to hydrolytically degradable alginate polymers. For example, Lueckgen *et al.* developed hydrolytically degradable crosslinked alginate hydrogels for potential uses in tissue engineering.[82] To do this, they oxidized the polymer backbone of alginate then modified the alginate by adding various ratios of norbornene and tetrazine onto the backbone, followed by crosslinking by carbodiimide chemistry. They were able to show these crosslinked networks retained high cell viability, were able to degrade in vivo, and promoted cell infiltration, rendering them useful for potential tissue engineering applications.

1.8.2   Synthetic Polymers

In comparison to natural polymers, synthetic degradable polymers offer many advantages such as the high versatility for a variety of applications, the ability to tailor the polymer properties to fit certain applications, and the possibility to tune the rate of degradation. Examples of synthetic polymers include polyesters, polyanhydrides, polyurethanes, polyphosphazanes, and poly(amino acids) to name of few. The most common class of biodegradable synthetic polymers are polyesters which can slowly degrade through their hydrolytically liable ester linkages or carbonate groups. Polyesters find many uses in drug delivery,[83] medical devices,[84] tissue regeneration[85] and in commercial food packaging[86] and although slow degradation can be useful in some applications, there is much interest in the ability to trigger polymer degradation on command.

1.8.2.1   Stimuli-Responsive Degradable Polymers

While the concept of depolymerization is not new, polymers that can depolymerize end-to-end upon application of a stimulus are known as self-immolative polymers (SIPs).[87,88] End-to-end depolymerization can occur following the cleavage of an end-cap (Figure 1-11A) or bond in the backbone (Figure 1-11B).[89]
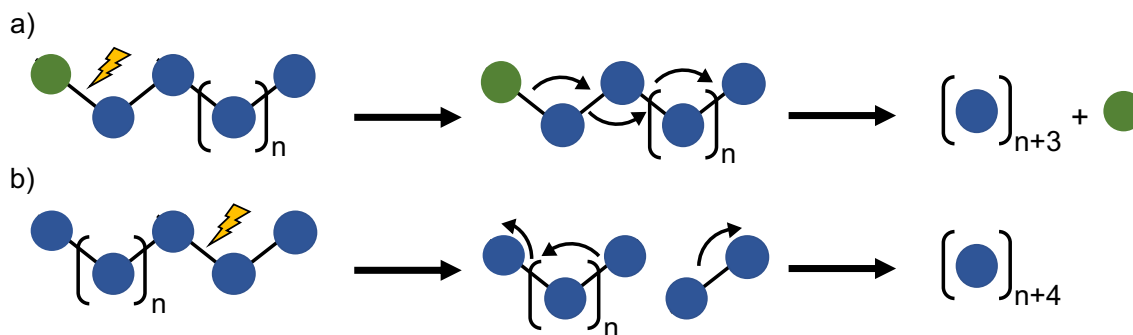
Figure 1-11 End-to-end depolymerization of polymers based on A) end-cap cleavage; B) backbone cleavage.

The major advantage of SIPs is their ability to degrade entirely as a result of a single bond cleavage by application of a stimulus. Stimuli-responsive end-caps have included groups responsive to fluoride ions,[90] redox changes,[91] enzymes,[92] mechanical force,[93] heat[94] and light.[95] The backbones of these polymers have included polycarbamates,[96] polycarbonates,[97] polyethers,[98] polyphthalaldehydes[99] and poly(glyoxylate)s.[100] Poly(glyoxylate)s are of particular interest as self-immolative polymers as they depolymerize to non-toxic products.

1.8.2.1.1 Poly(glyoxylate)s

Poly(glyoxylate)s are a class of polyaldehydes that can undergo depolymerization upon end-cap cleavage. Over the past few decades, poly(ethyl glyoxylate),[101] poly(methyl glyoxylate)[102] and poly(glyoxylic acid) salts have been reported and stabilized through end-capping. The polymers degraded by hydrolysis of the esters, backbone acetal cleavage, and depolymerization, leading to non-toxic products such as the corresponding alcohols and glyoxylic acid hydrate (Scheme 1-6).[103]
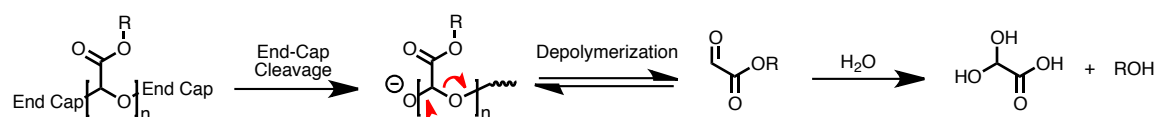
Scheme 1-6 Schematic representation of generic poly(glyoxylates) through end-cap cleavage and hydrolysis.

The first report of stimuli responsive end-caps added to poly(glyoxylate)s was in 2014 and allowed for triggered end to end depolymerization.[100] Ethyl glyoxylate was polymerized in dichloromethane using catalytic triethylamine at -20 °C to afford poly(ethyl glyoxylate) and then end-capped with 6-nitroveratryl carbonate, which was responsive to UV-light.[100] From here, a variety of different end-caps were synthesized to be responsive to a variety of different stimuli.[89] For example, block copolymers made from polyethylene glycol-poly(ethyl glyoxylate)-polyethylene glycol were synthesized and self-assembled into micelles with end-caps sensitive to reducing thiols and H_2O_2, which can be found in the body. These micelles were loaded with Nile red, doxorubicin and curcumin and showed triggered release upon application of the stimulus.[104]

1.8.2.1.2 Polyglyoxylamides

A newly synthesized class of self-immolative polymers was recently reported by the reaction of poly(ethyl glyoxylate) with a variety of different amines (Scheme 1-7).[105] The aim was to further stabilize the polymers by removing the hydrolytically sensitive ester groups. The addition of the amides drastically increased the T_g values of the polymers[105] and increased water solubility and stability.[106] Overall, there are many potential avenues of application for these polymers, one of which will be explored in this thesis.
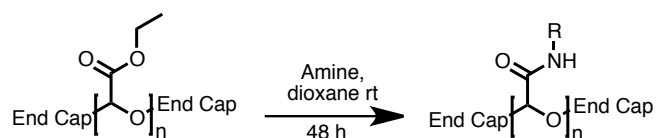
Scheme 1-7 Schematic representation of the conversion of poly(ethyl glyoxylate) to poly(glyoxylamide).

1.9 Scope of Thesis

This dissertation focuses on the use of various phosphonium salt-containing polymers to create polymer networks for uses in drug delivery and antibacterial surfaces. Chapter 2 focuses on incorporating three different phosphonium monomers into PEGDMA based covalent hydrogels for drug release. Anionic dyes and drug molecules were subsequently loaded into the hydrogels and released, and it was shown that release rates could be tuned

based on the chemical structure of the phosphonium and the ionic strength and pH of the release medium. Surface cell growth was also completed, but no growth of C2C12 cells was observed on the hydrogels indicating that they might resist fouling in biological systems.

Chapter 3 focuses on the use of phosphonium polymers to form polyelectrolyte complexes with hyaluronate for drug release. A variety of high molar mass phosphonium polymers were synthesized, characterized, and complexed with sodium hyaluronate to create ionic polymer networks. The swelling, rheology and self-healing properties were characterized for each complex. Anionic dyes and drug molecules were loaded into the complexes and released in phosphate buffered saline. It was determined that the identity of the phosphonium polymer affected the swelling, rheology and self-healing properties of the materials and that the identity of the phosphonium polymer and the anion also affected the rate of release from these complexes.

Chapter 4 compares phosphonium polymers and their analogous ammonium polymers in polyelectrolyte complexes to determine if the phosphorus or nitrogen has an impact on network properties or drug delivery. The anionic polymer in this study was chosen to be alginate, to also determine if this will have an effect on network properties and release rates as well. The swelling, rheology and self-healing properties were characterized for each complex. Anionic dyes and drug molecules were loaded into the complexes and released in phosphate buffered saline. It was determined that the substituents around phosphorus and nitrogen dictated the network properties and drug release abilities and the atom itself did not have a great effect.

Chapter 5 explores the initial reactivity to create self-immolative polymers with pendent phosphoniums to be used as antibacterials. This work outlines the synthesis and characterization of mixed copolymers containing pendent phosphoniums and allyl groups on poly(ethyl glyoxylate) and subsequent crosslinking via thiol-ene chemistry to create thin films. The resulting films can potentially act as antibacterials and should also degrade upon application of UV-light, allowing adhered bacteria or other fouling species to be shed from the surface.

1.10   References

(1)   Nicholson, J. W. *The Chemistry of Polymers*, 5th ed.; Royal Society of Chemistry: London, UK, 2017.

(2)   Jedvert, K.; Heinze, T. Cellulose Modification and Shaping - A Review. *J. Polym. Eng.* **2017**, *37*, 845–860.

(3)   Crick, F. H. C.; Watson, J. D. The Complementary Structure of Deoxyribonucleic Acid. *Proc. R. Soc. A* **1953**, *223*, 80–96.

(4)   Geyer, R.; Jambeck, J. R.; Law, K. L. Production, Use, and Fate of All Plastics Ever Made. *Sci. Adv.* **2017**, *3*, 25–29.

(5)   Dupont. *Teflon PTFE - Fluoropolymer Resin*; Dupont.

(6)   Board, G. DuPont Offers $670M Settlement For "Teflon" Chemical Contamination Of Water.

(8)   Gebhardt, C.; Bergin, C. STS-51L and STS-107 – Challenger and Columbia: A Legacy Honored.

(9)   Carothers, W. H. Polymerization. *Chem. Rev.* **1931**, *8*, 353–426.

(10)   Hoyle, C. E.; Lee, T. Y.; Roper, T. Thiol–Enes: Chemistry of the Past with Promise for the Future. *J. Polym. Sci,. Part A: Polym. Chem.* **2004**, *42*, 5301–5338.

(11)   Shukla, V.; Bajpai, M.; Singh, D. K.; Singh, M.; Shukla, R. Review of Basic Chemistry of UV-Curing Technology. *Pigm. Resin Technol.* **2004**, *33*, 272–279.

(12)   Segurola, J.; Allen, N. S.; Edge, M.; McMahon, A.; Wilson, S. Photoyellowing and Discolouration of UV Cured Acrylated Clear Coatings Systems: Influence of Photoinitiator Type. *Polym. Degrad. Stab.* **1999**, *64*, 39–48.

(13)   Schwalm, R. *UV Coatings: Basics, Recent Developments and New Applications*, First.; Elsevier: Amsterdam, The Netherlands, 2007.

(14) Reisch, A.; Tirado, P.; Roger, E.; Boulmedais, F.; Collin, D.; Voegel, J. C.; Frisch, B.; Schaaf, P.; Schlenoff, J. B. Compact Saloplastic Poly(Acrylic Acid)/Poly(Allylamine) Complexes: Kinetic Control over Composition, Microstructure, and Mechanical Properties. *Adv. Funct. Mater.* **2013**, *23*, 673–682.

(15) Laugel, N.; Betscha, C.; Winterhalter, M.; Voegel, J. C.; Schaaf, P.; Ball, V. Relationship between the Growth Regime of Polyelectrolyte Multilayers and the Polyanion/Polycation Complexation Enthalpy. *J. Phys. Chem. B* **2006**, *110*, 19443–19449.

(16) Fu, J.; Schlenoff, J. B. Driving Forces for Oppositely Charged Polyion Association in Aqueous Solutions: Enthalpic, Entropic, but Not Electrostatic. *J. Am. Chem. Soc.* **2016**, *138*, 980–990.

(17) Schlenoff, J. B.; Rmaile, A. H.; Bucur, C. B. Hydration Contributions to Association in Polyelectrolyte Multilayers and Complexes: Visualizing Hydrophobicity. *J. Am. Chem. Soc.* **2008**, *130*, 13589–13597.

(18) Reisch, A.; Roger, E.; Phoeung, T.; Antheaume, C.; Orthlieb, C.; Boulmedais, F.; Lavalle, P.; Schlenoff, J. B.; Frisch, B.; Schaaf, P. On the Benefi Ts of Rubbing Salt in the Cut : Self-Healing of Saloplastic PAA / PAH Compact Polyelectrolyte Complexes. *Adv. Mater.* **2014**, 1–5.

(19) Zhang, H.; Wang, C.; Zhu, G.; Zacharia, N. S. Self-Healing of Bulk Polyelectrolyte Complex Material as a Function of PH and Salt. *ACS Appl. Mater. Interfaces* **2016**, *8*, 26258–26265.

(20) Lin, W. C.; Yu, D. G.; Yang, M. C. PH-Sensitive Polyelectrolyte Complex Gel Microspheres Composed of Chitosan/Sodium Tripolyphosphate/Dextran Sulfate: Swelling Kinetics and Drug Delivery Properties. *Colloids Surf., B* **2005**, *44*, 143–151.

(21) Sepúlveda-Rivas, S.; Fritz, H. F.; Valenzuela, C.; Santiviago, C. A.; Morales, J. O. Development of Novel EE/Alginate Polyelectrolyte Complex Nanoparticles for

Lysozyme Delivery: Physicochemical Properties and in Vitro Safety. *Pharmaceutics* **2019**, *11*, 1-19.

(22)   Ghoussoub, Y. E.; Fares, H. M.; Delgado, J. D.; Keller, L. R.; Schlenoff, J. B. Antifouling Ion-Exchange Resins. *ACS Appl. Mater. Interfaces* **2018**, *10*, 41747–41756.

(23)   Liu, W.; Wijeratne, S.; Yang, L.; Bruening, M. Porous Star-Star Polyelectrolyte Multilayers for Protein Binding. *Polymer* **2018**, *138*, 267–274.

(24)   Schaaf, P.; Schlenoff, J. B. Saloplastics: Processing Compact Polyelectrolyte Complexes. *Adv. Mater.* **2015**, *27*, 2420–2432.

(25)   Pack, D. W.; Hoffman, A. S.; Pun, S.; Stayton, P. S. Design and Development of Polymers for Gene Delivery. *Nat. Rev. Drug Discovery* **2005**, *4*, 581–593.

(26)   Schmitt, C.; Sanchez, C.; Desobry-Banon, S.; Hardy, J. Structure and Technofunctional Properties of Protein-Polysaccharide Complexes: A Review. *Crit. Rev. Food Sci. Nutr.* **1998**, *38*, 689–753.

(27)   Voets, I. K.; de Keizer, A.; Cohen Stuart, M. A. Complex Coacervate Core Micelles. *Adv. Colloid Interface Sci.* **2009**, *147–148*, 300–318.

(28)   Forsyth, S. A.; Pringle, J. M.; MacFarlane, D. R. Ionic Liquids-An Overview. *Aust. J. Chem.* **2004**, *57*, 113–119.

(29)   Huddleston, J. G.; Visser, A. E.; Reichert, W. M.; Willauer, H. D.; Broker, G. A.; Rogers, R. D. Characterization and Comparison of Hydrophilic and Hydrophobic Room Temperature Ionic Liquids Incorporating the Imidazolium Cation. *Green Chem.* **2001**, *3*, 156–164.

(30)   Huddleston, J. G.; Willauer, H. D.; Swatloski, R. P.; Visser, A. E.; Rogers, R. D. Room Temperature Ionic Liquids as Novel Media for "clean" Liquid-Liquid Extraction. *Chem. Commun.* **1998**, 1765–1766.

(31)   Armand, M.; Endres, F.; MacFarlane, D. R.; Ohno, H.; Scrosati, B. Ionic-Liquid Materials for the Electrochemical Challenges of the Future. *Nat. Mater.* **2009**, *8*, 621–629.

(32)   Olivier-Bourbigou, H.; Magna, L. Ionic Liquids: Perspectives for Organic and Catalytic Reactions. *J. Mol. Catal. A: Chem.* **2002**, *182–183*, 419–437.

(33)   Tiyapiboonchaiya, C.; MacFarlane, D. R.; Sun, J.; Forsyth, M. Polymer-in-Ionic-Liquid Electrolytes. *Macromol. Chem. Phys.* **2002**, *203*, 1906–1911.

(34)   Wu, H.; Lai, X.; Li, Z.; Gu, L.; Ao, N. PEGylation Quaternary (Triphenyl-) Phosphonium Tosylate: A Class of Promising Carriers for Drug Delivery and Gene Delivery? *ChemistrySelect* **2018**, *3*, 11677–11679.

(35)   Haldar, J.; Kondaiah, P.; Bhattacharya, S. Synthesis and Antibacterial Properties of Novel Hydrolyzable Cationic Amphiphiles. Incorporation of Multiple Head Groups Leads to Impressive Antibacterial Activity. *J. Med. Chem.* **2005**, *48*, 3823–3831.

(36)   Rawlinson, L. A. B.; Ryan, S. M.; Mantovani, G.; Syrett, J. A.; Haddleton, D. M.; Brayden, D. J. Antibacterial Effects of Poly(2-(Dimethylamino Ethyl)Methacrylate) against Selected Gram-Positive and Gram-Negative Bacteria. *Biomacromolecules* **2010**, *11*, 443–453.

(37)   Hegstad, K.; Langsrud, S.; Lunestad, B. T.; Scheie, A. A.; Sunde, M.; Yazdankhah, S. P. Does the Wide Use of Quaternary Ammonium Compounds Enhance the Selection and Spread of Antimicrobial Resistance and Thus Threaten Our Health? *Microb. Drug Resist.* **2010**, *16*, 91–104.

(38)   Kim, D. Y.; Huh, S. C.; Kim, S. M. Enantioselective Michael Reaction of Malonates and Chalcones by Phase-Transfer Catalysis Using Chiral Quaternary Ammonium Salt. *Tetrahedron Lett.* **2001**, *42*, 6299–6301.

(39)   Zhang, C.; Cui, F.; Zeng, G. ming; Jiang, M.; Yang, Z. zhu; Yu, Z. gang; Zhu, M. ying; Shen, L. qing. Quaternary Ammonium Compounds (QACs): A Review on Occurrence, Fate and Toxicity in the Environment. *Sci. Total Environ.* **2015**, *518–*

519, 352–362.

(40)   Hemp, S. T.; Zhang, M.; Allen, M. H.; Cheng, S.; Moore, R. B.; Long, T. E. Comparing Ammonium and Phosphonium Polymerized Ionic Liquids: Thermal Analysis, Conductivity, and Morphology. *Macromol. Chem. Phys.* **2013**, *214*, 2099–2107.

(41)   Abdallah, D. J.; Lu, L.; Weiss, R. G. Thermoreversible Organogels from Alkane Gelators with One Heteroatom. *Chem. Mater.* **1999**, *11*, 2907–2911.

(42)   Liang, S.; Oreilly, M. V.; Choi, U. H.; Shiau, H. S.; Bartels, J.; Chen, Q.; Runt, J.; Winey, K. I.; Colby, R. H. High Ion Content Siloxane Phosphonium Ionomers with Very Low Tg. *Macromolecules* **2014**, *47*, 4428–4437.

(43)   Wang, S. W.; Liu, W.; Colby, R. H. Counterion Dynamics in Polyurethane-Carboxylate Ionomers with Ionic Liquid Counterions. *Chem. Mater.* **2011**, *23*, 1862–1873.

(44)   Domagk, G. Eine Neue Klasse von Desinfektionsmitteln. *Dtsch. Med. Wochenschr.* **1935**, *61*, 829–832.

(45)   Floch, V.; Loisel, S.; Guenin, E.; Herve, A. C.; Clement, J. C.; Yaouanc, J. J.; Des Abbayes, H.; Ferec, C. Cation Substitution in Cationic Phosphonolipids: A New Concept to Improve Transfection Activity and Decrease Cellular Toxicity. *J. Med. Chem.* **2000**, *43*, 4617–4628.

(46)   Kanazawa, A.; Ikeda, T.; Endo, T. Novel Polycationic Biocides: Synthesis and Antibacterial Activity of Polymeric Phosphonium Salts. *J. Polym. Sci., Part A: Polym. Chem.* **1993**, *31*, 335–343.

(47)   Kanazawa, A; Ikeda, T, Endo, T. Polymeric Phosphonium Salts as a Novel Class of Cationic Biocides. II. Effects of Counter Anion and Molecular Weight on Antibacterial Activity of Polymeric Phosphonium Salts. *J. Polym. Sci., Part A: Polym. Chem.* **1993**, *31*, 1441–1447.

(48)   Kanazawa, A.; Ikeda, T.; Endo, T. Polymeric Phosphonium Salts as a Novel Class of Cationic Biocides. III. Immobilization of Phosphonium Salts by Surface Photografting and Antibacterial Activity of the Surface-Treated Polymer Films. *J. Polym. Sci., Part A: Polym. Chem.* **1993**, *31*, 1467–1472.

(49)   Kanazawa, A.; Ikeda, T.; Endo, T. Polymeric Phosphonium Salts as a Novel Class of Cationic Biocides. VI. Antibacterial Activity of Fibers Surface-treated with Phosphonium Salts Containing Trimethoxysilane Groups. *J. Appl. Polym. Sci.* **1994**, *52*, 641–647.

(50)   Kanazawa, A.; Ikeda, T.; Endo, T. Polymeric Phosphonium Salts as a Novel Class of Cationic Biocides. IX. Effect of Side-Chain Length between Main Chain and Active Group on Antibacterial Activity. *J. Polym. Sci., Part A: Polym. Chem.* **1994**, *32*, 1997–2001.

(51)   Kanazawa, A.; Ikeda, T.; Endo, T. Polymeric Phosphonium Salts as a Novel Class of Cationic Biocides. IV. Synthesis and Antibacterial Activity of Polymers with Phosphonium Salts in the Main Chain. *J. Polym. Sci., Part A: Polym. Chem.* **1993**, *31*, 3031–3038.

(52)   Cuthbert, T. J.; Guterman, R.; Ragogna, P. J.; Gillies, E. R. Contact Active Antibacterial Phosphonium Coatings Cured with UV Light. *J. Mater. Chem. B*. **2015**, 1474–1478.

(53)   Cuthbert, T. J.; Harrison, T. D.; Ragogna, P. J.; Gillies, E. R. Synthesis, Properties, and Antibacterial Activity of Polyphosphonium Semi-Interpenetrating Networks. *J. Mater. Chem. B* **2016**, *4*, 4872–4883.

(54)   Hisey, B.; Ragogna, P. J.; Gillies, E. R. Phosphonium-Functionalized Polymer Micelles with Intrinsic Antibacterial Activity. *Biomacromolecules* **2017**, *18*, 914–923.

(55)   Cuthbert, T. J.; Hisey, B.; Harrison, T. D.; Trant, J. F.; Gillies, E. R.; Ragogna, P. J. Surprising Antibacterial Activity and Selectivity of Hydrophilic Polyphosphoniums Featuring Sugar and Hydroxy Substituents. *Angew*. *Chem*., *Int*. *Ed*. **2018**, *57*, 12707–12710.

(56)   Skarmoutsou, A.; Lolas, G.; Charitidis, C. A.; Chatzinikolaidou, M.; Vamvakaki, M.; Farsari, M. Nanomechanical Properties of Hybrid Coatings for Bone Tissue Engineering. *J. Mech. Behav. Biomed. Mater.* **2013**, *25*, 48–62.

(57)   Han, S.; Cheng, Q.; Wu, Y.; Zhou, J.; Long, X.; Wei, T.; Huang, Y.; Zheng, S.; Zhang, J.; Dong, A. Effects of Hydrophobic Core Components in Amphiphilic PDMAEMA Nanoparticles on SiRNA Delivery. *Biomaterials* **2015**, *48*, 45–55.

(58)   Liu, Y.; Cao, X.; Luo, M.; Le, Z.; Xu, W. Self-Assembled Micellar Nanoparticles of a Novel Star Copolymer for Thermo and PH Dual-Responsive Drug Release. *J. Colloid Interface Sci.* **2009**, *329*, 244–252.

(59)   Chen, M.; Tang, Y.; Wang, T.; Long, Q.; Zeng, Z.; Chen, H.; Feng, X. Enhanced Gene Delivery of Low Molecular Weight PEI by Flower-like ZnO Microparticles. *Mater. Sci. Eng. C* **2016**, *69*, 1367–1372.

(60)   Chen, L.; Ji, F.; Bao, Y.; Xia, J.; Guo, L.; Wang, J.; Li, Y. Biocompatible Cationic Pullulan-g-Desoxycholic Acid-g-PEI Micelles Used to Co-Deliver Drug and Gene for Cancer Therapy. *Mater. Sci. Eng. C* **2017**, *70*, 418–429.

(61)   Ornelas-Megiatto, C.; Wich, P. R.; Fréchet, J. M. J. Polyphosphonium Polymers for SiRNA Delivery: An Efficient and Nontoxic Alternative to Polyammonium Carriers. *J. Am. Chem. Soc.* **2012**, *134*, 1902–1905.

(62)   Hemp, S. T.; Allen, M. H.; Green, M. D.; Long, T. E. Phosphonium-Containing Polyelectrolytes for Nonviral Gene Delivery. *Biomacromolecules* **2012**, *13*, 231–238.

(63) Herma, R.; Wrobel, D.; Liegertová, M.; Müllerová, M.; Strašák, T.; Maly, M.; Semerádtová, A.; Štofik, M.; Appelhans, D.; Maly, J. Carbosilane Dendrimers with Phosphonium Terminal Groups Are Low Toxic Non-Viral Transfection Vectors for SiRNA Cell Delivery. *Int. J. Pharm.* **2019**, *562*, 51–65.

(64) Borguet, Y. P.; Khan, S.; Noel, A.; Gunsten, S. P.; Brody, S. L.; Elsabahy, M.; Wooley, K. L. Development of Fully Degradable Phosphonium-Functionalized Amphiphilic Diblock Copolymers for Nucleic Acids Delivery. *Biomacromolecules* **2018**, *19*, 1212–1222.

(65) Loczenski Rose, V.; Shubber, S.; Sajeesh, S.; Spain, S. G.; Puri, S.; Allen, S.; Lee, D. K.; Winkler, G. S.; Mantovani, G. Phosphonium Polymethacrylates for Short Interfering RNA Delivery: Effect of Polymer and RNA Structural Parameters on Polyplex Assembly and Gene Knockdown. *Biomacromolecules* **2015**, *16*, 3480–3490.

(66) Hemp, S. T.; Smith, A. E.; Bryson, J. M.; Allen, M. H.; Long, T. E. Phosphonium-Containing Diblock Copolymers for Enhanced Colloidal Stability and Efficient Nucleic Acid Delivery. *Biomacromolecules* **2012**, *13*, 2439–2445.

(67) Manavitehrani, I.; Fathi, A.; Badr, H.; Daly, S.; Shirazi, A. N.; Dehghani, F. Biomedical Applications of Biodegradable Polyesters. *Polymers* **2016**, *8*, 1–32.

(68) Doppalapudi, S.; Jain, A.; Khan, W.; Domb, A. J. Biodegradable Polymers-an Overview. *Polym. Adv. Technol.* **2014**, *25*, 427–435.

(69) Fraser, J. R. E.; Laurent, T. C.; Laurent, U. B. G. Hyaluronan: Its Nature, Distribution, Functions and Turnover. *J. Intern. Med.* **1997**, *242*, 27–33.

(70) Burdick, J. A.; Prestwich, G. D. Hyaluronic Acid Hydrogels for Biomedical Applications. *Adv. Mater.* **2011**, *23*, 41–56.

(71) Laurent, T. C.; Fraser, J. R. The Properties and Turnover of Hyaluronan. *Ciba Found. Symp.* **1986**, *124*, 9–29.

(72) Toole, B. P. Hyaluronan: From Extracellular Glue to Pericellular Cue. *Nat. Rev. Cancer* **2004**, *4*, 528–539.

(73) Wang, Y.; Lapitsky, Y.; Kang, C. E.; Shoichet, M. S. Accelerated Release of a Sparingly Soluble Drug from an Injectable Hyaluronan-Methylcellulose Hydrogel. *J. Controlled Release* **2009**, *140*, 218–223.

(74) Gupta, D.; Tator, C. H.; Shoichet, M. S. Fast-Gelling Injectable Blend of Hyaluronan and Methylcellulose for Intrathecal, Localized Delivery to the Injured Spinal Cord. *Biomaterials* **2006**, *27*, 2370–2379.

(75) Caicco, M. J.; Zahir, T.; Mothe, A. J.; Ballios, B. G.; Kihm, A. J.; Tator, C. H.; Shoichet, M. S. Characterization of Hyaluronan-Methylcellulose Hydrogels for Cell Delivery to the Injured Spinal Cord. *J. Biomed. Mater. Res., Part A* **2013**, *101 A*, 1472–1477.

(76) Delplace, V.; Ortin-Martinez, A.; Tsai, E. L. S.; Amin, A. N.; Wallace, V.; Shoichet, M. S. Controlled Release Strategy Designed for Intravitreal Protein Delivery to the Retina. *J. Controlled Release* **2019**, *293*, 10–20.

(77) Lee, K. L.; Mooney, D. J. Alginate : Properties and Biomedical Applications. *Prog. Polym. Sci.* **2012**, *37*, 106–126.

(78) Haug, A.; Larsen, B. Studies on the Sequence of Uronic Acid Residues in Alginic Acid. *Acta Chem. Scand.* **1967**, *21*, 691–704.

(79) Sun, J.; Tan, H. Alginate-Based Biomaterials for Regenerative Medicine Applications. *Materials* **2013**, *6*, 1285–1309.

(80) Lamelas, C.; Avaltroni, F.; Benedetti, M.; Wilkinson, K. J.; Slaveykova, V. I. Quantifying Pb and Cd Complexation by Alginates and the Role of Metal Binding on Macromolecular Aggregation. *Biomacromolecules* **2005**, *6*, 2756–2764.

(81) Tønnesen, H. H.; Karlsen, J. Alginate in Drug Delivery Systems. *Drug Dev. Ind. Pharm.* **2002**, *28*, 621–630.

(82)   Lueckgen, A.; Garske, D. S.; Ellinghaus, A.; Desai, R. M.; Stafford, A. G.; Mooney, D. J.; Duda, G. N.; Cipitria, A. Hydrolytically-Degradable Click-Crosslinked Alginate Hydrogels. *Biomaterials* **2018**, *181*, 189–198.

(83)   Nazemi, K.; Azadpour, P.; Moztarzadeh, F.; Urbanska, A. M.; Mozafari, M. Tissue-Engineered Chitosan/Bioactive Glass Bone Scaffolds Integrated with PLGA Nanoparticles: A Therapeutic Design for on-Demand Drug Delivery. *Mater. Lett.* **2015**, *138*, 16–20.

(84)   Haghighat, F.; Ravandi, S. A. H. Mechanical Properties and in Vitro Degradation of PLGA Suture Manufactured via Electrospinning. *Fibers Polym.* **2014**, *15*, 71–77.

(85)   Little, C. J.; Bawolin, N. K.; Chen, X. Mechanical Properties of Natural Cartilage and Tissue-Engineered Constructs. *Tissue Eng., Part B* **2011**, *17*, 213–227.

(86)   Li, W.; Coffin, D. R.; Jin, T. Z.; Latona, N.; Liu, C.-K.; Liu, B.; Zhang, J.; LinShu, L. Biodegradable Composites from Polyester and Sugar Beet Pulp with Antimicrobial Coating for Food Packaging. *J. Appl. Polym. Sci.* **2012**, *126*, 362–373.

(87)   Phillips, S. T.; Dilauro, A. M. Continuous Head-to-Tail Depolymerization: An Emerging Concept for Imparting Amplified Responses to Stimuli-Responsive Materials. *ACS Macro Lett.* **2014**, *3*, 298–304.

(88)   Wong, A. D.; DeWit, M. A.; Gillies, E. R. Amplified Release through the Stimulus Triggered Degradation of Self-Immolative Oligomers, Dendrimers, and Linear Polymers. *Adv. Drug Delivery Rev.* **2012**, *64*, 1031–1045.

(89)   Yardley, R. E.; Kenaree, A. R.; Gillies, E. R. Triggering Depolymerization: Progress and Opportunities for Self-Immolative Polymers. *Macromolecules* **2019**, *52*, 6342–6360.

(90)   Zhang, H.; Yeung, K.; Robbins, J. S.; Pavlick, R. A.; Wu, M.; Liu, R.; Sen, A.; Phillips, S. T. Self-Powered Microscale Pumps Based on Analyte-Initiated

Depolymerization Reactions. *Angew. Chem., Int. Ed.* **2012**, *51*, 2400–2404.

(91) Wong, A. D.; Güngör, T. M.; Gillies, E. R. Multiresponsive Azobenzene End-Cap for Self-Immolative Polymers. *ACS Macro Lett.* **2014**, *3*, 1191–1195.

(92) Weinstain, R.; Sagi, A.; Karton, N.; Shabat, D. Self-Immolative Comb-Polymers: Multiple-Release of Side-Reporters by a Single Stimulus Event. *Chem. - Eur. J.* **2008**, *14*, 6857–6861.

(93) Diesendruck, C. E.; Peterson, G. I.; Kulik, H. J.; Kaitz, J. A.; Mar, B. D.; May, P. A.; White, S. R.; Martínez, T. J.; Boydston, A. J.; Moore, J. S. Mechanically Triggered Heterolytic Unzipping of a Low-Ceiling-Temperature Polymer. *Nat. Chem.* **2014**, *6*, 623–628.

(94) Peterson, G. I.; Church, D. C.; Yakelis, N. A.; Boydston, A. J. 1,2-Oxazine Linker As a Thermal Trigger for Self-Immolative Polymers. *Polymer* **2014**, *55*, 5980–5985.

(95) De Gracia Lux, C.; McFearin, C. L.; Joshi-Barr, S.; Sankaranarayanan, J.; Fomina, N.; Almutairi, A. Single UV or near IR Triggering Event Leads to Polymer Degradation into Small Molecules. *ACS Macro Lett.* **2012**, *1*, 922–926.

(96) Wu, Y.; Zhang, L.; Zhang, M.; Liu, Z.; Zhu, W.; Zhang, K. Bottlebrush Polymers with Self-Immolative Side Chains. *Polym. Chem.* **2018**, *9*, 1799–1806.

(97) Gnaim, S.; Shabat, D. Self-Immolative Chemiluminescence Polymers: Innate Assimilation of Chemiexcitation in a Domino-like Depolymerization. *J. Am. Chem. Soc.* **2017**, *139*, 10002–10008.

(98) Xiao, Y.; Li, H.; Zhang, B.; Cheng, Z.; Li, Y.; Tan, X.; Zhang, K. Modulating the Depolymerization of Self-Immolative Brush Polymers with Poly(Benzyl Ether) Backbones. *Macromolecules* **2018**, *51*, 2899–2905.

(99) Poly, D.; Dilauro, A. M.; Robbins, J. S.; Phillips, S. T. Reproducible and Scalable Synthesis of End-Cap-Functionalized Depolymerizable Poly(Phthalaldehydes). *Macromolecules* **2013**, *46*, 2963–2968.

(100) Fan, B.; Trant, J. F.; Wong, A. D.; Gillies, E. R. Polyglyoxylates: A Versatile Class of Triggerable Self-Immolative Polymers from Readily Accessible Monomers. *J. Am. Chem. Soc.* **2014**, *136*, 10116–10123.

(101) Burel, F.; Rossignol, L.; Pontvianne, P.; Hartman, J.; Couesnon, N.; Bunel, C. Synthesis and Characterization of Poly(Ethyl Glyoxylate) - A New Potentially Biodegradable Polymer. *e-Polymers* **2003**, *3*, 1–12.

(102) Brachais, C. H.; Huguet, J.; Bunel, C. Synthesis, Characterization and Stabilization of Poly(Methyl Glyoxylate). *Polymer* **1997**, *38*, 4959–4964.

(103) Belloncle, B.; Burel, F.; Oulyadi, H.; Bunel, C. Study of the in Vitro Degradation of Poly(Ethyl Glyoxylate). *Polym. Degrad. Stab.* **2008**, *93*, 1151–1157.

(104) Fan, B.; Gillies, E. R. Poly(Ethyl Glyoxylate)-Poly(Ethylene Oxide) Nanoparticles: Stimuli-Responsive Drug Release via End-to-End Polyglyoxylate Depolymerization. *Mol. Pharm.* **2017**, *14*, 2548–2559.

(105) Sirianni, Q. E. A.; Rabiee Kenaree, A.; Gillies, E. R. Polyglyoxylamides: Tuning Structure and Properties of Self-Immolative Polymers. *Macromolecules* **2019**, *52*, 262–270.

(106) Ajiro, H.; Takemoto, Y.; Akashi, M.; Chua, P. C.; Kelland, M. A. Study of the Kinetic Hydrate Inhibitor Performance of a Series of Poly(N-Alkyl-N-Vinylacetamide)S. *Energy Fuels* **2010**, *24*, 6400–6410.

Chapter 2

2 Phosphonium Hydrogels for Controlled Release of Ionic Cargo

2.1 Introduction

Many traditional therapeutics suffer from limitations including side effects due to poor targeting, difficulty in controlling dosage and low patient compliance.[1] These challenges emphasize the need for superior controlled drug delivery systems. There are various approaches to delivering therapeutics that can release molecules in a controlled manner, ensuring sustained delivery.[2,3] The use of hydrogels, crosslinked networks containing a high fraction of water, is one of the commonly employed strategies. Hydrogels have been used in many applications such as wound dressings,[4] ocular aids,[5] and drug delivery.[6] Their high water content, and soft, rubbery properties can minimize inflammatory reactions of surrounding cells and tissues, imparting high biocompatibility.[7] In addition, they can be shaped and molded into many different structures that can be designed to match anatomical requirements.[8]

Many early examples of hydrogels involved relatively inert and non-functional polymers. For example, poly(ethylene glycol) (PEG) has been widely used in hydrogels because it has weak immunogenicity and is FDA approved in certain applications.[9] Recently, newer classes of hydrogels including those based on peptides[10] and those capable of responding to changes in conditions such as pH[11] or temperature,[12] to enable triggered drug release have been reported. The release of drugs can be controlled through network degradation,[13] mechanical deformation[14] or swelling/shrinking.[15] Alternatively specific interactions between the hydrogel and the drug can be incorporated, including covalent conjugation,[16] hydrophobic associations[17] or electrostatic interactions.[18]

Quaternary ammonium salts carry a positive charge at nitrogen and have been extensively studied as antimicrobial agents and electrostatic drug delivery vehicles.[19,20] Quaternary phosphonium cations also carry positive charges at phosphorus but exhibit different charge distributions and have been shown to have enhanced performance over their ammonium

counterparts in areas including antimicrobial activity[21] and nucleic acid binding.[22] While a limited number of phosphonium-containing hydrogels have been reported,[23,24] to our knowledge they have not been investigated for drug delivery. In this context, we report phosphonium-containing hydrogels as controlled delivery vehicles. The phosphonium monomers can be cured using UV light to create stable crosslinked hydrogels through a simple process. The hydrogel properties and drug release rates can be tuned by varying the monomer structures.

2.2   Results and Discussion

2.2.1   Monomer, Polymer and Hydrogel Synthesis

First, tris(hydroxypropyl)phosphine, tri-*n*-butylphosphine and triphenylphosphine were reacted with 4-vinylbenzyl chloride to generate the corresponding polymerizable phosphonium salts **T(hp)-P**, **Bu-P**, and **Ph-P**, respectively (Scheme 2-1).
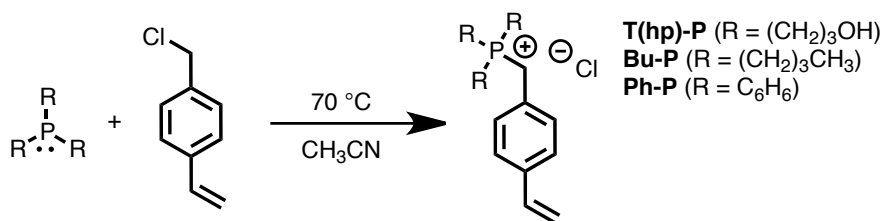
Scheme 2-1 Synthesis of phosphonium monomers.

These phosphonium derivatives were of specific interest because they have varying structures and hydrophobicities, potentially allowing their interactions with molecules in the hydrogels to be tuned. Tri-*n*-butyl(4-vinylbenzyl)ammonium chloride (**Bu-N**) was also investigated to enable comparison between phosphorus and nitrogen analogues (Figure A8). PEG dimethacrylate (PEGDMA) with an M_n of 11,900 g/mol was incorporated to provide crosslinking (Figure A9).

2.2.2 Hydrogel Synthesis and Characterization

The hydrogels were prepared from water-based formulations containing 89 wt% PEGDMA, 10 wt% onium salt (**T(hp)-P**, **Bu-P**, **Ph-P** and **Bu-N**) and 1 wt% photoinitiator 2-hydroxy-4'-(2-hydroxyethoxy)-2-methylpropiophenone (Igracure 2959) (Figure 2-1). Formulations were transferred to round Teflon® molds, purged with N_2 then cured by irradiation with UV light for 30 min.
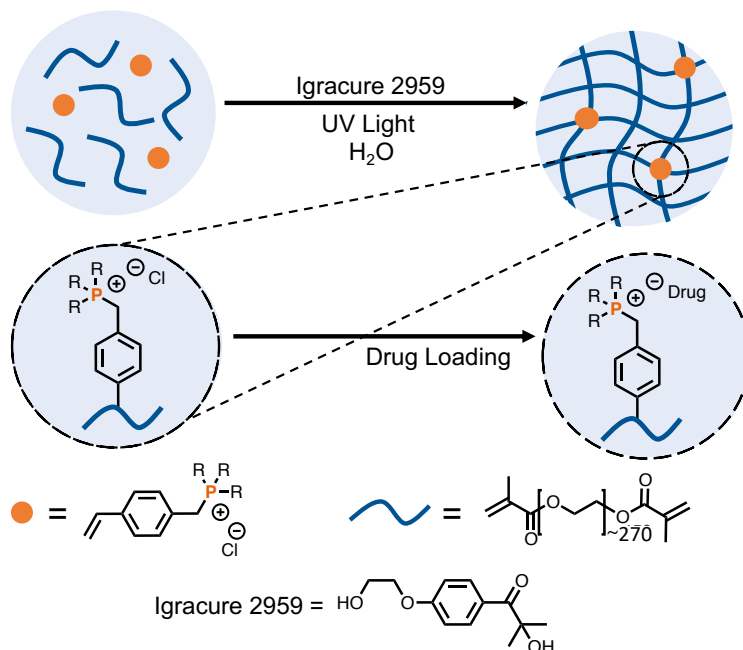
Figure 2-1 Schematic illustration of the synthesis and drug loading of phosphonium hydrogels.

The gel content was similar for the different phosphonium networks, ranging from 71-74%, while the ammonium network had a higher gel content of 92 % (Table 2-1). Dried hydrogels were then placed into either deionized (DI) H_2O or into citric acid/sodium phosphate buffer with pH of 5, 6 or 7.4 and the hydrogels were swelled at 37 °C. Swelling occurred over 2-6 h for each system (Figure 2-2). In each case, the swelling was highest in DI water, ranging from 1170 to 3700% of the dry weight. The swelling capacity was highest in pure H_2O due to the osmotic pressure. Conversely, when the hydrogels were placed into salt solutions, the osmotic pressure was much lower, resulting in less swelling.[25] Swelling varied slightly with pH due to the different buffer compositions (Table A1).[26]

Swelling was highest for the **T(hp)-P** hydrogel, followed by **Bu-P**, and was lowest for **Ph-P** and **Bu-N,** correlating with the decreasing hydrophilicities of the phosphonium salts and suggesting differences between the P and N-based gels perhaps due to their different gel contents.

Table 2-1 Swelling percentages, gel content and loading capacities of hydrogels. [a]% relative to one gram of hydrogel.

Hydrogel	Swelling (%)	Gel Content (%)	Loading Capacity (%)[a]
T(hp)-P	**DI Water**: 3700 ± 1100 **pH 5**: 1560 ± 12 **pH 6**: 1550 ± 33 **pH 7.4**: 1360 ± 75	73 ± 0.2	**Fluorescein**: 0.77 ± 0.03 **Diclofenac**: 3.9 ± 0.06
Bu-P	**DI Water**: 2290 ± 240 **pH 5**: 1510 ± 170 **pH 6**: 1460 ± 98 **pH 7.4**: 1260 ± 130	71 ± 2	**Fluorescein**: 0.60 ± 0.03 **Diclofenac**: 3.8 ± 0.08
Ph-P	**DI Water**: 1750 ± 340 **pH 5**: 870 ± 26 **pH 6**: 880 ± 33 **pH 7.4**: 800 ± 33	74 ± 1	**Fluorescein**: 0.71 ± 0.08 **Diclofenac**: 4.1 ± 0.34
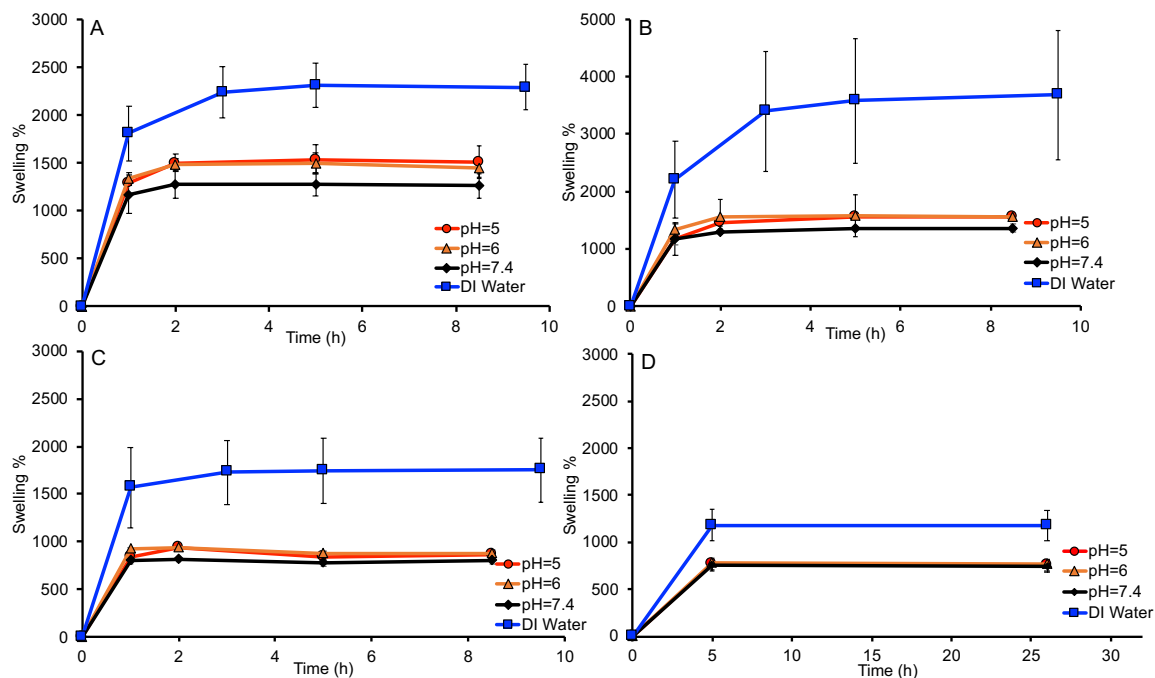
Figure 2-2 Swelling of each of the hydrogels in buffered solutions at pH= 5, 6, 7.4 and **DI** water A) **Bu-P** B) **T(hp)-P** C) **Ph-P** D) **Bu-N.**

Scanning electron microscopy (SEM) confirmed the microporous structures of all of the gels (Figure 2-3). **T(hp)-P** and **Bu-P** gels appeared to have the largest pores, which correlated with their higher degrees of swelling. Based on thermogravimetric analysis, all of the phosphonium-based networks had decomposition temperatures of ~240 °C, whereas the **Bu-N** network decomposed at 180 °C.
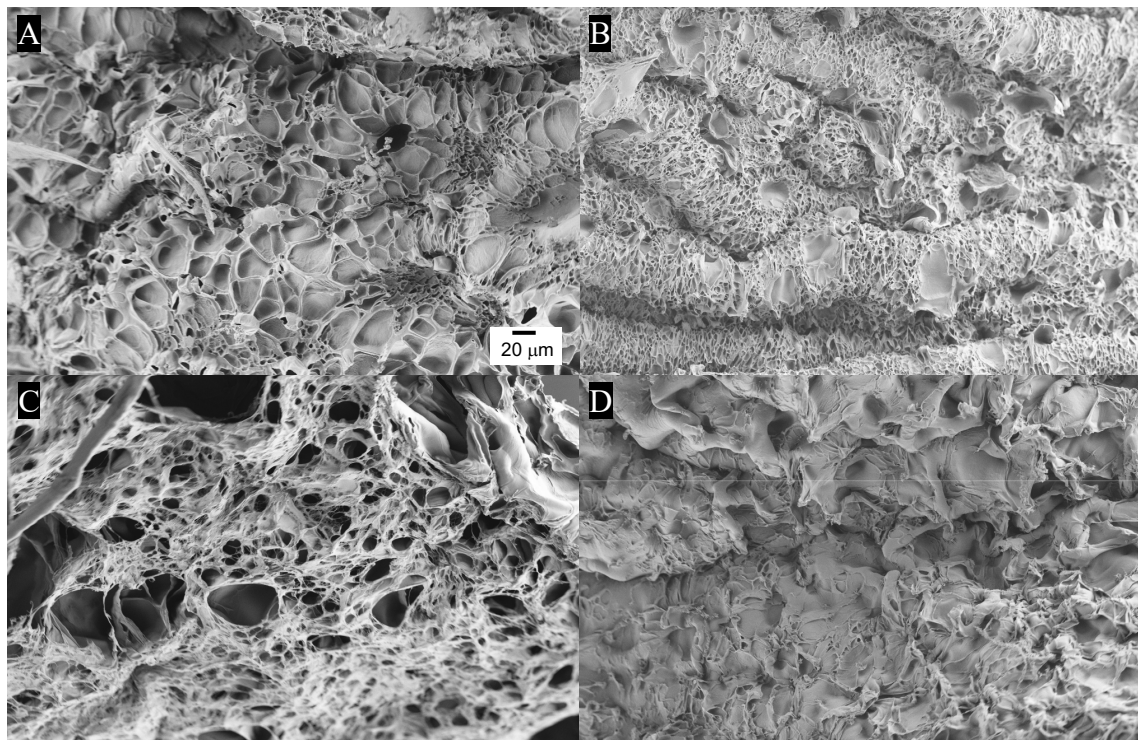
Figure 2-3 SEM images of hydrogels prepared from A) T(hp)-P; B) Ph-P; C) Bu-P D) Bu-N. Samples were prepared by the lyophilisation of gels that were swelled in deionized water, followed by coating with osmium.

2.2.3   Loading and Release Studies

To explore the abilities of the hydrogels to load anionic molecules and release them in a controlled manner, each hydrogel was first loaded with fluorescein sodium salt, an anionic dye. Loading was performed by immersing the hydrogels in a 1 wt% fluorescein sodium salt solution for 24 h. The gels were then washed in DI water to release all non-ionically bound fluorescein until no further dye was detected in the washings (Figure A10-A). A control hydrogel based only on PEGDMA was also evaluated. It was found that the onium-containing gels retained a deep red color after the washing procedure, while the PEGDMA gel did not retain any detectable dye (Figure 2-4). This indicated that anionic molecules could be retained in the onium-based networks. The ionically bound dye could be released from the hydrogels by immersion in a 1 wt% solution of cetyltrimethylammonium chloride (CTAC), allowing the amount of bound dye to be calculated as loading capacity (Table 2-1). The **Bu-N** gel released much more unbound dye during the washing compared with

the phosphonium gels (Figure A10-A). However, it also retained higher loading after washing.
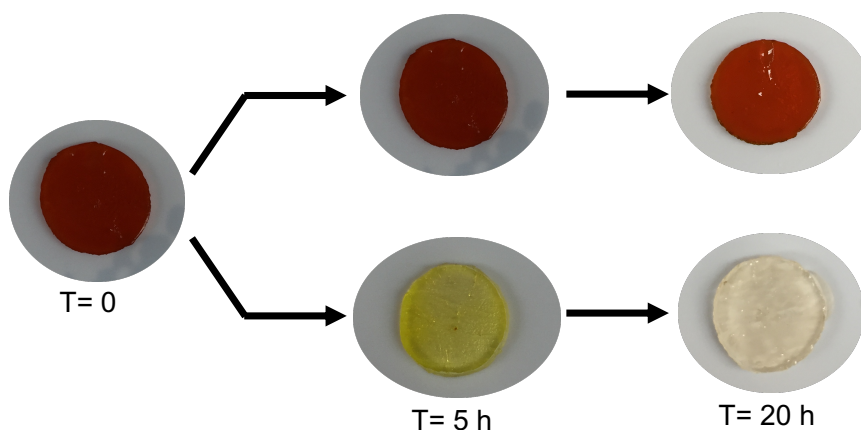
Figure 2-4 Bu-P hydrogel (top) and PEGDMA hydrogel (bottom) after washing with DU water for 5 h and 20 h. Hydrogel **Bu-P** retained its deep red colour after washing, whereas the control PEGDMA gel did not retain any detectable dye.

To measure the release rates under different conditions, each fluorescein-loaded hydrogel was placed into either DI water or buffered solutions at pH 5, 6 or 7.4 at 37 °C. The release rate of fluorescein was fastest from the **T(hp)-P** hydrogels in all buffers, with complete release over 24 h, likely due to their high hydrophilicity and high degree of swelling (Figure 2-5A). In contrast, **Ph-P** hydrogels released the fluorescein much more slowly, over at least 100 h (Figure 2-5B and A11-C). This can be attributed to the lower degree of swelling of this gel, which would slow diffusion of molecules out of the network. Furthermore, the phenyl groups on the phosphonium cation may interact with fluorescein through π stacking and van der Waals forces in addition to ionic interactions. Despite their different degrees of swelling, the **Bu-P** and **Bu-N** hydrogels exhibited similar fluorescein release rates in buffers and they were intermediate between those of the other phosphonium hydrogels (Figure 2-5B,D and A11-B,D).
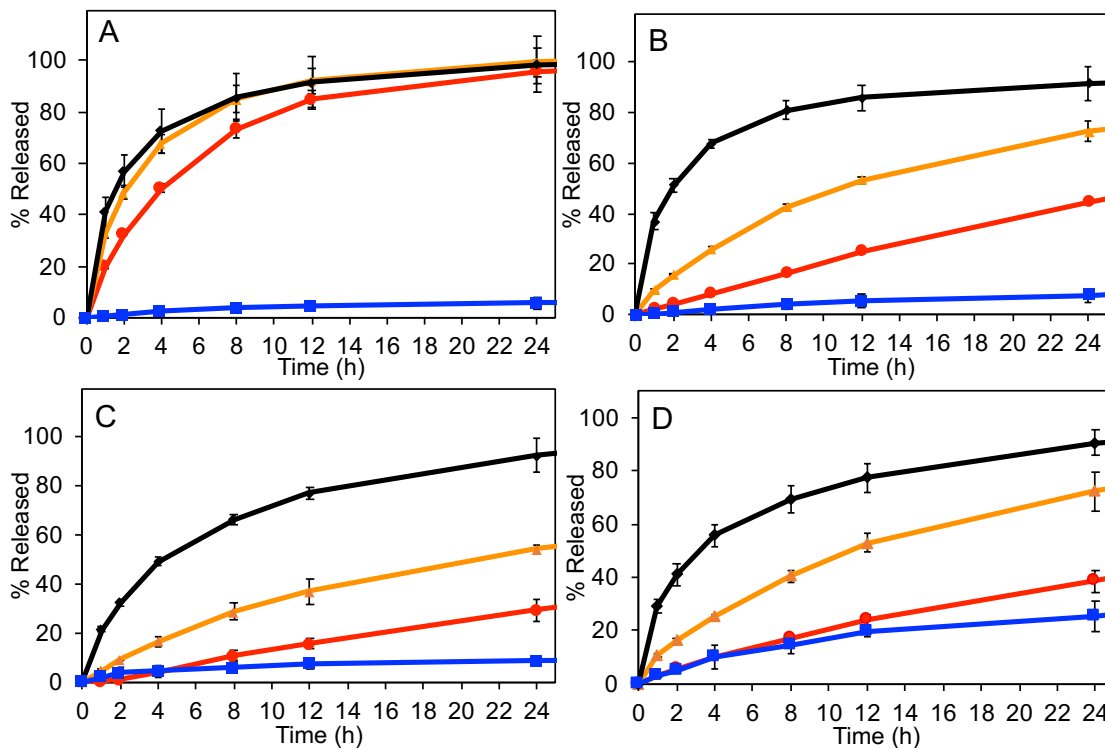
Figure 2-5 Release rates of fluorescein from hydrogels: **A) T(hp)-P;** B) **Bu-P;** C) **Ph-P;** D) **Bu-N** (Blue line – DI Water, Red – pH= 5, Orange – pH= 6, Black – pH= 7.4).

The release rates also depended on the pH, with fastest release at pH 7.4 and slowest release at pH 5 (Figure 2-5 and A11). Although the swelling was slightly lower at pH 7.4 than at the other pH values, which would favour slower release, the behaviour was dominated by the protonation state of fluorescein. Fluorescein has a pK_a value of 6.7,[27] and as the pH of the solution was decreased from pH 7.4 to pH 5, the molecule became less anionic, and consequently more hydrophobic . This favoured its retention in the hydrogel and slowed its release. Finally, although the hydrogels swelled much more in DI water than in the buffer solutions, the release in DI water was much slower for hydrogels **T(hp)-P**, **Bu-P**, **Ph-P**, as there were no anions to exchange with the fluorescein to enable its release. However, the release of fluorescein from the **Bu-N** hydrogel was much faster than from any of the phosphonium gels in DI water (Figure 2-5D, A11-D). Thus, the release rate depended on the ion structure as well as the pH and the presence of salt.

The loading and release of the non-steroidal anti-inflammatory drug diclofenac was then investigated. Notably, the loading capacities of the gels for diclofenac were ~5-fold higher than for fluorescein (Table 2-1), which may result from its higher hydrophobicity or the presence of a single ionizable site compared to fluorescein which can undergo multiple deprotonation events. The release of diclofenac from the hydrogels was then studied under the same conditions described above. As for fluorescein, **T(hp)-P** hydrogels released diclofenac most rapidly, with release complete in 24 h (Figure 2-6A, A12A). **Bu-P**, **Ph-P** and **Bu-N** hydrogels released diclofenac more slowly, with complete release requiring ~120 h (Figure 2-6B-D, A12-B-D). Like for fluorescein, the release of diclofenac from the **Bu-N** gel was much faster than from the other gels in DI water, suggesting that there may have been more non-specific binding of the drug in the **Bu-N** gel (Figure 2-6D, A12D). However, unlike fluorescein, the release rates were not very dependent on the pH for any system. The pK_a value for diclofenac is reported to be 4.1,[28] so it should remain primarily in its anionic state from pH 5-7.4. Lowering of the pH to 4 resulted in visible precipitation of diclofenac in the hydrogel. Thus, the pH-dependent release of drugs from the network depends on their specific chemical structures and pK_a values. Loading of an amino acid, tryptophan, was also attempted in deionized water, but due to its isoelectric point at 5.89, it existed predominately in its neutral form upon loading. When washed with water, all of the tryptophan was rapidly released (Figure A10-C).
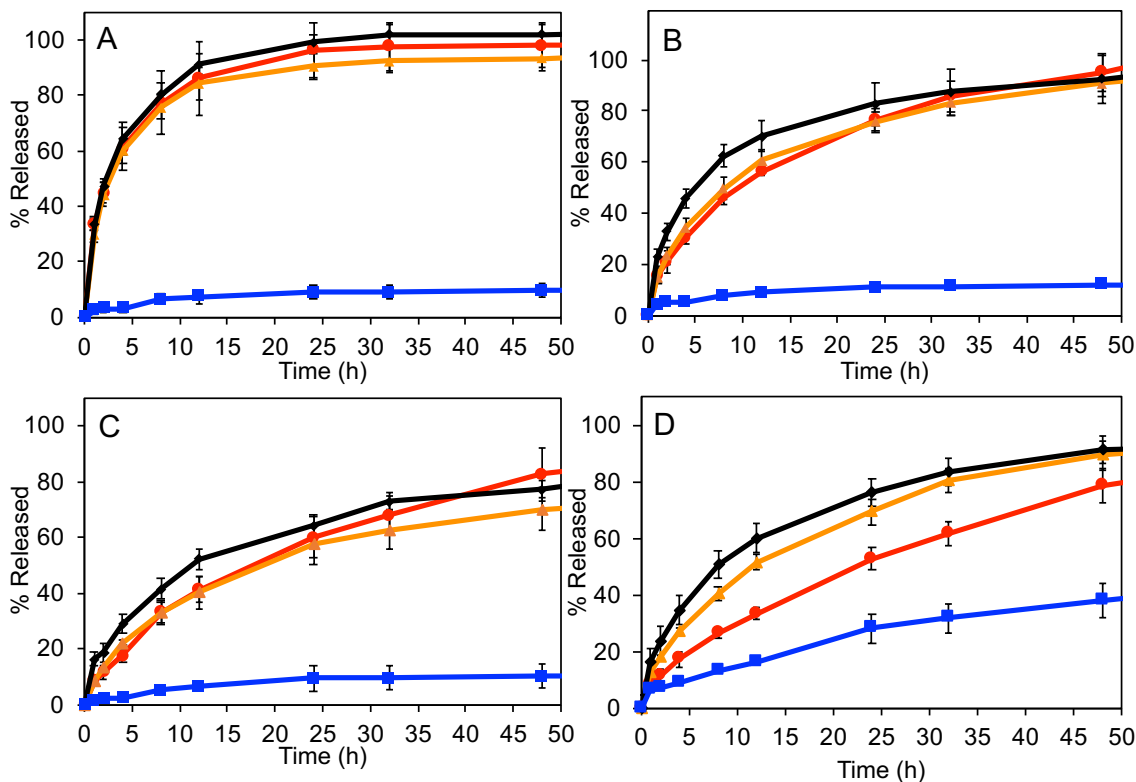
Figure 2-6 Release rates of diclofenac from hydrogels: A) **T(hp)-P;** B) **Bu-P;** C) **Ph-P** D) **Bu-N.** (Blue line – DI Water, Red – pH= 5, Orange – pH= 6, Black – pH= 7.4).

2.2.4   Growth of C2C12 Mouse Myoblast Cells

The growth of C2C12 mouse myoblast cells on the hydrogels was also studied. The hydrogels were seeded with C2C12 cells, incubated for 2 h, then washed to remove unadhered cells. After 72 h, the cells were fixed and stained with 4',6-diamidino-2-phenylindole (DAPI, blue, cell nuclei) and Alexa Fluor 568 (cytoskeletons, red). The glass slide (control) was an excellent substrate for cell attachment and proliferation (Figure 2-7A, C, E). The cells appeared healthy with normal cytoskeletons and were well spread over the entire surface. In contrast, for each of the **T(hp)-P**, **Bu-P**, and **Ph-P** hydrogels, no cells were detected on the surfaces (Figure 2-7B, D, F). To probe this further, the hydrogels were incubated in cell culture medium, then this medium was added to C2C12 cells. High cell viability was retained for each gel, as indicated by 3-(4,5-dimethylthiazol-2-yl)-2,5-diphenyl-tetrazolium bromide (MTT) assays (Figure A13-A-D), suggesting that the gels did not leach toxic species that would prevent the growth of cells. We also investigated the

toxicities of the onium monomers using MTT assays and found that it was dependent on the monomer structure. Greater than 80% viability was observed for **T(hp)-P** up to 1 mg/mL, whereas the other monomers exhibited toxicity at much lower concentrations (Figure A14-A-D). The fact that resistance to cell adhesion occurred for all gels, regardless of monomer structure suggests that adhesion properties were dominated by the high PEG content, as PEG is known to resist protein adsorption and consequently cell adhesion.[29] However, it is also possible that direct contact between cells and monomers covalently incorporated into the gels played a role in some cases.
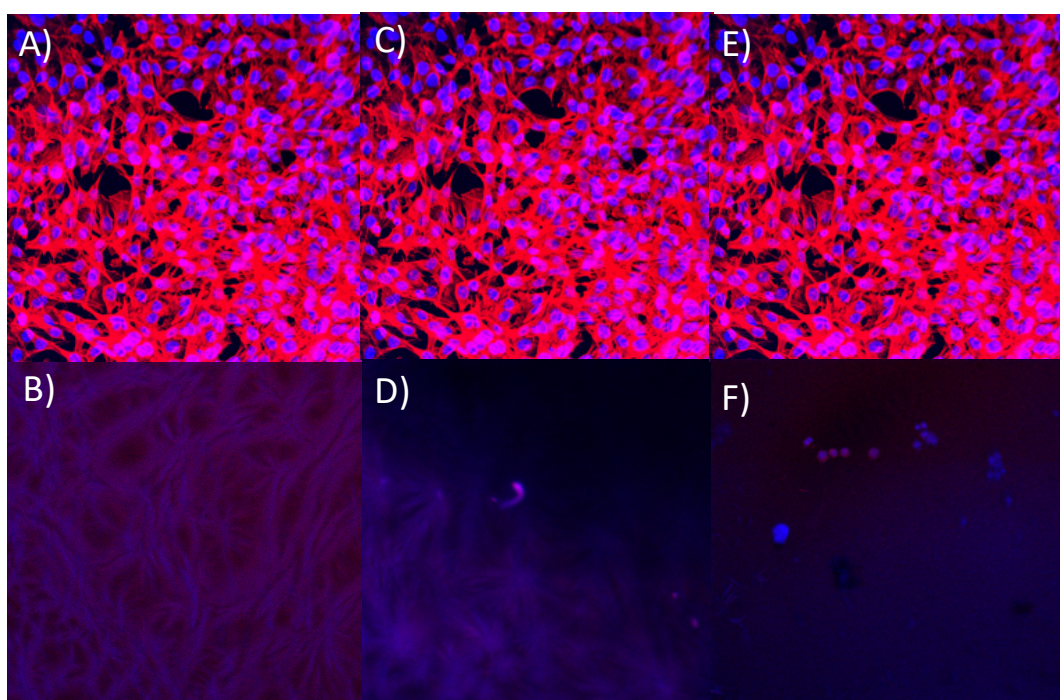
Figure 2-7 Confocal microscopy images of C2C12 cells adhered to A,C,E) glass slide (control); B) **T(hp)-P** hydrogel, D) **Bu-P** hydrogel and F) **Ph-P** hydrogel. The cell nuclei were stained blue with DAPI and cytoskeletons were stained red with Alexa Flour 568. Each image represents an area of 0.45 x 0.45 mm.

2.2.5   Conclusion

In conclusion, we have developed a new method for incorporating phosphonium cations into PEG based hydrogels to enable the ionic entrapment of anionic dyes and drug molecules. The hydrogel formation was completed rapidly and efficiently using UV light. The initial work to load anionic dyes and drug molecules has shown that the release rates can be tuned based on the chemical structures of the phosphoniums and anions, as well as the ionic strength and pH of the release medium. No growth of C2C12 cells was observed on the hydrogel surfaces, suggesting that they may resist fouling in biological systems.

2.3   Experimental

2.3.1   General Materials and Procedures

PEGDMA was synthesized as previously reported (Figure A9).[30] Solvents were purchased from Caledon Laboratory Chemicals (Georgetown, ON, Canada). Deuterated solvents were purchased from Cambridge Isotopes Laboratories (Tewskbury, MA, USA). Phosphines were supplied by Cytec Solvay (Niagara Falls, ON, Canada). Igracure 2959, tributylamine, 4-vinylbenzyl chloride and fluorescein sodium salt was purchased from Sigma-Aldrich and used as received. Triethylamine, methacrylic anhydride and diclofenac sodium salt were purchased from Alfa Aesar and used as received. Neutral alumina was purchased from Fisher Chemical and used as received. Nuclear Magnetic Resonance (NMR) spectroscopy was conducted on a Bruker AvIII HD 400 MHz Spectrometer (^{1}H 400.09 MHz, ^{31}P{^{1}H} 161.82 MHz, ^{13}C{^{1}H} 100.5 MHz). All ^{1}H and ^{13}C{^{1}H} NMR spectra were referenced relative to the residual solvent peak (H$_2$O: ^{1}H δ = 4.79). All ^{31}P{^{1}H} NMR spectra were referenced using an external standard (85% H$_3$PO$_4$: ^{31}P δ = 0). Coupling constants (J) are expressed in Hertz (Hz). Fourier transform infrared (FTIR) spectroscopy was conducted using a Perkin Elmer FT-IR Spectrum Two Spectrometer (Waltham, MA, USA) in the universal attenuated total reflectance mode (UATR), using a diamond crystal as well as the UATR sampling accessory (part number L1050231). Differential scanning calorimetry (DSC) was performed on a DSC Q20 TA Instruments (Waters, New Castle, DE, USA) at a heating rate of 10 °C per minute, under an N$_2$ atmosphere, in an aluminum Tzero™ pan with approximately 5 mg of sample. The melting temperature (T$_m$) and

crystallization temperature (T_c) was determined from the second heating cycle. Thermogravimetric analysis (TGA) was completed on a Q600 SDT TA Instruments and analyzed using TA Universal Analysis, under an N_2 atmosphere at a heating rate of 10 °C per minute up to 800 °C using a ceramic pan with approximately 5 mg of sample. The onset degradation temperatures were determined as the temperature at which 3% mass loss had occurred. UV-visible spectroscopy was conducted on a Tecan Infinite M1000 Pro plate reader. Costar 96 well UV plates (#3635) with UV transparent flat bottoms were used. Mass spectrometry was completed using a PE-Sciex API 365 instrument using electrospray ionization in positive mode. Curing of the hydrogels was performed in a UV-box from UV Process Supply Inc. (Chicago, IL, USA) equipped with a Mercury Bulb with an energy density of UVA (0.031 mJ cm^{-2}) and UVV (164 mJ cm^{-2}). This was determined by a PP2-H-U Power Puck II purchased from EIT Instrument Markets (Sterling, VA, USA). Scanning electron microscopy (SEM) was performed in the University of Western Ontario's Nanofabrication Facility using a LEO 1530 instrument, operating at 2.0 kV and a working distance of 4-6 mm. Samples were prepared by soaking them in deionized water for 24 h, freezing them, then lyophilizing. Samples were mounted to stubs covered in carbon tape and coated in osmium using a SPI Supplies, OC-60A plasma coater.

2.3.2   Monomer Synthesis

Synthesis of Trishydroxypropyl(4-vinylbenzyl)phosphonium chloride (T(hp)-P). Tris(hydroxypropyl)phosphine (13.9 g, 66.8 mmol), 4-vinylbenzyl chloride (10.8 g, 70.8 mmol), and acetonitrile (30 mL) were combined in a pressure tube with a stir bar under N_2 atmosphere and heated at 60 °C for 16 hours. A solid precipitated out of solution and was filtered and washed with acetonitrile, yielding a white powder (19.0 g, 79 %). **^{1}H NMR (400 MHZ, D$_2$O):** δ = 7.42 (d, $^3J_{H-H}$) = 8 Hz, 2H; CH) 7.20 (d, $^3J_{H-H}$) = 8 Hz, 2H; CH), 6.66 (dd, $^3J_{H-H}$) = 17.6 Hz (trans), $^3J_{H-H}$ = 10.8 Hz (cis), 1H; CH), 5.77 (d, $^3J_{H-H}$ 1H; CH) = 16 Hz, 5.25 (d, $^3J_{H-H}$) = 8 Hz, 1H; CH), 3.615 (d, $^2J_{P-H}$) = 12 Hz, 2H; CH$_2$), 3.55 (t, $^3J_{H-H}$ 6H; CH$_2$) = 12 Hz, 2.32 (m, 6H, CH$_2$), 2.32 (m, 6H, CH$_2$), 1.70 (m, 6H, CH$_2$). (Figure A1) **^{31}P{^{1}H} NMR (161.82 MHz, D$_2$O):** δ = 36.41 (s), 34.37 (s), 33.90 (s) (Figure A2). **^{13}C{^{1}H} NMR (100.5 MHz, D$_2$O):** δ =137.55 ((d, $^3J_{P-C}$) = 4 Hz), 135.82 ((d, $^5J_{P-C}$) = 2 Hz), 130.32 ((d, $^2J_{P-C}$)= 5Hz), 127.33 ((d, $^4J_{P-C}$)= 9 Hz), 127.25 ((d, $^6J_{P-C}$)= 3 Hz), 115.43 ((d, $^7J_{P-C}$)= 2 Hz), 60.94

((d, $^3J_{P-C}$)= 17.1 Hz), 25.66((d, $^3J_{P-C}$)= 45.2 Hz), 23.52 ((d, $^2J_{P-C}$)= 4 Hz), 14.87 ((d, $^1J_{P-C}$)= 49.2 Hz) (Figure A3). **ATR-FTIR (cm^{-1} (ranked intensity)):** 614(3), 862 (4), 910 (5), 1057 (1), 1410, 1511 (6), 2906 (7), 2938 (8), 3288 (2). **ESI-MS (m/z):** ESI+: 325.2 ([$C_{18}H_{29}O_3P$]$^+$), 685.4 [$C_{36}H_{58}O_6P_2Cl$]$^+$.

Synthesis of Tri-*n*-butyl(4-vinylbenzyl)phosphonium chloride (Bu-P). Tri-*n*-butylphosphine (10.9 g, 53.9 mmol) and 4-vinylbenzyl chloride (8.6 g, 56.5 mmol) were dissolved in CH$_3$CN (50 mL) under an N$_2$ atmosphere in a pressure tube and stirred at 70 °C for 16 hours. The solvent was then removed *in vacuo*. The resulting oil was dissolved in a minimal amount of CH$_2$Cl$_2$ (15 mL) and then precipitated in cold Et$_2$O (500 mL) and left to sit overnight in the freezer. The precipitate was then filtered and dried *in vacuo* yielding a white powder (14.3 g, 75%). Spectral data agreed with those previously reported.[31] ^{1}H and ^{31}P{^{1}H} NMR spectra are included (Figure A4-5)

Synthesis of Triphenyl(4-vinylbenzyl)phosphonium chloride (Ph-P). Triphenylphosphine (3.2 g, 12.1 mmol), 4-vinylbenzyl chloride (2.0 g, 13.3 mmol), and acetonitrile (30 mL) were combined in a pressure tube with a stir bar under N$_2$ atmosphere and heated at 60 °C for 72 hours. The solvent was then removed *in vacuo*. The resulting solid was dissolved in minimal dichloromethane (10 mL) and precipitated in diethylether (500 mL). The precipitate was filtered, washed with ether, and dried *in vacuo* yielding a white powder (4.4 g 88 %). Spectral data agreed with those previously reported.[31] ^{1}H and ^{31}P{^{1}H} NMR spectra are included (Figure A6-7)

Synthesis of Tri-*n*-butyl(4-vinylbenzyl)phosphonium chloride (Bu-P). Tributylamine (15.0 g, 80.9 mmol) and 4-vinylbenzyl chloride (12.4 g, 80.9 mmol) were dissolved in CH$_3$CN (25 mL) in a round bottom and stirred at 50 °C for 48 hours. The solvent was then removed *in vacuo*. The resulting oil was then washed with ethyl acetate to produce a white solid (22.3 g, 82%). Spectral data agreed with those previously reported.[32] A ^{1}H NMR spectrum is included (Figure A8).

2.3.3   Hydrogel Preparation

Synthesis of Tris(hydroxypropyl)(4-vinylbenzyl)phosphonium chloride (T(hp)-P) hydrogel. PEGDMA (1.22 g, 89 wt%), tris(hydroxypropyl)(4-vinylbenzyl)phosphonium chloride (0.14 g, 10 wt %), and Igracure 2959 (0.014 g, 1 wt %) were sonicated and dissolved in 3.75 mL of water. 300 μL of the formulation was then pipetted into round teflon molds with a diameter of 1 cm. The teflon molds were then placed into a closed curing box with a glass lid and purged with nitrogen to create an inert atmosphere. The box containing the teflon molds was then moved into the UV-curing box and irradiated for 30 minutes. The hydrogels were then taken out and cut into pieces. $T_m = 68$ °C; $T_c = 31$ °C; Onset Decomposition Temperature: 240 °C.

Synthesis of tri-*n*-butyl(4-vinylbenzyl)phosphonium chloride (Bu-P) hydrogel. PEGDMA (1.50 g, 89 wt%) and tri-*n*-butyl(4-vinylbenzyl)phosphonium chloride (0.17 g, 10 wt %) and Igracure 2959 (0.017 g, 1 wt %) were sonicated and dissolved in 4.6 mL of water. The hydrogels were then prepared as described above for **T(hp)-P**. $T_m = 60$ °C; $T_c = 40$ °C; Onset Decomposition Temperature: 242 °C.

Synthesis of triphenyl(4-vinylbenzyl)phosphonium chloride (Ph-P) hydrogel. PEGDMA (1.57 g, 89 wt%) and triphenyl(4-vinylbenzyl)phosphonium chloride (0.18 g, 10 wt %) and Igracure 2959 (0.018 g, 1 wt %) were sonicated an dissolved in 4.8 mL of water. The hydrogels were then prepared as described above for **T(hp)-P**. $T_m = 61$ °C. $T_c = 39$ °C. Onset Decomposition Temperature: 237 °C.

Synthesis of tri-*n*-butyl(4-vinylbenzyl)ammonium chloride (Bu-N) hydrogel. PEGDMA (0.82 g, 89 wt%) and tributyl(4-vinylbenzyl)ammonium chloride (0.092 g, 10 wt %) and Igracure 2959 (0.0090 g, 1 wt %) were sonicated an dissolved in 2.5 mL of water. The hydrogels were then prepared as described above for **T(hp)-P**. $T_m = 59$ °C. $T_c = 45$ °C. Onset Decomposition Temperature: 180°C.

2.3.4   Gel Content Measurements

Gels were prepared as described above, then cut into pieces with dry weight of 20-30 mg. Each piece was dried immediately under vacuum to remove any water from the initial formulation. The mass of each hydrogel was then recorded and each of the hydrogels was swelled in deionized water (25 mL) for 4 days, replacing the water every 24 h. This was done to remove any unreacted starting material from the hydrogels. The hydrogels were then taken out of solution and dried under vacuum. The hydrogels were weighed again. The percent mass remaining relative to the initial mass was determined to be the gel content. Each hydrogel was measured in triplicate and the results reported as the mean ± standard deviation.

2.3.5   Buffer Preparation

A 0.1 M citric acid/ 0.2 M disodium phosphate buffer was chosen as it covers a wide range from pH 2.2 to pH 8.0.[33] Citric Acid (0.1 M) and 0.2 M disodium phosphate were combined in such volumes to make 20 mL of pH 5, 6 and 7.4 solutions (Table A1).

2.3.6   Hydrogel Swelling Measurements

The swelling of each of the hydrogels was characterized. The swelling of each was measured by comparing the swelled weight (m_s) to the dried weight (m_i; Equation 1).

$$\text{Swelling \%} = \left(\frac{m_s - m_i}{m_i} \right) x \ 100\%$$

Equation 2-1

Each hydrogel was initially dried to remove any residual water and weighed. Each respective hydrogel was then placed in either the buffered solutions (pH 5, 6, 7.4) or DI water. Hydrogels were taken out at specific time intervals, placed in-between two paper towels to remove any residual water on the surface and weighed.

2.3.7   Loading and Release Studies

Hydrogels were initially placed in either 1 wt% (in DI water) fluorescein sodium salt, diclofenac sodium salt or tryptophan for 24 hours to allow time for anion exchange to occur. Hydrogels were then placed into deionized water to release any unbound molecules. When no further release occurred (as monitored by UV-visible spectroscopy, Figure A10), the washing of unbound molecules was deemed complete. Hydrogels were placed into solutions containing 25 mL of water, 0.1 citric acid/ 0.2 M sodium phosphate buffer (pH= 5, 6, 7.4), 0.1 M NaCl or a 1 wt% solution of cetytrimethylammonium chloride (CTAC) at 37 °C. Aliquots of 150 μL were then taken at specific time points and pipetted into the 96 well plates. The solutions were changed at each time point. To determine the total number of molecules in the hydrogel, CTAC was used to anion exchange with fluorescein sodium salt and 0.1 M NaCl was used to anion exchange with diclofenac and tryptophan. Calibration curves were prepared for each drug in each release medium (Figure A15-17).

2.3.8   Drug Loading Capacity Measurements

Drug loading capacity (%) was calculated by the equation:

$$\text{Drug Loading Capacity (\%)} \qquad\qquad \text{Equation 2-2}$$

$$= \frac{\text{mass of encapuslated drug}}{\text{dry mass of hydrogel used for encapuslation}} \text{ x } 100\%$$

This procedure was based on a previously reported method.[34] Each hydrogel was measured in triplicate and the results reported as the mean ± standard deviation.

2.3.9   Evaluation of Cell Growth on Films

C2C12 mouse myoblast cells were cultured in growth medium composed of Dulbecco's Modified Eagle Medium (DMEM) containing 10% fetal bovine serum (FBS) and supplemented with 1% Glutamax (100×) solution and antibiotics (Penicillin and Streptomycin, 100 units/mL each). Glass coverslips were placed into each well of a 12-well culture plate. The glass coverslips and hydrogels, which had a thickness of 170 μm

and surface area of 2.25 cm^2, were then sterilized with 70% ethanol for 30 minutes. The ethanol was aspirated and the hydrogels were exposed to UV light for a 2-3 hours. The hydrogels were conditioned overnight in Hank's Balanced Salt Solution (HBSS, 0.5 mL). The HBSS was then aspirated and the cells (2000 per well) were added directly onto the surfaces or control coverslip, and placed in the incubator for 2 hours. 0.5 mL of media were added to each well and the systems were incubated for 72 hours.

To mount and fix the cells after the 72-hour incubation, the media was removed, and each well was washed with phosphate buffered saline (PBS) (3 x 0.5 mL). Neutralized paraformaldehyde was prepared and 0.5 mL was added to each well and let stand for 10 minutes. The wells were then washed with PBS (3 x 0.5 mL) and 0.5 mL of cold acetone at -20 °C was then added to each well and let stand for 3-5 minutes. The wells were then washed with PBS (3 x 0.5 mL).

To stain the F-actin (cytoskeleton), phalloidin-Alex fluor 568 (Molecular Probes) was prepared at 20x dilution with PBS. 200 μL was added into each well and let sit for approximately 20 minutes. To stain the nucleus, 500x dilution DAPI (Molecular Probes) was added (150 μL) to each well and let stand for approximately 5 minutes. Each well was then washed with PBS (3 x 0.5 mL) and immersed in PBS for 1 hour. The hydrogels were removed with tweezers and placed face up on the slide. A drop of Prolong was the added directly on the hydrogel and coverslip and the coverslip was placed on top of the hydrogel. The hydrogels and coverslips were let to sit in darkness for 24 hours and the sides were sealed with nail polish.

2.3.10   Cell Toxicity Assays

C2C12 mouse myoblast cells were cultured as above and then seeded in a Nunclon 96-well U bottom transparent polystyrol plate to obtain approximately 10 000 cells/well in 100 μL of DMEM containing serum, glutamax, and antibiotics as described above. The cells were allowed to adhere to the plate in a 5% CO_2 incubator at 37 °C for 24 h. Meanwhile, for the leaching assays, samples of dry hydrogel (10 mg) were immersed in cell culture medium and incubated overnight to enable the leaching of potentially toxic species from the hydrogels over a period of 24 h.

The growth medium was then aspirated from the cells and replaced with either solutions of sodium dodecyl sulfate (SDS) in the cell culture medium at concentrations of 0.2, 0.15, 0.10, or 0.05 mg/mL, which were used as positive controls, serial 2-fold dilutions of the leachate in culture medium, serial 2-fold dilutions of the monomer in culture medium, or fresh medium as a negative control. The cells were then incubated at 37 °C (5% CO_2) for 24 h. The medium was again aspirated and replaced with 110 μL of fresh medium containing 0.5 mg/mL (3-(4,5-dimethylthiazol-2-yl)-2,5- diphenyltetrazolium bromide) (MTT). After 4 h of incubation (37 °C, 5% CO_2), the MTT solution was carefully aspirated and the purple crystals were dissolved by addition of 50 μL of spectroscopic grade dimethyl sulfoxide (DMSO). After shaking (1 s, 2 mm amp, 654 rpm), the absorbance of the wells at 540 nm was read using an M1000-Pro plate reader (Tecan). The absorbance of wells prepared in the same way but without cells was subtracted as a background and the cell viability was calculated relative to wells containing cells that were exposed only to the culture medium. No (0%) cell viability was detected for cells exposed to the highest concentrations of SDS, confirming the sensitivity of the assay.

2.4   References

(1)   Langer, R. Drug Delivery and Targeting. *Nature* **1998**, *392*, 5–10.

(2)   Tong, R.; Hemmati, H. D.; Langer, R.; Kohane, D. S. Photoswitchable Nanoparticles for Triggered Tissue Penetration and Drug Delivery. *J. Am. Chem. Soc.* **2012**, *134*, 8848–8855.

(3)   Lawrence, P. G.; Patil, P. S.; Leipzig, N. D.; Lapitsky, Y. Ionically Cross-Linked Polymer Networks for the Multiple-Month Release of Small Molecules. *Appl. Mater. Interfaces* **2016**, *8*, 4323–4335.

(4)   Mostafalu, P.; Kiaee, G.; Giatsidis, G.; Khalilpour, A.; Nabavinia, M.; Dokmeci, M. R.; Sonkusale, S.; Orgill, D. P.; Tamayol, A.; Khademhosseini, A. A Textile Dressing for Temporal and Dosage Controlled Drug Delivery. *Adv. Funct. Mater.* **2017**, *1702399*, 1–10.

(5)   Zhang, Z.; He, Z.; Liang, R.; Ma, Y.; Huang, W.; Jiang, R.; Shi, S.; Chen, H.; Li, X. Fabrication of a Micellar Supramolecular Hydrogel for Ocular Drug Delivery. *Biomacromolecules* **2016**, *13*, 798–807.

(6)   Buwalda, S. J.; Vermonden, T.; Hennink, W. E. Hydrogels for Therapeutic Delivery: Current Developments and Future Directions. *Biomacromolecules* **2017**, *18*, 316–330.

(7)   Kroschwitz, J. I.; Mark, H. F. *Encyclopedia of Polymer Science and Technology*; Wiley-Interscience: Hoboken, New Jersey, 2003.

(8)   Li, J.; Mooney, D. J. Designing Hydrogels for Controlled Drug Delivery. *Nat. Rev. Mater.* **2016**, *1*, 1–18.

(9)   Lin, C. C.; Anseth, K. S. PEG Hydrogels for the Controlled Release of Biomolecules in Regenerative Medicine. *Pharm. Res.* **2009**, *26*, 631–643.

(10)   Yu, Z.; Xu, Q.; Dong, C.; Lee, S.; Gao, L.; Li, Y.; D'Ortenzio, M.; Wu, J. Self-Assembling Peptide Nanofibrous Hydrogel as a Versatile Drug Delivery Platform. *Curr. Pharm. Des.* **2015**, *21*, 4342–4354.

(11)   Zhang, S.; Bellinger, A. M.; Glettig, D. L.; Barman, R.; Lee, Y. A. L.; Zhu, J.; Cleveland, C.; Montgomery, V. A.; Gu, L.; Traverso, G. A pH-Responsive Supramolecular Polymer Gel as an Enteric Elastomer for Use in Gastric Devices. *Nat. Mater.* **2015**, *14*, 1065–1071.

(12)   Dai, H.; Chen, Q.; Qin, H.; Guan, Y.; Shen, D.; Hua, Y.; Tang, Y.; Xu, J. A Temperature-Responsive Copolymer Hydrogel in Controlled Drug Delivery. *Macromolecules* **2006**, *39*, 6584–6589.

(13)   O'Shea, T. M.; Aimetti, A. A.; Kim, E.; Yesilyurt, V.; Langer, R. Synthesis and Characterization of a Library of In-Situ Curing, Nonswelling Ethoxylated Polyol Thiol-Ene Hydrogels for Tailorable Macromolecule Delivery. *Adv. Mater.* **2014**, *27*, 65–72.

(14) Huebsch, N.; Kearney, C. J.; Zhao, X.; Kim, J.; Cezar, C. A.; Suo, Z.; Mooney, D. J. Ultrasound-Triggered Disruption and Self-Healing of Reversibly Cross-Linked Hydrogels for Drug Delivery and Enhanced Chemotherapy. *Proc. Natl. Acad. Sci.* **2014**, *111*, 9762–9767.

(15) Mumper, R. J.; Huffman, A. S.; Puolakkainen, P. A.; Bouchard, L. S.; Gombotz, W. R. Calcium-Alginate Beads for the Oral Delivery of Transforming Growth Factor-B1 (TGF-B1): Stabilization of TGF-B1 by the Addition of Polyacrylic Acid within Acid-Treated Beads. *J. Controlled Release* **1994**, *30*, 241–251.

(16) Traub, S.; Morgner, J.; Martino, M. M.; Höning, S.; Swartz, M. A.; Wickström, S. A.; Hubbell, J. A.; Eming, S. A. The Promotion of Endothelial Cell Attachment and Spreading Using FNIII10 Fused to VEGF-A165. *Biomaterials* **2013**, *34*, 5958–5968.

(17) Thatiparti, T. R.; Shoffstall, A. J.; von Recum, H. A. Cyclodextrin-Based Device Coatings for Affinity-Based Release of Antibiotics. *Biomaterials* **2010**, *31*, 2335–2347.

(18) Shah, N. J.; Hyder, M. N.; Quadir, M. A.; Dorval Courchesne, N.-M.; Seeherman, H. J.; Nevins, M.; Spector, M.; Hammond, P. T. Adaptive Growth Factor Delivery from a Polyelectrolyte Coating Promotes Synergistic Bone Tissue Repair and Reconstruction. *Proc. Natl. Acad. Sci.* **2014**, *111*, 12847–12852.

(19) Liu, S. Q.; Yang, C.; Huang, Y.; Ding, X.; Li, Y.; Fan, W. M.; Hedrick, J. L.; Yang, Y. Y. Antimicrobial and Antifouling Hydrogels Formed in Situ from Polycarbonate and Poly(Ethylene Glycol) via Michael Addition. *Adv. Mater.* **2012**, *24*, 6484–6489.

(20) Peng, N.; Wang, Y.; Ye, Q.; Liang, L.; An, Y.; Li, Q.; Chang, C. Biocompatible Cellulose-Based Superabsorbent Hydrogels with Antimicrobial Activity. *Carbohydr. Polym.* **2016**, *137*, 59–64.

(21) Kanazawa, A.; Ikeda, T.; Endo, T. Novel Polycationic Biocides: Synthesis and Antibacterial Activity of Polymeric Phosphonium Salts. *J. Polym. Sci., Part A:*

Polym. Chem. **1993**, *31*, 335–343.

(22) Hemp, S. T.; Allen, M. H.; Green, M. D.; Long, T. E. Phosphonium-Containing Polyelectrolytes for Nonviral Gene Delivery. *Biomacromolecules* **2012**, *13*, 231–238.

(23) Watanabe, T.; Utsunomiya, M.; Kurihara, S.; Nonaka, T. Synthesis of Thermosensitive Hydrogels from Acryloyloxyethyl Trialkyl Phosphonium Chloride-N-Isopropylacrylamide-N,N′-Methylenebisacrylamide Terpolymers and Their Temperature Dependence of Water Absorption. *J. Polym. Sci., Part A: Polym. Chem.* **2001**, *39*, 1505–1514.

(24) Chung, C.; Lampe, K. J.; Heilshorn, S. C. Tetrakis(Hydroxymethyl) Phosphonium Chloride as a Covalent Cross-Linking Agent for Cell Encapsulation within Protein-Based Hydrogels. *Biomacromolecules* **2012**, *13*, 3912–3916.

(25) Gupta, N. V.; Shivakumar, H. G. Investigation of Swelling Behavior and Mechanical Properties of a PH-Sensitive Superporous Hydrogel Composite. *Iran. J. Pharm. Res.* **2012**, *11*, 481–493.

(26) Kohno, Y.; Gin, D.; Noble, R. D.; Ohno, H. A Thermoresponsive Poly(Ionic Liquid) Membrane Enables Concentration of Proteins from Aqueous Media. *Chem. Commun.* **2016**, *52*, 7497–7500.

(27) Doughty, M. J. PH Dependent Spectral Properties of Sodium Fluorescein Ophthalmic Solutions Revisited. *Ophthalmic Physiol. Opt.* **2010**, *30*, 167–174.

(28) Adeyeye, C. M.; Li, P.-K. Diclofenac Sodium. *Anal. Profiles Drug Subst.* **1990**, *19*, 123–144.

(29) Harris, J. M.; Zalipsky, S. *Poly(Ethylene Glycol) Chemistry and Biological Applications*; American Chemical Society: Washington, 1997.

(30) Lin-Gibson, S.; Bencherif, S.; Cooper, J. A.; Wetzel, S. J.; Antonucci, J. M.; Vogel, B. M.; Horkay, F.; Washburn, N. R. Synthesis and Characterization of PEG

Dimethacrylates and Their Hydrogels. *Biomacromolecules* **2004**, *5*, 1280–1287.

(31) Kanazawa, Akihiko; Ikeda, T. E. T. Novel Polycationic Biocides: Synthesis and Antibacterial Activity of Polymeric Phosphonium Salts. *J. Polym. Sci., Part A: Polym. Chem.* **1993**, *31*, 335–343.

(32) Itsuno, S.; Hashimoto, Y.; Haraguchi, N. Synthesis of Chiral Iridium Complexes Immobilized on Amphiphilic Polymers and Their Application to Asymmetric Catalysis. *J. Polym. Sci., Part A: Polym. Chem.* **2014**, *52*, 3037–3044.

(33) Mcilvaine, T. C. A Buffer Solution for Colorimetric Comparison. *J. Biol. Chem.* **1921**, 49, 183–186.

(34) Papadimitriou, S.; Bikiaris, D. Novel Self-Assembled Core-Shell Nanoparticles Based on Crystalline Amorphous Moieties of Aliphatic Copolyesters for Efficient Controlled Drug Release. *J. Controlled Release* **2009**, *138*, 177–184.

Chapter 3

3 Phosphonium Polyelectrolyte Complexes for the Encapsulation and Slow Release of Ionic Cargo

3.1 Introduction

Hydrogels have been extensively explored in biomedical applications such as drug delivery[1–3] and tissue engineering[4,5] over the past few decades. Their high water content and soft, elastomeric properties resemble those of many soft biological tissues, allowing hydrogels to be used *in vitro* for the culture of cells, as well as *in vivo*, with minimal host response. In the field of drug delivery, hydrogels have been surgically implanted,[6,7] injected,[8] or applied to the skin or wounds on the surface of the body.[9,10] They can provide a local release of drugs, which can be beneficial in terms of reducing side effects and reducing the frequency of dosing compared to conventional systemic drug administration. Crosslinking in hydrogels can be achieved through different approaches involving covalent bonding,[11–13] non-covalent interactions,[14–16] or a combination of both.[17–19]

One approach to non-covalent network formation in hydrogels is polyelectrolyte complexation. Polyelectrolytes are polymers composed of charged repeating units. Commonly used examples include the salts of poly(allylamine),[20,21] poly(acrylic acid),[22,23] poly(styrenesulfonate),[24,25] as well as biopolymers such as hyaluronic acid[26] and chitosan.[27] The polymers can have a fixed charge on each repeat unit or can become charged when protonated or deprotonated by acid or base. The combination of two oppositely charged polyelectrolytes leads to polyelectrolyte complexes (PECs) held together by Pol^-Pol^+ interactions between oppositely charged units on the polymers and by physical entanglements. The driving force for these interactions is the entropically favorable release of counterions[28,29] and water molecules[30] (Equation 3-1).

$$Pol^+Cl^- \bullet x H_2O + Pol^-Na^+ \bullet y H_2O \rightarrow Pol^+Pol^- \bullet i H_2O + Na^+ + Cl^- + z H_2O \qquad \text{Equation 3-1}$$
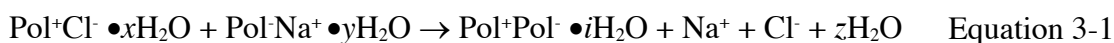
While weak, fluid-like complexes or dense precipitates of particles often form initially through the combination of oppositely charged polyelectrolytes, it has been found in recent years that ultracentrifugation or extrusion can lead to compacted PEC networks that exhibit useful properties such as high tensile strength, elongation, and elasticity, largely dependent on hydration by water.[31] The resulting materials can exhibit self-healing behavior in the presence of salt solutions[31] and have moduli in the range of 1 kPa – 10 MPa, similar to many biological tissues.[32] They have been explored as mimics of the nucleus pulposus of intervertebral disk, which contains negative polyelectrolyte.[33] They have also been functionalized with enzymes to obtain catalytically active PECs.[34] Because of the presence of numerous charged groups throughout their networks, compacted PECs can also potentially be used to electrostatically bind ionic drugs and release them in a controlled manner.

Polyphosphoniums have previously been used to prepare PEC thin films[35] and we recently reported the preparation of PEC networks composed of poly(acrylic acid) and poly[triethyl(4-vinylbenzyl)phosphonium chloride] (**P-Et-P**).[36] The networks exhibited swelling dependent on salt concentration and dynamic, self-healing behavior at physiologically relevant salt concentrations. These properties combined with the high capacity of the networks for ionic binding make them of interest for drug delivery applications. While it was desirable to retain the polyphosphonium component due to the possibility to easily modulate its structure and consequently network properties, drug binding, and release, we sought to replace the polyanion component with a biopolymer that would exhibit higher compatibility with biological tissues, as well as biodegradability, allowing eventual breakdown of the networks. Hyaluronic acid (HA) is a linear, anionic polysaccharide that is a natural component of the extracellular matrix. It has been used clinically in medical products for over three decades.[37] High molar mass HA has been shown to exhibit anti-angiogenic and anti-inflammatory properties.[38] PEC hydrogels composed of HA and various polycations such as chitosan have been explored for tissue engineering[39–41] and drug delivery applications.[42–44] However, the release of drugs from these hydrogels, as well as other PEC hydrogels was typically rapid, occurring over a period of a few hours to days.[42–44] To the best of our knowledge, ionic complexes of HA with phosphonium polymers have not yet been explored.

We report here the preparation of HA PEC complexes with phosphonium polymers. The phosphonium polymer structure was varied to include ethyl, *n*-butyl, phenyl, and 3-hydroxypropyl substituents on phosphorus and the thermal properties, swelling, rheology, and self-healing properties of the different networks were studied. The effects of salt on the networks were evaluated. Different anionic drugs and model drugs including fluorescein, diclofenac and adenosine-5'-triphosphate were loaded into the networks, leading to high drug content ranging from 5 – 16 wt%. Drug release rates depended on the structure of the drug and the PEC network, but it was possible to achieve sustained release over months, which is much longer than previously reported PECs that have been studied for drug delivery. We also evaluated the cytotoxicities of the networks and the polymers used to prepare them.

3.2   Results and Discussion

3.2.1   Monomer and Polymer Synthesis

Monomers were prepared as previously reported, by reacting tris(hydroxypropyl)phosphine, triphenylphosphine, tri(*n*-butyl)phosphine and triethylphosphine with 4-vinylbenzyl chloride to generate the corresponding polymerizable salts (**Hp-P**, **Ph-P**, **Bu-P** and **Et-P**, Scheme 3-1).[45,46] For the polymerization, conventional free radical polymerization was selected over controlled radical polymerization methods as it could more easily provide high molar mass polymers on large scale.[36] The presence of long polymer chains is beneficial for chain entanglement in the PEC networks. Shorter chains will also be present due to high dispersities in chain length and they can facilitate chain mobility, which can be important for properties such as self-healing.[47] Polymerization of the monomers to the corresponding polymers poly[tris(hydroxypropyl)(4-vinylbenzyl)phosphonium chloride] (**P-Hp-P**), poly[triphenyl(4-vinylbenzyl)phosphonium chloride] (**P-Ph-P**), poly[tri(*n*-butyl)(4-vinylbenzyl)phosphonium chloride] (**P-Bu-P**) and poly[triethyl(4-vinylbenzyl)phosphonium chloride] (**P-Et-P**) was performed in water at 60 °C using the thermal radical initiator 2,2'-azobis[2-(2-imidazolin-2-yl)propane]dihydrochloride (VA-044) for 16 h. Complete conversion of all monomers was observed by ^{1}H and ^{31}P{^{1}H} Nuclear Magnetic Resonance (NMR) spectroscopy (Figures B1-8).

The molar masses of **P-Ph-P** (M_w (weight average molar mass) = 138 kg/mol, Đ (dispersity) = 2.2) and **P-Bu-P** (M_w = 450 kg/mol, Đ = 2.6) were characterized by size exclusion chromatography (SEC) in dimethylformamide (DMF) containing 0.4 M tetrabutylammonium triflate and equipped with inert columns designed for ionic polymers (Figure B9). However, **P-Hp-P** and **P-Et-P** did not elute from this system or from an aqueous system, so they were analyzed by light scattering (LS) using Debye plots (Figure B10), providing M_w values of 666 and 588 kg/mol respectively. Thermal gravimetric analysis (TGA) was utilized to determine onset degradation temperatures (T_o) for the phosphonium polymers which ranged from 290 – 344 °C (Figure B11), while that of HA was 220 °C (Figure B12). Differential scanning calorimetry (DSC) was also performed on all polymers, and the glass transition temperatures (T_g) values were 115, 270, 180, 230 and 170 °C for **P-Hp-P**, **P-Ph-P**, **P-Bu-P**, **P-Et-P** and **HA** respectively (Figures B13-14). **P-Ph-P** has the highest T_g of 270 °C, likely due to the π-π stacking of the polymers. **P-Et-P** also had a high T_g which could be attributed to the better packing of the polymer chains and decreased segmental motion, compared to **P-Hp-P** and **P-Bu-P**, which have more bulky pendant groups.
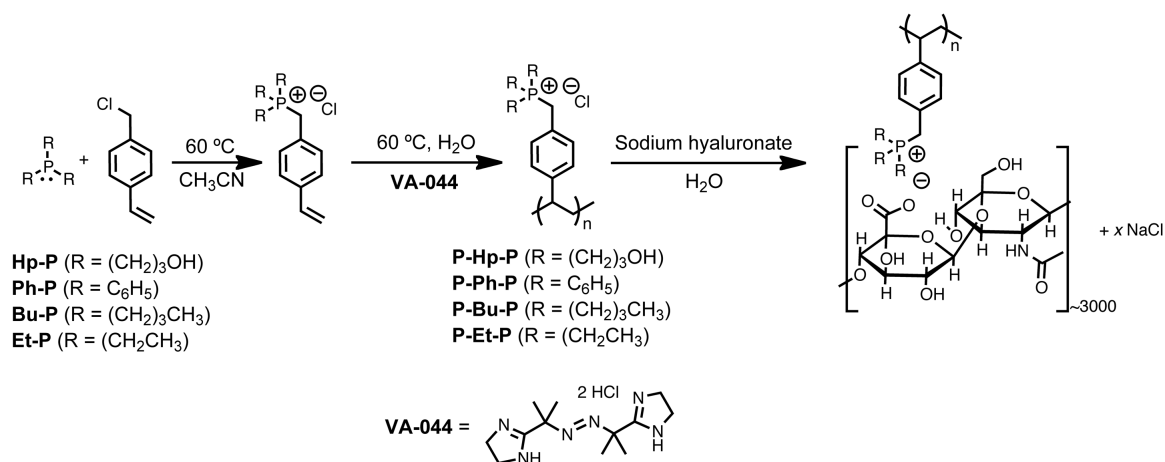
Scheme 3-1 Synthesis of monomers, polymers and PECs.

3.2.2   Network Preparation and Characterization

To prepare the PEC networks, the phosphonium polymer and HA were dissolved separately in deionized (DI) water, combined at 1:1 ratio of phosphonium to carboxylate, and then

mixed for 30 min to allow for network formation. HA with molar masses of 30 - 50 kg/mol and 1000 – 2000 kg/mol were initially investigated. The networks prepared from the lower molar mass HA exhibited predominantly fluid-like behavior and could not be processed for further study (Figure 3-1). This was attributed to a low degree of molecular entanglement between the polymer chains. Networks prepared using 1000 - 2000 kg/mol HA had gel-like behavior and higher structural integrity, so they were used for all subsequent studies. The networks were then ultracentrifuged, which has been reported to transform PECs from loosely packed networks into more compact, tough, transparent solids.[52] The resulting networks **P-Hp-P-HA**, **P-Ph-P-HA**, **P-Bu-P-HA** and **P-Et-P-HA** were then cut into pieces for characterization.
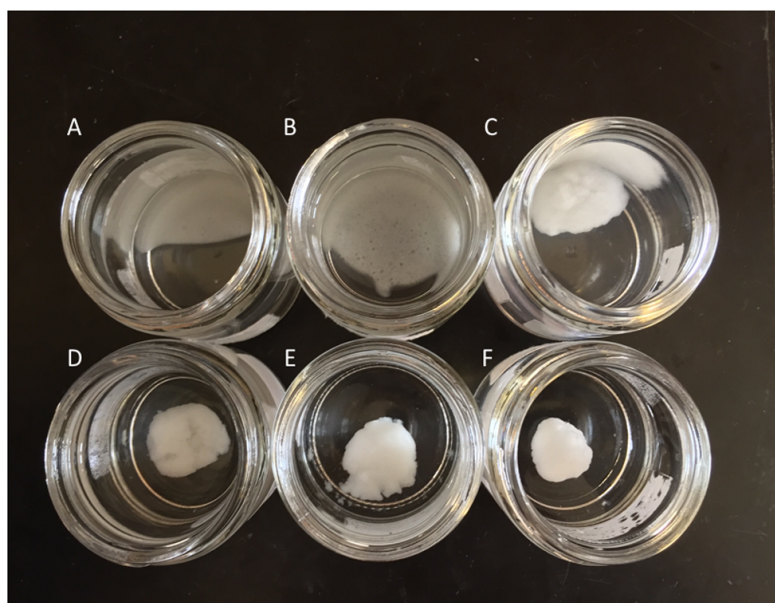
Figure 3-1 PEC networks of polyphosphoniums mixed with either 30 - 50 kg/mol or 1000 - 2000 kg/mol HA. A) **P-Et-P-(HA** 30 - 50 kg/mol); B) **P-Bu-P-(HA** 30-50 kg/mol); C) **P-Hp-P-(HA** 30 - 50 kg/mol); D) **P-Et-P-(HA** 1000 – 2000 kg/mol); E) **P-Bu-P-(HA** 1000 - 2000 kg/mol); F) **P-Hp-P-(HA** 1000 - 2000 kg/mol).

Thermal analysis was conducted on the dry PEC networks. TGA indicated that each network had a multi-step degradation with a T_o of ~210 °C corresponding to the decomposition of HA (Figure B15). The phosphonium polymers subsequently degraded at higher temperatures. DSC was also performed to examine possible phase separation. The DSC traces showed no glass transitions in the range of -10 to 200 °C (Figure B16). The absence of transitions for **P-Hp-P**, **P-Bu-P** and **HA** suggested that good mixing was obtained between these phosphonium polymers and HA. Unfortunately, higher temperatures could not be examined due to the degradation of **HA**, so it would not be possible to see the higher temperature glass transitions for **P-Ph-P** and **P-Et-P**.

The dry PEC networks were also analyzed by scanning electron microscopy-energy dispersive X-ray spectroscopy (SEM-EDX) to determine the ratios of carbon and phosphorus and thus the ratio of polyphosphonium to HA in the networks.[36] Atomic percentages of phosphorus relative to total carbon and phosphorus for **P-Hp-P-HA**, **P-Ph-P-HA**, **P-Bu-P-HA** and **P-Et-P-HA** were found to be 4.0 ± 0.4, 2.5 ± 0.2, 2.7 ± 0.3 and 2.8 ± 0.1 (mean ± std dev), corresponding to carboxylate:phosphonium ratios of (0.5 ± 0.2):1, (0.8 ± 0.2):1, (1.1 ± 0.3):1 and (1.4 ± 0.1):1 respectively (example calculation in experimental section 3.3.4). Therefore, the ratio of carboxylate:phosphonium ions in **P-Et-P-HA** is 1.4:1. The same procedure was used to calculate the ionic ratios for the other networks.

Thus, the **P-Hp-P-HA** network contained the highest polyphosphonium content relative to the other networks. This may arise from the high M_w and high hydrophilicity of **P-Hp-P**, which result in a highly extended conformation and efficient incorporation into the network. Lower incorporation of **P-Et-P** into the **P-Et-P-HA** network may be attributed to closer binding of the cation/anion pair in the phosphonium polymer, thus not allowing for efficient anion exchange with HA. It has been reported that the cation/anion pair is closer when there are less bulky substituents around phosphorus.[49] **P-Bu-P** and **P-Ph-P** formed networks with **HA** in about a 1:1 carboxylate:phosphonium ratio as expected.

3.2.3   PEC Network Swelling

PEC swelling has been implicated in the release of drugs and other molecules from PEC networks, as Pol^-Pol^+ or Pol^+Drug^- interactions can be sensitive to salt concentrations.[50–52] The presence of competing ions can induce increased mobility of polyions and the cleavage of ionic bonds in the network, causing swelling or network degradation.[53] Therefore it was of interest to investigate the stability and swelling of the PECs in different salt solutions. Dried PECs were placed in either deionized water, 0.1, 0.15, 0.25 M NaCl, or phosphate buffered saline (PBS) at 37 °C and their swelling was monitored over ~3 days. The network swelling varied depending on the concentration of salt and the PEC composition (Figure 3-2). In each case, the swelling was highest in 0.25 M NaCl. At this concentration, the structural integrity of the PECs was poor and they exhibited liquid-like properties. **P-Hp-P-HA**, **P-Bu-P-HA**, and **P-Et-P-HA** networks disintegrated and could not be further studied after about 1.5 days. The **P-Ph-P-HA** network remained intact at 0.25 M NaCl and swelled to the lowest degree at all salt concentrations, which can likely be attributed to increased hydrophobicity of the **P-Ph-P** polymer and additional interactions such as π-π stacking holding the network together.[45] In the solutions containing lower salt concentrations, all of the PECs maintained their structural integrity. **P-Et-P-HA** swelled the most, which likely results from its high hydrophilicity and lack of significant van der Waals or hydrogen bonding interactions in the network. Similar degrees of swelling were observed in PBS and 0.15 M NaCl for all of the networks, indicating that the identities of the ions do not impact swelling. In all salt solutions, the networks exhibited the "overshooting effect", which has been described as PEC swelling to a maximum value, then gradually deswelling due to chain relaxation until an equilibrium value is reached.[43] PECs swelled in DI water alone had the lowest degree of swelling due to the lack of ions in solution, and no overshooting effect was observed.
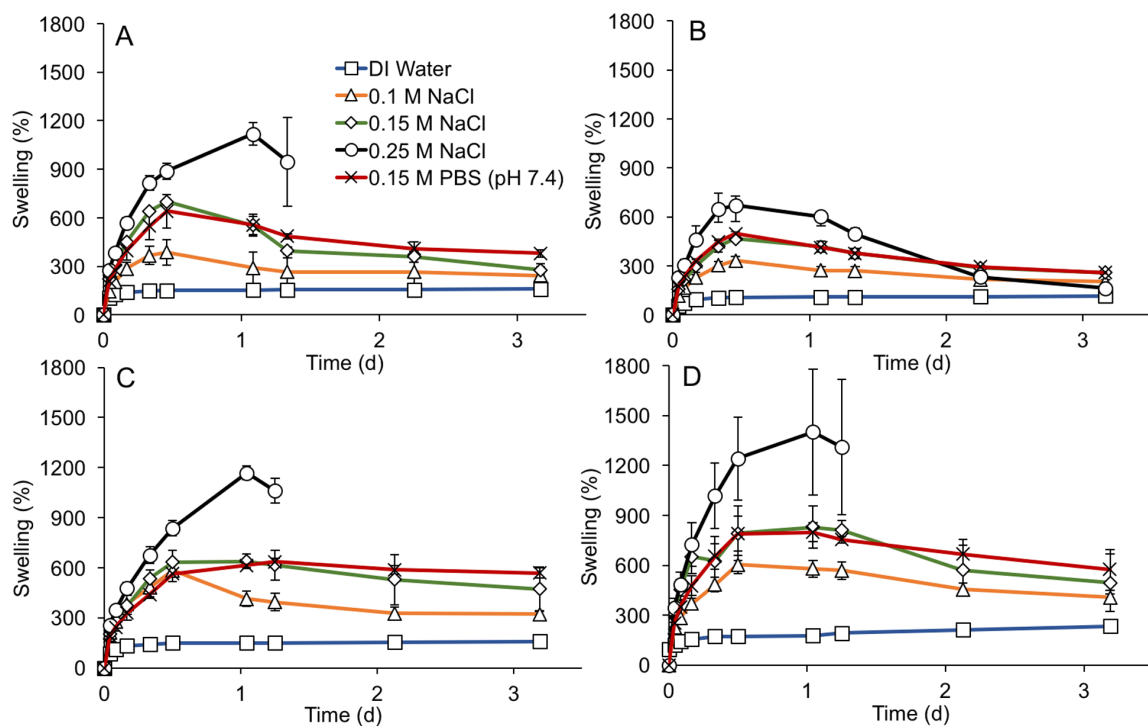
Figure 3-2 Swelling (wt%) of PECs relative to the dry state: A) **P-Hp-P-HA**; B) **P-Ph-P-HA**; C) **P-Bu-P-HA**; and D) **P-Et-P-HA**. Swelling depended on the salt concentration and network composition. **P-Hp-P-HA**, **P-Bu-P-HA**, and **P-Et-P-HA** disintegrated at 0.25 M NaCl after ~1.5 days. Error bars correspond to standard deviations (N = 3).

3.2.4   Scanning Electron Microscopy

The structures of the PEC networks in the dry state were examined by scanning electron microscopy (SEM). For PECs swelled in water, minimal porosity was observed (Figure 3-3), which may arise from their compact network structure in combination with artifacts of the drying process.
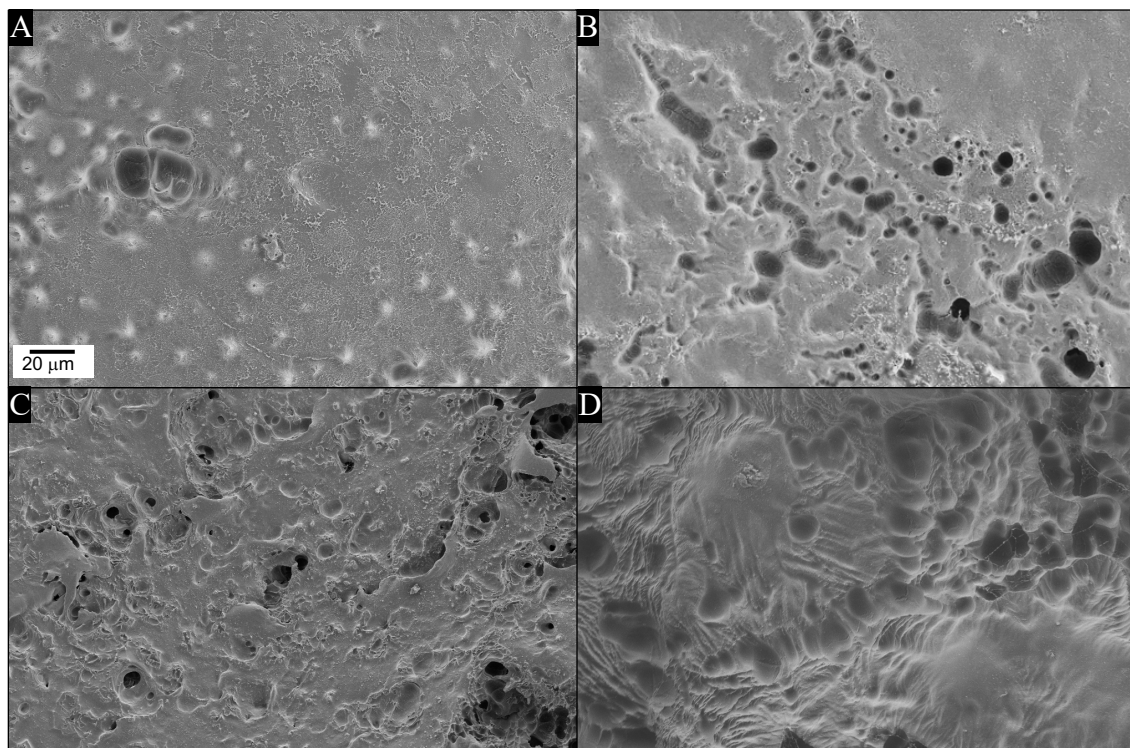
Figure 3-3 SEM images of PECs: A) **P-Hp-P-HA**; B) **P-Ph-P-HA**; C) **P-Bu-P-HA** D) **P-Et-P-HA**. Samples were prepared by the lyophilization of gels that were swelled in DI water for 24 h, followed by coating with 5 nm of osmium.

However, the porosity of **P-Ph-P-HA**, **P-Bu-P-HA**, and **P-Et-P-HA** networks swelled in PBS was clear from SEM (Figure 3-4). The **P-Et-P-HA** network, which had the highest degree of swelling, also appeared to have the largest pores. **P-Ph-P-HA** appeared to be the least porous, consistent with its lower degree of swelling.
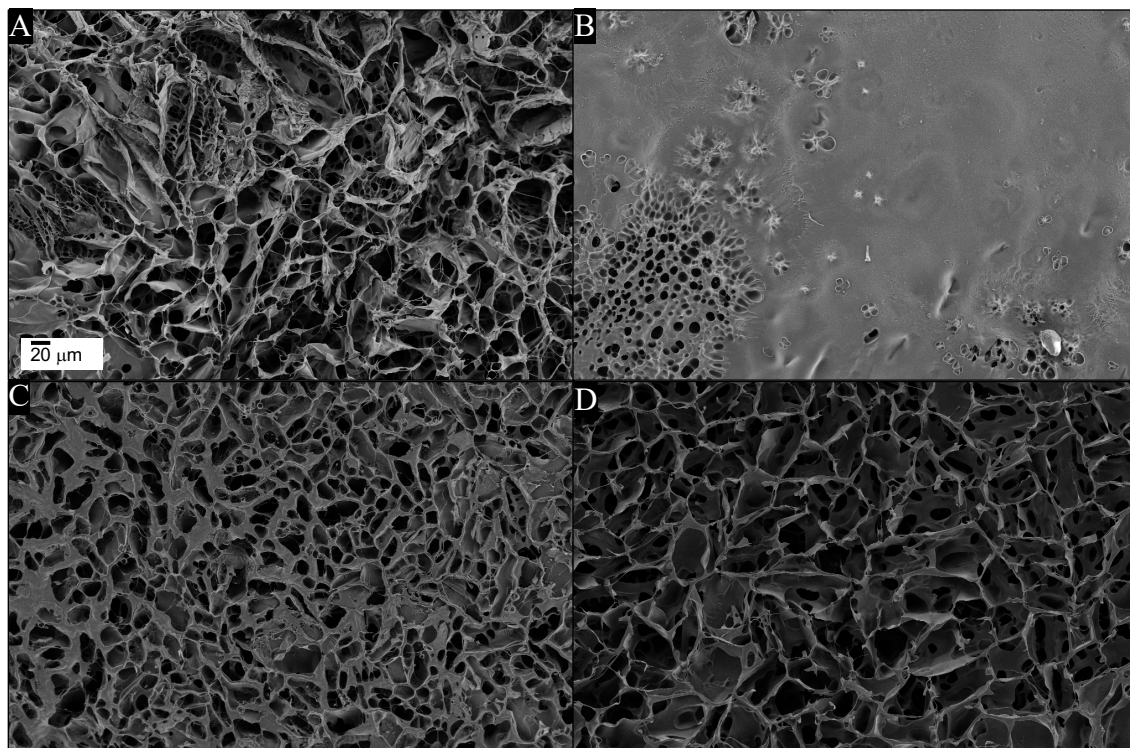
Figure 3-4 SEM images of PECs A) **P-Hp-P-HA**; B) **P-Ph-P-HA**; C) **P-Bu-P-HA** D) **P-Et-P-HA**. Samples were prepared by the lyophilization of gels that were swelled in PBS for 24 h then soaked in DI water for 1 min to remove surface salts, followed by coating with 5 nm of osmium.

3.2.5   Rheology

Rheology is useful to investigate the viscoelastic behavior of polymer systems.[54] It can also provide information on the time scale of network relaxation. After swelling in DI water or PBS, the elastic and viscous moduli, G' and G" respectively, of the PECs were measured over an angular frequency range of 0.01 to 100 rad/s (Figure 3-5). When swelled in DI water, all of the PECs exhibited gel-like behavior, with G' > G" over the entire frequency range. **P-Hp-P-HA**, **P-Ph-P-HA** and **P-Et-P-HA** had elastic moduli ranging from about 10 - 60 kPa and viscous moduli of 3 - 10 kPa. **P-Bu-P-HA** had lower elastic and viscous moduli, which can likely be attributed to the steric bulk or the hydrophobicity associated with the butyl groups limiting the extent of ionic crosslinking. G' and G" approached one another at low frequencies for each of the PECs in water. This suggests a crossover of the moduli at an angular frequency less than 0.01 rad/s, corresponding to relaxation times

greater than 100 s. There did not appear to be any significant trends relating the rheological properties to the degree of swelling in DI water.

When swelled in PBS, the networks had elastic and viscous moduli that were about an order of magnitude lower than those measured in DI water. The reduction in moduli can be attributed to the added salt disrupting ionic crosslinking, enhancing polymer chain mobility, and increasing swelling. However, the networks were still predominantly elastic over a broad frequency range, suggesting that the intermolecular bonds holding the networks together were still long-lived. **P-Hp-P-HA**, **P-Bu-P-HA** and **P-Et-P-HA** had moduli crossover frequencies of 0.010, 0.025, and 0.016 rad/s, corresponding to relaxation times of about 100, 40, and 63 s respectively. The shorter relaxation time for **P-Bu-P-HA** may again be attributed to weaker ionic bonding in this network. On the other hand, the moduli of **P-Ph-P-HA** did not crossover in the measured frequency range, suggesting longer relaxation times, due to strong bonding within this network. The longer relaxation time for **P-Ph-P-HA** may also result from its lower degree of swelling relative to the other networks; however, for the other networks no general relationship between the degree of swelling and the rheological properties was observed.
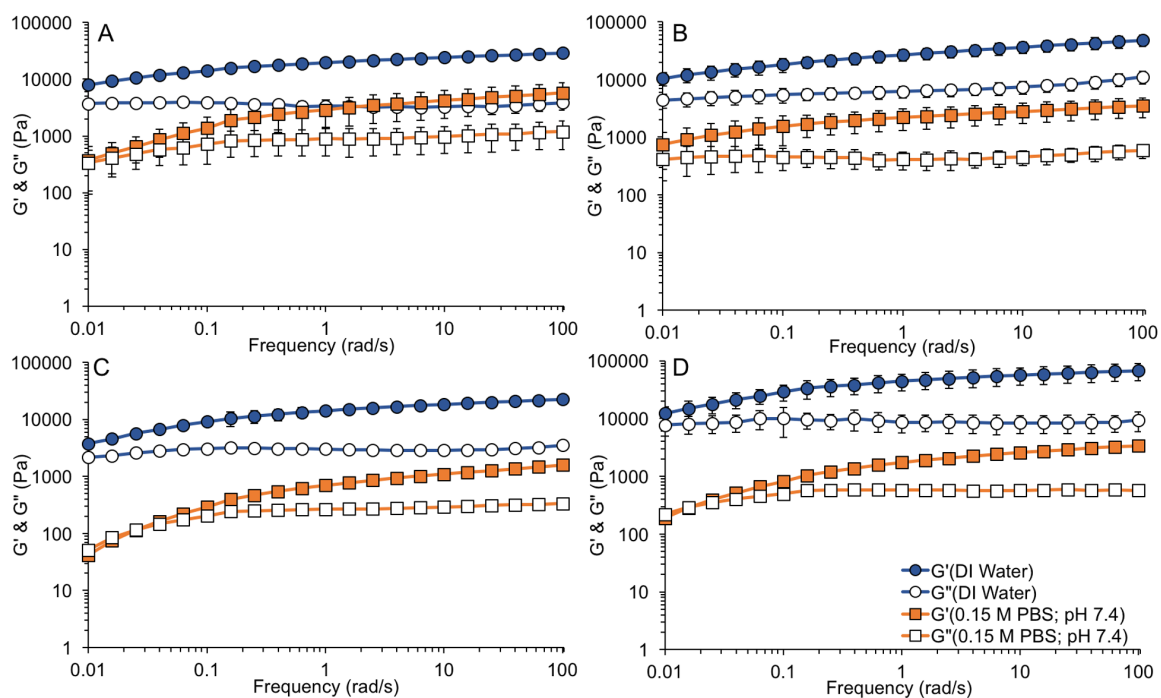
Figure 3-5 Rheology frequency sweeps for: A) **P-Hp-P-HA**; B) **P-Ph-P-HA**; C) **P-Bu-P-HA**; and D) **P-Et-P-HA** in DI water and PBS. Data points are means of 4 measurements at each frequency, and the error bars are standard deviations.

3.2.6   Self-Healing

The ability of the PECs to self-heal was studied qualitatively after damaging them by boring a ~0.5 mm hole with an 18-gauge needle, then incubating them in PBS at 37 °C for 18 h. Despite the longer relaxation time suggested by rheology, the **P-Ph-P-HA** had the shortest healing time of less than 2 hours (Figure 3-6B). It is possible that the lower M_w of **P-Ph-P** compared to the other polymers contributed to faster healing by facilitating flow. In addition, as the rheology measurements were performed in the linear regime, they would not have captured low frequency, non-linear viscosity behavior. **P-Hp-P-HA** networks had the longest healing time, with damage still detected at 18 h (Figure 3-6A). This may correlate with the relatively long relaxation time of this network as indicated by rheology, its high viscous modulus, and the high M_w of **P-Hp-P**. **P-Bu-P-HA** and **P-Et-P-HA** had fully healed by 18 h (Figure 3-6C-D). Self-healing was also investigated in DI water. All of the networks except for **P-Ph-P-HA** still had detectable damage after 18 h, indicating

that dynamic ion exchange facilitates healing (Figure 3-7). The capacities of the networks to self-heal may be of interest for delivery to tissues such as intervertebral disks or articular joints where loading may lead to deformation of the network, which could then self-heal when loading is removed, or for skin applications where they could conform to dynamic surfaces.[55]
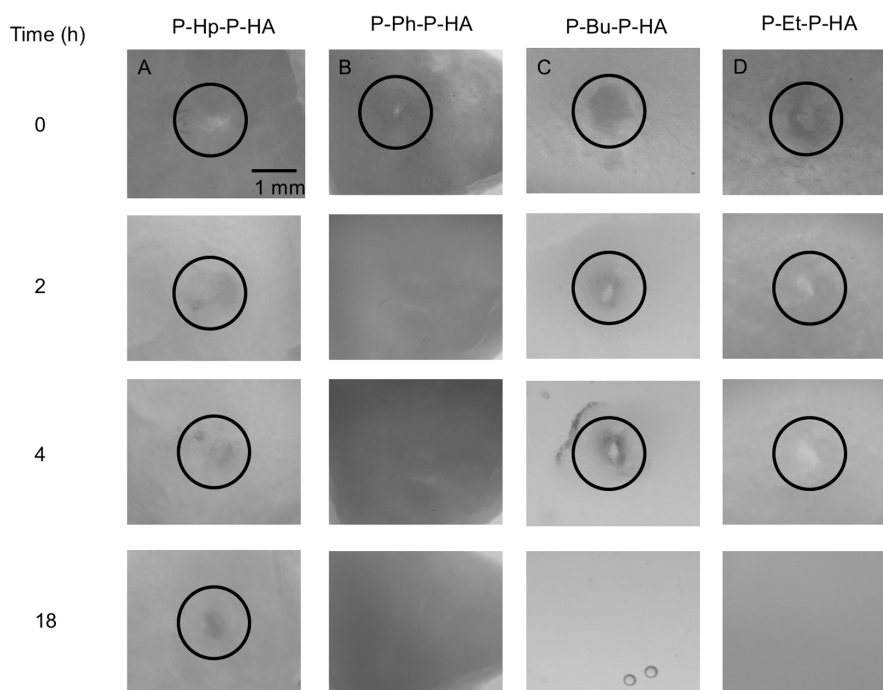
Figure 3-6 Digital images of PECs damaged by a 0.5 mm diameter hole, as indicated in the black circles, then healing over 18 h in PBS at 37 °C: A) **P-Hp-P-HA**; B) **P-Ph-P-HA**; C) **P-Bu-P-HA**; D) **P-Et-P-HA**. The black circles indicate the location of the initial damage. Bubbles were frequently observed for **P-Bu-P-HA**.
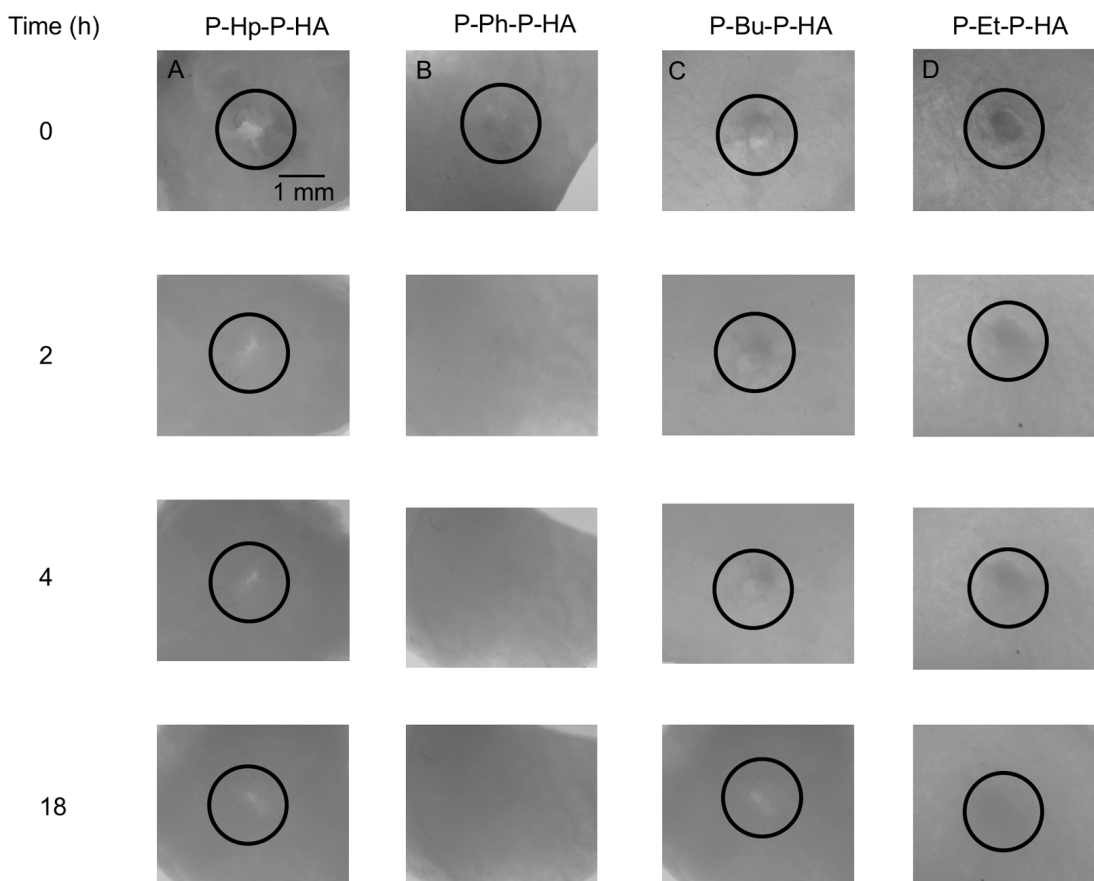
Figure 3-7 Digital images of PECs damaged by a 0.5 mm diameter hole, as indicated in the black circles, then healing over 18 h in DI-Water at 37 °C: A) **P-Hp-P-HA**; B) **P-Ph-P-HA**; C) **P-Bu-P-HA**; D) **P-Et-P-HA**. The black circles indicate the location of the initial damage.

3.2.7   Loading and Release Studies

Due to the capacities of the PEC networks to electrostatically bind charged molecules, we investigated the loading and release of three different anionic compounds and one neutral compound (Figure 3-8). Loading was performed by immersion of the PECs in ~0.05 wt% solutions of the compounds in DI water. In general, high loadings were obtained for all of the anionic molecules, whereas only ~1 wt% loading of the neutral compound paracetamol was obtained, demonstrating the importance of ionic interactions. Fluorescein was studied as it has been previously reported to bind well to accessible ammoniums and phosphoniums in polymer networks.[56,57] The highest loadings of fluorescein were obtained for **P-Hp-P-**

HA and **P-Bu-P-HA** (16 wt%), followed by **P-Et-P-HA** (14 wt%), and **P-Ph-P-HA** (9 wt%) (Table 3-1).The lower loading for **P-Ph-P-HA** could be attributed to its lower degree of swelling compared to the other networks or to less favorable interactions with fluorescein. Diclofenac sodium salt, a nonsteroidal anti-inflammatory drug, had loadings of 11 – 15 wt%, and there were no statistically significant differences between the networks ($p > 0.05$). The loading of adenosine-5'-triphosphate disodium salt hydrate (ATP), a dianion, was also investigated. **P-Hp-P-HA** afforded the highest loading of ATP (16 wt%), suggesting that hydrogen bonding to the **P-Hp-P** hydroxyls or the rheological properties of this network may have been important. **P-Ph-P-HA** afforded the lowest loading of 5 wt%, most likely again due to its lower swelling, while the other two networks had intermediate loading levels. Overall, **P-Hp-P-HA** had a trend towards higher drug loading than the other networks, which may relate to it also having the highest phosphonium:carboxylate ratio of 2:1 and thus highest density of uncomplexed cations. However, the other networks did not show correlations between drug loading and the phosphonium:carboxylate ratio.
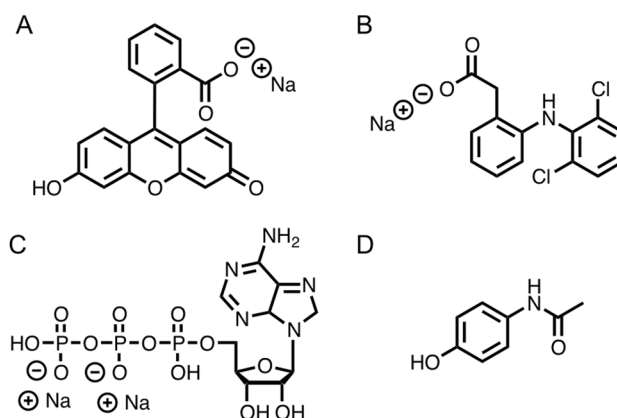
Figure 3-8 Anionic molecules, and a neutral control compound chosen for loading: A) fluorescein sodium salt; B) diclofenac sodium salt; C) adenosine 5′-triphosphate disodium salt; D) paracetamol.

Table 3-1 Loading content of the PEC networks (relative to dry weight of polymer). Error bars correspond to the standard deviations (N = 3).

PEC	Loading content (wt%)			
	Fluorescein	Diclofenac	ATP	Paracetamol
P-Hp-P-HA	16.2 ± 0.8	10.6 ± 0.6	16.5 ± 0.5	1.2 ± 0.2
P-Ph-P-HA	8.9 ± 1.7	12.0 ± 2.5	5.2 ± 0.4	0.8 ± 0.8
P-Bu-P-HA	16.4 ± 0.9	15.0 ± 1.7	8.0 ± 0.3	1.3 ± 0.4
P-Et-P-HA	13.4 ± 0.8	12.1 ± 2.4	8.9 ± 0.3	0.8 ± 0.3

Release of each of the anionic molecules from the networks was studied in PBS at 37 °C. The release of fluorescein ranged from 40 – 100% over 60 days (Figure 3-9A). **P-Ph-P-HA** exhibited the highest release rate. As it also had the lowest fluorescein content, the results suggest that binding of fluorescein to this network was likely weaker than to the other networks. **P-Hp-P-HA**, **P-Bu-P-HA** and **P-Et-P-HA** exhibited more sustained release of fluorescein over 60 days, with 40 – 60% released over this time frame. Release of diclofenac from the networks was also sustained, with 80 – 90% released over 60 days (Figure 3-9B). Similar to the results for the loading content, the release rates for diclofenac were not very dependent on the structure of the phosphonium polymer. Despite being a dianion that might exhibit stronger bivalent binding to the phosphonium polymer, ATP was rapidly released from all of the PEC networks, with 80 – 100% release over 1 day (Figure 3-9C). In addition to its different charge, ATP is also much more hydrophilic than fluorescein and diclofenac, suggesting that a combination of hydrophobic and ionic interactions may also be important for achieving slow drug release from the networks.
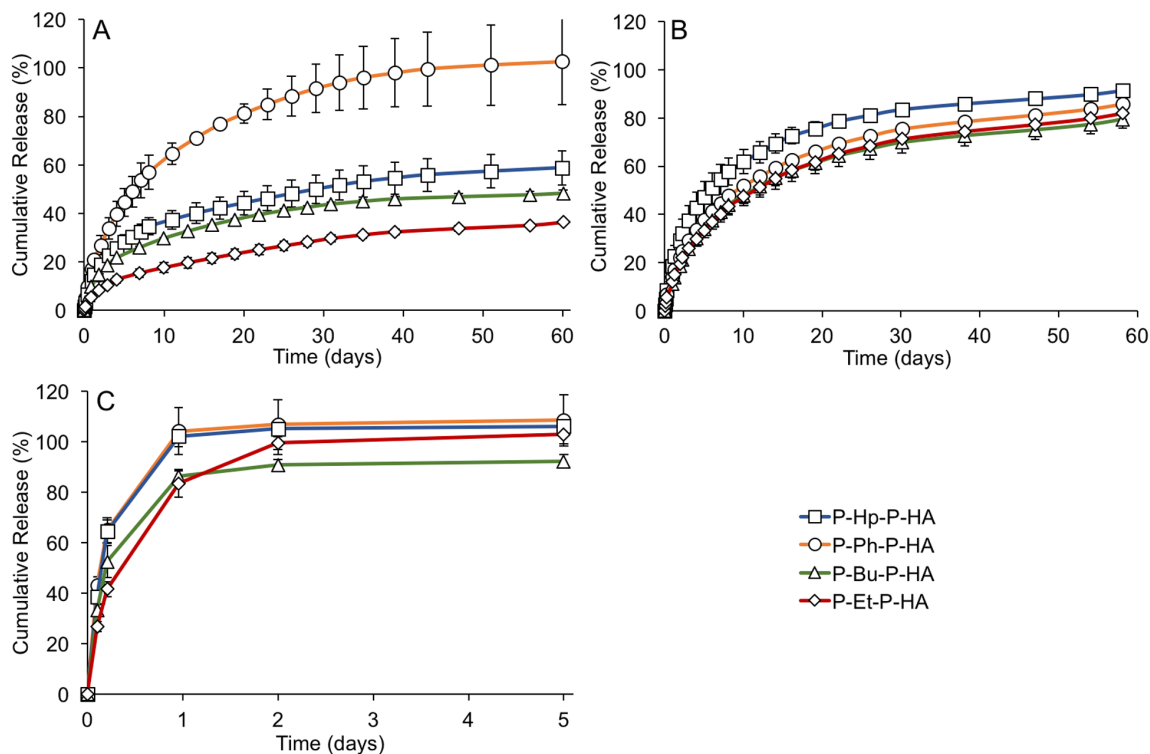
Figure 3-9 Release curves of A) fluorescein sodium salt, B) diclofenac sodium salt, C) ATP. Error bars correspond to the standard deviations (N = 3).

The anion release kinetics of fluorescein and diclofenac up to the time of 60% anion release were fit to the Korsmeyer-Peppas equation $M_t/M_\infty = kt^n$ where M_t is the amount of drug released at time t, M_∞ is the amount of drug released as time approaches infinity, k is a constant, and n is the diffusional exponent, which can indicate the transport mechanism (Figure B18).[58] Values of n ranged from 0.5 – 0.6 for fluorescein, and were ~0.6 for diclofenac. Although approaching the value of 0.45 expected for pure Fickian release from disks,[59] they fell in the range expected for anomalous transport, which can likely be attributed to their complex interactions with the PEC networks, as well as network swelling and possible degradation during the experiment. Overall, the slow release of fluorescein and diclofenac from our networks relative to previously reported systems can likely be attributed to the combination of ionic and hydrophobic interactions with the polymers in the network as well as the dense structure of the PECs that was achieved through ultracentrifugation.

3.2.8   *In Vitro* Toxicity Studies

The cytotoxicities of the PECs were first probed through the potential leaching of toxic molecules from the networks. To carry out the study, PECs were incubated in cell culture medium for 24 h, then this medium was added to cells at different dilutions. C2C12 mouse myoblast cells were selected as they have been widely used for *in vitro* work and a 3-(4,5-dimethylthiazol-2-yl)-2,5- diphenyltetrazolium bromide (MTT) assay was performed to assess cell metabolic activity after incubation with the leachate for 24 h. High cell metabolic activity (> 80 %) was retained for **P-Bu-Hp-HA**, **P-Ph-P-HA**, and **P-Et-P-HA**, suggesting that these networks did not leach toxic species (Figure 3-10). **P-Bu-P-HA** resulted in metabolic activities ranging from 65 – 83 % of the control. **P-Bu-P-HA** was the network with the lowest G' and G" values from rheology and also had the shortest relaxation time, suggesting that it was more dynamic and may be the most likely to release polyphosphonium chains into the culture medium.
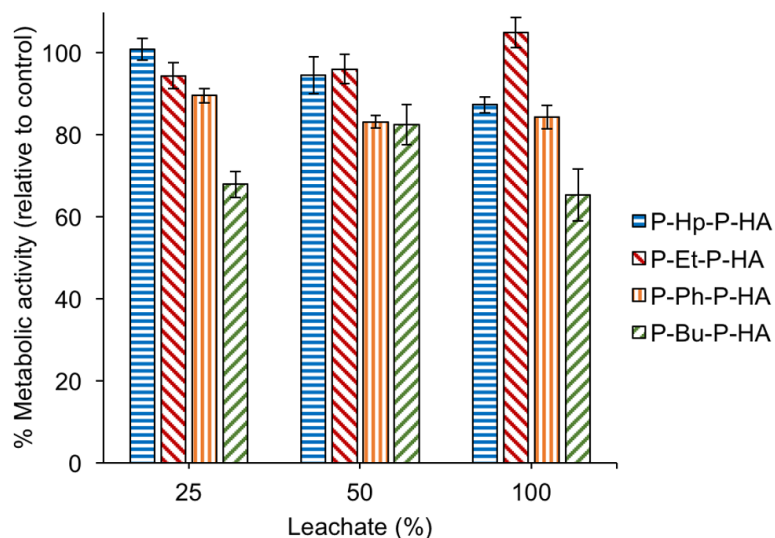
Figure 3-10 C2C12 metabolic activities measured by MTT assays on C2C12 cells incubated in culture medium that was exposed to the different PEC networks. 100 % metabolic activity corresponds to cells incubated in media that was not exposed to PEC. Error bars correspond to standard error on 6 measurements.

We also investigated the cytotoxicities of the phosphonium polymers and **HA** on their own using MTT assays. The metabolic activities of C2C12 cells incubated in culture medium containing the polymers for 24 h was dependent on the polymer concentration and structure (Figure 3-11). As expected based on the literature,[37] cells exposed to **HA** had the highest metabolic activities with > 90 % relative to the control up to 1 mg/ mL, the highest concentration evaluated. Phosphoniums, on the other hand, have been documented to act as biocides. Their mechanism of killing cells is thought to involve the disruption of cell membranes.[60] Despite this, **P-Ph-P** was found to have low cytotoxicity, with > 60 % metabolic activity relative to the control at 1 mg/mL, and greater than ~80 % metabolic activity at concentrations of 0.5 mg/mL and below. The remaining phosphonium polymers were more toxic, with low metabolic activities above 63 μg/mL. The toxicity of **P-Bu-P** likely explains the toxicity of **P-Bu-P-HA** networks observed in the leaching study. Thus, these initial biological studies suggest that **P-Bu-P-HA** may not be an ideal material for *in vivo* use. In comparing the toxicity results for the networks with those of the free polymers, **P-Hp-P** and **P-Et-P** were much less toxic in the networks, in agreement with previous results where the toxicities of cationic ammonium polyelectrolytes were reduced upon complexation with polyanions.[61] The toxicity results for **P-Hp-P** and **P-Et-P** also suggest that these polycations were not released from their corresponding networks during the leaching study. However, they should be used cautiously due to their toxicity at high concentrations. Given the low toxicity of **P-Ph-P**, it is not possible to determine based on these toxicity studies whether it leached from **P-Ph-P-HA** networks. However, leaching of **P-Ph-P** does not appear to be a major concern based on these initial experiments due to its low cytotoxicity. A more comprehensive study of the biological properties of the networks will be required in future studies.
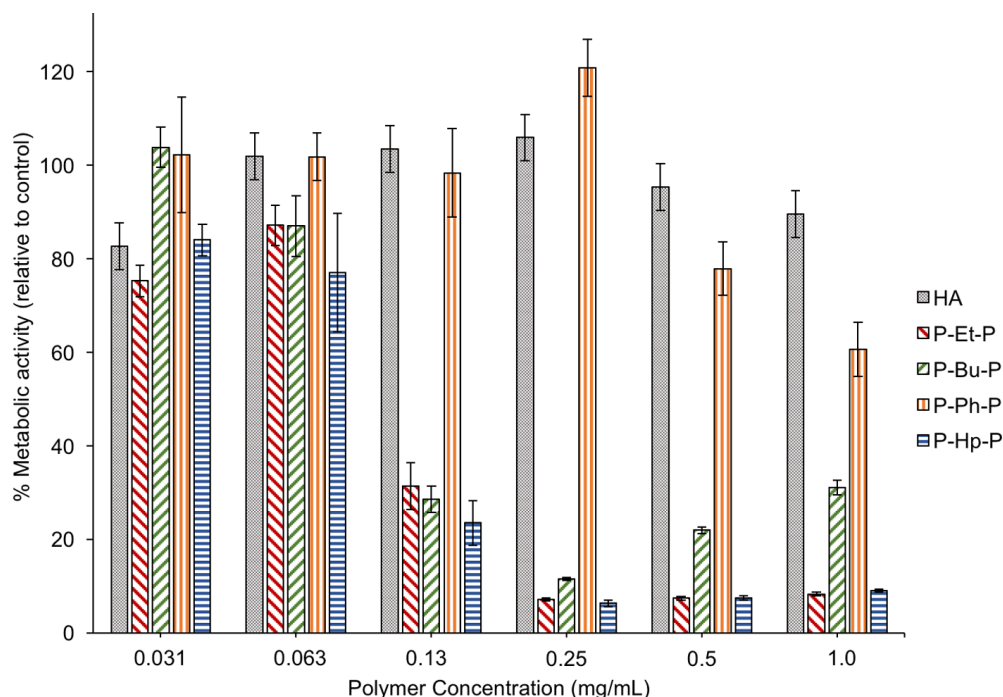
Figure 3-11 C2C12 metabolic activities measured by MTT assays on C2C12 cells incubated with varying concentrations of polymers dissolved in culture medium. 100 % metabolic activity corresponds to cells incubated in media that was not exposed to PEC. Error bars correspond to the standard error (N=6).

3.2.9   Conclusions

New PEC networks were prepared by mixing phosphonium polymers with HA and then using ultracentrifugation to compact the networks. The properties of the networks, such as their swelling, viscoelastic moduli, and relaxation times measured by rheology depended on the structure of the phosphonium polymer and on the presence of salts, which can both influence the strength of ionic interactions in the networks. **P-Ph-P-HA** afforded networks with less swelling and long relaxations times, while the **P-Hp-P-HA**, **P-Bu-P-HA**, and **P-Et-P-HA** networks exhibited higher swelling and shorter relaxation times. Qualitative self-healing tests showed that **P-Ph-P-HA** healed the fastest, **P-Hp-P-HA** healed more slowly, and that the presence of salt in PBS facilitated healing. Ionic molecules including fluorescein, diclofenac, and ATP could be loaded into the different networks leading to good loadings of 5 – 16 wt%, while very low loading (1 wt%) was obtained for the nonionic molecule paracetamol. Fluorescein and diclofenac were released very slowly from the

networks over 60 days, which we attribute to the dense ionic network structure, combined with ionic and hydrophobic interactions. ATP, a more hydrophilic dianion, was released much more rapidly over 1-2 days. *In vitro* cytotoxicity studies suggested that only the **P-Bu-P-HA** network released toxic concentrations of polymers into cell culture media, which can be attributed to its dynamic properties that were revealed by rheology. **P-Hp-P** and **P-Et-P** were also toxic when added directly to cell culture media, but were not released from the networks at toxic concentrations over 24 h. **P-Ph-P** exhibited low cytotoxicity, despite the presence of cationic and hydrophobic groups on the polymer. Thus, the choice of phosphonium polymer has important implications on the physical and biological properties of the resulting PEC network and should be selected according to the target application. In future work, it will be interesting to investigate the loading of cationic drugs, and also to explore the effect of different network compositions (e.g. anion:cation ratio) on the drug loading. Furthermore, it will also be desirable to investigate degradable phosphonium polymers.

3.3   Experimental

3.3.1   General Materials

Tri(*n*-butyl)(4-vinylbenzyl)phosphonium chloride (**Bu-P**), triethyl(4-vinylbenzyl)phosphonium chloride (**Et-P**), triphenyl(4-vinylbenzyl)phosphonium chloride (**Ph-P**) and tris(hydroxypropyl)(4-vinylbenzyl)phosphonium chloride (**Hp-P**) were synthesized as previously reported.[45,56,62] Deionized (DI) water was obtained from a Barnstead Easypure II system and had a resistivity of 15 MΩ•cm or greater. Hyaluronic acid sodium salt (HA) (1000-2000 or 30-50 kg/mol) was purchased form CarboSynth (Berkshire, United Kingdom) and used as received. Phosphines were donated by Solvay (Niagara Falls, ON, Canada) and used as received. D_2O, 4-vinylbenzyl chloride, fluorescein sodium salt, paracetamol and all cell culture reagents were purchased from Sigma-Aldrich and used as received. Diclofenac sodium salt and adenosine-5'-triphosphate disodium salt hydrate (ATP) were purchased from Alfa Aesar and used as received. Phosphate buffered saline contained 137 mM NaCl, 2.7 mM KCl, 10 mM Na_2HPO_4, and 1.8 mM KH_2PO_4 with a pH of 7.4.

3.3.2   General Methods

Differential scanning calorimetry (DSC) was performed on a DSC Q20 from TA Instruments (New Castle, DE) at a ramp rate of 10 °C/min under a N_2 atmosphere in an aluminum T_{zero} pan containing 5–10 mg of sample. Glass transition temperatures (T_g) were obtained from the second heating cycle. Thermogravimetric analysis (TGA) to determine the onset degradation temperatures (T_o) was performed on a Q600 SDT from TA Instruments and analyzed at a ramp rate of 10 °C/min up to 800 °C using a ceramic pan containing 5–10 mg of dry sample. Nuclear Magnetic Resonance (NMR) spectroscopy was conducted on a Bruker AvIII HD 400 MHz Spectrometer from (^{1}H 400.08 MHz, ^{31}P{^{1}H} 161.82 MHz). The chemical shifts (δ, ppm) in all ^{1}H NMR spectra were referenced relative to the residual H_2O peak (^{1}H $\delta = 4.79$). All ^{31}P{^{1}H} NMR spectra were referenced using an external standard (85% H_3PO_4: ^{31}P $\delta = 0$). UV-visible spectroscopy was conducted on a Tecan Infinite M1000 Pro plate reader. Costar 96 well UV plates (#3635) with UV transparent flat bottoms were used. Scanning electron microscopy (SEM) was performed in the University of Western Ontario's Nanofabrication Facility using a Zeiss LEO 1530 instrument, operating at 3.0 kV and a working distance of 4-7 mm. Samples were prepared by soaking them in DI water or PBS for 24 h, freezing them, then lyophilizing. Samples soaked in PBS were soaked in DI water for 1 min prior to lyophilization to remove surface salt that would interfere with imaging. Samples were mounted to stubs covered in carbon tape and coated in 5 nm osmium using a SPI Supplies, OC-60A plasma coater. Energy dispersive X-ray spectroscopy (EDX) was performed using a Hitachi S-3400N variable pressure microscope with a turbomolecular pump. Samples were analyzed at an accelerating voltage of 20 kV and analyzed by EDX analysis using an INCA EDAX system and software.

Size exclusion chromatography (SEC) of the polymers was performed using a Malvern Viscotek GPCmax instrument equipped with a Viscotek VE 3580 RI detector and two Inert series columns (P101609 and Q10183) at a constant temperature of 50 °C. The eluent was 0.4 M tetrabutylammonium triflate in N,N-dimethylformamide (DMF) with a flow rate of 1 mL/min. Calibration was performed using poly(methyl methacrylate) (PMMA) standards to determine the number average molar mass (M_n), weight average molar mass (M_w), and dispersity ($Đ$). The M_w values for **P-Hp-P** and **P-Et-P** were measured by light scattering

(LS) using a Malvern Zetasizer Nano-ZS instrument as previously reported.[63] The differential refractive index increment (dn/dc) for **P-Et-P** has been reported previously.[49] The differential refractive index increment (dn/dc) of **P-Hp-P** has not been reported so dn/dc of **P-Et-P** was assumed to be similar and used for both. Time averaged scattered light intensities were measured for each polymer at a series of concentrations from 0.1 to 1.0 mg/mL in 54/23/23 (v/v/v) water/methanol/acetic acid containing 0.1 M sodium acetate. This ternary mixture was used as it prevented aggregation of polymers.[49] Toluene was used as a standard for the measurements. Using these data, the M_w for each polymer was determined from the Rayleigh equation, $KC/R_\theta = (1/M_w + 2A_2C)P(\theta)$, using a Debye plot: KC/R_θ is plotted as a function of C, allowing $1/M_w$ to be determined as the y-intercept. Here C is the polymer concentration; R_θ is the excess Rayleigh ratio - the ratio of scattered to incident light intensity; A_2 is the second viral coefficient, which is a measure of solute-solvent interactions; $P(\theta)$ is a scattering function which relates the angular variation in scattering intensity to the mean square radius of the particle; $K = 4\pi^2/\lambda_o^4 N_A[n_o(dn/dc)]^2$, where λ_o is the vacuum wavelength of incident light; N_A is Avogadro's number; and n_o is the refractive index of the solvent.

3.3.3   Polymer Synthesis

Synthesis of poly[tris(hydroxypropyl)(4-vinylbenzyl)phosphonium chloride] (P-Hp-P). Hp-P (16.7 g, 46.3 mmol), 2,2'-azobis[2-(2-imidazolin-2-yl)propane]dihydrochloride (VA-044) (75.0 mg, 0.23 mmol) and DI water (210 mL) were combined in a round bottom flask with a stir bar, and the flask was sealed with Teflon tape. N_2 was bubbled through the solution using a needle with stirring at room temperature for 30 min to degas the reaction mixture. The reaction mixture was then heated at 60 °C for 16 h. The solvent was then removed in vacuo. No further purification was necessary as no monomer peaks were visible in the resulting ^{1}H NMR spectrum. Yield = 15.9 g, 95 %. ^{1}H NMR (400 MHz, D$_2$O) δ: 1.55 (broad s, 9 H, P-CH$_2$-C<u>H$_2$</u>-CH$_2$-OH and backbone C<u>H</u> and C<u>H$_2$</u>), 2.09 (broad s, 6 H, P-C<u>H$_2$</u>-(CH$_2$)$_2$-OH), 3.48 (broad s, 8 H, P-(CH$_2$)$_2$-C<u>H$_2$</u>-OH, Ar-C<u>H$_2$</u>-P-(CH$_2$)$_3$-OH), 6.49 (broad s, 2 H, Ar-<u>H</u>), 7.06 (broad s, 2 H, Ar-<u>H</u>) ppm. ^{31}P{^{1}H} NMR (162 MHz, D$_2$O) δ: 34.2; T_g = 115 °C, T_o = 290 °C; LS: M_w = 666 kg/mol.

Synthesis of poly[triphenyl(4-vinylbenzyl)phosphonium chloride] (P-Ph-P). The synthesis was carried out as described above for **P-Hp-P** except that the following compounds and quantities were used: **Ph-P** (17.8 g 43.0 mmol); VA-044 (70.0 mg, 0.22 mmol); DI water (220 mL). Yield = 16.4 g, 92 %. ^{1}H NMR (400 MHz, D$_2$O) δ: 0.99 (broad, C$\underline{H}_2$ and C$\underline{H}$), 4.33 (broad, Ar-C$\underline{H}_2$-P-C$_5$H$_5$) 5.91 (broad, Ar-$\underline{H}$), 6.45 (broad, Ar-$\underline{H}$), 7.30 (broad, Ar-$\underline{H}$) 7.60 ((broad, Ar-$\underline{H}$) ppm. ^{31}P{^{1}H} NMR (162 MHz, D$_2$O) δ: 22.15 ppm; T_g = 270 °C, T_o = 314 °C; M_n = 60 kg/mol, M_w = 138 kg/mol, $Đ$ = 2.2.

Synthesis of poly[tri(*n*-butyl)(4-vinylbenzyl)phosphonium chloride] (P-Bu-P). The synthesis was carried out as described above for **P-Hp-P** except that the following compounds and quantities were used: **Bu-P** (9.60 g, 27.1 mmol); VA-044 (44.0 mg, 0.14 mmol); DI water (120 mL). Yield = 8.80 g, 92 %. ^{1}H NMR (400 MHz, D$_2$O) δ: 0.76 (broad s, 10 H, P-(CH$_2$)$_3$-C$\underline{H}_3$ and backbone C$\underline{H}$), 1.29 (broad s, 14 H, P-CH$_2$-(C$\underline{H}_2$)$_2$-CH$_3$ and backbone C$\underline{H}_2$), 2.05 (broad s, 6 H, P-C$\underline{H}_2$-(CH$_2$)$_2$-CH$_3$), 3.69 (broad s, 2H Ar-C$\underline{H}_2$-P-(CH$_2$)$_3$-CH$_3$), 6.42 (broad s, 2 H, Ar-$\underline{H}$), 7.14 (broad s, 2 H, Ar-$\underline{H}$). ^{31}P{^{1}H} NMR (162 MHz, D$_2$O) δ: 31.71, 35.75 ppm; T_g = 180 °C, T_o = 344 °C; SEC: M_n = 170 kg/ mol, M_w = 450 kg/mol, $Đ$ = 2.6.

Synthesis of poly[triethyl(4-vinylbenzyl)phosphonium chloride] (P-Et-P). The synthesis was carried out as described above for **P-Hp-P** except that the following compounds and quantities were used: **Et-P** (10.1 g, 37.4 mmol); VA-044 (60.0 mg, 0.19 mmol); DI water (130 mL). Yield = 9.30 g, 92 %. ^{1}H NMR (400 MHz, D$_2$O) δ: 0.93 (broad s, 10 H, P-CH$_2$-C$\underline{H}_3$ and backbone C$\underline{H}$), 1.45 (broad s, 2 H, backbone C$\underline{H}_2$), 2.02 (broad s, 6 H, P-C$\underline{H}_2$-CH$_3$), 3.61 (broad s, 2 H, Ar-C$\underline{H}_2$-P-CH$_2$-CH$_3$), 6.44 (broad s, 2 H, Ar-$\underline{H}$), 7.09 (broad s, 2 H, Ar-$\underline{H}$) ppm. ^{31}P{^{1}H} NMR (162 MHz, D$_2$O) δ: 36.94 ppm; T_g = 230 °C, T_o = 330 °C; LS: M_w = 588 kg/mol.

3.3.4 Calculation of phosphorus content in the PEC networks from SEM-EDX

Following a previously reported procedure,[2] **P-Hp-P-HA**, **P-Ph-P-HA**, **P-Bu-P-HA** and **P-Et-P-HA** networks were washed with water for 24 h to remove salts, and dried overnight at 25 °C in a vacuum oven. The dry PEC networks were the mounted on carbon tabs and coated with 5 nm of osmium. SEM-EDX analysis was used to measure the carbon and phosphorus atomic %, in triplicate.

Knowing that each phosphonium monomer contains x C (with x depending on the specific polymer) and 1 P atom, while the carboxylate monomer contains 14 C atoms, the measured atomic % of P relative to that of C could be converted to a carboxylate:phosphonium ratio. For example, the expected atomic P % relative to C for different ratios is summarized in the following table for complex **P-Et-P-HA**:

Table 3-2 Expected atomic P % relative to C for different ratios for **P-Et-P-HA**.

Stoichiometry of carboxylate: phosphonium monomers	Total C & P atoms in the given ratio	Atomic % of P relative to P and C
1:3	62	4.84
1:2	46	4.35
1:1	30	3.33
2:1	44	2.27
3:1	58	1.72
4:1	72	1.39

Example calculation for **P-Et-P-HA**:

$$2.8 \text{ atomic \% P relative to P and C} = \left(\frac{1 \, P \, atom}{x \, total \, C \, and \, P \, atoms}\right) 100\%$$

$$x = \frac{100}{2.8} = 35.7 \text{ total C and P atoms in the ratio of monomers}$$

For one P atom in the ion pair, we have 16 total atoms attributable to the phosphonium monomer (1 P and 15 C atoms).

$35.7 - 16 = 19.7$ carbon atoms attributable to the carboxylate monomer

$$\frac{19.7 \, atoms}{14 \, carbon \, atoms \, per \, carboxylate \, monomer} = 1.4$$

Therefore the ratio of carboxylate:phosphonium ions in **P-Et-P-HA** is 1.4:1. The same procedure was used to calculate the ionic rations for the other networks.

3.3.5   Measurement of Swelling

Each network (about 150 mg, performed in triplicate) was initially dried to remove any residual water and accurately weighed to determine the dried mass (m_i). The networks were then placed into 25 mL of solution at 37 °C with NaCl concentrations of 0 M (DI water), 0.1 M, 0.15 M, 0.25 M or into PBS. Networks were taken out at specific time points, blotted dry with paper towel to remove surface liquid, and weighed to provide the swollen mass (m_s). The swelling was determined using the equation:

$$\text{Swelling \%} = \left(\frac{m_s - m_i}{m_i}\right) x \, 100 \qquad\qquad \text{Equation 3-2}$$

3.3.6   Healing Experiments

PECs were punctured with an 18-gauge needle, and the material was removed to create a 0.5 mm diameter hole. Damaged networks were imaged initially and then soaked in PBS and imaged at 2, 4, and 18 h using a Zeiss StereoLumar V12 microscope at 35x magnification.

3.3.7   Anion loading

PECs (150 mg) were placed in solutions (25 mL) containing 0.05 wt% fluorescein sodium salt, diclofenac sodium salt, ATP or paracetamol (not anionic) for 7 days to allow time for anion exchange to occur. The PECs were then taken out of solution and quickly rinsed with deionized water to remove any unbound surface molecules. The mass of encapsulated compound was then calculated for each of the PECs by using UV-visible spectroscopy at a defined wavelength to compare the initial concentration of anion in the solution to the concentration after loading the PEC. The molar absorptivities (ε, in units of L mol^{-1} cm^{-1}) determined from calibration curves were 13265 for fluorescein sodium salt (490 nm), 4493 for diclofenac sodium salt (276 nm), 6658 for ATP (260 nm), and 4087 for paracetamol (240 nm). Loading content (LC) was then calculated as:

$$LC = \frac{m_D}{m_N} \text{ x } 100\%$$

Equation 3-3

where m_D is the mass of anion encapsulated in the network and m_N is the dry mass of the network. The experiments were performed in triplicate.

3.3.8   Anion release

Anion-loaded PECs (~ 150 mg, accurately weighed) were each placed into 25 mL of PBS and incubated at 37 °C. Aliquots of 150 µL were then taken from the solutions at specific time points and transferred into 96-well plates. The absorbances of the solutions were measured on a plate reader at the appropriate wavelength for each anion (see above) to determine the concentration and thus the quantity of drug that had been released at each time point. The PBS solutions in which the PECs were incubated were changed at each time point to maintain sink conditions. To determine the percent release, the cumulative mass of drug released at each time point was divided by the total mass of encapsulated drug in the network. The experiments were performed in triplicate.

3.3.9   Rheology

PECs were prepared as described above, but after ultracentrifugation they were pressed between two Teflon sheets using a Carver 3851-0C melt press to a thickness ~1 mm. Sheets of material were then punched into thin disks with diameters of 5 cm then soaked in DI water or PBS at 37 °C for 24 h prior to testing. Viscous and elastic moduli were measured at 37 °C on an Anton Paar MCR 302 shear rheometer with a 5 cm diameter parallel plate tool (PP50). Fine grit sandpaper was affixed to the bottom plate and top plate to prevent slip when measuring the samples soaked in PBS. For samples soaked in DI water, small-amplitude oscillatory shear measurements were performed over the angular frequency range of 0.01 – 100 rad/s with a stress amplitude of 250 dyn/cm^2. For samples soaked in PBS, small-amplitude oscillatory shear measurements were performed over the angular frequency range of 0.01 – 100 rad/s with a stress amplitude of 10 dyn/cm^2. It was confirmed that these stress amplitudes were in the linear viscoelastic region (Figure B17). Sweeps from low to high frequency and from high to low frequency were each performed in duplicate to ensure reproducibility.

3.3.10   Cell toxicity assays

C2C12 mouse myoblast cells were cultured in medium consisting of 500 mL of Dulbecco's Modified Eagle's Medium (DMEM) supplemented with 10 mL of penicillin-streptomycin (1000 units/mL), 5 mL of L-Glutamine (200 mM) and 50 mL of fetal bovine serum, at 37 °C in an incubator with 5% CO_2. They were then seeded in a Nunclon 96-well U bottom transparent polystyrol plate to obtain approximately 10000 cells/well in 100 μL of culture medium. The cells were then incubated for 24 h prior to performing the assay. For the leaching assays, samples of dry hydrogel (~50 mg) were immersed in 3 mL of culture medium and incubated overnight to enable the leaching of potentially toxic species from the hydrogels over a period of 24 h.

The growth medium was then aspirated from the cells and replaced with either solutions of sodium dodecyl sulfate (SDS) in the cell culture medium at concentrations of 0.2, 0.15, 0.10, or 0.05 mg/mL, which were used as positive controls; serial 2-fold dilutions of the leachate in culture medium; serial 2-fold dilutions of the polymers in culture medium; or fresh medium as a negative control (6 wells per concentration). The cells were then

incubated at 37 °C (5% CO_2) for 24 h. The medium was again aspirated and replaced with 110 μL of fresh medium containing 0.5 mg/mL of 3-(4,5-dimethylthiazol-2-yl)-2,5-diphenyltetrazolium bromide (MTT). After 4 h of incubation (37 °C, 5% CO_2), the medium was carefully aspirated, and the purple crystals were dissolved by addition of 50 μL of spectroscopic grade dimethyl sulfoxide (DMSO). After shaking (1 s, 2 mm amp, 654 rpm), the absorbance of the wells at 540 nm was read using a Tecan M1000-Pro plate reader. The absorbance of wells prepared in the same way but without cells was subtracted as a background and the cell viability was calculated relative to wells containing cells that were exposed only to the culture medium. No (0%) cell viability was detected for cells exposed to the highest concentrations of SDS, confirming the sensitivity of the assay.

3.4   References

(1)   Li, J.; Mooney, D. J. Designing Hydrogels for Controlled Drug Delivery. *Nat. Rev. Mater.* **2016**, *1*, 1–18.

(2)   Buwalda, S. J.; Vermonden, T.; Hennink, W. E. Hydrogels for Therapeutic Delivery: Current Developments and Future Directions. *Biomacromolecules* **2017**, *18*, 316–330.

(3)   Hoare, T. R.; Kohane, D. S. Hydrogels in Drug Delivery: Progress and Challenges. *Polymer* **2008**, *49*, 1993–2007.

(4)   Wang, H.; Heilshorn, S. C. Adaptable Hydrogel Networks with Reversible Linkages for Tissue Engineering. *Adv. Mater.* **2015**, *27*, 3717–3736.

(5)   Khademhosseini, A.; Langer, R. A Decade of Progress in Tissue Engineering. *Nat. Protoc.* **2016**, *11*, 1775–1781.

(6)   Dash, A. K.; Cudworth, G. C. Therapeutic Applications of Implantable Drug Delivery Systems. *J. Pharmacol. Toxicol. Methods* **1998**, *40*, 1–12.

(7)   Lee, S. C.; Kwon, I. K.; Park, K. Hydrogels for Delivery of Bioactive Agents: A Historical Perspective. *Adv. Drug Delivery Rev.* **2013**, *65*, 17–20.

(8)   Nguyen, Q. V.; Huynh, D. P.; Park, J. H.; Lee, D. S. Injectable Polymeric Hydrogels for the Delivery of Therapeutic Agents: A Review. *Eur. Polym. J.* **2015**, *72*, 602–619.

(9)   Tellechea, A.; Silva, E. A.; Min, J.; Leal, E. C.; Auster, M. E.; Pradhan-nabzdyk, L.; Shih, W.; Mooney, D. J.; Veves, A. Alginate and DNA Gels Are Suitable Delivery Systems for Diabetic Wound Healing. *Int. J. Low. Extrem. Wounds* **2015**, *14*, 146–153.

(10)   Di, J.; Yao, S.; Ye, Y.; Cui, Z.; Yu, J.; Ghosh, T. K.; Zhu, Y.; Gu, Z. Stretch-Triggered Drug Delivery from Wearable Elastomer Films Containing Therapeutic Depots. *ACS Nano* **2015**, *9*, 9407–9415.

(11)   Sawhney, A. S.; Pathak, C. P.; Hubbell, J. A. Bioerodible Hydrogels Based on Photopolymerized Poly(Ethylene Glycol)-Co-Poly (α-Hydroxy Acid) Diacrylate Macromers. *Macromolecules* **1993**, *26*, 581–587.

(12)   Quick, D. J.; Anseth, K. S. DNA Delivery from Photocrosslinked PEG Hydrogels: Encapsulation Efficiency, Release Profiles, and DNA Quality. *J. Controlled Release* **2004**, *96*, 341–351.

(13)   Nimmo, C. M.; Owen, S. C.; Shoichet, M. S. Diels-Alder Click Cross-Linked Hyaluronic Acid Hydrogels for Tissue Engineering. *Biomacromolecules* **2011**, *12*, 824–830.

(14)   Liow, S. S.; Dou, Q.; Kai, D.; Karim, A. A.; Zhang, K.; Xu, F.; Loh, X. J. Thermogels: In Situ Gelling Biomaterial. *ACS Biomater. Sci. Eng.* **2016**, *2*, 295–316.

(15)   Moore, A. N.; Hartgerink, J. D. Self-Assembling Multidomain Peptide Nanofibers for Delivery of Bioactive Molecules and Tissue Regeneration. *Acc. Chem. Res.* **2017**, *50*, 714–722.

(16)   Lee, K. L.; Mooney, D. J. Alginate : Properties and Biomedical Applications. *Prog. Polym. Sci.* **2012**, *37*, 106–126.

(17)   Hiemstra, C.; Zhou, W.; Zhong, Z.; Wouters, M.; Feijen, J. Rapidly in Situ Forming Biodegradable Robust Hydrogels by Combining Stereocomplexation and Photopolymerization. *J. Am. Chem. Soc.* **2007**, *129*, 9918–9926.

(18)   Cheng, J.; Liu, F.; Dan, S.-; Yang, Z.; Ding, C.; Zhao, L.; Qu, X.; Gu, J.; Liu, C. Dually Responsive Injectable Hydrogel Prepared by In Situ Cross-Linking of Glycol Chitosan and Benzaldehyde-Capped PEO-PPO-PEO. *Biomacromolecules* **2010**, *11*, 1043–1051.

(19)   Boere, K. W. M.; Van Den Dikkenberg, J.; Gao, Y.; Visser, J.; Hennink, W. E.; Vermonden, T. Thermogelling and Chemoselectively Cross-Linked Hydrogels with Controlled Mechanical Properties and Degradation Behavior. *Biomacromolecules* **2015**, *16*, 2840–2851.

(20)   Silva, U. K. De; Weik, B. E.; Lapitsky, Y. Simple Preparation of Polyelectrolyte Complex Beads for the Long-Term Release of Small Molecules. *Langmuir* **2014**, *30*, 8915–8922.

(21)   Rydzek, G.; Pakdel, A.; Witecka, A.; Noorfazidah, D.; Shri, A.; Gaudie, F.; Nicolosi, V.; Mokarian-tabari, P.; Schaaf, P.; Ariga, K. PH-Responsive Saloplastics Based on Weak Polyelectrolytes: From Molecular Processes to Material Scale Properties. *Macromolecules* **2018**, *51*, 4424–4434.

(22)   Smith, R. J.; Long, C. T.; Grunlan, J. C. Transparent Polyelectrolyte Complex Thin Films with Ultralow Oxygen Transmission Rate. *Langmuir* **2018**, *34*, 11086–11091.

(23)   Mikhael, J.; Schoof, S.; Andrieu-brunsen, A.; Baier, G.; Sonja, K. Immobilization of A-Amylase in Polyelectrolyte Complexes. *J. Appl. Polym. Sci.* **2017**, *134*, 45036.

(24)   Fares, H. M.; Ghoussoub, Y. E.; Delgado, J. D.; Fu, J.; Urban, V. S.; Schleno, J. B. Scattering Neutrons along the Polyelectrolyte Complex/Coacervate Continuum. *Macromolecules* **2018**, *51*, 4945–4955.

(25)   Fu, J.; Wang, Q.; Schlenoff, J. B. Extruded Superparamagnetic Saloplastic Polyelectrolyte Nanocomposites. *Appl. Mater. Interfaces* **2015**, *7*, 895–901.

(26) Tang, J. D.; Caliari, S. R.; Lampe, K. J. Temperature-Dependent Complex Coacervation of Engineered Elastin-like Polypeptide and Hyaluronic Acid Polyelectrolytes. *Biomacromolecules* **2018**, *19*, 3925–3935.

(27) Gallardo-rivera, R.; Aguilar-santamaría, M. D. L. Á.; Silva-bermúdez, P.; García-lópez, J.; Tecante, A.; Velasquillo, C.; Román-guerrero, A. Polyelectrolyte Complex of Aloe Vera, Chitosan, and Alginate Produced Fibroblast and Lymphocyte Viabilities and Migration. *Carbohydr. Polym.* **2018**, *192*, 84–94.

(28) Laugel, N.; Betscha, C.; Winterhalter, M.; Voegel, J. C.; Schaaf, P.; Ball, V. Relationship between the Growth Regime of Polyelectrolyte Multilayers and the Polyanion/Polycation Complexation Enthalpy. *J. Phys. Chem. B* **2006**, *110*, 19443–19449.

(29) Fu, J.; Schlenoff, J. B. Driving Forces for Oppositely Charged Polyion Association in Aqueous Solutions: Enthalpic, Entropic, but Not Electrostatic. *J. Am. Chem. Soc.* **2016**, *138*, 980–990.

(30) Schlenoff, J. B.; Rmaile, A. H.; Bucur, C. B. Hydration Contributions to Association in Polyelectrolyte Multilayers and Complexes: Visualizing Hydrophobicity. *J. Am. Chem. Soc.* **2008**, *130*, 13589–13597.

(31) Schaaf, P.; Schlenoff, J. B. Saloplastics: Processing Compact Polyelectrolyte Complexes. *Adv. Mater.* **2015**, *27*, 2420–2432.

(32) Akhtar, R.; Sherratt, M. J.; Cruickshank, J. K.; Derby, B. Characterizing the Elastic Properties of Tissues. *Mater Today* **2012**, *14*, 96–105.

(33) Porcel, C. H.; Schlenoff, J. B. Compact Polyelectrolyte Complexes: "Saloplastic" Candidates for Biomaterials. *Biomacromolecules* **2009**, *10*, 2968–2975.

(34) Tirado, P.; Reisch, A.; Roger, E.; Boulmedais, F.; Jierry, L.; Lavalle, P.; Voegel, J.; Schaaf, P.; Schlenoff, J. B.; Frisch, B. Catalytic Saloplastics: Alkaline Phosphatase Immobilized and Stabilized in Compacted Polyelectrolyte Complexes. *Adv. Funct. Mater.* **2013**, *23*, 4785–4792.

(35) Al-Hariri, L. A.; Reisch, A.; Schlenoff, J. B. Exploring the Heteroatom Effect on Polyelectrolyte Multilayer Assembly: The Neglected Polyoniums. *Langmuir* **2011**, *27*, 3914–3919.

(36) Cuthbert, T. J.; Jadischke, J. J.; De Bruyn, J. R.; Ragogna, P. J.; Gillies, E. R. Self-Healing Polyphosphonium Ionic Networks. *Macromolecules* **2017**, *50*, 5253–5260.

(37) Burdick, J. A.; Prestwich, G. D. Hyaluronic Acid Hydrogels for Biomedical Applications. *Adv. Mater.* **2011**, *23*, 41–56.

(38) Stern, R.; Asari, A. A.; Sugahara, K. N. Hyaluronan Fragments: An Information-Rich System. *Eur. J. Cell Biol.* **2006**, *85*, 699–715.

(39) Costa, R. R.; Soares, D.; Reis, R. L.; Pashkuleva, I. Bioinspired Baroplastic Glycosaminoglycan Sealants for Soft Tissues. *Acta Biomater.* **2019**, *87*, 108–117.

(40) Brekke, J. H.; Scott, C. M.; Chai, Y. W.; Ulrich, C.; Sandquist, L.; Kokkoli, E.; Brien, T. D. O. A Chitosan-Hyaluronan-Based Hydrogel-Hydrocolloid Supports In Vitro Culture and Differentiation of Human Mesenchymal Stem/Stromal Cells. *Tissue Eng. Part A* **2015**, *21*, 1952–1962.

(41) Rajaram, A.; Schreyer, D. J.; Chen, D. X. B.; Rajaram, A.; Schreyer, D. J.; Chen, D. X. B. Use of the Polycation Polyethyleneimine to Improve the Physical Properties of Alginate – Hyaluronic Acid Hydrogel during Fabrication of Tissue Repair Scaffolds. *J. Biomater. Sci. Polym. Ed.* **2015**, *26*, 433–445.

(42) Lai, W.; Shum, H. C. Hypromellose-Graft-Chitosan and Its Polyelectrolyte Complex as Novel Systems for Sustained Drug Delivery. *Appl. Mater. Interfaces* **2015**, *7*, 10501–10510.

(43) Gierszewska, M.; Ostrowska-czubenko, J.; Chrzanowska, E. PH-Responsive Chitosan/ Alginate Polyelectrolyte Complex Membranes Reinforced by Tripolyphosphate. *Eur. Polym. J.* **2018**, *101*, 282–290.

(44) Chen, L.; Zheng, Y.; Feng, L.; Liu, Z.; Guo, R.; Zhang, Y. Novel Hyaluronic Acid Coated Hydrophobically Modi Fi Ed Chitosan Polyelectrolyte Complex for the Delivery of Doxorubicin. *Int. J. Biol. Macromol.* **2019**, *126*, 254–261.

(45) Harrison, T. D.; Ragogna, P. J.; Gillies, E. R. Phosphonium Hydrogels for Controlled Release of Ionic Cargo. *Chem. Commun.* **2018**, *54*, 11164–11167.

(46) Kanazawa, Akihiko; Ikeda, T. E. T. Novel Polycationic Biocides: Synthesis and Antibacterial Activity of Polymeric Phosphonium Salts. *J. Polym. Sci., Part A: Polym. Chem.* **1993**, *31*, 335–343.

(47) Tsenoglou, C. Molecular Weight Polydispersity Effects on the Viscoelasticity of Entangled Linear Polymers. *Macromolecules* **1991**, *24*, 1762–1767.

(48) Porcel, C.; Schlenoff, J. Compact Polyelectrolyte Complexes:"Saloplastic" Candidates for Biomaterials. *Biomacromolecules* **2009**, *10*, 2968–2975.

(49) Hemp, S. T.; Zhang, M.; Allen, M. H.; Cheng, S.; Moore, R. B.; Long, T. E. Comparing Ammonium and Phosphonium Polymerized Ionic Liquids: Thermal Analysis, Conductivity, and Morphology. *Macromol. Chem. Phys.* **2013**, *214*, 2099–2107.

(50) Yan, J. K.; Wang, Y. Y.; Qiu, W. Y.; Wu, J. Y. Construction and Characterization of Nanosized Curdlan Sulfate/Chitosan Polyelectrolyte Complex toward Drug Release of Zidovudine. *Carbohydr. Polym.* **2017**, *174*, 209–216.

(51) Tan, C.; Celli, B. G.; Lee, M.; Licker, J.; Abbaspourrad, A. Polyelectrolyte Complex Inclusive Biohybrid Microgels for Tailoring Delivery of Copigmented Anthocyanins. *Biomacromolecules* **2018**, *19*, 1517–1527.

(52) Lawrence, P. G.; Patil, P. S.; Leipzig, N. D.; Lapitsky, Y. Ionically Cross-Linked Polymer Networks for the Multiple-Month Release of Small Molecules. *Appl. Mater. Interfaces* **2016**, *8*, 4323–4335.

(53) *Multilayer Thin Films: Sequential Assembly of Nanocomposite Materials*, Second.; Decher, G., Schlenoff, J. B., Eds.; Wiley-VCH Verlag GmbH & Co. KGaA: Weinheim, Germany, 2012.

(54) Chen, D. T. N.; Wen, Q.; Janmey, P. A.; Crocker, J. C.; Yodh, A. G. Rheology of Soft Materials. *Annu. Rev. Condens. Matter Phys.* **2010**, *1*, 301–322.

(55) Khan, T. A.; Peh, K. K.; Seng, H. Mechanical, Bioadhesive Strength and Biological Evaluations of Chitosan Films for Wound Dressing. *J. Pharm. Pharm. Sci.* **2000**, *3*, 303–311.

(56) Cuthbert, T. J.; Harrison, T. D.; Ragogna, P. J.; Gillies, E. R. Synthesis, Properties, and Antibacterial Activity of Polyphosphonium Semi-Interpenetrating Networks. *J. Mater. Chem. B* **2016**, *4*, 4872–4883.

(57) Murata, H.; Koepsel, R. R.; Matyjaszewski, K.; Russell, A. J. Permanent, Non-Leaching Antibacterial Surface 2: How High Density Cationic Surfaces Kill Bacterial Cells. *Biomaterials* **2007**, *28*, 4870–4879.

(58) Siepmann, J.; Peppas, N. A. Higuchi Equation: Derivation, Applications, Use and Misuse. *Int. J. Pharm.* **2011**, *418*, 6–12.

(59) Ritger, P. L.; Peppas, N. A. A Simple Equation for Description of Solute Release I. Fickian and Non-Fickian Release from Non-Swellable Devices in the Form of Slabs, Spheres, Cylinders or Discs. *J. Controlled Release* **1987**, *5*, 23–36.

(60) Kenawy, E.-R.; Worley, S. D.; Broughton, R. The Chemistry and Applications of Antimicrobial Polymers: A State-of-the-Art Review. *Biomacromolecules* **2007**, *8*, 1359–1384.

(61) Martinez, J. S.; Keller, T. C. S.; Schlenoff, J. B. Cytotoxicity of Free versus Multilayered Polyelectrolytes. *Biomacromolecules* **2011**, *12*, 4063–4070.

(62) Kanazawa, A.; Ikeda, T.; Endo, T. Novel Polycationic Biocides: Synthesis and Antibacterial Activity of Polymeric Phosphonium Salts. *J. Polym. Sci., Part A: Polym. Chem.* **1993**, *31*, 335–343.

(63)   Bonduelle, C. V.; Karamdoust, S.; Gillies, E. R. Synthesis and Assembly of Butyl Rubber-Poly(Ethylene Oxide) Graft Copolymers: From Surface Patterning to Resistance to Protein Adsorption. *Macromolecules* **2011**, *44*, 6405–6415.

Chapter 4

4 Phosphonium vs. Ammonium Salt-containing Polymers – Which is Better for the Delivery of Ionic Cargo?

4.1 Introduction

Many traditional therapeutics suffer from limitations such as low patient compliance, side effects due to poor targeting and difficulty controlling dosage.[1] For example, oral administration of drugs which is a very popular approach, is limited by poor targeting and a short circulation time of less than 12 hours.[2] To address these issues, controlled drug delivery systems based on nanoparticles[3,4] micelles,[5,6] liposomes[7,8] and hydrogels[9,10] have been of interest over the past few decades. These systems have been tuned to controllably release their payload to specific areas of the body over long periods of time. Hydrogels, in particular, have been extensively explored for drug delivery and are made up of crosslinked polymer networks that have high water content and mechanical properties similar to soft tissues which can minimize inflammatory reactions of surrounding cells and tissues.[11]

Although hydrogels have found many uses in medicine, some disadvantages arise from their high swellability as the delivery of therapeutics can be hindered if the pore size is too large or there is no means to entrap and slow the release of molecules.[12] To address this issue, pore sizes can be tuned[13] and drugs can be entrapped in networks by covalent[14,15] or ionic[16,17] interactions.

While covalent bonding has been extensively employed for the preparation of hydrogels, they can also be held together though physical entanglements or ionic interactions.[18] The mixture of two oppositely charged polymers can create polyelectrolyte complexes (PECs) where the driving force for network formation is the entropic release of bound counterions[19,20] and water molecules[21] (Equation 4-1).

$$\text{Pol}^+\text{Cl}^- \bullet x\text{H}_2\text{O} + \text{Pol}^-\text{Na}^+ \bullet y\text{H}_2\text{O} \rightarrow \text{Pol}^+\text{Pol}^- \bullet i\text{H}_2\text{O} + \text{Na}^+ + \text{Cl}^- + z\text{H}_2\text{O} \qquad \text{Equation 4-1}$$

Many different polycation/ polyanion pairs have been developed for the creation of ionic networks,[22–24] for example complexes based on poly(acrylic acid)/ poly(allylamine) have been extensively studied by Schlenoff for use as self-healable materials.[18,25,26] In these materials ammonium-based polycations have been most popular while their analogous polyphoshonium salts have been less explored. Our group recently reported ionically crosslinked polymer networks prepared from poly(acrylic acid) and poly(triethyl(4-vinylbenzyl)phosphonium chloride) that were able to self-heal in physiologically relevant salt concentrations.[27] We also reported ionic networks composed of a more biologically relevant polyanion, sodium hyaluronate and four different polyphosphoniums for drug release applications.[28] These networks exhibited the ability to self-heal in less than 24 hours and had prolonged drug delivery times of 60 days, making them promising candidates for applications in the biomedical area. While ammonium and phosphonium polymers have been investigated for hydrogel formation, only one direct comparison of ammonium and phosphonium polymers in polyelectrolyte multilayer buildup has been reported[29] and to the best of our knowledge, they have not been directly compared for drug release and self-healable materials. There are many differences between ammonium and phosphonium salts that could have an effect on ionic network formation and mechanical properties. For example ammonium salts are smaller than their phosphonium analogues and also have shorter C-N (~ 1.53 A) bonds when compared to C-P (~1.81 A), which allows them to be closer to their anionic counterions.[30] Furthermore, the cationic charge distribution is more localized on phosphorus, while more delocalized through the carbons next to nitrogen.[31,32]

For biomedical applications, naturally occurring anionic polysaccharides are of significant interest. Alginates, for example, are unbranched polysaccharides which contain varying amounts of 1,4'-linked β-D-mannuronic acid (M) and α-L-guluronic acid (G) residues.[33] The residues vary in sequence and can be arranged in consecutive M residues (MMMM) or G residues (GGGG) or alternating M and G residues (MGMGMG) (Figure 4-1). Divalent Ca^{2+} ions are typically employed as the crosslinking agent to create alginate hydrogels and the mechanical properties of the hydrogels can be tuned by changing the amount of Ca^{2+} added.[33] The divalent cations are believed to bind only to the guluronate blocks of the alginate chains as the structure of these blocks allows for a high degree of

coordination of the divalent ions. The guluronate blocks of one polymer can then interact with adjacent guluronate chains in an egg-box model of crosslinking.[34] Alginate gels have been used for many different applications such as wound healing[35] and drug delivery vehicles, although as drug delivery vehicles these systems have shown relatively fast release of drugs and proteins in aqueous media.[36–38]
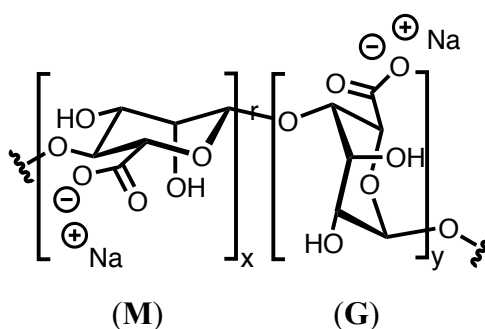

Figure 4-1 Sodium alginate polymer containing blocks of (1,4)-linked β-D-mannuronate (**M**) and α-L-guluronate (**G**) residues.

Here we report PEC hydrogels based on 5 different poly(oniums) and sodium alginate for controlled drug release. First, commercially available triethylphosphine, triethylamine, tri-*n*-butylphosphine, tributylamine and tris(hydroxypropyl)phosphine were reacted with 4-vinylbenzyl chloride to generate the corresponding polymerizable phosphonium salts **Et-P**, **Et-N**, **Bu-P**, **Bu-N**, and **Hp-P**, respectively. Each monomer was then polymerized by free-radical polymerization to generate high molar mass polymers **P-Et-P**, **P-Et-N**, **P-Bu-P**, **P-Bu-N**, and **P-Hp-P.** These polyelectrolytes were then dissolved in water and simultaneously mixed with sodium alginate to create PECs. The thermal properties, swelling, rheology and self-healing properties of the PECs were studied and compared. PECs were loaded with a dye molecule and two anionic drugs to see if the release rates would differ based on the central atom (i.e. P or N), R-groups around each quaternary pnictogen, or if drug architecture played a more dominant role.

4.2 Results and Discussion

4.2.1 Monomer and Polymer Synthesis

Monomers were prepared as previously reported by reacting triethylphosphine, triethylamine, tri(*n*-butyl)phosphine, tributylamine, tris(hydroxypropyl)phosphine, with 4-vinylbenzyl chloride to generate the corresponding salts (**Et-P**, **Et-N**, **Bu-P**, **Bu-N**, **Hp-P**; Scheme 4-1).[39–41] Tris(hydroxypropyl)amine was also reacted with 4-vinylbenzyl chloride, but the reaction did not go to completion and upon work-up the products swelled extensively and could not be purified. Polymerization of the remaining monomers was completed in water at 60 °C using the thermal initiator 2,2'-azobis[2-(2-imidazolin-2-yl)propane]dihydrochloride (VA-044) over 16 hours. Free radical polymerization was chosen over controlled radical polymerization as it could provide high molar mass polymers on a large scale. As previously reported, **Et-P**, **Bu-P**, and **Hp-P** polymerized to complete conversion and the weight-average molar masses (M_w) were 588 kg/mol for **P-Et-P**, 442 kg/mol for **P-Bu-P**, and 666 kg/mol for **P-Hp-P**.[28] The polymerization of **Et-N** yielded complete conversion (Figure C1) but the polymerization of **Bu-N** did not and the resulting polymer was purified using dialysis (Figure C2). The molar masses of **P-Et-N** (M_w = 315 kg/mol, Dispersity (*Đ*) = 2.3) and **P-Bu-N** (M_w = 220 kg/mol, *Đ* = 3.4) were characterized by size exclusion chromatography (SEC) in dimethylformamide (DMF) containing 0.4 M tetrabutylammonium triflate relative to poly(methyl methacrylate) (PMMA) standards (Figure C3).
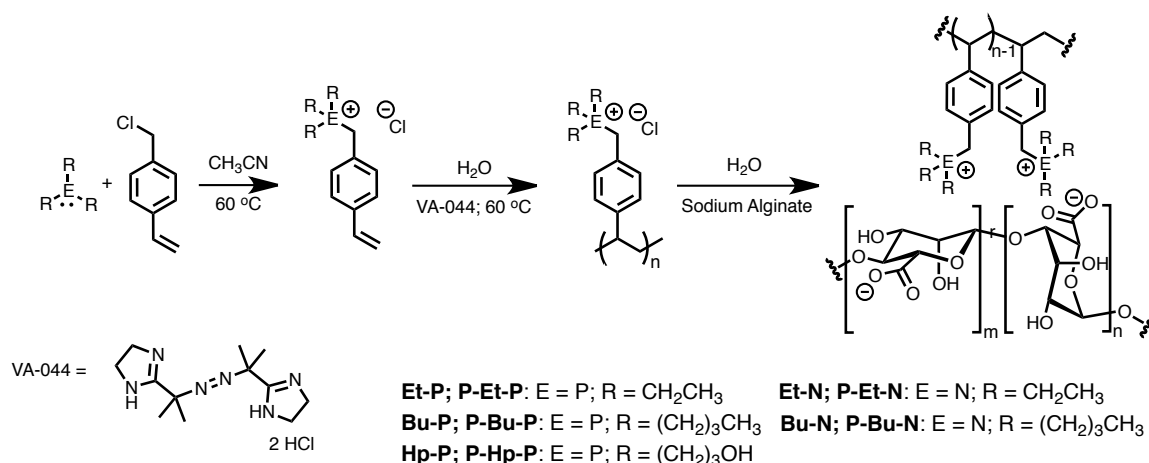
Scheme 4-1 Monomer, polymer and ionic network synthesis.

Based on thermogravimetric analysis (TGA), onset decomposition temperatures (T_o) for the phosphonium polymers ranged from 290 – 344 °C (Table 4-1; Figures C4A-6A), with that of sodium alginate at 220 °C (Figure C6B). Onset decomposition temperatures were much lower for the ammonium polymers, ranging from 184 – 275 °C (Table 4-1; Figure C4B,5B). The lower thermal stability of polyammonium salts has been well documented and can be explained by nucleophilic substitution or Hoffman elimination occurring at much lower temperatures (Scheme 4-2).[40] For polymers **P-Et-N** and **P-Bu-N**, initial mass losses of ~25 and ~50 wt% were observed at T_o, indicating a reverse nucleophilic substitution degradation pathway. For polymer **P-Hp-P**, the degradation went through a two-step mechanism that is hypothesized to be Hoffman elimination, as the initial mass loss was ~ 20 %.

Table 4-1 Polymer T_o, T_g and network T_o, T_g and carboxylate:onium ratios.

Polymers	T_o (°C)	T_g (°C)	Networks	T_o (°C)	T_g (°C)	Carboxylate: Onium Ratio
P-Et-P	328	230	**P-Et-P-Alg**	232	-	$1.44 \pm 0.15{:}1$
P-Et-N	184	-	**P-Et-N-Alg**	209	-	$2.18 \pm 0.81{:}1$
P-Bu-P	344	180	**P-Bu-P-Alg**	245	145	$1.72 \pm 0.24{:}1$
P-Bu-N	275	-	**P-Bu-N-Alg**	218	-	3.63 ± 0.80
P-Hp-P	290	115	**P-Hp-P-Alg**	246	-	$1.53 \pm 0.14{:}1$
SA	220	-				
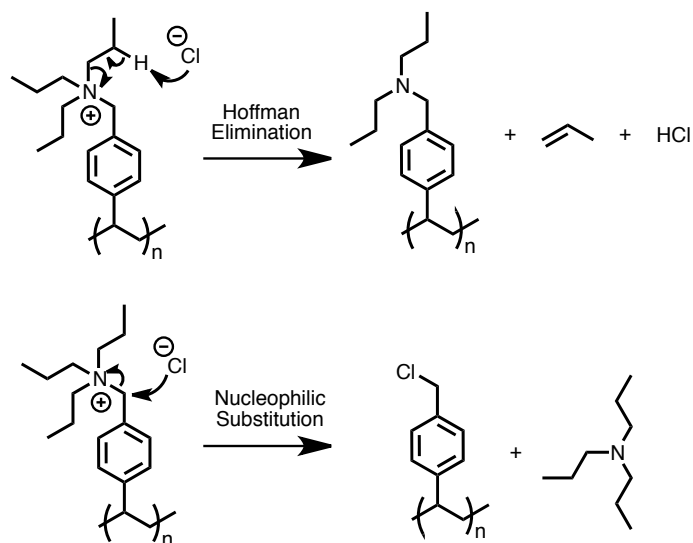
Scheme 4-2 Thermal degradation of ammonium polymers through Hoffman elimination or nucleophilic substitution.

Differential scanning calorimetry (DSC) was also performed on all polymers to determine their glass transition temperatures (T_g). T_g values of **P-Et-P**, **P-Bu-P** and **P-Hp-P** were 230, 180 and 115 °C, respectively (Table 4-1, Figures C7A-9A). **P-Et-P** had the highest T_g which could be attributed to the better packing of the polymer chains and decreased segmental motion in comparison to **P-Bu-P** and **P-Hp-P**, which have more bulky pendent groups. No T_g values of **P-Et-N** and **P-Bu-N** were observed, as they degraded thermally before reaching the T_g, in agreement with previous results for similar polymers (Figure C7B-8B).[40] Similarly, no T_g for sodium alginate was observed below its degradation temperature (Figure C9B).

4.2.2   Network Preparation and Characterization

To prepare the PECs, P or N-based polyelectrolyte and sodium alginate were dissolved separately in deionized (DI) water at a concentration of 0.1 M in terms of the ions (onium or carboxylate). Equal volumes of solution were then mixed in a 1:1 ratio of onium to carboxylate and left to stir for 30 minutes. The networks were then ultracentrifuged to compact the PEC networks[42] and the newly formed PECs **P-Et-P-Alg**, **P-Et-N-Alg**, **P-Bu-P-Alg**, **P-Bu-N-Alg**, **P-Hp-P-Alg** were then cut into pieces for characterization.

Thermal analysis was completed on the dried PEC networks (Table 4-1) which revealed that all PECs followed a two-step decomposition pathway, with the initial decomposition due to alginate at ~220 °C (Figures C10-12). DSC was also completed on all PECs, but no T_g values were observed for **P-Et-P-Alg**, **P-Et-N-Alg**, **P-Bu-N-Alg**, **P-Hp-P-Alg**, indicating the polymers were mixed well, and there was no phase separation (Figures C13-15). The T_g of **P-Bu-P-Alg** (Figure C14A) is observed at 145 °C and is attributed to phase separation of the phosphonium and alginate given the bulky substituents around phosphorus that can hinder binding.

Dry PEC networks were also analyzed by scanning electron microscopy-energy dispersive X-ray spectroscopy (SEM-EDX) to determine the ratio of carbon to phosphorus or nitrogen, and thus the ratio of poly(onium) to **Alg** as the order and rate of addition of polyelectrolytes to create PECs can affect the amount of each in the complex.[18] Atomic weight percent values of phosphorus or nitrogen relative to carbon for PECs **P-Et-P-Alg**,

P-Et-N-Alg, **P-Bu-P-Alg**, **P-Bu-N-Alg** and **P-Hp-P-Alg** were found to be 4.1 ± 0.2, 3.5 ± 0.6, 3.1 ± 0.1, 2.2 ± 0.2 and 3.6 ± 0.1, respectively. This corresponds to carboxylate:onium ratios of 1.44 ± 0.15:1, 2.18 ± 0.81:1, 1.72 ± 0.24:1, 3.6 ± 0.8:1 and 1.53 ± 0.14:1, respectively (example calculation in experimental section 4.4.5). From these values it is clear that there is excess carboxylate in all of the networks, regardless of simultaneous addition. Upon closer comparison, PECs **P-Et-P-Alg** and **P-Et-N-Alg** had very similar carboxylate:onium ratios as they were within experimental error with each other. Upon comparison of **P-Bu-P-Alg** and **P-Bu-N-Alg**, there is more carboxylate in the network of **P-Bu-N-Alg** which could result from a bigger charge distribution around nitrogen binding to more carboxylate.[32,43]

4.2.3   Network Swelling

Physical properties of PECs can be changed by the addition of salt to break ion pairs and cause disruption of the network.[44] Therefore, it was of interest to determine the stability of the PECs in solutions containing different concentrations of NaCl and PBS. Dried PECs were placed into either 0, 0.1, 0.15, 0.25 M NaCl or 0.15 M PBS with a pH of 7.4. The PECs were placed in sealed containers at 37 °C and the swelling was monitored for ~ 2 weeks (Figure 4-2). As expected, swelling varied based on the concentration of salt in solution and polymer composition. At 0 M, all PECs swelled rapidly, turned white, and fragmented within a few hours. This phenomenon has been reported previously and can be attributed to the pores growing rapidly in water to a point where they become so big, they destroy the integrity of the PEC.[45] In addition, all of the PECs, except for **P-Hp-P-Alg**, that were swelled in 0.25 M NaCl disintegrated over the first few hours and could not be measured further. This was expected, as high salt concentrations have led to PEC degradation in related systems.[41] The additional hydrogen bonding in PEC **P-Hp-P-Alg**, most likely aided in the prolonged stability in 0.25 M NaCl for 6 days. In 0.1 M NaCl, **P-Et-P-Alg** swelled to ~250 % and **P-Et-N-Alg** swelled to ~230 % after 24 h and remained relatively stable. At the same concentration, **P-Bu-P-Alg** swelled to ~220% and **P-Bu-N-Alg** only swelled to ~170 %. In 0.15 M NaCl and 0.15 M PBS, **P-Et-P-Alg** swelled to ~ 300% where **P-Et-N-Alg** swelled to only 250 %, indicating that the networks containing phosphonium swelled to a higher degree. This trend was also seen in **P-Bu-P-Alg** and **P-**

Bu-N-Alg where **P-Bu-P-Alg** swelled to ~ 310 % in comparison to **P-Bu-N-Alg** only swelled to ~230 %. **P-Et-P-Alg** and **P-Bu-P-Alg** swelled the highest in 0.1, 0.15 M NaCl and 0.15 M PBS, which could be due to the disruption of the more localized charge on phosphorus. PEC **P-Hp-P-Alg** swelled the least at all salt concentrations, which could be a result of the added hydrogen bonding keeping the network packed tighter and allowing less water to inflate. Swelling of all PECs in 0.1, 0.15 M NaCl and in 0.15 M PBS (pH – 7.4) remained stable over ~ 16 days. Most importantly, the PECs were stable in 0.15 M PBS which will later be used as a drug release medium as it mimics the pH and salt concentration of the human body.
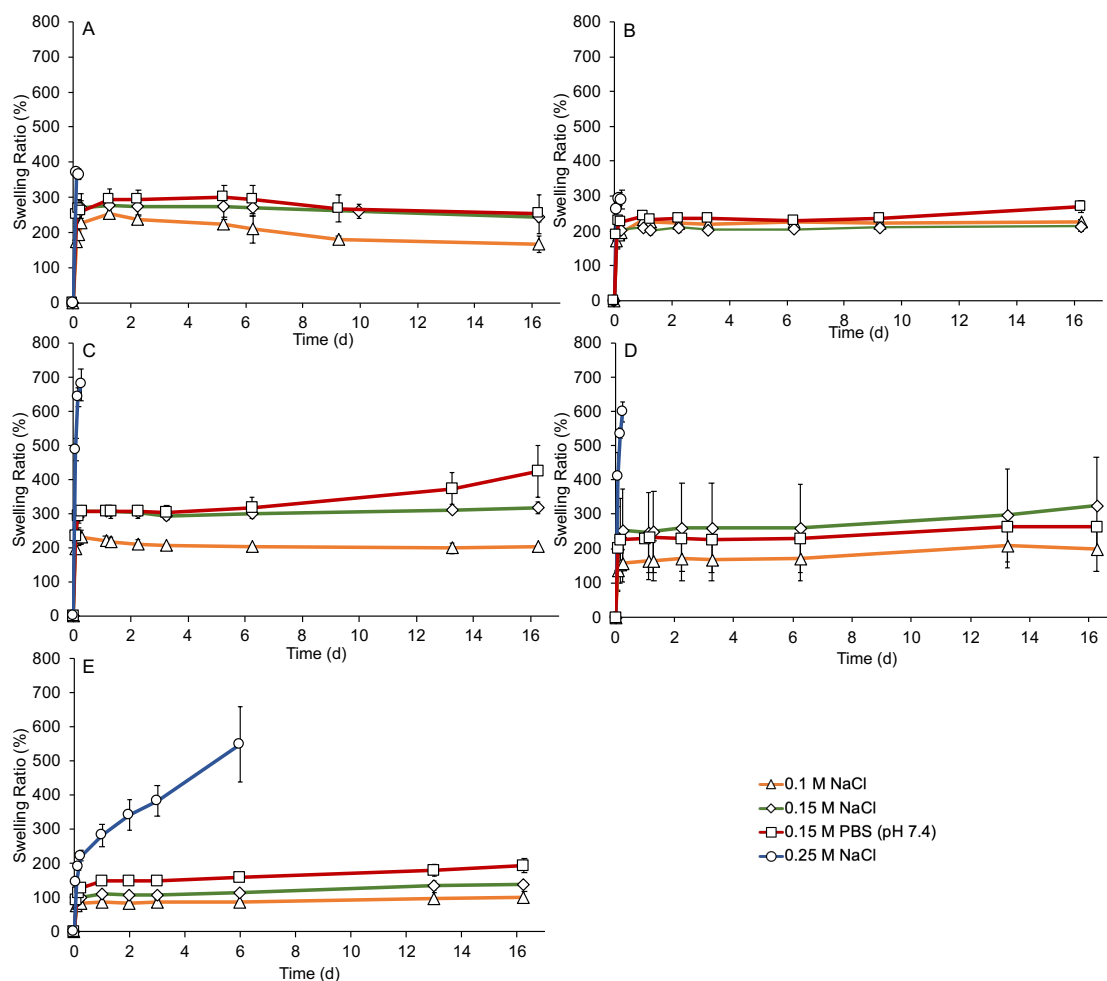
Figure 4-2 Swelling (wt%) of PECs relative to the dry state: A) **P-Et-P-Alg**; B) **P-Et-N-Alg**; C) **P-Bu-P-Alg**; D) **P-Bu-N-Alg**; and E) **P-Hp-P-Alg**. Swelling depended on the salt concentration and network composition. **P-Et-P-Alg**, **P-Et-N-Alg**, **P-Bu-P-Alg** and **P-Bu-N-Alg** disintegrated at 0.25 M NaCl after ~ 6 hours and **P-Hp-P-Alg** disintegrated after 6 days. Error bars correspond to standard deviations (N = 3).

4.2.4 SEM Images of Network Structure

The structures of the PEC networks in the dry state were examined by SEM. The PECs were swelled in PBS and their porosity can be seen (Figure 4-3). Generally, the porosities are highest for PECs **P-Bu-P-Alg** and **P-Bu-N-Alg**, followed by **P-Hp-P-Alg** then **P-Et-P-Alg** and **P-Et-N-Alg**. However, caution must be taken in interpreting these results as changes in morphology and artifacts can occur as a result of drying the samples for SEM.
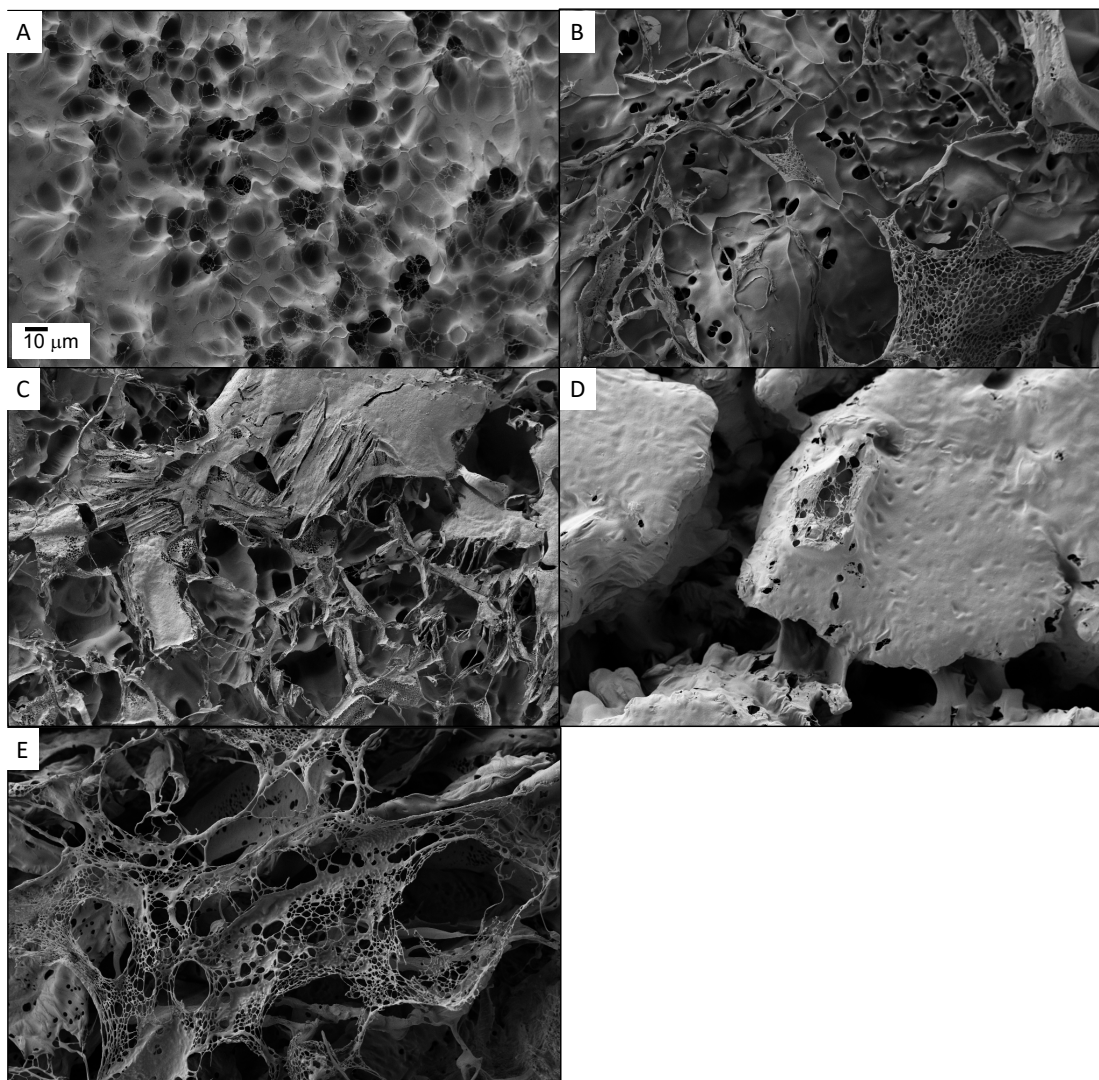
Figure 4-3 SEM images of PECs A) **P-Et-P-Alg;** B) **P-Et-N-Alg;** C) **P-Bu-P-Alg;** D) **P-Bu-N-Alg**; and E) **P-Hp-P-Alg.** Samples were prepared by the lyophilization of gels that were swelled in PBS for 24 h then soaked in DI water for 1 min to remove surface salts, followed by coating with 5 nm of osmium.

4.2.5   Rheology

Rheology can provide information on the time scale of network relaxation and on the viscoelastic behavior of polymeric systems.[46] Depending on the degree of crosslinking as well as other aspects of a network, the material's viscous and elastic response to an applied force can be drastically different. The viscous (G") and elastic (G') moduli of the PECs, swelled in PBS were characterized over a frequency range of 0.01 to 100 rad s^{-1} with an

applied stress of 100 dyn cm^{-1} (Figure 4-4). All PECs had elastic moduli values ranging from 0.04 – 20.00 kPa and viscous moduli from 0.07 - 6.00 kPa. **P-Et-P-Alg** and **P-Et-N-Alg** had crossover frequencies of 0.063 and 0.251 rad/s, respectively, corresponding to relaxation times of 16 and 4 s. The longer relaxation time of phosphonium containing network indicates stronger bonding of the phosphonium to the alginate in this network. **P-Bu-P-Alg** and **P-Bu-N-Alg** had the lowest (G") and (G') compared to all the other networks, with crossover frequencies of 0.40 rad/s and a relaxation time of 2.5 s. The short relaxation time of both of these networks could be due to the more hindered binding of the onium and carboxylate as both oniums contain bulky butyl groups. **P-Hp-P-Alg** did not cross over in the measured frequency range, suggesting a relaxation time of longer than 100 s due to strong bonding in this network. This longer relaxation time may also result from its lower degree of swelling relative to all other networks.
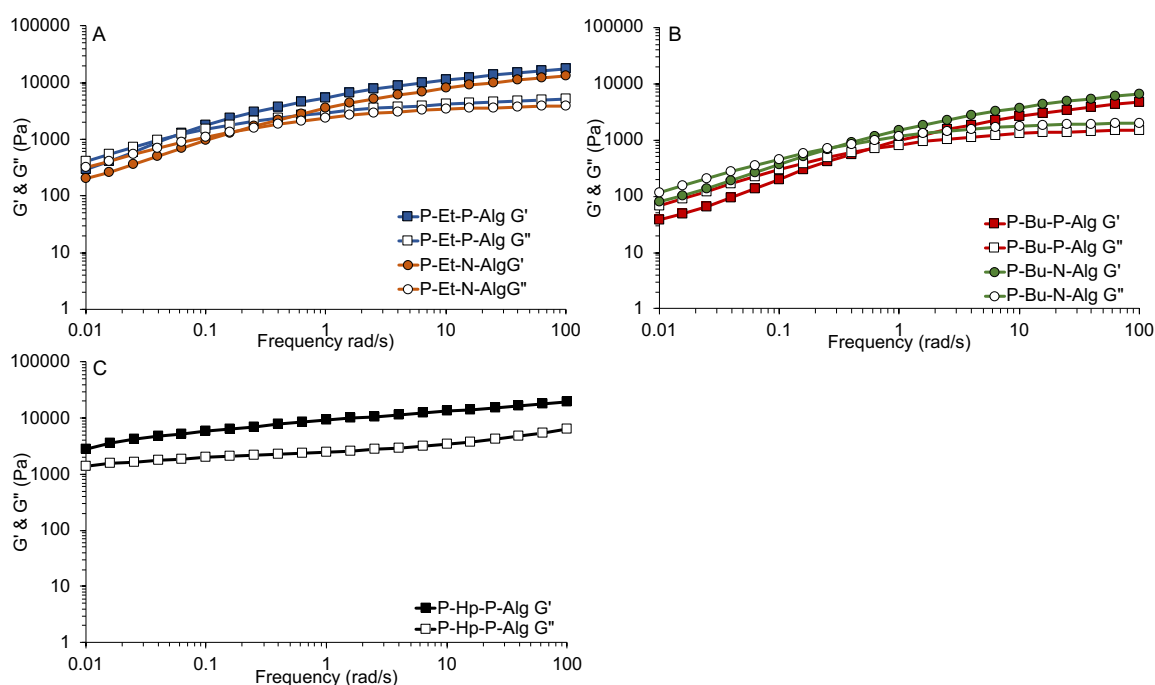

Figure 4-4 Rheology frequency sweeps for (A) **P-Et-P-Alg**, **P-Et-N-Alg**; (B) **P-Bu-P-Alg**, **P-Bu-N-Alg**; and (C) **P-Hp-P-Alg** in PBS. Data points are means of four measurements at each frequency, and the error bars are standard deviations.

4.2.6   Self-Healing

The ability of the PECs to self-heal was studied qualitatively after damage by boring a 0.5 mm hole, then incubating in PBS at 37 °C for 48 h (Figure 4-5). After 24 h, the only networks to fully heal were **P-Et-P-Alg** and **P-Bu-P-Alg**. After 48 h, **P-Et-N-Alg** had fully healed but **P-Bu-N-Alg** and **P-Hp-P-Alg** had not. **P-Hp-P-Alg** networks had the longest healing time, with damage still detected after 48 h. This may correlate with the long relaxation time of the network as indicated by rheology, its high viscous modulus and high M_w. The ability of most networks to heal indicated that ionic bonding is dynamic.
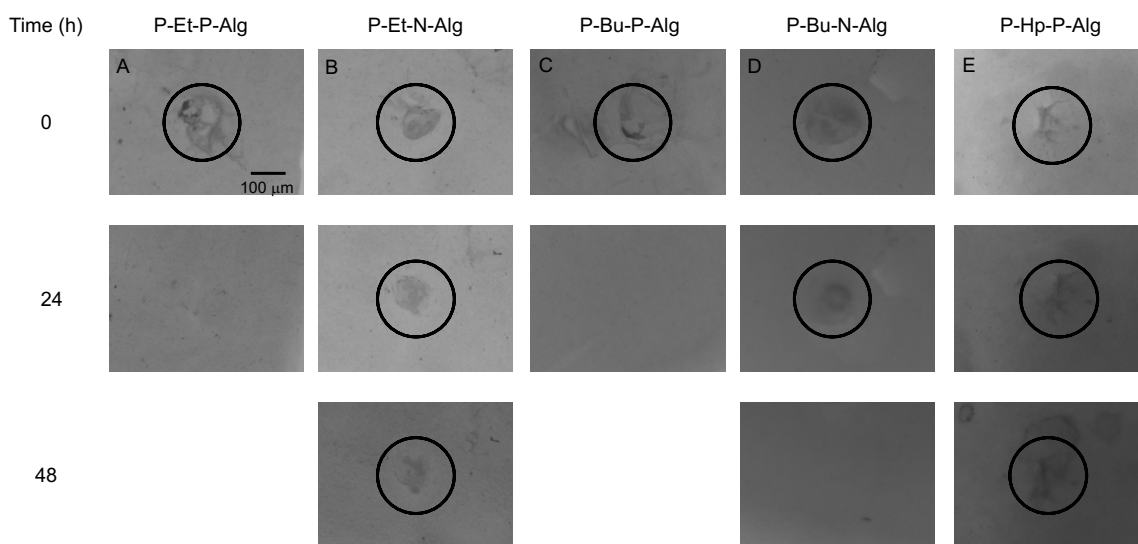
Figure 4-5 Digital images of PECs damaged by a 0.5 mm diameter hole, as indicated in the black circles, then healing over 48 h in PBS at 37 °C: (A) **P-Et-P-Alg**, (B) **P-Et-N-Alg**, (C) **P-Bu-P-Alg**, (D) **P-Bu-N-Alg**, (E) **P-Hp-P-Alg**.

4.2.7   Loading and Release Studies

The loading and release of three different anionic molecules was probed. Each PEC was loaded with the salts of fluorescein, etodolac or methotrexate (Figure 4-6) at concentrations of 0.05 wt% in 0.1 M NaCl and the loading capacity (LC, weight % relative to polymer) and encapsulation efficiency (EE) were calculated (Table 4-2).
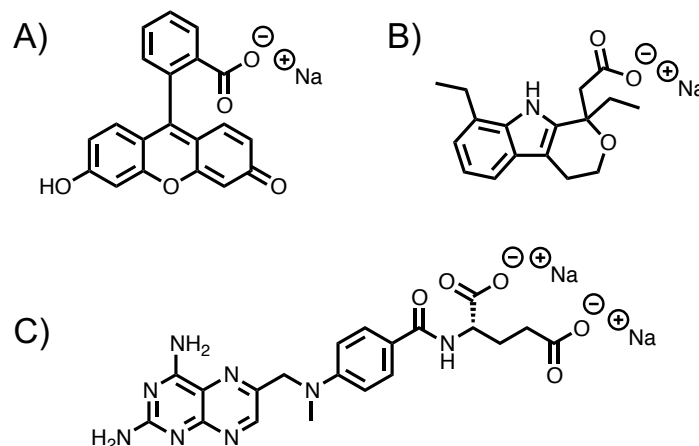
Figure 4-6 Molecules chosen for loading: (a) fluorescein sodium salt; (b) etodolac sodium salt and (c) methotrexate disodium salt

Table 4-2 Loading capacity and encapsulation efficiency of fluorescein, etodolac and methotrexate into PECs **P-Et-P-Alg**, **P-Et-N-Alg**, **P-Bu-P-Alg**, **P-Bu-N-Alg** and **P-Hp-P-Alg**.

	Fluorescein		Etodolac		Methotrexate	
	LC (%)	EE (%)	LC (%)	EE (%)	LC (%)	EE (%)
P-Et-P-Alg	12.1 ± 0.1	93.3 ± 0.1	14.3 ± 0.1	79.5 ± 0.8	11.7 ± 0.2	66.7 ± 0.9
P-Et-N-Alg	11.7 ± 0.1	90.3 ± 0.5	13.3 ± 0.1	74.1 ± 0.7	12.4 ± 0.1	70.6 ± 0.6
P-Bu-P-Alg	11.2 ± 0.4	84.1 ± 0.5	14.6 ± 0.1	81.2 ± 0.3	7.1 ± 0.2	40.4 ± 1.1
P-Bu-N-Alg	10.9 ± 0.1	84.2 ± 0.9	14.0 ± 0.1	78.0 ± 0.3	8.5 ± 0.2	48.3 ± 1.2
P-Hp-P-Alg	11.1 ± 0.3	85.9 ± 2.4	8.0 ± 0.8	44.5 ± 4.7	5.1 ± 0.2	29.0 ± 1.3

The loading of fluorescein in **P-Et-P-Alg** (~12.1 %) was significantly different, but close to that of **P-Et-N-Alg** (~11.7 %) and these networks yielded the highest loading of fluorescein of all the PECs. The loadings of **P-Bu-P-Alg** (~11.2 %) and **P-Bu-N-Alg** (~10.9 %), were similar and not significantly different, indicating similar affinity for

fluorescein. The LC of **P-Hp-P-Alg** (~11.1 %) was also very similar to the other PECs. Overall, the loading of fluorescein in all PECs was very similar, indicating that loading did not depend heavily on the onium structure.

The LC for etodolac was then probed. The loadings of **P-Et-P-Alg** (~14.3 %) and **P-Et-N-Alg** (~13.3 %) were high, but slightly lower when compared to the LC of **P-Bu-P-Alg** (~14.6 %) and **P-Bu-N-Alg** (~14.0 %), as there could be a more favourable hydrophobic interaction with the butyl substituents. Interestingly, the loading of **P-Hp-P-Alg** with etodolac was very low (~8.0 %). This could again be due to the hydrophobicity associated with etodolac and its lack of hydrophobic interactions with the more hydrophilic polymer **P-Hp-P**.

For methotrexate, the LC of **P-Et-N-Alg** (~12.4 %) was higher but very similar to that of **P-Et-P-Alg** (~11.7 %). These two PECs had the highest loadings of methotrexate, which could be attributed to the closer binding of methotrexate to the onium. The LC of **P-Bu-N-Alg** (~8.5 %) was also higher but similar to that of **P-Bu-P-Alg** (~7.1 %). The loading of methotrexate in these PECs was significantly lower than **P-Et-N-Alg** and **P-Et-P-Alg** which could be due to the added steric bulk. Finally, the LC of **P-Hp-P-Alg** was very low (~5.1 %), indicating again the increased steric bulk and hydrophilicity of this network could cause lower loading.

Release of the molecules from the networks was studied in PBS at 37 °C. The release of fluorescein ranged from 30 – 100 % in the first 8 days (Figure 4-7A, C17A). The fastest release occurred from **P-Bu-P-Alg** (~100 %) and **P-Bu-N-Alg** (~90 %), followed by **P-Hp-P-Alg** (~50 %) and **P-Et-P-Alg** (~50 %) and **P-Et-N-Alg** (~30 %). Although, very similar loading capacities were obtained for all networks, the fastest release of fluorescein was from the networks containing the butyl substituents. This could be due to the bulkiness associated with these oniums hindering the strong binding of fluorescein. The release of the etodolac (Figure 4-7B, C17B) was much faster than that of fluorescein from all of the networks. 100 % release from networks **P-Bu-P-Alg** and **P-Bu-N-Alg** was reached in 4 days at very similar rates. 80% release of etodolac was reached in 8 days from **P-Hp-P-Alg**, **P-Et-P-Alg** and **P-Et-N-Alg**. The release of methotrexate disodium salt (Figure 4-7C,

C17C) followed the same trends as that of etodolac, with the fastest from **P-Bu-P-Alg** and **P-Bu-N-Alg**. This was followed by **P-Hp-P-Alg** and **P-Et-P-Alg**, and **P-Et-N-Alg**.

The overall release rates from the networks were fastest from substituents butyl>hydroxypropyl>ethyl and can be tuned by changing the substituent on the onium and that atom, (N or P) actually does not have a large impact. The SEM images (Figure 4-3) suggest that the pore sizes are highest for **P-Bu-P-Alg**, **P-Bu-N-Alg**, followed by **P-Hp-P-Alg** then **P-Et-P-Alg**, **P-Et-N-Alg**, aligning with fastest release rates coming from networks with the bigger pore sizes. In comparison to our previous system involving poly(phosphonium)s complexed with hyaluronate[28] the rate of release from this system is much more rapid. In phosphonium/hyaluronate system, fluorescein had the most sustained release of over 60 days which was attributed to hydrophobic and ionic interactions with the networks. In this system, release of fluorescein is much faster suggesting that choice of polysaccharide can affect network properties and release rates. Upon comparison of the release of fluorescein to etodolac and methotrexate in this system, it is more sustained, indicating that hydrophobic and ionic interactions between the drugs and the networks is important for achieving slow delivery.
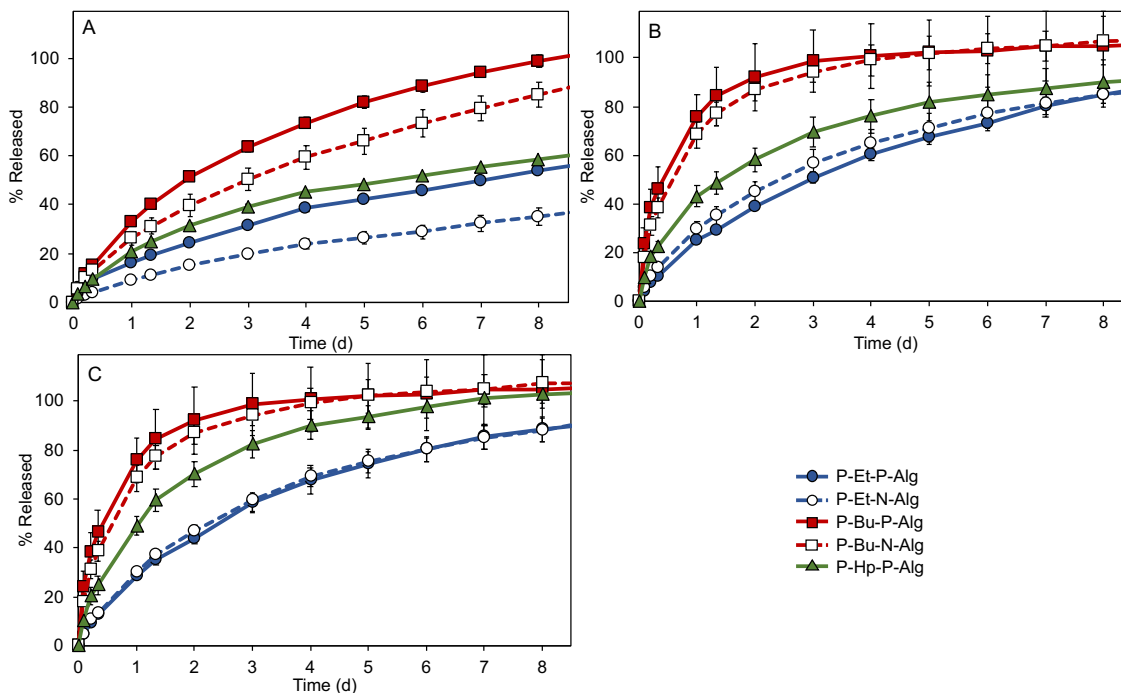
Figure 4-7 Release curves of A) fluorescein sodium salt, B) etodolac sodium salt, C) methotrexate sodium salt. Error bars correspond to the standard deviations (N = 3).

The anion release kinetics of fluorescein, etodolac and methotrexate, up to the time of 60% anion release, were fit to the Korsmeyer-Peppas equation $M_t/M_\infty = kt^n$ where M_t is the amount of drug released at time t, M_∞ is the amount of drug released as time approaches infinity, k is a constant, and n is the diffusional exponent, which can indicate the transport mechanism (Figure C18).[47] Values of n ranged from 0.50 – 0.71 for all release kinetics. Although approaching the value of 0.45 expected for pure Fickian release from disks,[48] they fell in the range expected for anomalous transport, which can likely be attributed to their complex interactions with the PEC networks, as well as network swelling and possible degradation during the experiment. Overall, the slow release of fluorescein, etodolac and methotrexate from our networks relative to previously reported systems can likely be attributed to the combination of ionic and hydrophobic interactions with the polymers in the network as well as the dense structure of the PECs that was achieved through ultracentrifugation.

4.2.8   *In Vitro* Toxicity Assays

The probe the toxicity of the PECs, a -(4,5-dimethylthiazol-2-yl)-2,5-diphenyl- tetrazolium bromide (MTT) assay was performed using various concentrations of PEC leachate to assess the cytotoxicity of molecules that could diffuse out of the networks to C2C12 mouse myoblast cells. The assay was performed to access cell metabolic activity after incubation with the leachate for 24 h. High cell metabolic activity (> 80 %) for **P-Bu-P-Alg**, **P-Bu-N-Alg** and **P-Hp-P-Alg** was retained, indicating these networks did not leach toxic species. **P-Et-P-Alg** and **P-Et-N-Alg** had metabolic activities of 56 and 27 % respectively, indicating that most likely some onium polymers were leaching into the culture medium (Figure 4-8).
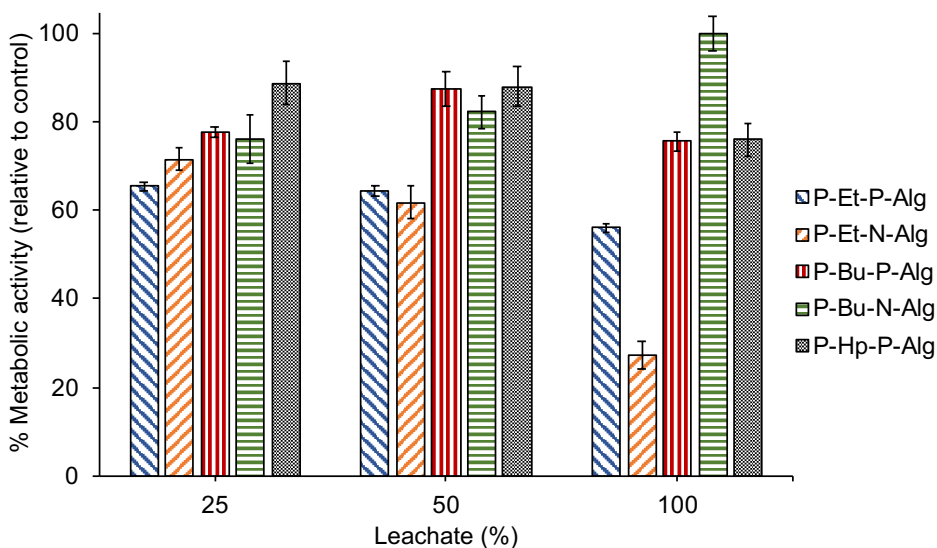
Figure 4-8 C2C12 metabolic activities measured by MTT assays on C2C12 cells incubated in culture medium that was exposed to the different PEC networks. 100% metabolic activity corresponds to cells incubated in media that was not exposed to PEC. Error bars correspond to standard error on six measurements.

Cytotoxicities of the polymers were studied by incubation with C2C12 cells for 24 hours then performing MTT assays. Cytotoxicity of **P-Et-P**, **P-Bu-P** and **P-Hp-P** have previously been reported to have low metabolic activities above 63 µg/mL and are shown here for comparison (Figure 4-9).[28] **P-Bu-N** also has low metabolic activities above 63 µg/mL, similar to the phosphoniums, but **P-Et-N** has an even lower metabolic activities

above 30 µg/mL. The very low metabolic activity of **P-Et-N** could explain network toxicity of **P-Et-N-Alg**, as very low concentrations of **P-Et-N** leaching can be toxic. The lower metabolic activity of **P-Et-P-Alg** could be due to it containing one of lowest ratios of carboxylate:phosphonium (1.44 $\pm$ 0.15:1) indicating there is higher amounts of **P-Et-P** in this network. This higher amount of **P-Et-P** could leach out more easily and cause a lower metabolic activity. Upon comparing toxicities of **P-Bu-P**, **P-Bu-N** and **P-Hp-P** to their respective networks, the polymers are much less toxic when complexed with alginate, which aligns with previously results in a study where toxicities of cationic ammonium polyelectrolytes were reduced upon complexation with polyanions.[49]
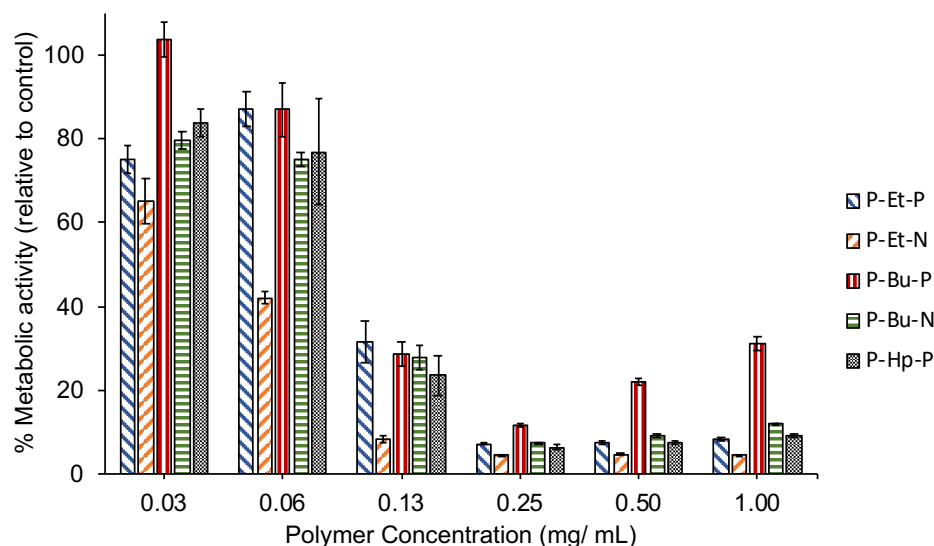
Figure 4-9 C2C12 metabolic activities measured by MTT assays on C2C12 cells incubated with varying concentrations of polymers dissolved in culture medium. 100% metabolic activity corresponds to cells incubated in media that was not exposed to PEC. Error bars correspond to the standard error (N = 6). C2C12 metabolic activities incubated with polymers **P-Et-P**, **P-Bu-P** and **P-Hp-P** were reported previously[28] but are reported here for comparison.

4.3   Conclusions

PECs were prepared by mixing phosphonium and ammonium polymers with sodium alginate, and then were ultracentrifuged to create compact networks. Network properties were characterized by swelling and viscoelastic moduli as measured from rheology. **P-Hp-P-Alg** networks yielded the lowest swelling and longest relaxation times, most likely due to the additional hydrogen bonding in these networks. **P-Bu-P-Alg** and **P-Bu-N-Alg** networks had the lowest relaxation times of 2.5 s, which could be attributed to the more loosely bonded network, compared to **P-Et-P-Alg** and **P-Et-N-Alg**, which both had longer times. Qualitative self-healing tests showed that **P-Hp-P-Alg** and **P-Et-N-Alg** did not fully heal over 48 h, but both **P-Et-P-Alg** and **P-Bu-P-Alg** healed after 24 hours, most likely due to the shorter relaxation times. Loading of all networks with the salts of fluorescein, etodolac and methotrexate was completed. The loading of fluorescein in all networks were very similar, indicating that loading did not depend heavily on the onium structure. The loadings for etodolac was very similar for all expect for **P-Hp-P-Alg**, which could be attributed to the more hydrophilic nature of **P-Hp-P** and hydrophobic nature of etodolac. The loadings for methotrexate were highest for **P-Et-P-Alg** and **P-Et-N-Alg** and lower for **P-Bu-P-Alg**, **P-Bu-N-Alg** and **P-Hp-P-Alg** indicating that the more sterically bulky networks could have more trouble binding with methotrexate. The release rate of all drugs from the polyonium and alginate system was completed and occurred over 1 week. This was much quicker compared to the networks consisting of phosphonium and hyaluronate, which had sustained delivery for up to 2 months. Fluorescein dye was the only anionic molecule used in both studies and due to its quick release from the polyphosphonium/ alginate networks and long sustained release from the phosphonium/hyaluronate network, it can be concluded that the chosen anionic polysaccharide does affect release rates. The release of the three anionic molecules from the polyonium and alginate networks also depended on the structure of each onium and not the identity of nitrogen or phosphorus. The release rates for all molecules were fastest from **P-Bu-P-Alg**, **P-Bu-N-Alg** followed by **P-Hp-P-Alg** and then **P-Et-P-Alg**, **P-Et-N-Alg**. Network images as characterized by SEM, showed the biggest pore sizes for **P-Bu-P-Alg**, **P-Bu-N-Alg** followed by **P-Hp-P-Alg** and then **P-Et-P-Alg**, **P-Et-N-Alg** which could be the reason for the faster release from **P-Bu-P-Alg**, **P-Bu-N-Alg**, although caution must be taken in interpreting these results as

changes in morphology and artifacts can occur as a result of drying the samples for SEM. Fluorescein released at the slowest of all the molecules which could be attributed to its ionic and more hydrophobic interactions with the networks. *In vitro* cytotoxicity studies suggested that networks **P-Bu-P-Alg**, **P-Bu-N-Alg** and **P-Et-P-Alg** did not leach toxic species into the cell culture media, whereas **P-Et-P-Alg** and **P-Et-N-Alg** did which could be attributed to the higher toxicity of **P-Et-N** in comparison to all other polymers and also to the higher ration of **P-Et-P** to carboxylate in **P-Et-P-Alg**.

4.4   Experimental

4.4.1   General Materials

Triethyl(4-vinylbenzyl)phosphonium chloride (**Et-P**), Triethyl(4-vinylbenzyl)ammonium chloride (**Et-N**), tri-*n*-butyl(4-vinylbenzyl)phosphonium chloride (**Bu-P**), tributyl(4-vinylbenzyl)ammonium chloride (**Bu-N**) and tris(hydroxypropyl)(4-vinylbenzyl)phosphonium chloride (**Hp-P**) were synthesized as previously reported.[40,41] Poly(triethyl(4-vinylbenzyl)phosphonium chloride) (**P-Et-P**), poly(tri-*n*-butyl (4-vinylbenzyl)phosphonium chloride) (**P-Bu-P**) and poly(tris(hydroxypropyl)(4-vinylbenzyl)phosphonium chloride) (**P-Hp-P**) were also synthesized as previously reported.[28] Triethylamine, tributylamine, 4-vinylbenzyl chloride, fluorescein sodium salt and D_2O were purchased from Sigma Aldrich and used as received. Sodium alginate – low viscosity was purchased from Carbosynth and used as received. Phosphines were donated by Solvay (Niagara Falls, ON, Canada) and used as received. Etodolac and methotrexate were purchased from Ontario Chemicals Inc. and used as received. Phosphate buffered saline contained 137 mM NaCl, 2.7 mM KCl, 10 mM Na_2HPO_4, and 1.8 mM KH_2PO_4 with a pH of 7.4.

4.4.2   General Methods

Differential scanning calorimetry (DSC) was performed on a DSC Q20 from TA Instruments (Waters, New Castle, DE) at a ramp rate of 10 °C min^{-1} under an N_2 atmosphere in an aluminum T_{zero} pan using 5−10 mg of sample. Thermogravimetric analysis (TGA) was completed on a Q600 SDT TA Instruments and analyzed at a ramp rate of 10 °C min^{-1} up to 800 °C using a ceramic pan with 5−10 mg of sample. Nuclear

Magnetic Resonance (NMR) spectroscopy was conducted on a Bruker AvIII HD 400 MHz Spectrometer (^{1}H 400.08 MHz, ^{31}P{^{1}H} 161.82 MHz). All ^{1}H spectra were referenced relative to the residual solvent peak (H$_2$O: ^{1}H d = 4.79). All ^{31}P{^{1}H} NMR spectra were referenced using an external standard (85% H$_3$PO$_4$: ^{31}P d = 0). UV-visible spectroscopy was conducted on a Tecan Infinite M1000 Pro plate reader. Costar 96 well UV plates (#3635) with UV transparent flat bottoms were used. Scanning electron microscopy was performed in the University of Western Ontario's Nanofabrication Facility using a LEO 1540XB instrument, operating at 1.0 kV and a working distance of ~ 4 mm. Samples were prepared by soaking in PBS for 24 h, rinsing with DI water, freezing, then lyophilizing. Samples were mounted to stubs covered in carbon tape and coated in 7 nm osmium using a SPI Supplies, OC-60A plasma coater. Energy dispersive X-ray spectroscopy (EDX) was also performed on the same instrument. Samples were analyzed at an accelerating voltage of 20 kV and analyzed by EDX analysis using an INCA EDAX system and software. Size exclusion chromatography (SEC) of the polymers was performed using a Malvern Viscotek GPCmax instrument equipped with a Viscotek VE 3580 RI detector and two Inert series columns (P101609 and Q10183) at a constant temperature of 50 °C. The eluent was 0.4 M tetrabutylammonium triflate in N,N-dimethylformamide (DMF) with a flow rate of 1 mL/min. Calibration was performed using poly(methyl methacrylate) (PMMA) standards to determine the number average molar mass (M_n), weight average molar mass (M_w), and dispersity (Đ).Rheological measurements were carried out at 37 °C on an Anton Paar MCR 302 shear rheometer with a 50 mm diameter parallel plate tool (PP50).

4.4.3   Polymer Synthesis

Synthesis of poly(triethyl(4-vinylbenzyl)ammonium chloride) (P-Et-N).

Et-N (10.2 g, 40.18 mmol), 2,2'-azobis[2-(2-imidazolin-2-yl)propane]dihydrochloride (VA-044) (65.0 mg, 0.20 mmol) and deionized water (205 mL) were combined in a round bottom flask with a stir bar, and the flask was sealed with Teflon tape. N$_2$ was bubbled through the solution using a needle with stirring at room temperature for 30 min to degas the reaction mixture. The reaction mixture was then heated at 60 °C for 16 h. The solvent was then removed by lyophilization. No further purification was necessary as no monomer peaks were visible in the resulting ^{1}H NMR. Yield = 9.90 g, 97 %. ^{1}H NMR (400.08 MHz,

D$_2$O) δ: 1.18 (broad s, 12 H, N-(CH$_2$)-C$\underline{H}_3$, backbone C$\underline{H}_2$ and C$\underline{H}$), 3.03 (broad s, 6 H, N-C$\underline{H}_2$-CH$_3$), 4.24 (broad s, 2H, Ar-C$\underline{H}_2$-N), 6.55 (broad s, 2H, Ar–H), 7.20 (broad s, 2H, Ar–H). $T_g =$ none, $T_{o, 3\%} =$ 184 °C; SEC: $M_n =$ 136 kg/ mol, $M_w =$ 315 kg/mol, $Đ = 2.3$.

Synthesis of poly(tri-*n*-butyl(4-vinylbenzyl)ammonium chloride) (P-Bu-N).

Bu-N (9.60 g, 28.30 mmol), 2,2'-Azobis[2-(2-imidazolin-2-yl)propane]dihydrochloride (VA-044) (46.0 mg, 0.14 mmol) and deionized water (190 mL) were combined in a round bottom flask with a stir bar, and the flask was sealed with Teflon tape. N$_2$ was bubbled through the solution using a needle with stirring at room temperature for 30 min to degas the reaction mixture. The reaction mixture was then heated at 60 °C for 16 h. The reaction mixture was then dialyzed using 3.5 kg mol^{-1} molar mass cutoff (MWCO) membrane against 1 L of DI water for 48 h, changing the DI water once, half way through. Yield = 9.00 g, 94 %. ^{1}H NMR (400.08 MHz, D$_2$O) δ: 0.79 (broad s, 11 H, N-(CH$_2$)$_3$-C$\underline{H}_3$ and backbone C$\underline{H}_2$), 1.19 (broad s, 7 H, N-(CH$_2$)$_2$-C$\underline{H}_2$-CH$_3$ and backbone CH), 1.57 (broad s, 6 H, N-CH$_2$-C$\underline{H}_2$-CH$_2$-CH$_3$), 2.94 (broad s, 6 H, N-C$\underline{H}_2$-(CH$_2$)$_2$-CH$_3$), 4.35 (broad s, 2H, Ar-C$\underline{H}_2$-N), 6.55 (broad s, Ar–H), 7.24 (broad s, Ar–H). $T_g =$ none, $T_{o, 3\%} =$ 275 °C; SEC: $M_n =$ 63 kg/ mol, $M_w =$ 218 kg/mol, $Đ = 3.5$.

4.4.4   Ionic Network Preparation

Phosphonium or ammonium polymer and sodium alginate were dissolved separately in deionized (DI) water at concentrations of 0.1 M in terms of the ions. With vigorous stirring, each of the solutions were combined into a large beaker and left to stir for 30 minutes. The liquid was then decanted leaving polymer network. The polymer network was then packed into ultracentrifuge tubes and centrifuged for one hour at 187,000 *g*. The networks were removed from the tubes and cut into narrow pellets and dried until a constant weight was obtained.

4.4.5 Procedure for the Calculation of Phosphorus Content using SEM-EDX

Samples **P-Et-P-Alg**, **P-Bu-P-Alg** and **P-Hp-P-Alg** were mounted on carbon tabs and coated with 5 nm of osmium. SEM-EDX analysis was completed to determine carbon and phosphorus atomic %, in triplicate. For each sample, the measured atomic % of phosphorus relative to that of carbon could be converted to a carboxylate:phosphonium ratio knowing that each phosphonium monomer contains x C and 1 P atom, while the carboxylate monomer contains 6 C atoms. For example, the expected atomic phosphorus % relative to carbon for different ratios is summarized in the following table for complex **P-Et-P-Alg**:

Table 4-3 Expected atomic P % relative to C for different ratios for **P-Et-P-Alg**.

Stoichiometry of carboxylate: phosphonium monomers	Total C & P atoms in the given ratio	Atomic % of P relative to P and C
1:3	54	5.56
1:2	38	5.26
1:1	22	4.55
2:1	28	3.57
3:1	34	2.94
4:1	40	2.5

Calculation of the ratio **for P-Et-P-Alg**:

$$3.9 \text{ atomic \% P relative to P and C} = \left(\frac{1\ P\ atom}{x\ total\ C\ and\ P\ atoms}\right) 100\%$$

$$x = \frac{100}{3.9} = 25.4 \text{ total C and P atoms in the ratio of monomers}$$

For one P atom in the ion pair, we have 16 total atoms attributable to the phosphonium monomer (1 P and 15 C atoms).

$$25.4 - 16 = 9.4 \text{ carbon atoms attributable to the carboxylate monomer}$$

$$\frac{9.4\ atoms}{6\ carbon\ atoms\ per\ carboxylate\ monomer} = 1.4$$

Therefore, the ratio of carboxylate:phosphonium ions in **P-Et-P-Alg** is 1.4:1. The same procedure was used to calculate the ionic ratios for the other PECs.

4.4.6 Measurement of Swelling

The swelling of each of the networks was characterized by comparing the swollen weight (m_s) to the dried weight (m_i) (Equation 4-2). Each network (about 150 mg) was initially dried to remove any residual water and accurately weighed to determine m_i. The networks were then placed into 25 mL of solutions at 37 °C with NaCl concentrations of 0 M (DI water), 0.1 M, 0.15 M, 0.25 M or into pH 7.4 PBS. Networks were taken out at specific time points, blotted dry with paper towel to remove surface liquid, and weighed. The experiments were carried out in triplicate.

$$\text{Swelling \%} = \left(\frac{m_s - m_i}{m_i}\right) x\ 100 \qquad\qquad \text{Equation 4-2}$$

4.4.7   Healing Experiments

For the puncture tests, PECs were punctured with an 18-gauge needle, and the material was removed to create a 0.5 mm diameter hole. Damaged networks were imaged initially and then soaked in PBS and imaged at 0, 24 and 48 h using a Zeiss StereoLumar V12 microscope at 35x magnification.

4.4.8   Loading Studies

PECs (~150 mg) were placed in 0.1 M NaCl solutions containing 0.05 wt% fluorescein sodium salt, etodolac sodium salt or methotrexate disodium salt at 0.0058 grams of network/mL, for 7 days to allow time for anion exchange to occur. The PECs were then taken out of solution and quickly rinsed with deionized water to remove any unbound surface molecules. The loading capacity (LC) was then calculated for each of the PECs by use of UV-visible spectroscopy. The absorbance of the solution before loading was compared to the absorbance after loading and from this difference, the mass of anion in each PEC was determined. The molar absorptivities were: fluorescein sodium salt (490 nm, ε = 29817 L mol^{-1} cm^{-1}),[41] etodolac (274 nm, ε = 3409 L mol^{-1} cm^{-1}),[41] or methotrexate (372 nm, ε = 3072 L mol^{-1} cm^{-1}) in 0.1 M NaCl and were calculated from calibration curves. Both etodolac and methotrexate were purchased in their acidic forms, so each of the loading solutions were brought to a pH of 8 by the addition of NaOH. Loading capacities were then calculated from Equation 4-3 where m_D is the mass of drug encapsulated in the network and m_N is the dry mass of the network. The experiments were performed in triplicate.

$$LC = \frac{M_D}{M_N} \text{ x } 100 \text{ \%}$$

Equation 4-3

Encapsulation efficiency was calculated by **Equation 4-4** where M_E is the mass of drug encapsulated in the PEC and M_I is the mass of drug in the solution before loading.

$$EE = \frac{M_E}{M_I} \text{ x } 100\%$$

Equation 4-4

4.4.9   Release Studies

Drug-loaded PECs ($\sim$ 150 mg accurately weighed) were each placed into 25 mL of PBS and incubated at 37 °C. Aliquots of 150 μL were then taken from the solutions at specific time points and transferred into 96 well plates. The absorbances of the solutions were measured on a plate reader at the appropriate wavelength for each drug (see above) to determine the concentration and thus quantity of released drug at each time point. The PBS solutions in which the PECs were incubated were changed at each time point. To determine the percent release, the cumulative mass of drug released at each time point was divided by the total mass of encapsulated drug in the network. The experiments were performed in triplicate.

4.4.10   Rheology

Networks were prepared as outlined above, but after ultracentrifugation they were pressed in between two Teflon® sheets using a Carver 3851-0C melt press to a thickness $\sim$ 1 mm. Sheets of material were then punched into circles with a diameter of 5 cm then soaked in PBS at 37 °C for 24 hours prior to testing. Rheological measurements were then performed at 37 °C on an Anton Paar MCR 302 shear rheometer with a 50 mm diameter parallel plate tool (PP50). Fine grit sandpaper was affixed to the bottom plate and top plate to prevent slip when measuring the samples soaked in PBS. Small-amplitude oscillatory shear measurements were performed over the frequency range of 0.01 – 100 rad s^{-1} with a stress amplitude of 100 dyn cm^{-2} for all samples. It was confirmed that these stress amplitudes were in the linear viscoelastic region (Figure C16). Frequency sweeps from 0.01 – 100 rad/s and from 100 – 0.01 rad/s were each performed in duplicate to ensure reproducibility.

4.4.11   Cell Toxicity Assays

C2C12 mouse myoblast cells were cultured in medium consisting of 500 mL of Dulbecco's Modified Eagle's Medium (DMEM) supplemented with 10 mL of penicillin-streptomycin (1000 units/ mL), 5 mL of L-Glutamine (200 mM) and 50 mL of fetal bovine serum, at 37

°C in an incubator with 5% CO_2. They were then seeded in a Nunclon 96-well U bottom transparent polystyrol plate to obtain approximately 10000 cells/well in 100 μL of culture medium. The cells were then incubated for 24 h prior to performing the assay. For the leaching assays, samples of dry hydrogel (~ 50 mg) were immersed in 3 mL of cell culture medium and incubated overnight to enable the leaching of potentially toxic species from the hydrogels over a period of 24 h.

The growth medium was then aspirated from the cells and replaced with either solutions of sodium dodecyl sulfate (SDS) in the cell culture medium at concentrations of 0.2, 0.15, 0.10, or 0.05 mg/mL, which were used as positive controls, serial 2-fold dilutions of the leachate in culture medium, serial 2-fold dilutions of the polymers in culture medium, or fresh medium as a negative control (6 wells per concentration). The cells were then incubated at 37 °C (5% CO_2) for 24 h. The medium was again aspirated and replaced with 110 μL of fresh medium containing 0.5 mg/mL (3-(4,5-dimethylthiazol-2-yl)-2,5-diphenyltetrazolium bromide) (MTT). After 4 h of incubation (37 °C, 5% CO_2), the medium was carefully aspirated, and the purple crystals were dissolved by addition of 50 μL of spectroscopic grade dimethyl sulfoxide (DMSO). After shaking (1 s, 2 mm amp, 654 rpm), the absorbance of the wells at 540 nm was read using a Tecan M1000-Pro plate reader. The absorbance of wells prepared in the same way but without cells was subtracted as a background and the cell viability was calculated relative to wells containing cells that were exposed only to the culture medium. No (0%) cell viability was detected for cells exposed to the highest concentrations of SDS, confirming the sensitivity of the assay. Statistical analyses were conducted using JMP version 14 (SAS Institute). The data were analyzed using a one-way analysis of variance (ANOVA) to compare differences amongst groups and followed by Tukey's multiple comparison test.

4.5   References

(1)   Langer, R. Drug Delivery and Targeting. *Nature* **1998**, *392*, 5–10.

(2)   Florence, A. T.; Jani, P. U. Novel Oral Drug Formulations. *Drug Saf.* **1994**, *10*, 233–266.

(3)   Shelley, H.; Babu, R. J. Role of Cyclodextrins in Nanoparticle-Based Drug Delivery Systems. *J. Pharm. Sci.* **2018**, *107*, 1741–1753.

(4)   Tang, L.; Zheng, Y.; Melo, M. B.; Mabardi, L.; Castaño, A. P.; Xie, Y. Q.; Li, N.; Kudchodkar, S. B.; Wong, H. C.; Irvine, D. J. Enhancing T Cell Therapy through TCR-Signaling-Responsive Nanoparticle Drug Delivery. *Nat. Biotechnol.* **2018**, *36*, 707-716.

(5)   Zhou, Q.; Zhang, L.; Yang, T. H.; Wu, H. Stimuli-Responsive Polymeric Micelles for Drug Delivery and Cancer Therapy. *Int. J. Nanomed.* **2018**, *13*, 2921–2942.

(6)   Zhou, Z.; Li, G.; Wang, N.; Guo, F.; Guo, L.; Liu, X. Synthesis of Temperature/PH Dual-Sensitive Supramolecular Micelles from β-Cyclodextrin-Poly(N-Isopropylacrylamide) Star Polymer for Drug Delivery. *Colloids Surf., B* **2018**, *172*, 136–142.

(7)   Francolini, I.; Giansanti, L.; Piozzi, A.; Altieri, B.; Mauceri, A.; Mancini, G. Glucosylated Liposomes as Drug Delivery Systems of Usnic Acid to Address Bacterial Infections. *Colloids Surf., B* **2019**, *181*, 632–638.

(8)   Shtenberg, Y.; Goldfeder, M.; Prinz, H.; Shainsky, J.; Ghantous, Y.; Abu El-Naaj, I.; Schroeder, A.; Bianco-Peled, H. Mucoadhesive Alginate Pastes with Embedded Liposomes for Local Oral Drug Delivery. *Int. J. Biol. Macromol.* **2018**, *111*, 62–69.

(9)   Roth-Konforti, M. E.; Comune, M.; Halperin-Sternfeld, M.; Grigoriants, I.; Shabat, D.; Adler-Abramovich, L. UV Light–Responsive Peptide-Based Supramolecular Hydrogel for Controlled Drug Delivery. *Macromol. Rapid Commun.* **2018**, *39*, 1–7.

(10)   Li, J.; Mooney, D. J. Designing Hydrogels for Controlled Drug Delivery. *Nat. Rev. Mater.* 2016.

(11)   Kroschwitz, J. I.; Mark, H. F. *Encyclopedia of Polymer Science and Technology*; Wiley-Interscience: Hoboken, New Jersey, 2003.

(12)   Hoare, T. R.; Kohane, D. S. Hydrogels in Drug Delivery: Progress and Challenges. *Polymer* **2008**, *49*, 1993–2007.

(13)   Huebsch, N.; Kearney, C. J.; Zhao, X.; Kim, J.; Cezar, C. A.; Suo, Z.; Mooney, D. J. Ultrasound-Triggered Disruption and Self-Healing of Reversibly Cross-Linked Hydrogels for Drug Delivery and Enhanced Chemotherapy. *Proc. Natl. Acad. Sci. U. S. A.* **2014**, *111*, 9762–9767.

(14)   Mann, B. K.; Schmedlen, R. H.; West, J. L. Tethered-TGF-β Increases Extracellular Matrix Production of Vascular Smooth Muscle Cells. *Biomaterials* **2001**, *22*, 439–444.

(15)   Kolate, A.; Baradia, D.; Patil, S.; Vhora, I.; Kore, G.; Misra, A. PEG - A Versatile Conjugating Ligand for Drugs and Drug Delivery Systems. *J. Controlled Release* **2014**, *192*, 67–81.

(16)   Shah, N. J.; Hyder, M. N.; Quadir, M. A.; Dorval Courchesne, N.-M.; Seeherman, H. J.; Nevins, M.; Spector, M.; Hammond, P. T. Adaptive Growth Factor Delivery from a Polyelectrolyte Coating Promotes Synergistic Bone Tissue Repair and Reconstruction. *Proc. Natl. Acad. Sci.* **2014**, *111*, 12847–12852.

(17)   Macdonald, M. L.; Samuel, R. E.; Shah, N. J.; Padera, R. F.; Beben, Y. M.; Hammond, P. T. Tissue Integration of Growth Factor-Eluting Layer-by-Layer Polyelectrolyte Multilayer Coated Implants. *Biomaterials* **2011**, *32*, 1446–1453.

(18)   Reisch, A.; Tirado, P.; Roger, E.; Boulmedais, F.; Collin, D.; Voegel, J. C.; Frisch, B.; Schaaf, P.; Schlenoff, J. B. Compact Saloplastic Poly(Acrylic Acid)/Poly(Allylamine) Complexes: Kinetic Control over Composition,

Microstructure, and Mechanical Properties. *Adv. Funct. Mater.* **2013**, *23*, 673–682.

(19)   Laugel, N.; Betscha, C.; Winterhalter, M.; Voegel, J. C.; Schaaf, P.; Ball, V. Relationship between the Growth Regime of Polyelectrolyte Multilayers and the Polyanion/Polycation Complexation Enthalpy. *J. Phys. Chem. B* **2006**, *110*, 19443–19449.

(20)   Fu, J.; Schlenoff, J. B. Driving Forces for Oppositely Charged Polyion Association in Aqueous Solutions: Enthalpic, Entropic, but Not Electrostatic. *J. Am. Chem. Soc.* **2016**, *138*, 980–990.

(21)   Schlenoff, J. B.; Rmaile, A. H.; Bucur, C. B. Hydration Contributions to Association in Polyelectrolyte Multilayers and Complexes: Visualizing Hydrophobicity. *J. Am. Chem. Soc.* **2008**, *130*, 13589–13597.

(22)   Fu, J.; Fares, H. M.; Schlenoff, J. B. Ion-Pairing Strength in Polyelectrolyte Complexes. *Macromolecules* **2017**, *50*, 1066–1074.

(23)   Wang, H.; Wang, Z.; Yang, J.; Xu, C.; Zhang, Q.; Peng, Z. Ionic Gels and Their Applications in Stretchable Electronics. *Macromol. Rapid Commun.* **2018**, *39*, 1–17.

(24)   Stanzione, J. F.; Jensen, R. E.; Costanzo, P. J.; Palmese, G. R. Synthesis and Characterization of Ionic Polymer Networks in a Room-Temperature Ionic Liquid. *ACS Appl. Mater. Interfaces* **2012**, *4*, 6142–6150.

(25)   Reisch, A.; Roger, E.; Phoeung, T.; Antheaume, C.; Orthlieb, C.; Boulmedais, F.; Lavalle, P.; Schlenoff, J. B.; Frisch, B.; Schaaf, P. On the Benefi Ts of Rubbing Salt in the Cut : Self-Healing of Saloplastic PAA / PAH Compact Polyelectrolyte Complexes. *Adv. Mater.* **2014**, 1–5.

(26)   Shamoun, R. F.; Reisch, A.; Schlenoff, J. B. Extruded Saloplastic Polyelectrolyte Complexes. *Adv. Funct. Mater.* **2012**, *22*, 1923–1931.

(27)   Cuthbert, T. J.; Jadischke, J. J.; De Bruyn, J. R.; Ragogna, P. J.; Gillies, E. R. Self-

Healing Polyphosphonium Ionic Networks. *Macromolecules* **2017**, *50*, 5253–5260.

(28) Harrison, T. D.; Yunyaeva, O.; Borecki, A.; Hopkins, C. C.; DeBruyn, J. R.; Ragogna, P. J.; Gillies, E. R. Phosphonium Polyelectrolyte Complexes for the Encapsulation and Slow Release of Ionic Cargo. *Biomacromolecules*, **2020**, *21*, 152–162.

(29) Al-Hariri, L. A.; Reisch, A.; Schlenoff, J. B. Exploring the Heteroatom Effect on Polyelectrolyte Multilayer Assembly: The Neglected Polyoniums. *Langmuir* **2011**, *27*, 3914–3919.

(30) Abdallah, D. J.; Lu, L.; Weiss, R. G. Thermoreversible Organogels from Alkane Gelators with One Heteroatom. *Chem. Mater.* **1999**, *11*, 2907–2911.

(31) Liang, S.; Oreilly, M. V.; Choi, U. H.; Shiau, H. S.; Bartels, J.; Chen, Q.; Runt, J.; Winey, K. I.; Colby, R. H. High Ion Content Siloxane Phosphonium Ionomers with Very Low Tg. *Macromolecules* **2014**, *47*, 4428–4437.

(32) Wang, S. W.; Liu, W.; Colby, R. H. Counterion Dynamics in Polyurethane-Carboxylate Ionomers with Ionic Liquid Counterions. *Chem. Mater.* **2011**, *23*, 1862–1873.

(33) Lee, K. L.; Mooney, D. J. Alginate : Properties and Biomedical Applications. *Prog. Polym. Sci.* **2012**, *37*, 106–126.

(34) Grant, G. T.; Morris, E. R.; Rees, D. A.; Smith, P. J. C.; Thom, D. Biological Interactions between Polysaccharides and Divalent Cations: The Egg-Box Model. *FEBS Lett.* **1973**, *32*, 195–198.

(35) Lv, X.; Liu, Y.; Song, S.; Tong, C.; Shi, X.; Zhao, Y.; Zhang, J.; Hou, M. Influence of Chitosan Oligosaccharide on the Gelling and Wound Healing Properties of Injectable Hydrogels Based on Carboxymethyl Chitosan/Alginate Polyelectrolyte Complexes. *Carbohydr. Polym.* **2019**, *205*, 312–321.

(36) Maiti, S.; Singha, K.; Ray, S.; Dey, P.; Sa, B. Adipic Acid Dihydrazide Treated

Partially Oxidized Alginate Beads for Sustained Oral Delivery of Flurbiprofen Oxidized Alginate Beads of Flurbiprofen. *Pharm. Dev. Technol.* **2009**, *14*, 461–470.

(37)   Lv, X.; Zhang, W.; Liu, Y.; Zhao, Y.; Zhang, J.; Hou, M. Hygroscopicity Modulation of Hydrogels Based on Carboxymethyl Chitosan/Alginate Polyelectrolyte Complexes and Its Application as PH-Sensitive Delivery System. *Carbohydr. Polym.* **2018**, *198*, 86–93.

(38)   Ferreira, N. N.; Caetano, B. L.; Boni, F. I.; Sousa, F.; Magnani, M.; Sarmento, B.; Ferreira Cury, B. S.; Daflon Gremião, M. P. Alginate-Based Delivery Systems for Bevacizumab Local Therapy: In Vitro Structural Features and Release Properties. *J. Pharm. Sci.* **2019**, *108*, 1559–1568.

(39)   Kanazawa, A.; Ikeda, T.; Endo, T. Polymeric Phosphonium Salts as a Novel Class of Cationic Biocides. VII. Synthesis and Antibacterial Activity of Polymeric Phosphonium Salts and Their Model Compounds Containing Long Alkyl Chains. *J. Appl. Polym. Sci.* **1994**, *53*, 1237–1244.

(40)   Hemp, S. T.; Zhang, M.; Allen, M. H.; Cheng, S.; Moore, R. B.; Long, T. E. Comparing Ammonium and Phosphonium Polymerized Ionic Liquids: Thermal Analysis, Conductivity, and Morphology. *Macromol. Chem. Phys.* **2013**, *214*, 2099–2107.

(41)   Harrison, T. D.; Ragogna, P. J.; Gillies, E. R. Phosphonium Hydrogels for Controlled Release of Ionic Cargo. *Chem. Commun.* **2018**, *54*, 11164–11167.

(42)   Porcel, C.; Schlenoff, J. Compact Polyelectrolyte Complexes:"Saloplastic" Candidates for Biomaterials. *Biomacromolecules* **2009**, *10*, 2968–2975.

(43)   Ornelas-Megiatto, C.; Wich, P. R.; Fréchet, J. M. J. Polyphosphonium Polymers for SiRNA Delivery: An Efficient and Nontoxic Alternative to Polyammonium Carriers. *J. Am. Chem. Soc.* **2012**, *134*, 1902–1905.

(44)   Wang, Q.; Schlenoff, J. B. The Polyelectrolyte Complex/Coacervate Continuum.

Macromolecules **2014**, *47*, 3108–3116.

(45)   Fares, H. M.; Wang, Q.; Yang, M.; Schlenoff, J. B. Swelling and Inflation in Polyelectrolyte Complexes. *Macromolecules* **2019**, *52*, 610–619.

(46)   Chen, D. T. N.; Wen, Q.; Janmey, P. A.; Crocker, J. C.; Yodh, A. G. Rheology of Soft Materials. *Annu. Rev. Condens. Matter Phys.* **2010**, *1*, 301–322.

(47)   Siepmann, J.; Peppas, N. A. Higuchi Equation: Derivation, Applications, Use and Misuse. *Int. J. Pharm.* **2011**, *418*, 6–12.

(48)   Ritger, P. L.; Peppas, N. A. A Simple Equation for Description of Solute Release I. Fickian and Non-Fickian Release from Non-Swellable Devices in the Form of Slabs, Spheres, Cylinders or Discs. *J. Controlled Release* **1987**, *5*, 23–36.

(49)   Martinez, J. S.; Keller, T. C. S.; Schlenoff, J. B. Cytotoxicity of Free versus Multilayered Polyelectrolytes. *Biomacromolecules* **2011**, *12*, 4063–4070.

Chapter 5

5 Progress Towards Self-Immolative Polymer Networks Containing Pendent Phosphonium Salts

5.1 Introduction

Infections caused by bacteria are becoming more difficult to treat, and sometimes impossible, now that cornerstone treatments are becoming less effective.[1] In 2018, 26 % of bacterial infections were resistant to first-line antibiotics in Canada, and it was estimated that well over 5400 deaths were a result of these infections.[2] It is also predicted that by the year 2050, resistance to first-line antibiotics will reach 40 %, increasing the number of deaths.[2] Without the development of new antibacterials to treat and combat the spread of infections, the world is heading towards an age where many infections will once again become fatal. Bacteria can be found on many common surfaces such as door handles,[3] computers,[4] telephones,[4] table surfaces[5] and can be easily spread through direct contact[6] and some bacteria have even been known to survive on these common surfaces for up to nine weeks.[5] Therefore, the attachment and proliferation of bacteria on common surfaces is a concern. Furthermore, bacterial colonization of surfaces can lead to biofilm formation.

Biofilm formation can initially occur by bacteria accumulating on a surface and secreting adhesion proteins to bind irreversibly (Figure 5-1; Step 1).[7] Upon attachment, proliferation and colony formation can occur, as does the formation of a thick peptidoglycan layer to act as protection (Figure 5-1; Step 2).[8] Under this layer, multiple different bacteria can grow and proliferate causing a pressure buildup and eventual rupture, allowing bacteria to colonize other surfaces (Figure 5-1; Step 3).[9]

1. Initial bacterial adhesion

2. Proliferation, colonization and peptidoglycan layer formation

3. Biofilm maturation and eventual rupture
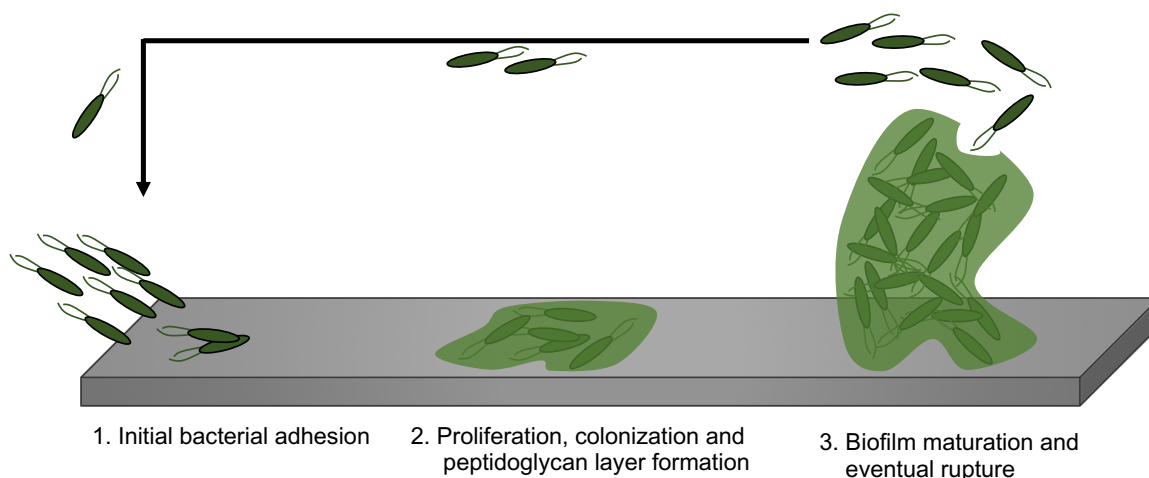
Figure 5-1 Illustration of biofilm formation. Bacteria initially adhere to the surface of a material irreversibly (Step 1). This is followed by proliferation, colonization, and the formation of a peptidoglycan layer (Step 2). Finally, the biofilm matures, rupture occurs and the spread of bacterial to a new surface re-starts this cycle (Step 3).

One method to prevent the bacterial spread and also kill bacteria is to use antibacterial surfaces. These are classified into two categories: passive and active. Passive surfaces prevent the growth of bacteria by minimizing their adhesion to surfaces, whereas active surfaces interact with the negatively charged surface of a bacteria cell wall and cause cell death.[10] Common examples of passive surface polymers include poly(ethylene glycol),[11] poly(dimethyl siloxane)[12] and fluorinated materials.[13] Common examples of active systems include cationic polymers such as quaternary ammonium/phosphonium ionomers[14,15] and antibacterial peptides.[16] Cationic biocidal polymers such as polyammonium salts have been extensively studied for antibacterial applications,[17] whereas there has been much less research on polyphosphoniums derivatives,[18] despite exhibiting higher antibacterial activity,[19] and chemical and thermal stability.[20]

Cationic biocidal polymers have also been used as surface coatings to kill bacteria. Our group has reported cationic thin film coatings that have shown antibacterial activity against both *S. aureus* and *E.coli*.[21,22] Although these coatings are useful, there is a potential that these materials could eventually become fouled.[23] To address the issue, 'self-cleaning surfaces' have been developed. For example, Cao *et al*. used a polyzwitterionic material

consisting of antibacterial N,N-dimethyl-2-morpholinone.[24] In this system, N,N-dimethyl-2-morpholinone polymers were attached to a surface and were cationic when ring closed, allowing them to kill bacteria, but upon hydrolysis could become ring opened and zwitterionic to release dead bacteria (Figure 5-2). Bieser *et al*. also developed a 'self-cleaning' surface that involved grafting antibacterial N,N-dimethyldodecylammonium to cellulose and then coating these polymers on glass slides.[25] They reported that upon attachment of bacteria, cell lysis and death occurred, causing leaching of the enzyme cellulase, which induced coating degradation.
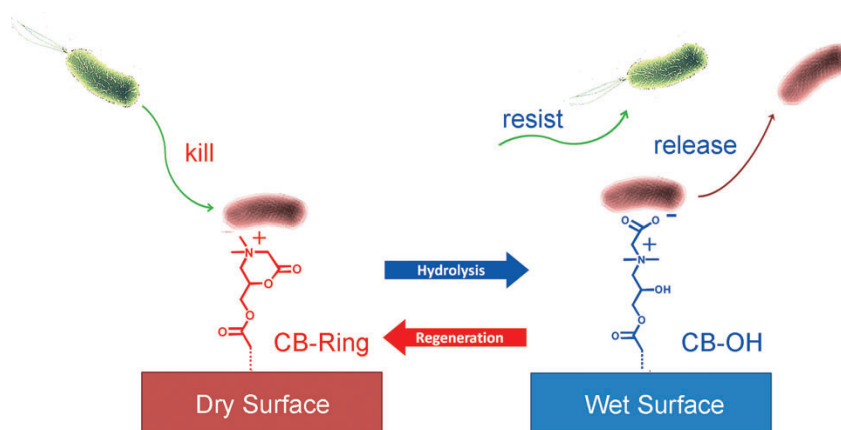
Figure 5-2 Cationic morpholine-based polymer surface that can be switched to a zwitterionic state by hydrolysis, yielding a bacteria-repellant and resistant material. Reproduced with permission of the publisher (Appendix E).

Degradable materials have received substantive attention recently because of the environmental and societal impacts of plastic pollution. While degradable polymers such as polysaccharides[26] and polyesters[27] are not new, the ability to trigger end-to-end degradation upon application of a specific stimulus has been a new focus. Polymers that can accomplish this are called self-immolative polymers (SIPs). Since their first introduction in 2008,[28] different backbones including poly(carbamates),[29]

poly(benzyl ether)s,[30] poly(phathaldehydes)[31] and poly(glyoxylates)[32] have been developed (

Figure 5-3). In their uncapped form, these polymers are not stable as they can revert back to their monomers or convert to other degradation species, so to stabilize these polymers, end-caps are added. The end-caps can be tuned to induce degradation in response to applied stimuli such as pH,[33] heat,[34] redox changes,[35] and light,[36] enabling the polymers to be used in applications such as sensors,[37] membranes,[38] and drug delivery systems.[39]

Poly(benzyl carbamate)   Poly(benzyl ether)   Poly(phthalaldehyde)   Poly(glyoxylate)
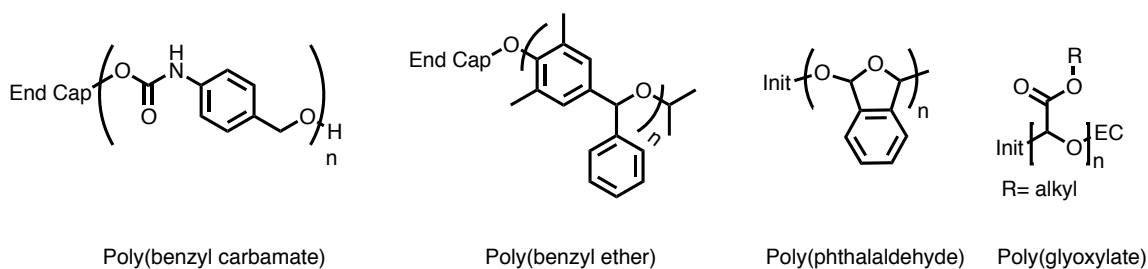
Figure 5-3 Common examples self-immolative polymers.

Our group has reported the synthesis and end-capping of poly(glyoxylate)s with stimuli-responsive groups.[32] Poly(glyoxylate)s can be synthesized from commercially available monomers, such as ethyl glyoxylate, and the degradation products are ultimately glyoxylic acid hydrate[40] which is nontoxic to the environment, as well as the corresponding alcohol.[41] Although they find use in many applications, one limitation these polymers have faced is the eventual hydrolysis of the ester side chains, revealing carboxylic acids. These newly formed carbocyclic acid groups can then intramolecularly catalyze backbone acetal hydrolysis, leading to depolymerization. To increase their stability, new derivatives of these polymers were developed where the ester groups have been converted to amides through an aminolysis reaction (Scheme 5-1). These new derivatives, termed poly(glyoxylamide)s (**PGAms**),[42] can be prepared by reaction with a wide variety of primary amines (Scheme 5-1), and have higher T_g values[42] and increased water solubility and stability[43] compared to analogous poly(glyoxylate)s.
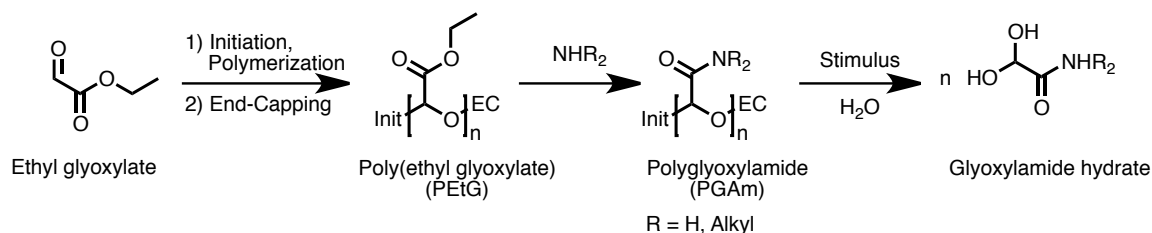
Scheme 5-1 Synthesis of poly(ethyl glyoxylate)s, poly(glyoxylamide)s and their degradation to glyoxylamide hydrate.

To further build on this new generation of **PGAms** it was of interest to introduce cationic pendant groups with antibacterial functionalities to create **PGAm** biocidal SIPs. Biocidal SIPs are a relatively new class of polymers and have only recently been reported.[44,45] To date they have not been explored with quaternary phosphonium salts, or with **PGAms**. Therefore, in this work we report the first UV-responsive **PGAm** self-immolative polymers containing quaternary phosphonium salts. The substituents on the phosphonium salt were varied to include ethyl, *n*-butyl or phenyl. We also report random copolymer **PGAms** consisting of allyl amide and the aforementioned phosphoniums salts to allow for thin film cross-linking via thiol-ene chemistry. The thin films are to be used as antibacterial surfaces that can be degraded upon exposure to UV-light, to prevent biofilm formation (**Figure 5-4**).
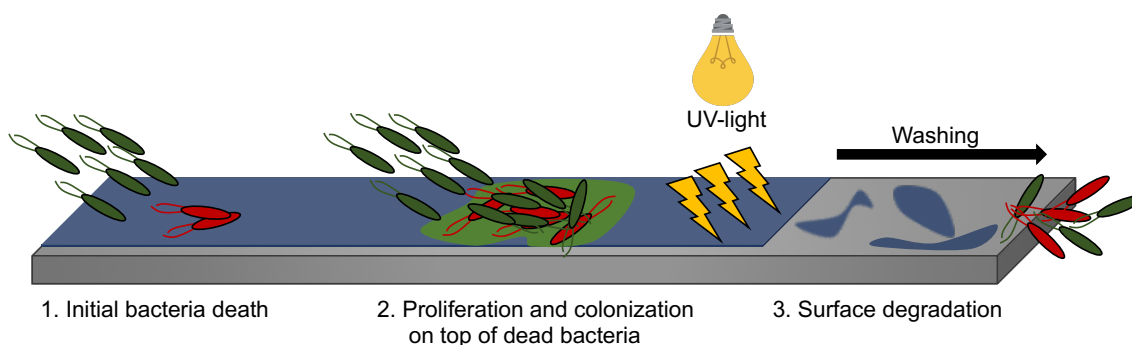
Figure 5-4 Illustration of initial bacterial adhesion to and killing by the proposed antibacterial surface (1). After bacterial death, more bacteria can proliferate and colonize on top of the dead bacteria (2). Exposing the surface to UV-light can initiate degradation and surface shedding (3).

5.1 Results and Discussion

5.1.1 Phosphonium Salt Synthesis

Monomers were prepared by reacting triethylphosphine, tri-*n*-butylphosphine and triphenylphosphine with 3-bromopropylamine hydrobromide stoichiometrically under N_2 atmosphere to generate the corresponding salts triethyl(3-aminopropyl)phosphonium bromide hydrobromide (**EtP**), tri-*n*-butyl(3-aminopropyl)phosphonium bromide hydrobromide (**BuP**)[46] and triphenyl(3-aminopropyl)phosphonium bromide hydrobromide (**PhP**)[47] (Scheme 5-2). The reaction products were characterized by ^1H, $^{13}C\{^1H\}$ and $^{31}P\{^1H\}$ NMR spectroscopy (Figures D1-9).

R = Et, Bu, Ph
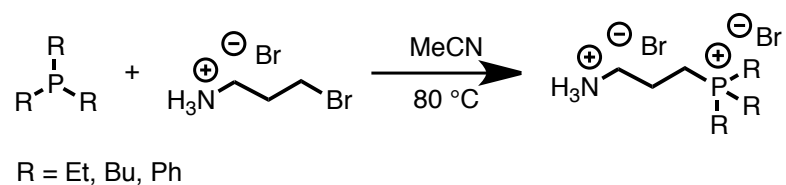
Scheme 5-2 Synthesis of **EtP**, **BuP** and **PhP**.

5.1.2 Self-Immolative Polymer Synthesis

Poly(ethyl glyoxylate) with a UV-responsive endcap (**PEtG**), was synthesized by first treating 2-nitrobenzyl alcohol with lithium bis(trimethylsilyl)amide to generate the initiator, then using it to polymerize purified ethyl glyoxylate.[48] Addition of triethylamine and benzyl chloromethyl ether were added to yield poly(ethyl glyoxylate) (**PEtG**; $M_n = 5$ kg mol^{-1} $Đ = 1.8$) (Scheme 5-3) (Figure D10).
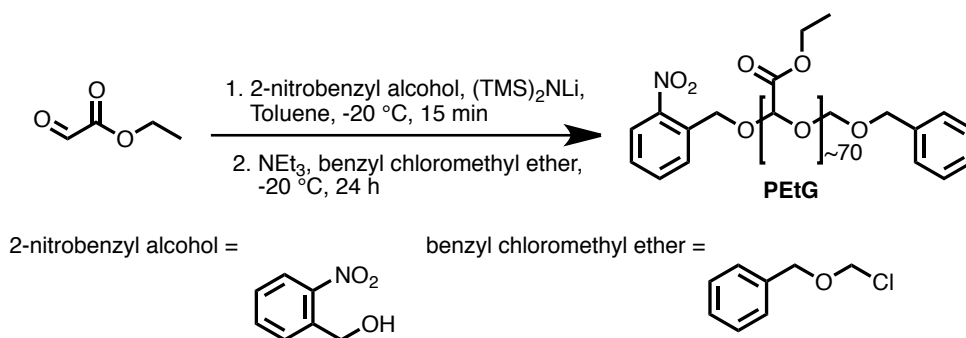
Scheme 5-3 Synthesis of poly(ethyl glyoxylate) with a UV-responsive end cap.

5.1.3   Triggered Depolymerization

To assess the depolymerization percentage of **PEtG**, ^{1}H NMR spectroscopy experiments were performed in the absence and presence of UV light. The percent of depolymerization was quantified by comparing the integration of the signal at ~ 5.5 ppm corresponding to the polymer backbone to that of the peak at 5.1 ppm corresponding to the methine proton of the monomer hydrate depolymerization product. Depolymerization was studied in 9:1 $CD_3CN:D_2O$, a solvent mixture that has previously been used to study the depolymerization of polyglyoxylates.[32] The polymer degraded to 50 % over 40 hours (Figure 5-5).
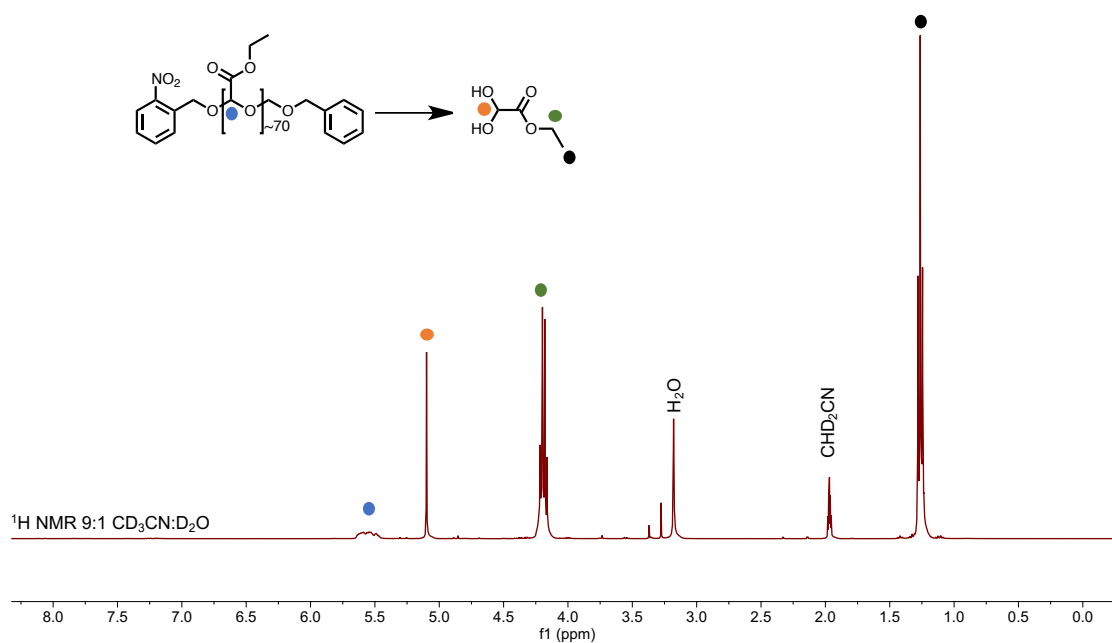
Figure 5-5 ¹H NMR Spectrum of **PEtG** after UV irradiation (400 MHz, 9:1 CD₃CN:D₂O).

5.1.4   Addition of Phosphonium Salts to Poly(ethyl glyoxylate)

The addition of **EtP**, **BuP** and **PhP** to **PEtG** was attempted through an aminolysis reaction, using 2 equivalents of NEt₃ to deprotonate the amino groups on the phosphoniums (Scheme 5-4).
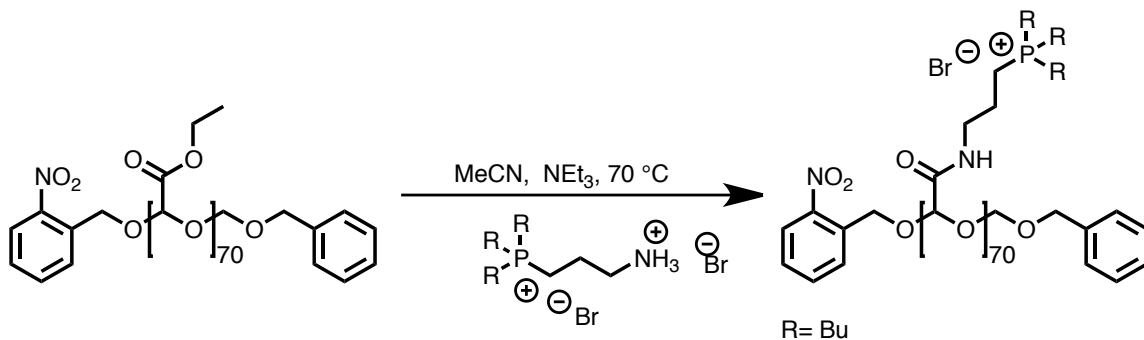
Scheme 5-4 Addition of **BuP** to **PEtG** in the presence of two stoichiometric equivalents of NEt₃ at 70 °C.

This reaction was monitored by ^{1}H NMR spectroscopy over five days but yielded no conversion. The notable expected changes in the ^{1}H NMR spectrum should include the signal corresponding to the backbone methine proton changing from a broad multiplet at ~5.5 ppm to a broad singlet ~5.3 ppm after the amide has formed.[42] In addition, the peaks corresponding to the ester CH_2 and CH_3 at 4.2 and 1.3 ppm should disappear, and the new peaks associated with the **BuP** were expected to appear. Based on the appearance of the ^{1}H NMR spectrum of this reaction (Figure 5-6), there were no changes in the peak at ~5.5 ppm and the ester CH_2 and CH_3 at 4.2 and 1.3 ppm respectively were still visible, indicating no addition occurred. The equivalents of **BuP** were then increased to 2 and 3 and combined with 4 and 6 equivalents of NEt_3, respectfully, and added to **PEtG** but again no changes in the ^{1}H NMR spectrum were observed. (Figure D12, 14). A reaction containing 10 equivalents of NEt_3 and 1 equivalent of **BuP** and **PEtG** was also carried out, but again no changes in the ^{1}H NMR spectrum were observed (Figure D16). Upon careful examination of the ^{31}P $\{^1$H$\}$ NMR spectrum in each of the aforementioned reactions, the singlet at 34 ppm from **BuP** has converted into multiple signals ~ 34 ppm after mixing, indicating side products could be forming (Figure D11, 13, 15).
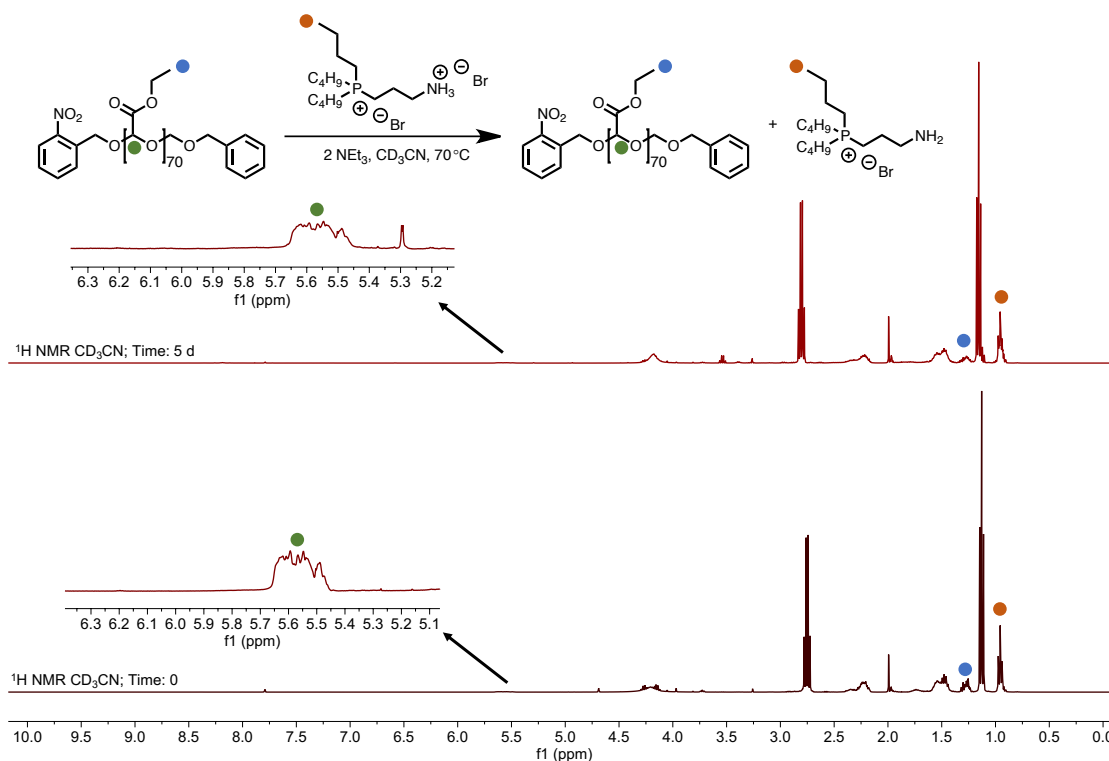
Figure 5-6 ^{1}H NMR spectrum of the attempted addition of **BuP** to **PEtG** in the presence of two stoichiometric equivalents of NEt$_3$ at 70 °C over 5 days. The bottom spectrum represents T = 0 and the top represents T = 5 days (400 MHz, CD$_3$CN).

5.1.5 Reactions using TBD

As no addition of **BuP** to **PEtG** could be accomplished with the NEt$_3$, the use of a well-known organocatalyst, 1,5,7-triazabicyclo[4.4.0]dec-5-ene (**TBD**) was explored. 1,5,7-triazabicyclo[4.4.0]dec-5-ene (**TBD**) is a cyclic guanidine molecule, which is well known to be an effective catalyst for the formation of amides from esters and primary amines.[49,50] **TBD** was recently employed in the ester to amide conversion of poly(methyl acrylate)s to yield a variety of different poly(*n*-alkyl acrylamides), with different functialities[51] and it appeared that this catalyst could be employed in the current system to facilitate addition of the phosphonium salts. **TBD** first reacts with the ester to form intermediate I, where the protonated nitrogen then allows for easy proton transfer forming species II and release of

the alcohol. Finally, hydrogen bond activation of the amine facilitates amide formation and the regeneration of **TBD** (Scheme 5-5).[50]
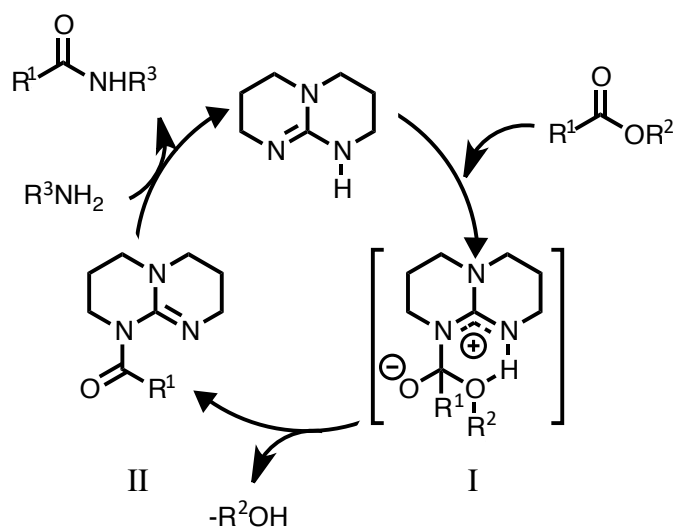
Scheme 5-5 Mechanism proposed for the aminolysis of esters catalyzed by TBD.[50]

5.1.6   Addition of Phosphonium Salts to Poly(ethyl glyoxylate)

The addition of **TBD** did indeed facilitate the addition of **BuP** onto **PEtG** to create **PEtG$_{BuP}$** (Scheme 5-6) as a new broad peak was observed upfield at ~5.25 ppm, in the crude ^{1}H NMR spectrum and broadening of the alkyl peaks on the phosphonium was also observed (Figure 5-7). The reaction was left to stir for 15 minutes at room temperature and was accompanied to by the appearance of light yellow colour in the reaction solution.
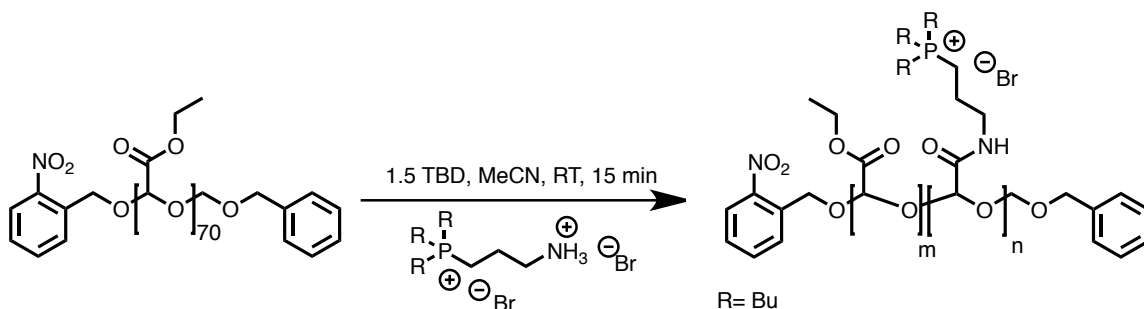
Scheme 5-6 Schematic illustration of the addition of BuP to PEtG in the presence of 1.5 stoichiometric equivalents of TBD.

From the ^{31}P{^{1}H} spectra, there were again multiple signals at ~ 34 ppm, indicating again that there could be side products forming. The reaction was then carried out with the same conditions for **EtP** and **PhP**. The formation of **PGAm$_{EtP}$** was successful (Figure 5-8), but no addition was observed for **PhP**. The equivalents of **TBD** were increased, and the reaction was heated to 70 °C, but again no reaction was observed. As the **PhP** is very bulky, steric hindrance could prevent this reaction. **PGAm$_{BuP}$** and **PGAm$_{EtP}$** were then purified by dialysis and dried *in vacuo* to yield light yellow powders (Figures D17-20).
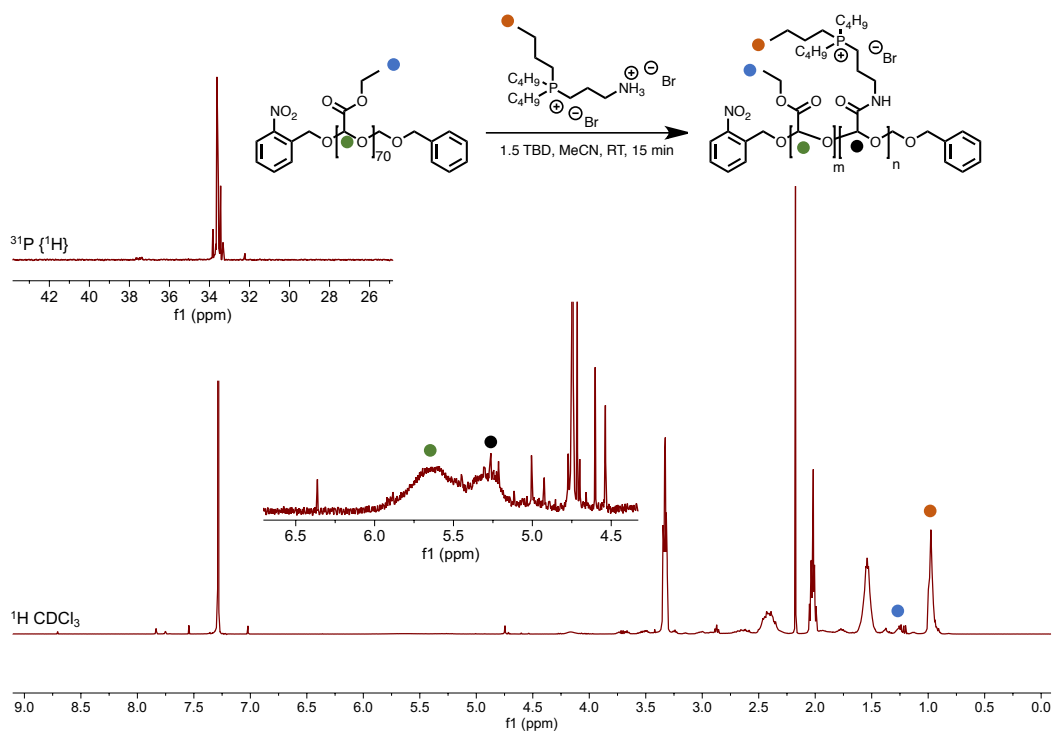
Figure 5-7 ^{1}H NMR and ^{31}P{^{1}H} spectrum of the attempted addition of **BuP** to **PEtG** in the presence of 1.5 stoichiometric equivalents of TBD at room temperature (400 MHz, CDCl$_3$) to make **PGAm$_{BuP}$**.
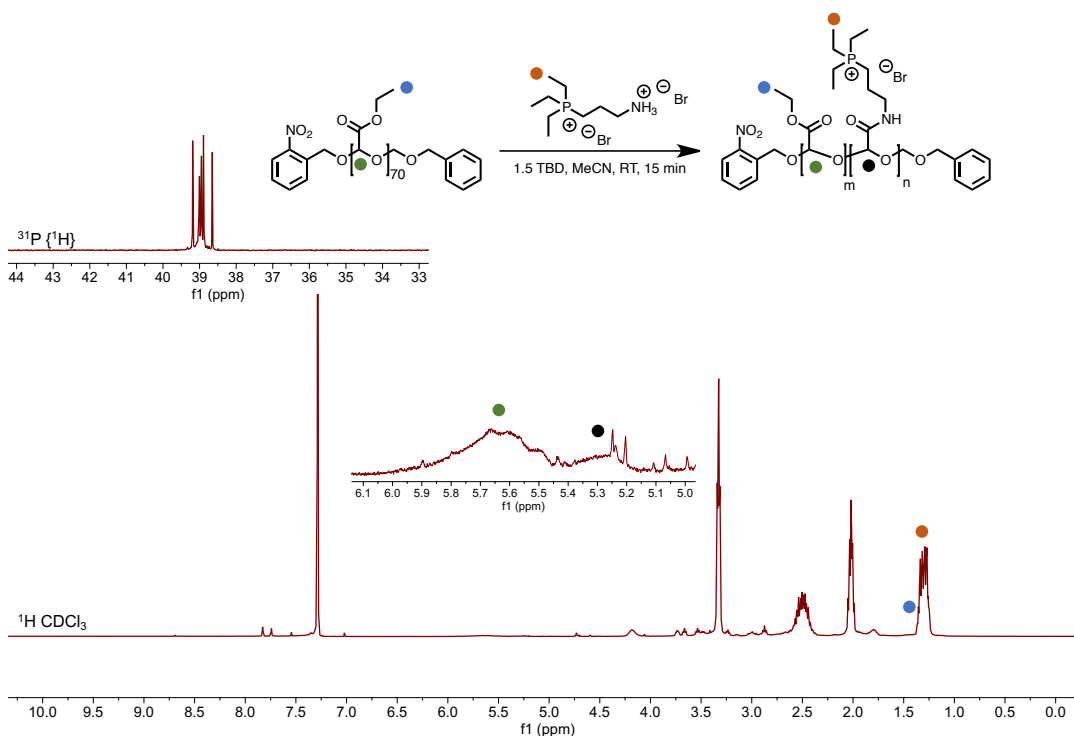
Figure 5-8 ^{1}H NMR and ^{31}P{^{1}H} spectrum of the attempted addition of **EtP** to **PEtG** in the presence of 1.5 stoichiometric equivalents of TBD at room temperature (400 MHz, CDCl$_3$) to make **PGAm$_{EtP}$**.

5.1.7   Extent of Phosphonium Salt Addition

The conversion of ethyl esters to amides in **PGAm$_{BuP}$** and **PGAm$_{EtP}$** was important to determine and is tabulated in Table 5-1. For **PGAm$_{BuP}$**, the integration of the terminal CH$_3$ group on the phosphonium at 0.94 ppm was set to 9 and compared to the integration of the terminal CH$_3$ group on the residual glyoxylate at 1.27 ppm. The ratio of these two was calculated to be 2.1 ethyl glyoxylate units:1 **BuP** unit, which corresponded to 30 % **BuP** and 70 % ethyl glyoxylate units on the polymer. For **PGAm$_{EtP}$,** the terminal CH$_3$ group on **EtP** and the ethyl glyoxylate units overlapped so the signals corresponding to methine backbone peaks from each were integrated and the polymer was calculated to consist of about 50 % **EtP** and 50 % ethyl glyoxylate repeat units. The higher conversion rate for **PGAm$_{EtP}$** compared to **PGAm$_{BuP}$** could be due to the lower steric bulk associated with **EtP**.

Table 5-1 Ratio of repeat units on **PGAm_{BuP}** and **PGAm_{EtP}**.

Polymer	Ethyl Glyoxylate Repeat units (%)	Phosphonium Salt Repeat units (%)
PGAm_{BuP}	30	70
PGAm_{EtP}	50	50

5.1.8   Addition of Allylamine to **PGAm_{BuP}** and **PGAm_{EtP}**

After the synthesis of **PGAm_{BuP}** and **PGAm_{EtP}** was completed, the addition of a functional group with potential crosslinking abilities by thiol-ene chemistry was desired. **PGAm_{BuP}** and **PGAm_{EtP}** were then reacted with 6 molar equivalents of allylamine to convert the remaining esters to amides and form **PGAm_{BuP-AllylAm}** and **PGAm_{EtP-AllylAm}** (Scheme 5-7) (Figures D20-24).
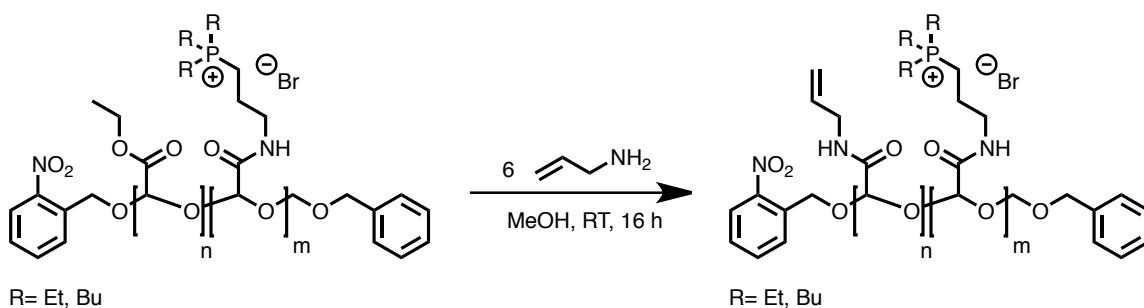
Scheme 5-7 Synthesis of **PGAm_{BuP-AllylAm}** and **PGAm_{EtP-AllylAm}**.

5.1.9   Initial Network Formation

Initial network formation was carried out by thiol-ene crosslinking and involved mixing **PGAm_{EtP-AllylAm}**, pentaerythritol tetrakis(3-mercaptopropionate) and azobisisobutyronitrile (AIBN) in weight percent ratios of 71/28/1 (Figure 5-9). This ratio was chosen to keep the ratio of allyl to thiols groups 1:1. During preparation of the formulation, it was realized

that solvent was necessary to dissolve all of the components and dimethylsulfoxide (DMSO) was the only solvent that could achieve this. The formulation was then drop cast on a glass slide that had both ends wrapped in electrical tape and another glass slide on top. The glass slides were then transferred to an oven and cured for 24 hours at 60 °C (Figure 5-9). After curing, the films were separated from the glass slides and measured with a caliper to have a thickness of ~ 150 μm. Films also had a much smaller diameter than initially expected, indicating that too much DMSO must have been added, but were now insoluble indicating crosslinking. In future network synthesis, the formulation will be tuned so less DMSO is added.
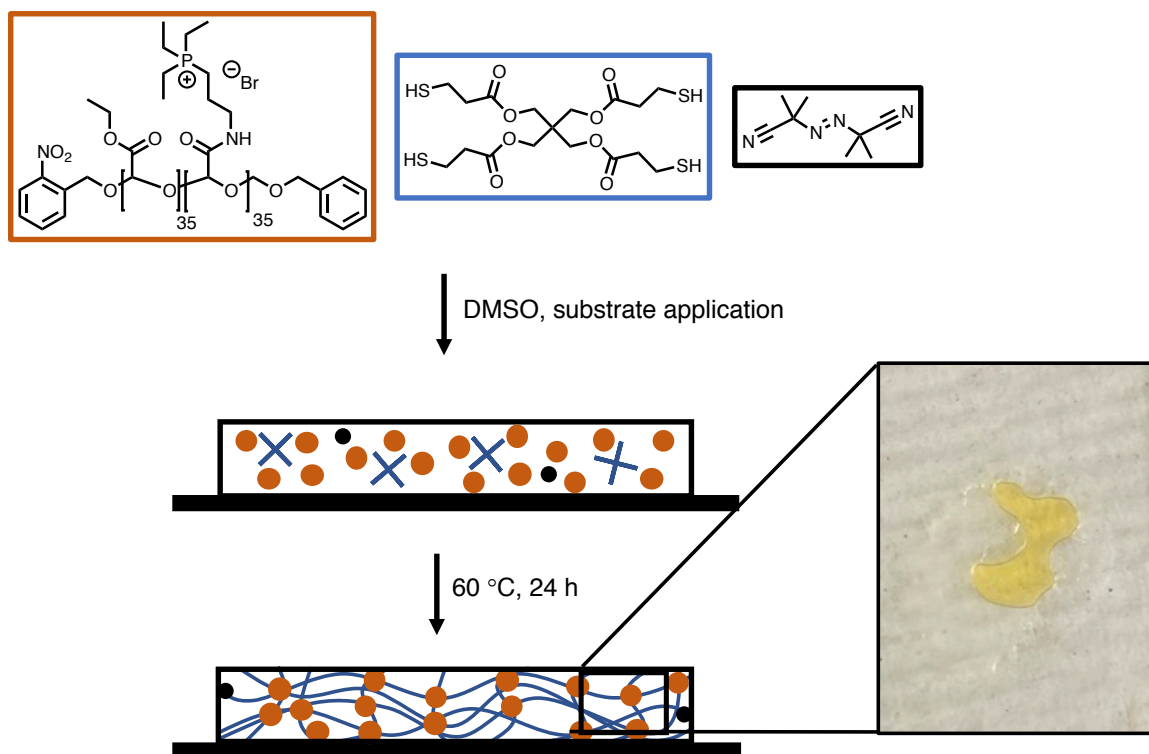
Figure 5-9 Polymer network formation via thiol-ene chemistry.

5.2   Conclusions

We have demonstrated for the first time that phosphonium salts can be added onto poly(ethyl glyoxylate) to yield **PGAm$_{BuP}$** and **PGAm$_{EtP}$**. Conditions for the addition of **BuP** and **EtP** required the presence of **TBD** to facilitate the reaction as uncatalyzed reactions were unsuccessful. **PhP** could not be added onto **PEtG** in either uncatalyzed or catalyzed

reactions which could be due to steric bulk. The extent of amidation was then calculated for **PGAm$_{BuP}$** and **PGAm$_{EtP}$** by use of signal integrations from ^{1}H NMR spectroscopy to show that 30 % of the initial ester groups had been converted to amides for **PGAm$_{BuP}$** compared to 50 % for **PGAm$_{EtP}$**. The lower conversion of **PGAm$_{BuP}$** could be attributed to steric bulk associated with **BuP**. The resulting ester groups on **PGAm$_{BuP}$** and **PGAm$_{EtP}$** were further functionalized with excess allylamine to create **PGAm$_{BuP-AllylAm}$** and **PGAm$_{EtP-}$** **$_{AllylAm}$** that could be used with thiol-ene crosslinking to create polymer networks. Initial network formation to produce insoluble films involved the reaction of **PGAm$_{EtP-AllylAm}$** with pentaerythritol tetrakis(3-mercaptopropionate) and AIBN, using DMSO, but the amount of DMSO added was too high which caused film shrinkage.

5.3   Future Work

Future work will first involve re-visiting the synthesis of **PGAm$_{BuP}$** and **PGAm$_{EtP}$** to try and complete an aminolysis reaction without the use of **TBD** to simplify purification. **BuP** or **EtP** will be deprotonated with NEt$_3$ and separated by determining the solubilities of each in a variety of different solvents. A large excess of 6 equivalents of deprotonated **BuP** or **EtP** will then be added to one equivalent of ester on **PEtG** to see if this will yield **PGAm$_{BuP}$** or **PGAm$_{EtP}$** (Scheme 5-8). If this yields **PGAm$_{BuP}$** and **PGAm$_{EtP}$** unreacted **BuP** and **EtP** can simply be collected by dialysis, dried to remove ethanol, and reused.
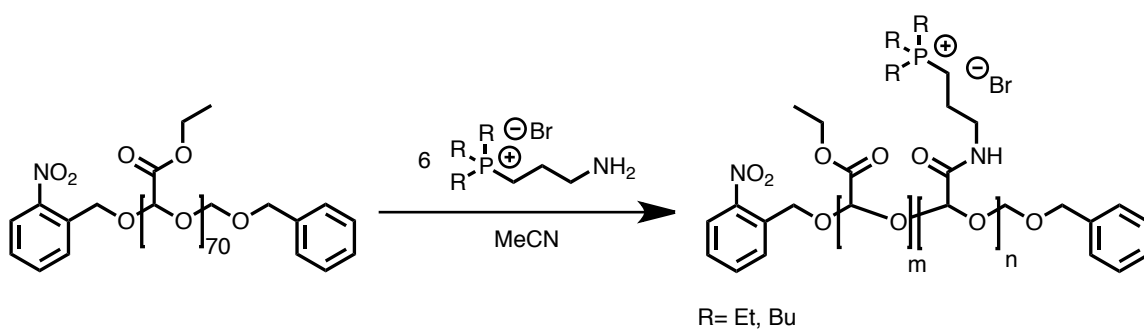
Scheme 5-8 Hypothesized synthesis of PGAms with a large excess of **EtP** or **BuP**.

If the proposed reaction is successful, reaction optimization will then be carried out to attempt to normalize the amount of **BuP** and **EtP** added onto **PEtG.** As the previous work demonstrated that only 30% ester-to-amide conversion was obtained in **PGAm$_{BuP}$**, 30 %

conversion will be attempted for **PGAm$_{EtP}$.** This will be important for comparing antibacterial properties in future work. A less bulky, third phosphonium containing **PGAm** can also be made with trimethylphosphine to expand the substrate scope as well. After this reaction step is completed, the remaining ester groups can be converted to amides with allylamine and degradation studies of **PGAm$_{BuP-AllylAm}$**, **PGAm$_{EtP-AllylAm}$** and **PGAm$_{MeP-AllylAm}$** will be carried out.

Ideally, formulations of each polymer can then be created without the use of DMSO and a more cost-effective solvent such as water could be used. **PGAm$_{BuP-AllylAm}$** and **PGAm$_{EtP-AllylAm}$** are both water-soluble, so changing to a water-soluble crosslinker such as 2,2′-(ethylenedioxy)diethanethiol, could be easily done. Networks will be formed between glass slides as described above and network properties will be studied. After the coatings are prepared, bacteria toxicity testing can be completed along with network degradation studies.

5.4 Experimental

5.4.1 General Materials

3-Bromopropylamine hydrobromide, allylamine and pentaerythriyol tetrakis(3-mercaptopropionate), 2-nitrobenzyl alcohol, lithium bis(trimethylsilyl)amide and benzyl chloromethyl ether were purchased from Sigma Aldrich and used as received. Phosphines were donated from Solvay (Niagara Falls). Acetonitrile, methanol, toluene and dimethyl sulfoxide were purchased from Caledon. Triethylamine was purchased from Fisher Scientific. 1,5,7-triazabicyclo[4.4.0]dec-5-ene was purchased from AK Scientific.

5.4.2 General Methods

Differential scanning calorimetry (DSC) was performed on a DSC Q20 from TA Instruments (New Castle, DE) at a ramp rate of 10 °C/min under a N$_2$ atmosphere in an aluminum T$_{zero}$ pan containing 5–10 mg of sample. Glass transition temperatures (T$_g$) were obtained from the second heating cycle. Thermogravimetric analysis (TGA) to determine the onset degradation temperatures (T$_o$) was performed on a Q600 SDT from TA Instruments and analyzed at a ramp rate of 10 °C/min up to 800 °C using a ceramic pan

containing 5–10 mg of dry sample. Size-exclusion chromatograms were obtained using a THF chromatograph. The THF chromatograph was equipped with a Viscotek GPC Max VE2001 solvent module, a Viscotek VE3580 RI detector, and S3 two Agilent Polypore (300 × 7.5mm) columns connected in series to a Polypore guard column. Samples were dissolved in THF (glass-distilled grade) at a concentration of ~5 mg/mL, filtered through a 0.2 μm polytetrafluoroethylene (PTFE) syringe filter, and injected using a 100 μL loop. Samples were run at a flow rate of 1 mL/min for 30 min at 30 ºC. Molar masses of the samples were calculated relative to polystyrene standards. Nuclear Magnetic Resonance (NMR) spectroscopy was conducted on a Bruker AvIII HD 400 MHz spectrometer from (^{1}H 400.08 MHz, ^{31}P{^{1}H} 161.82 MHz). The chemical shifts (δ, ppm) in all ^{1}H NMR spectra were referenced relative to the residual proton signal in the solvent (H_2O: ^{1}H δ = 4.79, $CHCl_3$ ^{1}H δ = 7.26). All ^{31}P{^{1}H} NMR spectra were referenced using an external standard (85% H_3PO_4:^{31}P δ = 0).

5.4.3   Phosphonium Salt Synthesis

Synthesis of triethyl(3-aminopropyl)phosphonium bromide hydrobromide (EtP). Triethylphosphine (0.600 g, 5.1 mmol), 3-bromopropylamine hydrobromide (1.10 g, 5.1 mmol) and acetonitrile (25 mL) were combined in a pressure tube with a stir bar under N_2 atmosphere and heated at 60 °C for 24 hours. A solid precipitate out of solution and was filtered and washed with excess acetonitrile to yield a white powder (0.700 g, 43 %). **^{1}H NMR (400 MHz, D_2O):** δ = 1.19 ((dt, $^3J_{P-H}$ = 20 Hz, $^3J_{H-H}$ = 8 Hz) = 9H, CH_3), 1.98-1.88 (m, 2H; CH_2), 2.32-2.18 (m, 8H; CH_2), 3.10 ((t, $^3J_{H-H}$) = 8 Hz, 2H; CH_2).**^{31}P{^{1}H} NMR (161.82 MHz, D_2O):** δ = 39.11 (s). **^{13}C{^{1}H} NMR (100.5 MHz, D_2O):** δ = 39.6 ((d,$^3J_{P-C}$) = 19.1 Hz), 19.2 ((d, $^2J_{P-C}$) = 3.0 Hz), 14.6 ((d, $^1J_{P-C}$) = 50.3 Hz), 10.9 ((d, $^1J_{P-C}$) = 49.3 Hz), 4.8 ((d, $^2J_{P-C}$) = 6.0 Hz). **ATR-FTIR (cm^{-1} (ranked intensity)):** 771 (1), 801 (6), 1581 (10), 2469 (8), 2535 (7), 2705 (5), 2764 (4), 2888 (3), 2918 (2). **ESI-MS (m/z):** ESI+: 176.2 ([$C_9H_{23}NP$]$^+$).

Synthesis of tri-*n*-butyl(3-aminopropyl)phosphonium bromide hydrobromide (BuP).

Tri-*n*-butyl(3-aminopropyl)phosphonium bromide hydrobromide was synthesized as previously reported.[46] Briefly, tri-*n*-butylphosphine (4.50 g, 22.4 mmol), 3-bromopropylamine hydrobromide (4.90 g, 22.4 mmol) and acetonitrile (25 mL) were combined in a pressure tube with a stir bar under N_2 atmosphere and heated at 60 °C for 24 hours. The solvent was then removed *in vacuo,* yielding a clear and colourless viscous liquid (9.20 g, 98 %). **¹H NMR (400 MHz, D_2O):** δ = 3.15 ((t, $^3J_{H-H}$) = 8 Hz, 2H; CH_2), 2.37-2.21 (m, 8H; CH_2), 2.03-1.94 (m, 2 H; CH_2), 1.63-1.56 (m, 6H; CH_2), 1.53-1.44 (m, 6H; CH_2), 0.95 ((t, $^3J_{H-H}$) = 8 Hz, 9H: CH_3). **³¹P{¹H} NMR (161.82 MHz, D_2O):** δ = 37.60 (s), 33.82 (s). **¹³C{¹H} NMR (100.5 MHz, D_2O):** δ = 39.9 ((d, $^3J_{P-C}$) = 20.1 Hz), 23.3 ((d, $^2J_{P-C}$) = 15.1 Hz), 22.7 ((d, $^3J_{P-C}$) = 5 Hz), 19.26 ((d, $^2J_{P-C}$) = 4 Hz), 17.6 ((d, $^1J_{P-C}$) = 48.2 Hz), 15.8 ((d, $^1J_{P-C}$) = 50.3 Hz), 12.5 ((s, $^4J_{P-C}$). **ATR-FTIR (cm⁻¹ (ranked intensity)):** 719 (3), 907 (5), 969 (4), 1097 (7), 1232 (6), 1461 (2), 1599 (8), 2035 (9), 2869 (1). **ESI-MS (m/z):** ESI+: 260.2 ($[C_{15}H_{35}NP]^+$); 601.3 ($[C_{30}H_{71}N_2P_2Br]^{2+}$).

Synthesis of triphenyl(3-aminopropyl)phosphonium bromide hydrobromide (PhP).

Triphenyl(3-aminopropyl)phosphonium bromide hydrobromide was synthesized as previously reported.[47] Briefly, triphenylphosphine (7.10 g, 27.1 mmol), 3-bromopropylamine hydrobromide (5.90 g, 27.1 mmol) and acetonitrile (100 mL) were combined in a pressure tube with a stir bar under N_2 atmosphere and heated at 60 °C for 7 days. Upon cooling to room temperature, a white precipitate formed and was filtered and washed with excess acetonitrile (11.0 g, 89 %). **¹H NMR (400 MHz, D_2O):** δ = 1.96-2.06 (m, 2H; CH_2), 3.11 ((t, $^3J_{H-H}$) = 8 Hz, 2H; CH_2), 3.33-3.40 (m, 2H; CH_2), 7.63-7.83 (m, 15H; CH). **³¹P{¹H} NMR (161.82 MHz, D_2O):** δ = 23.09 (s). **¹³C{¹H} NMR (100.5 MHz, D_2O):** δ = 135.27 ((d, $^4J_{P-C}$) = 3.0 Hz), 133.58 ((d, $^3J_{P-C}$) = 11.1 Hz), 130.58 ((d, $^2J_{P-C}$) = 12.1 Hz), 130.58 ((d, $^2J_{P-C}$) = 12.1 Hz), 117.28 ((d, $^1J_{P-C}$) = 87.4 Hz), 39.39 ((d, $^3J_{P-C}$) = 21.1 Hz), 20.11 ((d, $^2J_{P-C}$) = 2.0 Hz), 19.27 ((d, $^1J_{P-C}$) = 55.3 Hz). **ATR-FTIR (cm⁻¹ (ranked intensity)):** 497 (9), 531 (2), 717 (1), 738 (3), 796 (6), 1107 (4), 1155 (7), 1481 (5), 1516 (8), 2897 (10). **ESI-MS (m/z):** ESI+: 320.2 ($[C_{21}H_{23}NP]^+$)

5.4.4   Poly(ethyl glyoxylate) Synthesis (**PEtG**)

In a Schlenk flask and at 20 °C, 2-nitrobenzyl alcohol (153 mg, 1.0 mmol) and (TMS)$_2$NLi (167 mg, 1.0 mmol) were combined in dry toluene (80 mL) and stirred for 5 min, before the rapid addition of freshly distilled EtG (20.0 mL, 200 mmol). The resulting solution was then cooled to –20 °C and vigorously stirred for 15 min. NEt$_3$ (1.20 mL, 9 mmol) was added and the solution was stirred for another 20 minutes. Benzyl chloromethyl ether (4.0 mL, 17 mmol) was instantly added and the resulting mixture was stirred for 3 h at –20 °C, before sealing the flask under N$_2$ gas, and transferring it into a –20 °C freezer where it was kept for 21 h. The polymerization mixture was then precipitated into methanol (1.0 L). The solvent was decanted, and the resulting residue was dried under vacuum. Yield = 16.0 g, 80%. **^{1}H NMR (400 MHz, CDCl$_3$):** δ = 1.31 (s, 3H; CH$_3$), 4.24 (s, 2H; CH$_2$), 5.54-5.73 (m, 1H, CH). Initiator and endcap peaks cannot be integrated accurately as they are very broad in the baseline. SEC: M$_n$ = 5.0 kg/mol, M$_w$ = 9.0 kg/mol, Đ = 1.8. T_o = 190 °C. T_g = - 12 °C.

5.4.5   Synthesis of **PGAm$_{BuP}$** and **PGAm$_{EtP}$**

Synthesis of PGAm$_{BuP}$ using NEt$_3$. PEtG (0.0100 g, 0.1 mmol of ester units), **BuP** (0.0413 g, 0.1 mmol), triethylamine (27 μL, 0.2 mmol) were mixed in 711 μL of MeCN-D$_3$ to keep the concentration of the reaction 0.1 g mL^{-1}. This solution was then transferred to an NMR tube and reacted in the dark at 70 °C for 5 days. Reactions involving higher equivalents of **BuP** and triethylamine were prepared by the same method.

Synthesis of PGAm$_{BuP}$ using TBD. PEtG (0.160 g, 1.56 mmol of ester units) dissolved in 1.6 mL of MeCN was added to a stirring solution of **BuP** (0.657 g, 1.56 mmol) and **TBD** (0.326 g, 2.34 mmol) in 9.83 mL of MeCN and left to stir in the dark for 15 minutes at room temperature. The light-yellow solution was then dried *in vacuo*, then redissolved in a minimal amount of MeOH. This solution was then transferred to 3.5 kDa regenerated cellulose (RC) dialysis tubing and dialyzed against 500 mL MeOH, changing the solution 3 times over 24 hours. The remaining solution was then dried *in vacuo* to yield a yellow solid (0.100 g, 12 %).

¹H NMR (400 MHz, CDCl₃): δ = 0.94 (broad, P-CH₂-CH₃-CH₂-C<u>H₃</u>), 1.27 (broad, O-CH₂-C<u>H₃</u>), 1.50 (broad, P-CH₂-C<u>H₃</u>-C<u>H₂</u>-CH₃), 1.96 (broad, NH-CH₂-C<u>H₂</u>-CH₂-P), 2.29 (broad P-C<u>H₂</u>-CH₃-CH₂-CH₃), 2.52 (NH-CH₂-CH₂-C<u>H₂</u>-P), 3.30 (broad, NH-C<u>H₂</u>-CH₂-CH₂-P), 4.17 (broad, O-C<u>H₂</u>-CH₃), 5.35 (broad, backbone CH from glyoxylamide), 5.65 (backbone CH from glyoxylate). **³¹P{¹H} NMR (161.82 MHz, D₂O):** δ = 33.64 (s).

Synthesis of PGAm_EtP using TBD. PEtG (0.218 g, 2.14 mmol of ester units) dissolved in 2.18 mL of MeCN was added to a stirring solution of **EtP** (0.722 g, 2.14 mmol) and **TBD** (0.447 g, 3.21 mmol) in 11.69 mL of MeCN and left to stir in the dark for 15 minutes at room temperature. The light-yellow solution was then dried *in vauco*, then redissolved in a minimal amount of MeOH. This solution was then transferred to 3.5 kDa RC dialysis tubing and dialyzed against 500 mL MeOH, changing the solution 3 times over 24 hours. The remaining solution was then dried *in vacuo* to yield a yellow solid (0.110 g, 15 %).**¹H NMR (400 MHz, D₂O):** δ = 1.03 (broad, P-CH₂-C<u>H₃</u>), 1.14 (broad, O-CH₂-C<u>H₃</u>), 1.66 (broad, NH-CH₂-C<u>H₂</u>-CH₂-P), 2.06 (broad, NH-CH₂-CH₂-C<u>H₂</u>-P and P-C<u>H₂</u>-CH₃), 3.64 (broad, NH-C<u>H₂</u>-CH₂-CH₂-P), 4.07 (broad, O-C<u>H₂</u>-CH₃), 5.09 (broad, backbone CH from glyoxylamide), 5.35 (backbone CH from glyoxylate). **³¹P{¹H} NMR (161.82 MHz, D₂O):** δ = 39.07 (s).

Synthesis of PGAm_BuP-AllylAm. Allylamine (116 uL, 1.5 mmol) was added to a stirring solution of **PGAm_BuP** (0.0750 g, 0.25 mmol) in 2 mL of MeOH. This solution was left to stir for 16 hours in the dark then precipitated into diethyl ether three times to remove residual amine. The resulting material was then dried to a yellow solid (0.0800 g, 60 %). Spectra coming this week. **¹H NMR (400 MHz, CDCl₃):** δ = 0.94 (broad, P-CH₂-CH₃-CH₂-C<u>H₃</u>), 1.49 (broad, P-CH₂-C<u>H₃</u>-C<u>H₂</u>-CH₃), 1.84 (broad, NH-CH₂-C<u>H₂</u>-CH₂-P), 2.26 (broad, P-C<u>H₂</u>-CH₃-CH₂-CH₃ and NH-CH₂-CH₂-C<u>H₂</u>-P), 3.28 (broad, NH-C<u>H₂</u>-CH₂-CH₂-P), 3.82 (broad NH-C<u>H₂</u>-CH-CH₂), 5.01-5.18 (broad NH-CH₂-CH-C<u>H₂</u> and backbone CH's from glyoxylamides), 5.86 (broad, NH-CH₂-C<u>H</u>-CH₂). **³¹P{¹H} NMR (161.82 MHz, D₂O):** δ = 33.64 (s). T_o = 135 °C T_g = 85 °C.

Synthesis of PGAm$_{EtP-AllylAm}$. Allylamine (154 uL, 2.0 mmol) was added to a stirring solution of **PGAm$_{EtP}$** (0.100 g, 0.3 mmol) in 2 mL of MeOH. This solution was left to stir for 16 hours in the dark the dried *in vauco* to remove residual amine and solvent. then precipitated into diethyl ether three times to remove residual amine. The resulting material was then dried to a yellow solid (0.0800 g, 50 %). **¹H NMR (400 MHz, D₂O):** δ = 1.10-1.17 (m, P-CH₂-C$\underline{H}$₃), 1.74 (broad, NH-CH₂-C$\underline{H}$₂-CH₂-P), 2.14 (broad, NH-CH₂-CH₂-C$\underline{H}$₂-P and P-C$\underline{H}$₂-CH₃), 3.27 (broad, NH-C$\underline{H}$₂-CH₂-CH₂-P), 3.75 (broad, NH-C$\underline{H}$₂-CH-CH₂) 5.10-5.22 (broad, NH-CH₂-CH-C$\underline{H}$₂ and backbone CH from glyoxylamide with pendant phosphonium), 5.44 (broad, backbone CH from glyoxylamide with pendant allyl group), 5.78 (broad NH-CH₂-C$\underline{H}$-CH₂), 7.35 (broad, aromatic protons from initiator and end cap). **³¹P{¹H} NMR (161.82 MHz, D₂O):** δ = 39.07 (s). T_o = 140 °C T_g = 70 °C.

5.4.6   General Film Preparation

Formulation samples of 25 μL were drop casted onto glass slides with one strip of electrical tape at each end. A second glass slide was then mounted on top of the glass slide/formulation. The formulation was then placed in a 60 °C for 24 hours to cure. The formulation consisted of **PGAm$_{EtP}$** (78 wt %), pentaerythriyol tetrakis(3-mercaptopropionate) (28 wt %), AIBN (1 wt %) and 0.33 g of DMSO.

5.5   References

(1)   Antimicrobial resistance https://www.who.int/news-room/fact-sheets/detail/antimicrobial-resistance (accessed Nov 1, 2019).

(2)   Prytula, M. A. *When Antibiotics Fail*; 2019.

(3)   Oie, S.; Hosokawa, I.; Kamiya, A. Contamination of Room Door Handles by Methicillin-Sensitive/ Methicillin-Resistant Staphylococcus Aureus. *J. Hosp. Infect.* **2002**, *51*, 140–143.

(4)   Ciragil, P.; Gul, M.; Aral, M. Bacterial Contamination of Computers and Telephones in a University Hospital in Turkey. *J. Hosp. Infect.* **2006**, *62*, 247–248.

(5)   Weinstein, R. A.; Hota, B. Contamination, Disinfection, and Cross-Colonization: Are Hospital Surfaces Reservoirs for Nosocomial Infection? *Clin. Infect. Dis.* **2004**,

39, 1182–1189.

(6)   Page, K.; Wilson, M.; Parkin, I. Antimicrobial Surfaces and Their Potential in Reducing the Role of the Inanimate Environment in the Incidence of Hospital-Acquired Infections. *J. Mater. Chem.* **2009**, *19*, 3819–3831.

(7)   Lichter, J. A.; Van Vlietpa, K. J.; Rubner, M. F. Design of Antibacterial Surfaces and Interfaces: Polyelectrolyte Multilayers as a Multifunctional Platform. *Macromolecules* **2009**, *42*, 8573–8586.

(8)   Stewart, P. S.; Costerton, J. W. Antibiotic Resistance of Bacteria in Biofilms. *Lancet* **2001**, *358*, 135–138.

(9)   Gupta, P.; Sarkar, S.; Das, B.; Bhattacharjee, S.; Tribedi, P. Biofilm, Pathogenesis and Prevention—a Journey to Break the Wall: A Review. *Arch. Microbiol.* **2016**, *198*, 1–15.

(10)   Huang, K. S.; Yang, C. H.; Huang, S. L.; Chen, C. Y.; Lu, Y. Y.; Lin, Y. S. Recent Advances in Antimicrobial Polymers: A Mini-Review. *Int. J. Mol. Sci.* **2016**, *17*, 1-14.

(11)   Zhang, F.; Kang, E. T.; Neoh, K. G.; Wang, P.; Tan, K. L. Surface Modification of Stainless Steel by Grafting of Poly(Ethylene Glycol) for Reduction in Protein Adsorption. *Biomaterials* **2001**, *22*, 1541–1548.

(12)   Lee, S.; Vörös, J. An Aqueous-Based Surface Modification of Poly(Dimethylsiloxane) with Poly(Ethylene Glycol) to Prevent Biofouling. *Langmuir* **2005**, *21*, 11957–11962.

(13)   Gyo, M.; Nikaido, T.; Okada, K.; Yamauchi, J.; Tagami, J.; Matin, K. Surface Response of Fluorine Polymer-Incorporated Resin Composites to Cariogenic Biofilm Adherence. *Appl. Environ. Microbiol.* **2008**, *74*, 1428–1435.

(14)   Kanazawa, A; Ikeda, T, Endo, T. Polymeric Phosphonium Salts as a Novel Class of Cationic Biocides. II. Effects of Counter Anion and Molecular Weight on Antibacterial Activity of Polymeric Phosphonium Salts. *J. Polym. Sci., Part A: Polym. Chem.* **1993**, *31*, 1441–1447.

(15) Rahn, O.; Eseltine, W. P. Quaternary Ammonium Compounds. *Annu. Rev. Microbiol.* **1947**, *1*, 173–192.

(16) Waghu, F. H.; Joseph, S.; Ghawali, S.; Martis, E. A.; Madan, T.; Venkatesh, K. V.; Idicula-Thomas, S. Designing Antibacterial Peptides with Enhanced Killing Kinetics. *Front. Microbiol.* **2018**, *9*, 1–10.

(17) Domagk, G. Eine Neue Klasse von Desinfektionsmitteln. *Dtsch. Med. Wochenschr.* **1935**, *61*, 829–832.

(18) Kanazawa, A.; Ikeda, T.; Endo, T. Novel Polycationic Biocides: Synthesis and Antibacterial Activity of Polymeric Phosphonium Salts. *J. Polym. Sci., Part A: Polym. Chem.* **1993**, *31*, 335–343.

(19) Kanazawa, A.; Ikeda, T.; Endo, T. Novel Polycationic Biocides: Synthesis and Antibacterial Activity of Polymeric Phosphonium Salts. *J. Polym. Sci., Part A: Polym. Chem.* **1993**, *31*, 335–343.

(20) Bradaric, C. J.; Downard, A.; Kennedy, C.; Robertson, A. J. Industrial Preparation of Phosphonium Ionic Liquids. *Green Chem.* **2003**, *5*, 143–152.

(21) Cuthbert, T. J.; Guterman, R.; Ragogna, P. J.; Gillies, E. R. Contact Active Antibacterial Phosphonium Coatings Cured with UV Light. *J. Mater. Chem. B.* 2015, pp 1474–1478.

(22) Cuthbert, T. J.; Harrison, T. D.; Ragogna, P. J.; Gillies, E. R. Synthesis, Properties, and Antibacterial Activity of Polyphosphonium Semi-Interpenetrating Networks. *J. Mater. Chem. B* **2016**, *4*, 4872–4883.

(23) Asri, L. A. T. W.; Crismaru, M.; Roest, S.; Chen, Y.; Ivashenko, O.; Rudolf, P.; Tiller, J. C.; Van Der Mei, H. C.; Loontjens, T. J. A.; Busscher, H. J. A Shape-Adaptive, Antibacterial-Coating of Immobilized Quaternary-Ammonium Compounds Tethered on Hyperbranched Polyurea and Its Mechanism of Action. *Adv. Funct. Mater.* **2014**, *24*, 346–355.

(24) Cao, Z.; Mi, L.; Mendiola, J.; Ella-Menye, J. R.; Zhang, L.; Xue, H.; Jiang, S. Reversibly Switching the Function of a Surface between Attacking and Defending

against Bacteria. *Angew. Chem., Int. Ed.* **2012**, *51*, 2602–2605.

(25) Bieser, A. M.; Thomann, Y.; Tiller, J. C. Contact-Active Antimicrobial and Potentially Self-Polishing Coatings Based on Cellulose. *Macromol. Biosci.* **2011**, *11*, 111–121.

(26) Vasanthi, K. Biodegradable Polymers - A Review. *Polym. Sci.* **2017**, *3*, 1–7.

(27) Mueller, R. J. Biological Degradation of Synthetic Polyesters-Enzymes as Potential Catalysts for Polyester Recycling. *Process Biochem.* **2006**, *41*, 2124–2128.

(28) Sagi, A.; Weinstain, R.; Karton, N.; Shabat, D. Self-Immolative Polymers. *J. Am. Chem. Soc.* **2008**, *130*, 5434–5435.

(29) Wu, Y.; Zhang, L.; Zhang, M.; Liu, Z.; Zhu, W.; Zhang, K. Bottlebrush Polymers with Self-Immolative Side Chains. *Polym. Chem.* **2018**, *9*, 1799–1806.

(30) Xiao, Y.; Li, H.; Zhang, B.; Cheng, Z.; Li, Y.; Tan, X.; Zhang, K. Modulating the Depolymerization of Self-Immolative Brush Polymers with Poly(Benzyl Ether) Backbones. *Macromolecules* **2018**, *51*, 2899–2905.

(31) Poly, D.; Dilauro, A. M.; Robbins, J. S.; Phillips, S. T. Reproducible and Scalable Synthesis of End-Cap-Functionalized Depolymerizable Poly(Phthalaldehydes). *Macromolecules* **2013**, *46*, 2963–2968.

(32) Fan, B.; Trant, J. F.; Wong, A. D.; Gillies, E. R. Polyglyoxylates: A Versatile Class of Triggerable Self-Immolative Polymers from Readily Accessible Monomers. *J. Am. Chem. Soc.* **2014**, *136*, 10116–10123.

(33) Gisbert-Garzaran, M.; Lozano, D.; Vallet-Regí, M.; Manzano, M. Self-Immolative Polymers as Novel PH-Responsive Gate Keepers for Drug Delivery. *RSC Adv.* **2017**, *7*, 132–136.

(34) Peterson, G. I.; Church, D. C.; Yakelis, N. A.; Boydston, A. J. 1,2-Oxazine Linker As a Thermal Trigger for Self-Immolative Polymers. *Polymer* **2014**, *55*, 5980–5985.

(35) Wong, A. D.; Güngör, T. M.; Gillies, E. R. Multiresponsive Azobenzene End-Cap for Self-Immolative Polymers. *ACS Macro Lett.* **2014**, *3*, 1191–1195.

(36) De Gracia Lux, C.; McFearin, C. L.; Joshi-Barr, S.; Sankaranarayanan, J.; Fomina,

N.; Almutairi, A. Single UV or near IR Triggering Event Leads to Polymer Degradation into Small Molecules. *ACS Macro Lett*. **2012**, *1*, 922–926.

(37)   Lewis, G. G.; Robbins, J. S.; Phillips, S. T. Phase-Switching Depolymerizable Poly(Carbamate) Oligomers for Signal Amplification in Quantitative Time-Based Assays. *Macromolecules* **2013**, *46*, 5177–5183.

(38)   Esser-Kahn, A. P.; Sottos, N. R.; White, S. R.; Moore, J. S. Programmable Microcapsules from Self-Immolative Polymers. *J*. *Am*. *Chem*. *Soc*. **2010**, *132*, 10266–10268.

(39)   Gambles, M. T.; Fan, B.; Borecki, A.; Gillies, E. R. Hybrid Polyester Self-Immolative Polymer Nanoparticles for Controlled Drug Release. *ACS Omega* **2018**, *3*, 5002–5011.

(40)   Belloncle, B.; Burel, F.; Oulyadi, H.; Bunel, C. Study of the in Vitro Degradation of Poly(Ethyl Glyoxylate). *Polym*. *Degrad*. *Stab*. **2008**, *93*, 1151–1157.

(41)   Belloncle, B.; Bunel, C.; Menu-Bouaouiche, L.; Lesouhaitier, O.; Burel, F. Study of the Degradation of Poly(Ethyl Glyoxylate): Biodegradation, Toxicity and Ecotoxicity Assays. *J*. *Polym*. *Environ*. **2012**, *20*, 726–731.

(42)   Sirianni, Q. E. A.; Rabiee Kenaree, A.; Gillies, E. R. Polyglyoxylamides: Tuning Structure and Properties of Self-Immolative Polymers. *Macromolecules* **2019**, *52*, 262–270.

(43)   Ree, L. H. S.; Sirianni, Q. E. A.; Gillies, E. R.; Kelland, M. A. Systematic Study of Polyglyoxylamides as Powerful, High-Cloud-Point Kinetic Hydrate Inhibitors. *Energy Fuels* **2019**, *33*, 2067–2075.

(44)   Ergene, C.; Palermo, E. F. Self-Immolative Polymers with Potent and Selective Antibacterial Activity by Hydrophilic Side Chain Grafting. *J*. *Mater*. *Chem*. *B* **2018**, *6*, 7217–7229.

(45)   Ergene, C.; Palermo, E. F. Cationic Poly(Benzyl Ether)s as Self-Immolative Antimicrobial Polymers. *Biomacromolecules* **2017**, *18*, 3400–3409.

(46)   Zhang, Y.; Zhang, S.; Lu, X.; Zhou, Q.; Fan, W.; Zhang, X. P. Dual Amino-

Functionalised Phosphonium Ionic Liquids for CO2 Capture. *Chem. - Eur. J.* **2009**, *15*, 3003–3011.

(47) Kuang, Y.; Sechi, M.; Nurra, S.; Ljungman, M.; Neamati, N. Design and Synthesis of Novel Reactive Oxygen Species Inducers for the Treatment of Pancreatic Ductal Adenocarcinoma. *J. Med. Chem.* **2018**, *61*, 1576–1594.

(48) Rabiee Kenaree, A.; Gillies, E. R. Controlled Polymerization of Ethyl Glyoxylate Using Alkyllithium and Alkoxide Initiators. *Macromolecules* **2018**, *51*, 5501–5510.

(49) Kiesewetter, M. K.; Scholten, M. D.; Kirn, N.; Weber, R. L.; Hedrick, J. L.; Waymouth, R. M. Cyclic Guanidine Organic Catalysts: What Is Magic About Triazabicyclodecene? *J. Org. Chem.* **2009**, *74*, 9490–9496.

(50) Sabot, C.; Kumar, K. A.; Meunier, S.; Mioskowski, C. A Convenient Aminolysis of Esters Catalyzed by 1,5,7-Triazabicyclo[4.4.0]Dec-5-Ene (TBD) under Solvent-Free Conditions. *Tetrahedron Lett.* **2007**, *48*, 3863–3866.

(51) Van Guyse, J. F. R.; Verjans, J.; Vandewalle, S.; De Bruycker, K.; Du Prez, F. E.; Hoogenboom, R. Full and Partial Amidation of Poly(Methyl Acrylate) as Basis for Functional Polyacrylamide (Co)Polymers. *Macromolecules* **2019**, *52*, 5102–5109.

Chapter 6

6 Conclusions and Future Work

6.1 Conclusions

The work presented in this thesis demonstrated the utility of incorporating phosphonium salts into crosslinked polymer networks. The variety of applications in drug delivery, self-healing materials and anti-bacterial surfaces demonstrate that materials containing phosphonium salts are tunable and useful in a wide variety of applications.

Chapter 2 outlined the synthesis of three different phosphonium salts and their reaction with poly(ethylene glycol) dimethacrylate (PEGDMA) to create cationic hydrogels. The hydrogels were loaded with an anionic dye, fluorescein and an anionic anti-inflammatory drug, diclofenac. The ability of the hydrogels to retain the anionic molecules was first monitored by loading with fluorescein dye. The networks that contained the phosphonium salts remained red after washing indicating fluorescein retention, but networks of pure PEGDMA did not retain any detectable dye. The release of the molecules was then completed in buffered solutions at pH at 5, 6 and 7.4 and could be tuned based on the structure of phosphonium, the ionic strength of the solution and the pH. Release in a control solution of deionized (DI) water was also completed and yielded very low levels of release. From these results, it can be concluded that these networks were able to load anionic molecules through electrostatic interactions and retain them until a stimulus was applied. The identity of the phosphonium was also important as the networks containing more hydrophilic phosphonium salts released fluorescein and diclofenac more rapidly than the networks containing the hydrophobic phosphonium salts.

Chapter 3 introduced the use of polyphosphoniums in ionic polymer networks for drug delivery. It was anticipated that these highly charged networks would be able to retain anionic molecules and that the release could be sustained for long periods of time due to the high charge density. Four different phosphonium monomers with varying hydrophobicities were created and polymerized to produce their corresponding polyphosphoniums. Ionic polymer networks were then formed by mixing the

polyphosphoniums with a biologically relevant anionic polysaccharide, sodium hyaluronate. Network properties were characterized by swelling studies, rheology and self-healing abilities and it was concluded that network properties could be tuned based on the identity of the polyphosphonium and the medium in which the network was immersed. Drug release rates were also studied with fluorescein, diclofenac and ATP where fluorescein and diclofenac were released very slowly from the networks over 60 days. The slow release was attributed to the dense ionic network structure, combined with ionic and hydrophobic interactions. ATP, a more hydrophilic dianion, was released much more rapidly over 1-2 days. These materials demonstrated self-healing abilities in physiologically relevant salt concentrations, making them promising candidates for applications in the biomedical field. In conclusion, it was clear that the ionic networks could retain anionic molecules and release them over longer periods of time as compared with the hydrogels prepared in Chapter 2. This could be due to the high charge density and dense packing that these networks have.

Chapters 2 and 3 compare the release of a variety of anionic molecules including fluorescein and diclofenac from covalent hydrogels and ionic polymer networks. In each case, the release of fluorescein and diclofenac was more sustained from the ionic polymer networks due to the higher charge density and denser packing. In both of these chapters, phosphonium salts or polyphosphonium salts were utilized for drug or dye binding. Therefore, in Chapter 4 it was of interest to perform a study comparing network properties and release rates in analogous phosphonium and ammonium based ionic polymer networks. Ionic polymer networks were again chosen because of the sustained drug release and self-healing abilities of the networks prepared in Chapter 3. Sodium alginate was used in this study to probe whether or not incorporating a different polysaccharide would have an impact on the network properties and release rates. Network properties were characterized by swelling studies, rheology and self-healing abilities. Networks prepared with identical phosphoniums and either hyaluronate and alginate swelled in PBS exhibited similar elastic and viscous moduli over the tested frequency range. When the networks were swelled in PBS, higher swelling occurred in the phosphonium/hyaluronate networks. All networks also exhibited self-healing abilities in the presence of salt. The anions chosen for release from the polyonium and alginate system were fluorescein, an anti-inflammatory drug

etodolac, and the chemotherapy agent methotrexate. The release rates of all drugs from the polyonium and alginate system was much quicker (~1 week) compared to the networks consisting of phosphonium and hyaluronate, which had sustained delivery for up to 2 months. Fluorescein dye was the only anionic molecule used in both studies and due to its rapid release rate from the polyphosphonium and alginate networks, it can be concluded that the chosen anionic polysaccharide does affect release rates. The release of the three anionic molecules from the polyonium and alginate networks depended on the structure of each onium and not the identity of nitrogen or phosphorus. The release rates for all molecules were fastest from **P-Bu-P-Alg**, **P-Bu-N-Alg** followed by **P-Hp-P-Alg** and then **P-Et-P-Alg** and **P-Et-N-Alg**. Network images as characterized by SEM, showed the largest pore sizes for **P-Bu-P-Alg**, **P-Bu-N-Alg** followed by **P-Hp-P-Alg** and then **P-Et-P-Alg**, **P-Et-N-Alg** which could be the reason for the faster release from **P-Bu-P-Alg**, **P-Bu-N-Alg**, although caution must be taken in interpreting these results as changes in morphology and artifacts can occur as a result of drying the samples for SEM. Fluorescein released at the slowest rate of all the molecules which could be attributed to its ionic and more hydrophobic interactions with the networks. From these studies it can be concluded that the anionic polysaccharide does affect network properties and drug delivery rates. The substituents surrounding the pnictogen (nitrogen or phosphorus) does have a big effect on release rates the identity if the pnictogen does not.

The work described in Chapter 5 aimed to combine degradable polymers developed in the Gillies lab with the antibacterial phosphoniums developed in the Ragogna and Gillies labs. This chapter outlined progress towards creating self-immolative polymers with pendent phosphonium salts, which have not been reported to date. This work can be applied for the development of degradable antibacterial surface coatings.

6.2   Future Work

6.2.1   Polyplexes Combining DNA/RNA with Poly(phosphoniums)

While the use of self-immolative polymers with pendent phosphonium cations in Chapter 5 was explored, the ability of these polymers to bind different anionic groups, was not. In recent years, there has been growing interest in polymer-based delivery systems for

polynucleotides such as ribonucleic acid (RNA) or deoxyribonucleic acid (DNA). Synthetic polymers are of interest because of their wide range of polymerization techniques and the ability to modify the polymers post-polymerization. One of the most common techniques to deliver nucleotides is to complex them into polyplexes, where the negatively charged nucleotide is bound to cationic polymers by ionic interactions (Figure 6-1).
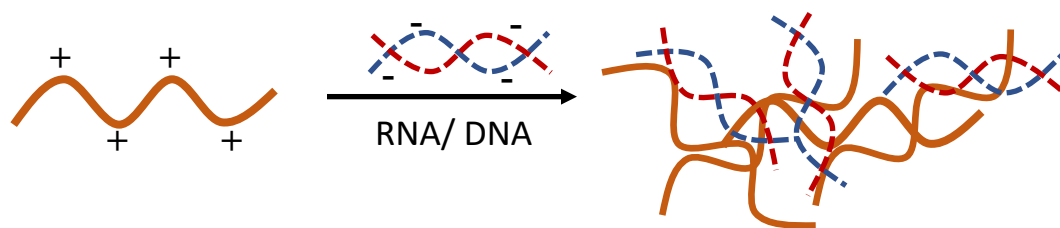
Figure 6-1 Illustration of polyplex formation.

To form these polyplexes, ammonium-based polymers have been studied extensively, whereas phosphonium based polymers have not been explored as heavily.[1] Poly(ethyl glyoxylate)s could be synthesized to contain redox or acid sensitive endcaps, where these would be relevant to the delivery location desired. Phosphonium salts could then be added to the backbone through an amidation reaction as discovered in Chapter 5. Upon purification, the polyphosphoniums and RNA/DNA could be complexed then implanted or injected into the desired region. Degradation of the polyphosphonium would then release the complexed DNA/RNA for use.

6.2.2   Improving Stability of Phosphonium/ Hyaluronate PECs

The polymer networks described in Chapter 3 showed promising results for applications in self-healing and sustained drug delivery. Nevertheless, the structural integrity of the networks decreased over time as the bonds became disrupted by salt. To improve this and increase the material lifetime, light crosslinking of the hyaluronic acid could be incorporated which is hypothesized to increase their mechanical strength. One crosslinker to consider is 1,4-butanediol diglycidyl ether, which in the presence of NaOH can react with hydroxyl groups on hyaluronic acid to provide crosslinking.[2] The synthesis of these networks would remain unchanged. After formation of the network they could be swelled into a solution containing 1,4-butanediol diglycidyl ether to allow for these molecules to

be taken up by the network. Then, the solution could be basified to crosslink (Figure 6-2). Varying the crosslinking ratio could be studied to examine the effect on release rates.
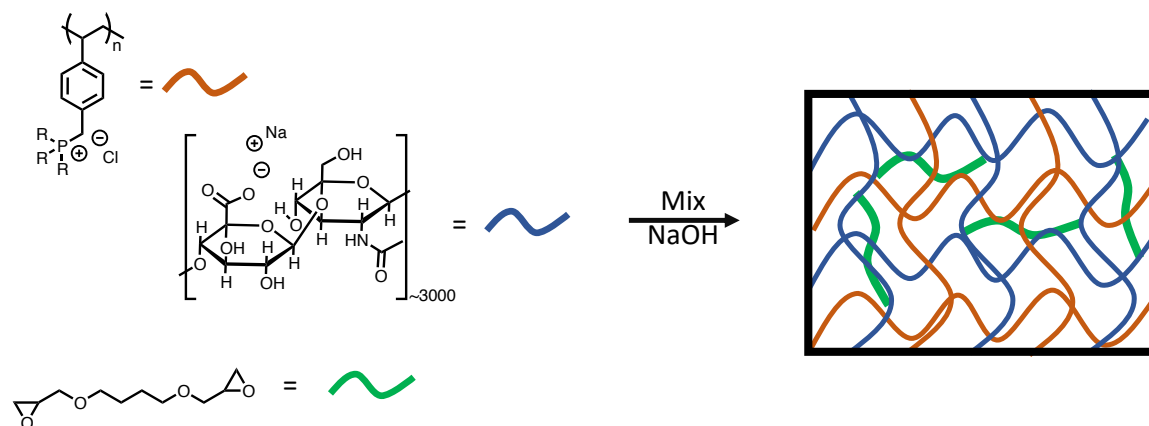
Figure 6-2 Proposed ionic network formation and additional covalent crosslinking.

6.2.3   Oxygen and Metal Scavenging Materials

In the 1960's, Pellon reported that primary phosphines could undergo radical mediated hydrophosphination, similar to hydrothiolation in their analogous thiols.[3] More recently, our group developed a method to create polymer networks using hydrophosphination chemistry.[4] In this work, networks were formed by the reaction of a diphosphine with various crosslinkers to create soft or brittle materials that imposed different physical and chemical properties. The high phosphine content in the networks also allowed for oxygen scavenging properties but some limitations can arise after oxidation, such as the lack of degradability. To build on this concept, the introduction of a degradable oxygen scavenging materials could allow for controlled degradation once the materials become fully oxidized. One option is to utilize the degradable poly(glyoxylamide)s our group has developed. In this proposal, poly(ethyl glyoxylate) could be synthesized to contain relevant end-caps related to the desired degradation stimulus. After the polymer is synthesized, excess allylamine could be added to the polymer to form the corresponding poly(glyoxylamide). Then this polymer cold be reacted with PH$_3$ on our specialized PH$_3$ line to create a network (Scheme 6-1).Upon application and oxidation of this new material it could then be

degraded upon exposure to a stimulus and a new layer applied if necessary. These polymer networks could also find use as metal scavengers. We also recently reported polymer networks prepared from phosphane-ene chemistry that successfully sequestered rhodium and ruthenium from hydrogenation and ring closing metathesis reactions.[5] If the metal coordination is successful in the degradable networks, they could serve as useful platforms for heavy metal sequestration in contaminated industrial water. Upon full saturation of metals, these materials could be degraded upon command.
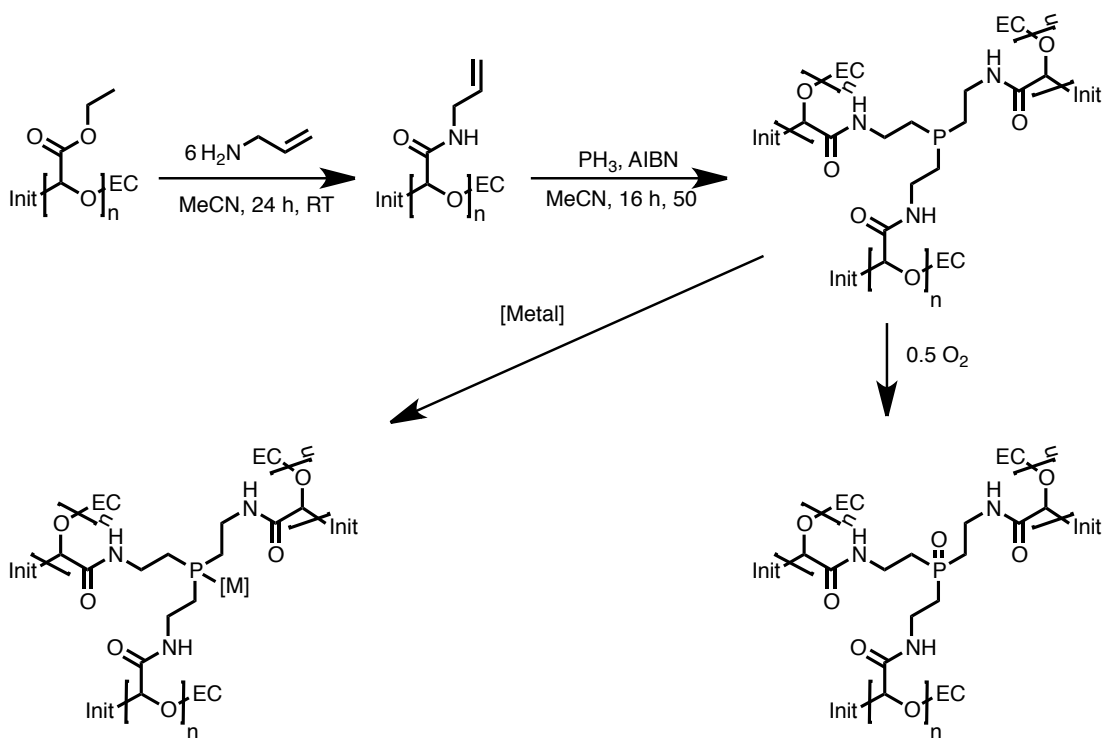
Scheme 6-1 Proposed pathway to create degradable oxygen and metal scavenging materials.

6.2.4 Self-Regenerating Surfaces

Although the progress towards degradable films was completed in Chapter 5, one main issue involves the re-application needed after fouling and subsequent degradation of the surface. To build on this idea, if a material was able to shed its fouled top surface to reveal another layer, this could extend the life-time of the coating dramatically. Layer-by-layer approaches have been developed but due to interpenetration of the polymers as the layers increase, shedding a specific layer is very challenging.[6] An improved method could involve

polymer multi-layer stacks, where each layer is much thicker.[7] In this proposed project, a covalently bound bottom layer would be applied, then an antibacterial layer could be coated on top followed by a stimuli-responsive layer. In the purposed system, poly(ethyl glyoxylate) would be synthesized and reacted with (3-aminopropyl)triethoxylsilane which could then be deposited on a glass substrate (Figure 6-3).[8] The antibacterial phosphonium layer could then be added by spin coating and polymerized by heat. Poly(ethyl glyoxylate), without the pendent siloxane, could be deposited on this surface to act as the degradable layer and this could then be repeated to create *n* layers. The exposed top layer would be the phosphonium layer and upon fouling, this surface could be irradiated with light and the top layer could be released. Ideally the applied light would only initiate depolymerization in the first sacrificial layer and not subsequent layers leaving an exposed new phosphonium layer that is now against active bacteria.
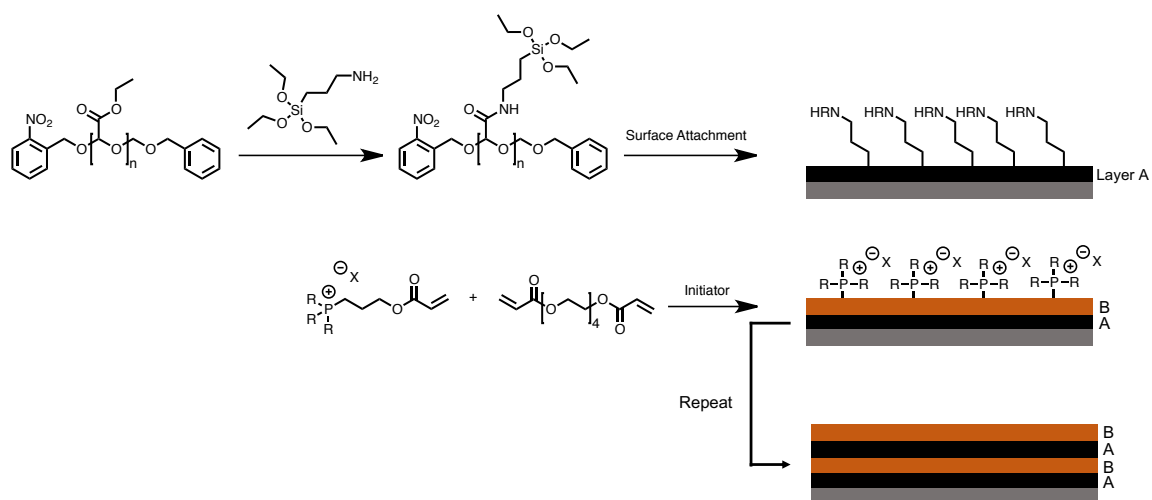
Figure 6-3 Proposed multi-layer stack incorporating antibacterial phosphoniums and degradable poly(ethyl glyoxylate).

6.3   References

(1)   Loczenski Rose, V.; Mastrotto, F.; Mantovani, G. Phosphonium Polymers for Gene Delivery. *Polym. Chem.* **2017**, *8*, 353–360.

(2)   Khunmanee, S.; Jeong, Y.; Park, H. Crosslinking Method of Hyaluronic-Based Hydrogel for Biomedical Applications. *J. Tissue Eng.* **2017**, *8*, 204173141772646.

(3)   Pellon, J. Reversibility in the Reaction of Phosphinyl Radicals with Olefins. *J. Am. Chem. Soc.* **1961**, *83*, 1915–1916.

(4)   Guterman, R.; Rabiee Kenaree, A.; Gilroy, J. B.; Gillies, E. R.; Ragogna, P. J. Polymer Network Formation Using the Phosphane–Ene Reaction: A Thiol–Ene Analogue with Diverse Postpolymerization Chemistry. *Chem. Mater.* **2015**, *27*, 1412–1419.

(5)   Cuthbert, T. J.; Evoy, E.; Bow, J. P. J.; Guterman, R.; Stubbs, J. M.; Gillies, E. R.; Ragogna, P. J.; Blacquiere, J. M. CapturePhos-A Phosphorus-Rich Polymer as a Homogeneous Catalyst Scavenger. *Catal. Sci. Technol.* **2017**, *7*, 2685–2688.

(6)   Wood, K. C.; Boedicker, J. Q.; Lynn, D. M.; Hammond, P. T. Tunable Drug Release from Hydrolytically Degradable Layer-by-Layer Thin Films. *Langmuir* **2005**, *21*, 1603–1609.

(7)   Riga, E. K.; Gillies, E.; Lienkamp, K. Self-Regenerating Antimicrobial Polymer Surfaces via Multilayer-Design—Sequential and Triggered Layer Shedding under Physiological Conditions. *Adv. Mater. Interfaces* **2019**, *6*, 1–12.

(8)   Wang, W.; Vaughn, M. W. Morphology and Amine Accessibility of (3-Aminopropyl) Triethoxysilane Films on Glass Surfaces. *Scanning* **2008**, *30*, 65–77.

Chapter 7

7 Appendices

7.1 Appendix A: Supporting Information for Chapter 2
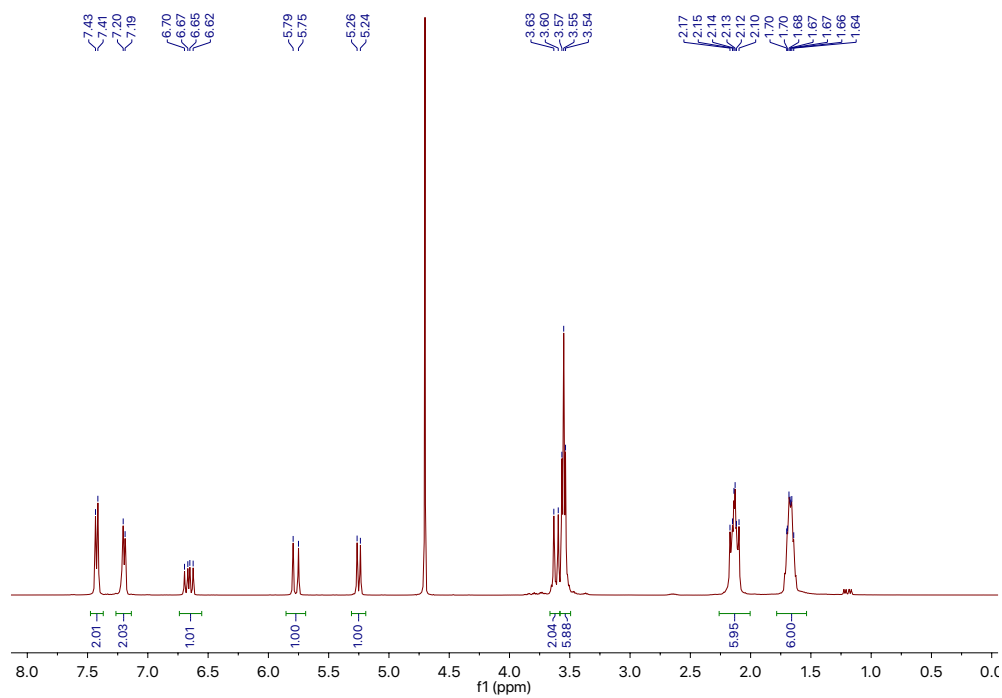
Figure A1. ^{1}H NMR spectrum of **T(hp)-P** monomer (400 MHz, D$_2$O).
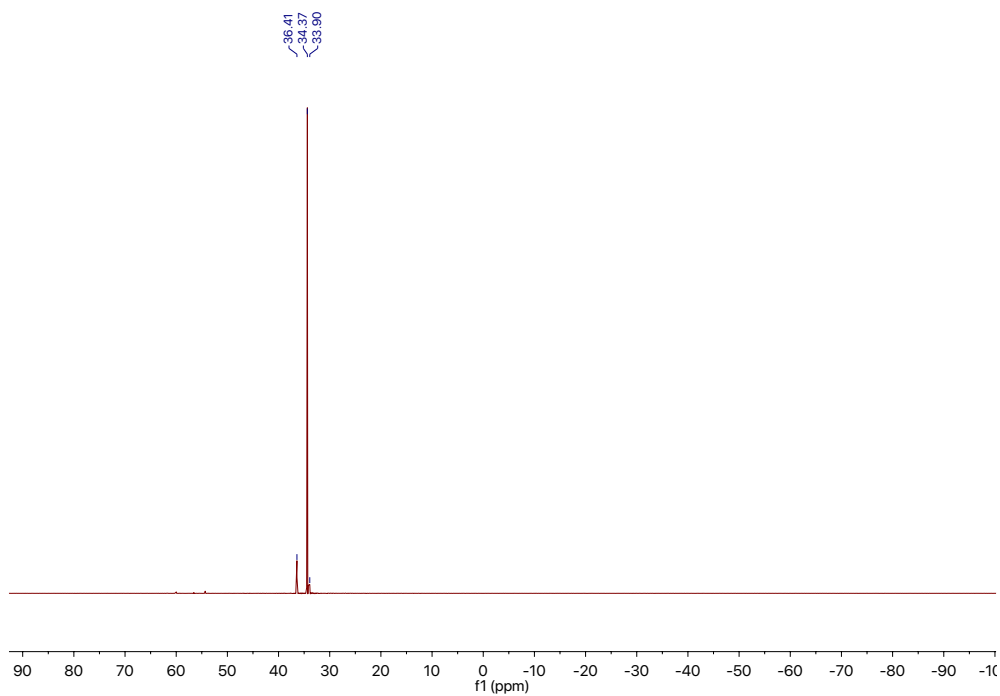
Figure A2. $^{31}P\{^1H\}$ NMR spectrum of **T(hp)-P** monomer (161.8 MHz, D$_2$O).
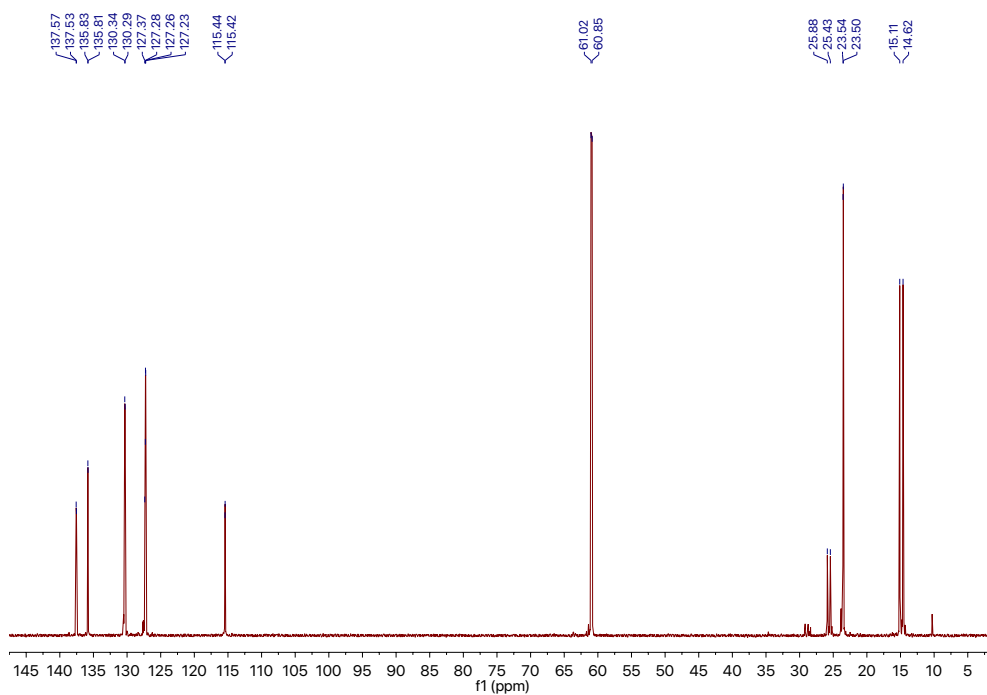
Figure A3. $^{13}C\{^1H\}$ NMR spectrum of **T(hp)-P** monomer (100.5 MHz, D$_2$O).
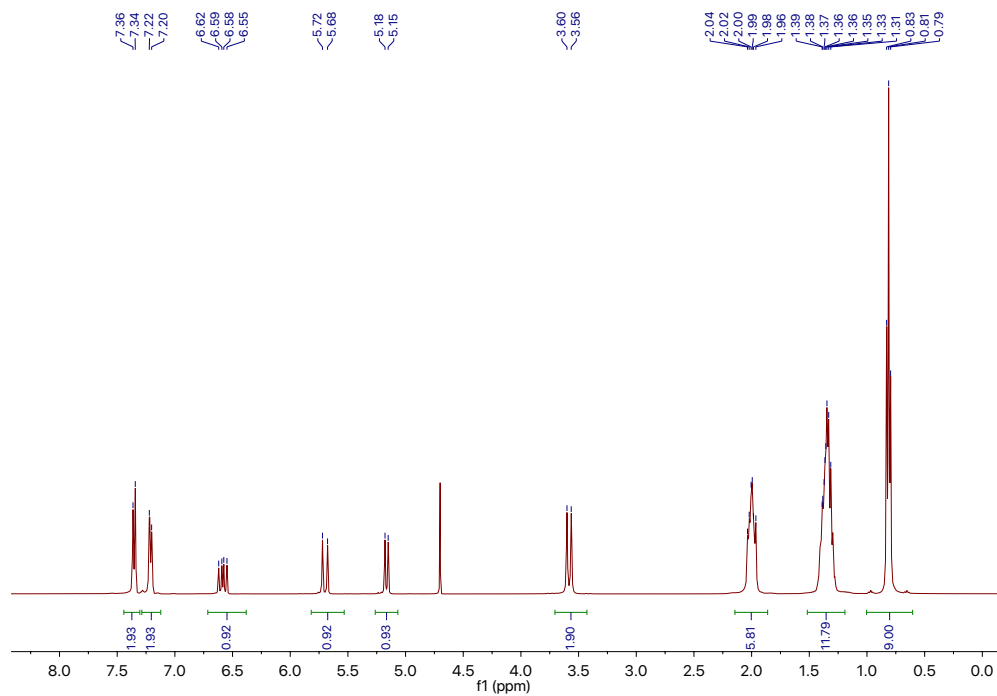
Figure A4. ^{1}H NMR spectrum of **Bu-P** monomer (400 MHz, D$_2$O).
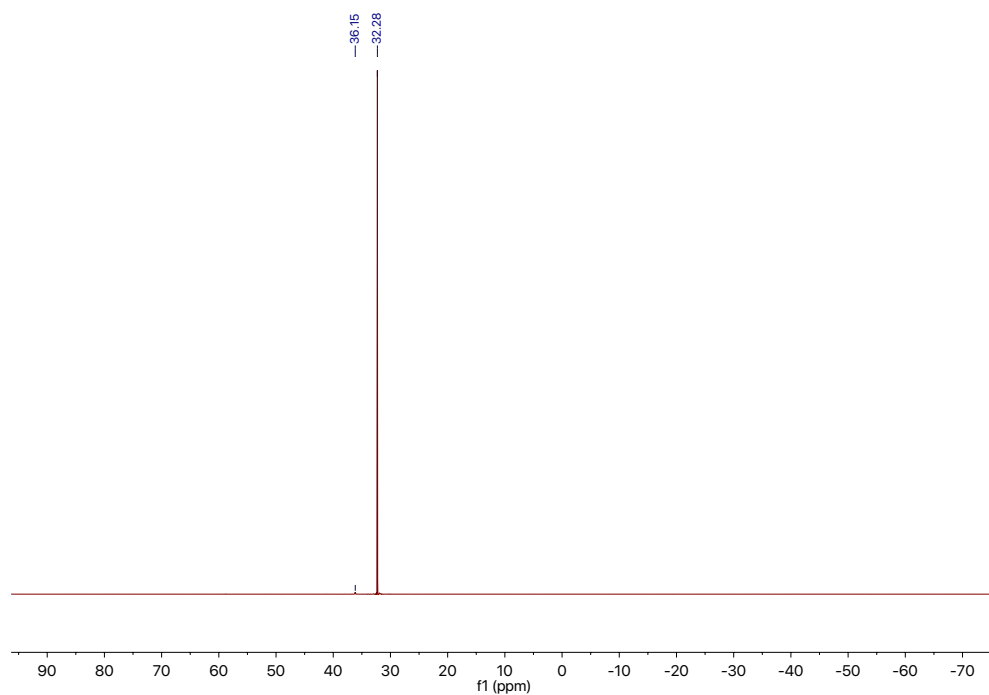
Figure A5. ^{31}P{^{1}H} NMR spectrum of **Bu-P** monomer (161.8 MHz, D$_2$O).
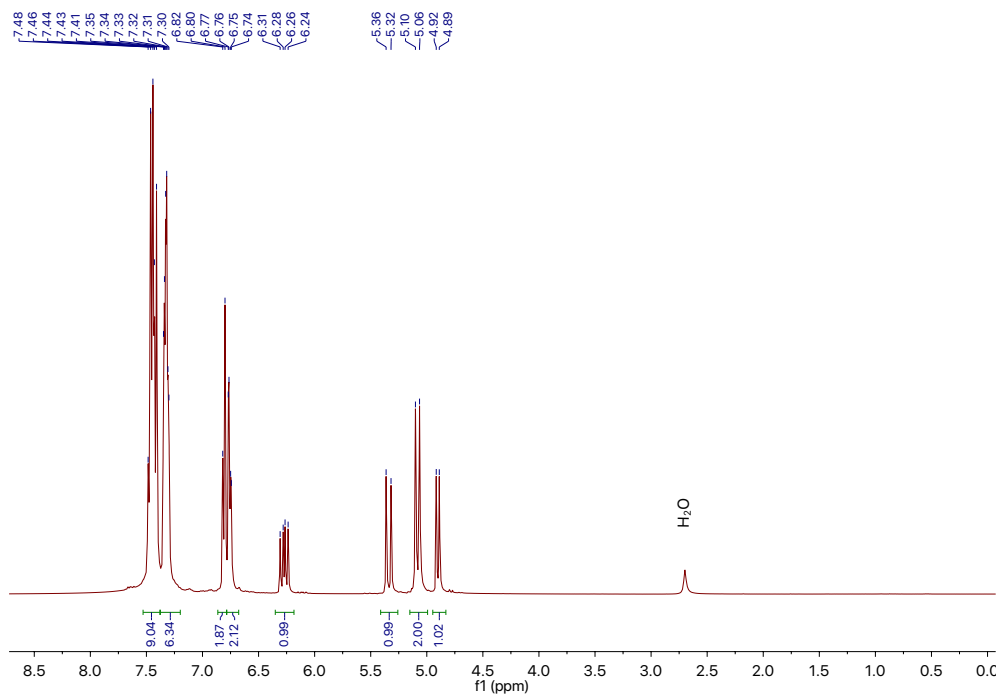
Figure A6. ^{1}H NMR spectrum of **Ph-P** monomer (400 MHz, CDCl$_3$).
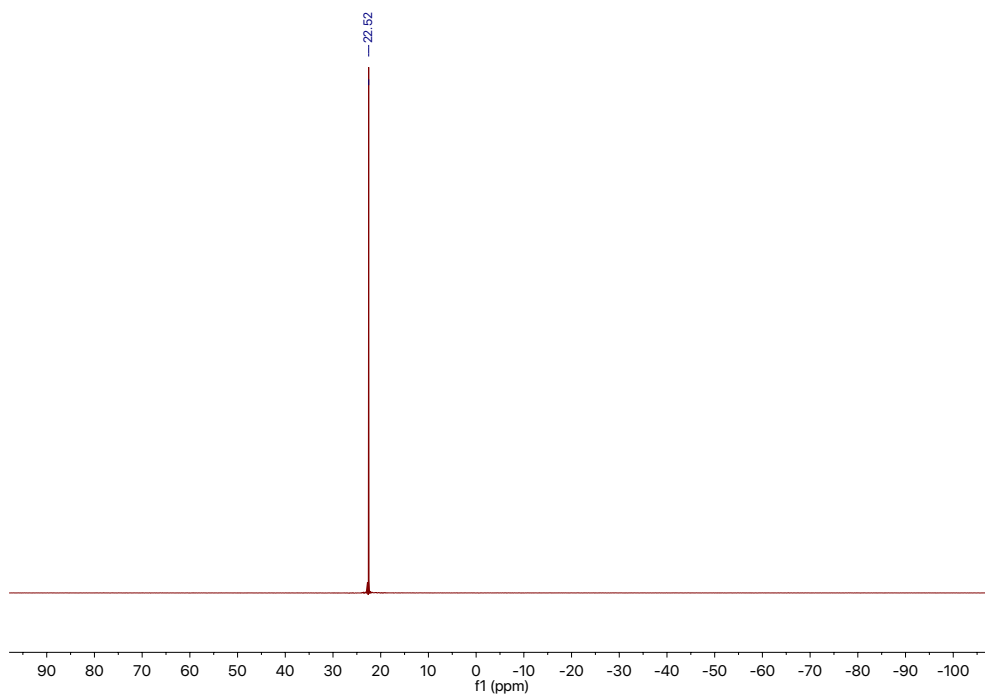
Figure A7. ^{31}P{^{1}H} NMR spectrum of **Ph-P** monomer (161.8 MHz, CDCl$_3$).
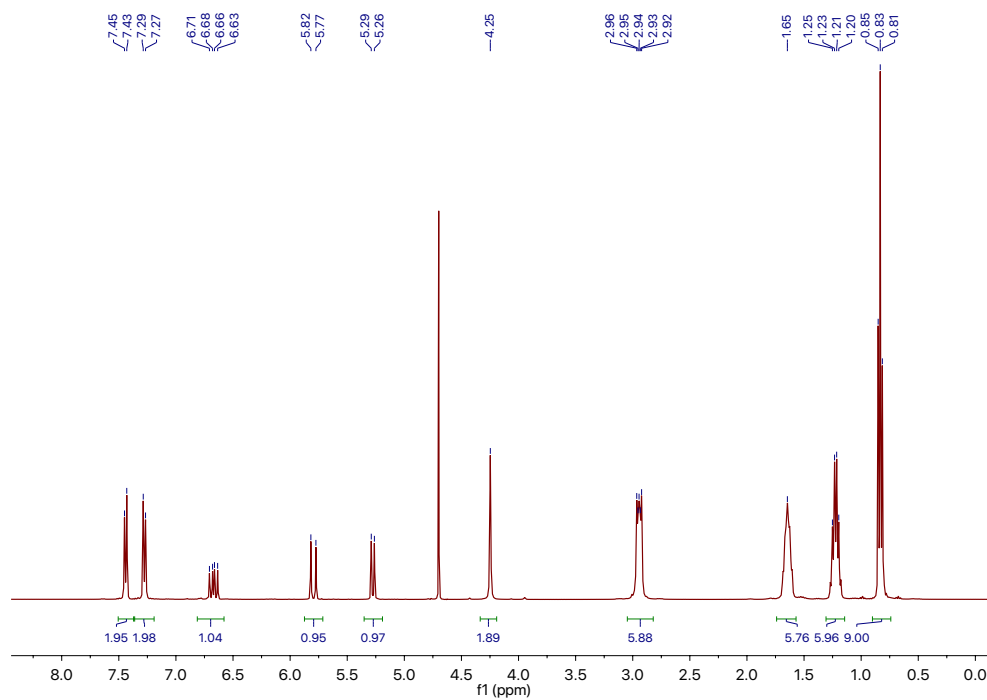
Figure A8. ^{1}H NMR spectrum of **Bu-N** monomer (400 MHz, D$_2$O).
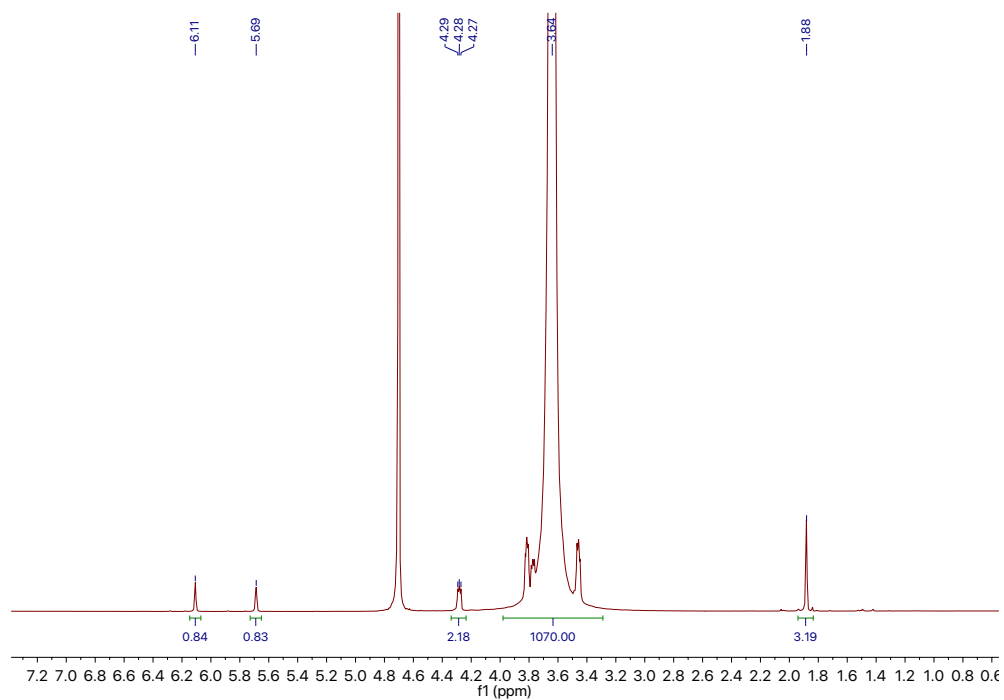
Figure A9. ^{1}H NMR spectrum of **PEGDMA** monomer (400 MHz, D$_2$O).

Table A1. Volumes required of 0.1 M citric acid/ 0.2 M disodium phosphate to create the buffer.

pH required	0.2 M Na$_2$HPO$_4$ (mL)	0.1 M citric acid (mL)
5	10.30	9.70
6	12.63	7.37
7.4	18.17	1.83
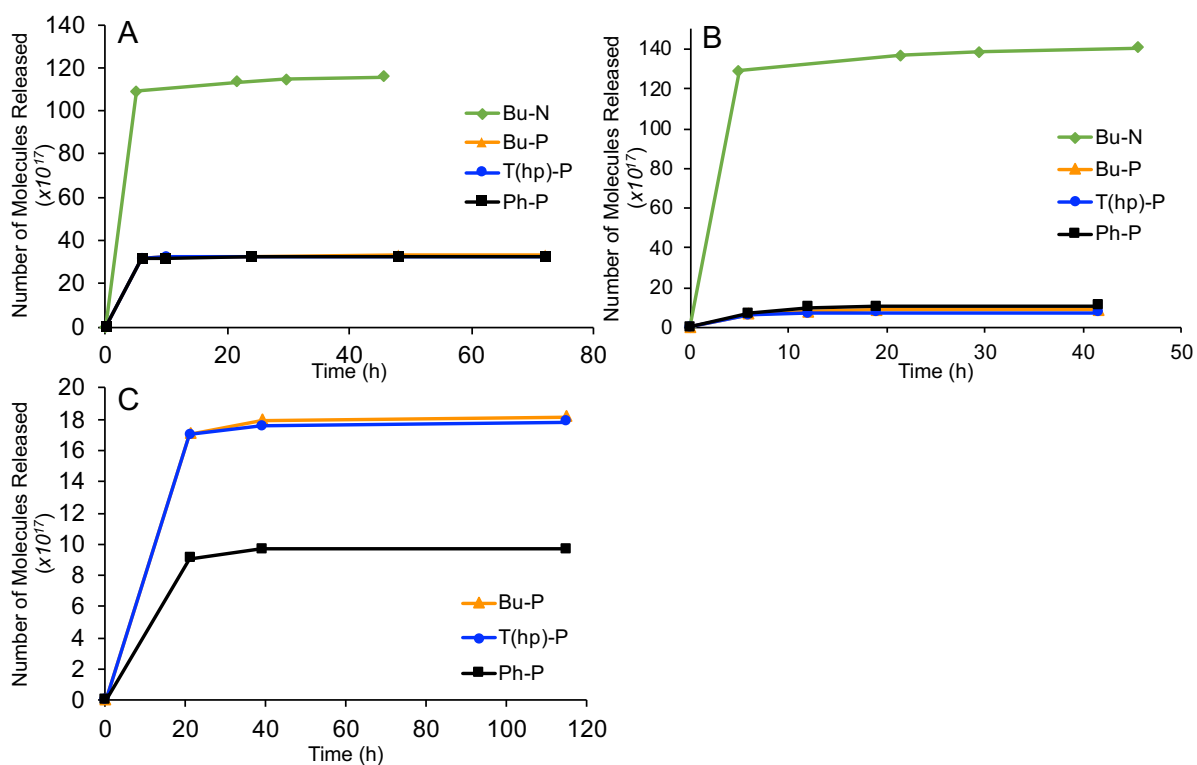
Figure A10. Release of anionic molecules during washing with deionized water to confirm that any non-ionically bound molecules had been removed prior to the release studies. When no further release occurred, the washing of unbound molecules was deemed complete. A) fluorescein sodium salt B) diclofenac sodium salt C) tryptophan in DI water.
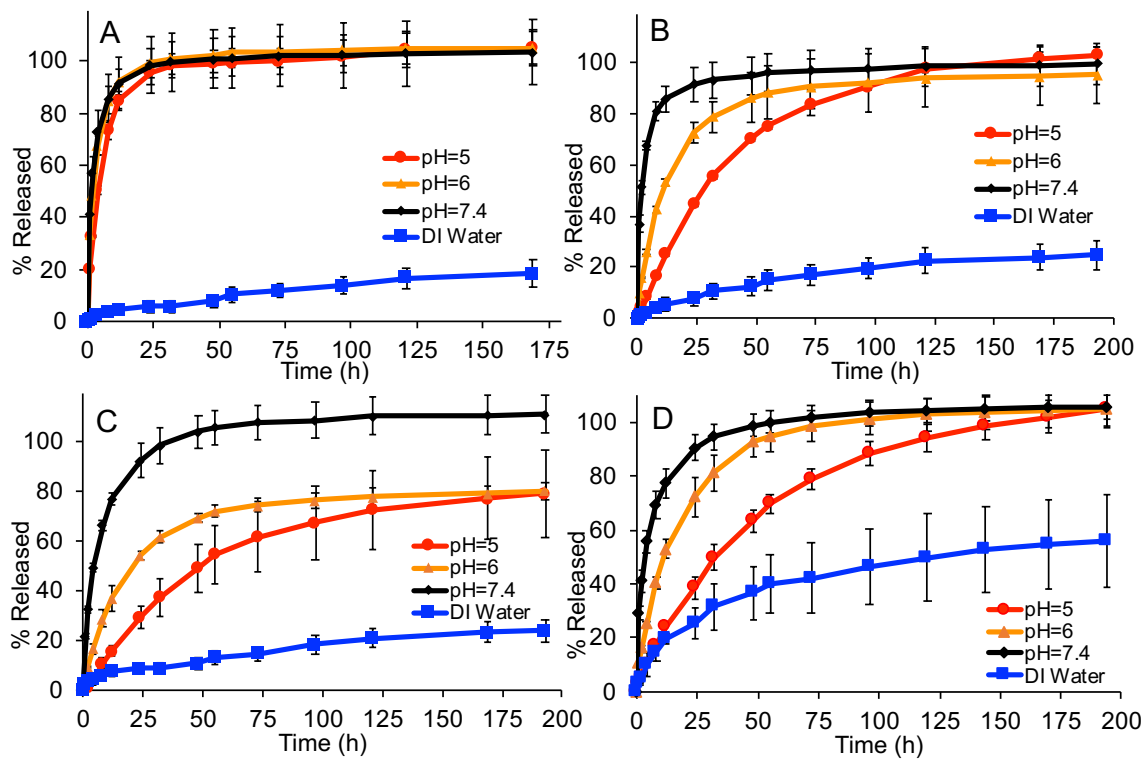
Figure A11. Release rates of fluorescein from hydrogels: A) **T(hp)-P**; B) **Bu-P**; C) **Ph-P**;
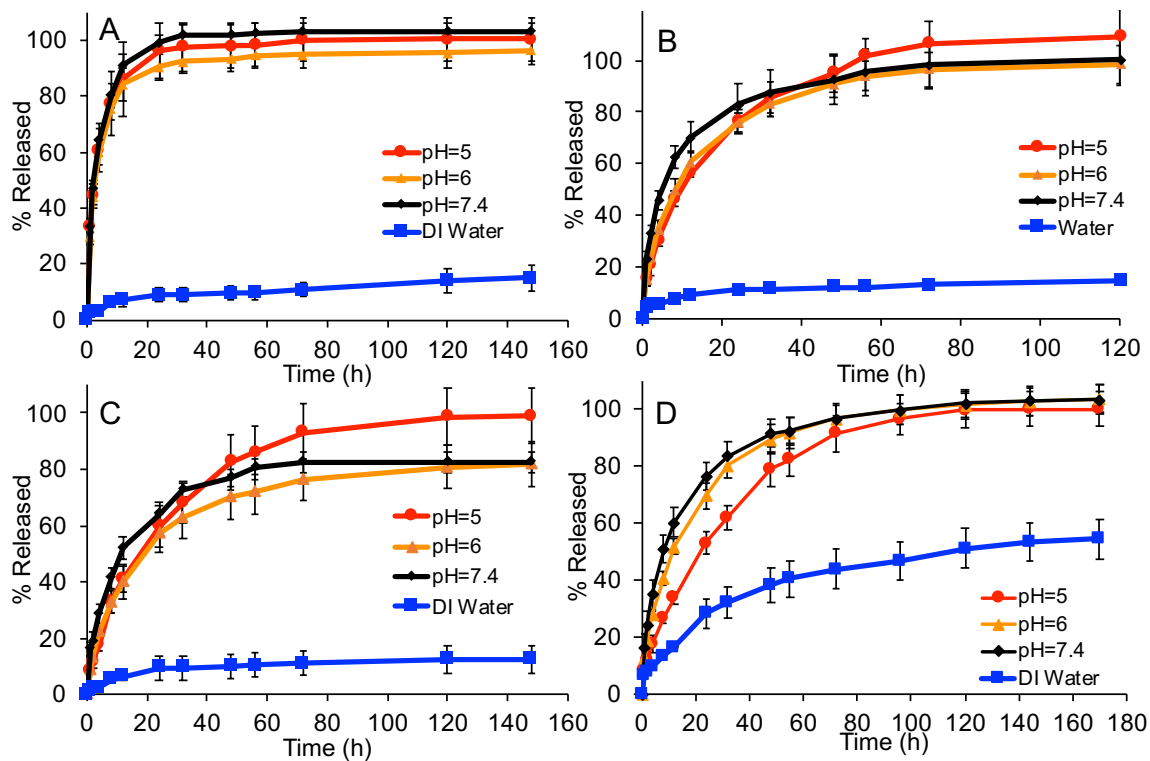
D) **Bu-N**.

Figure A12. Release rates of diclofenac from hydrogels: A) **T(hp)-P**; B) **Bu-P**; C) **Ph-P**
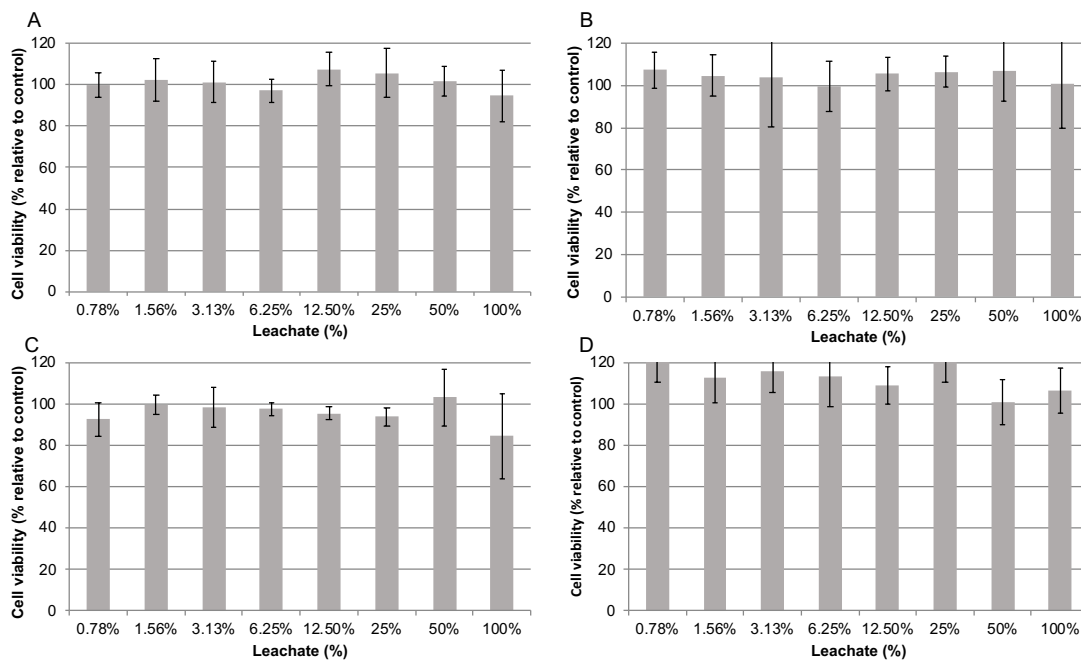
D) **Bu-N**.

Figure A13. In vitro cytotoxicity of leachate obtained from A) **T(hp)-P** hydrogel, B) **Bu-P** hydrogel, C) **Ph-P** hydrogel, and D) **Bu-N** hydrogel as measured by MTT assays following 24 h incubations with C2C12 mouse myoblast cells. Data represent the mean and standard deviation of six replicates per concentration.
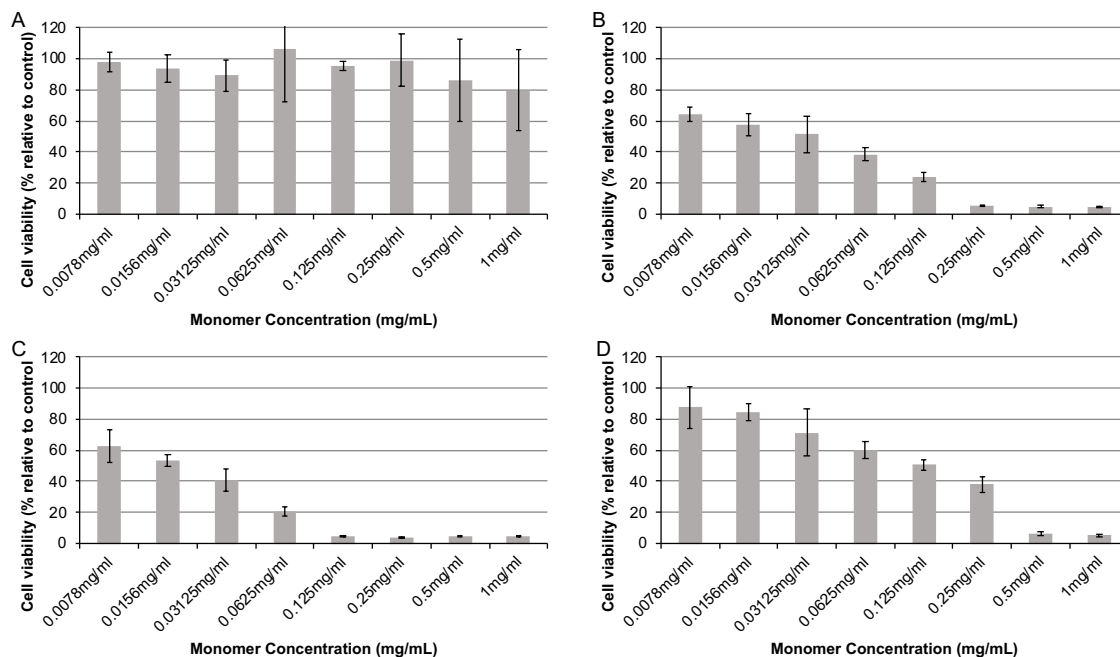
Figure A14. In vitro cytotoxicity of A) monomer **T(hp)-P**, B) monomer **Bu-P**, C) monomer **Ph-P**, and D) monomer **Bu-N** as measured by MTT assays following 24 h incubations with C2C12 mouse myoblast cells. Data represent the mean and standard deviation of six replicates per concentration.
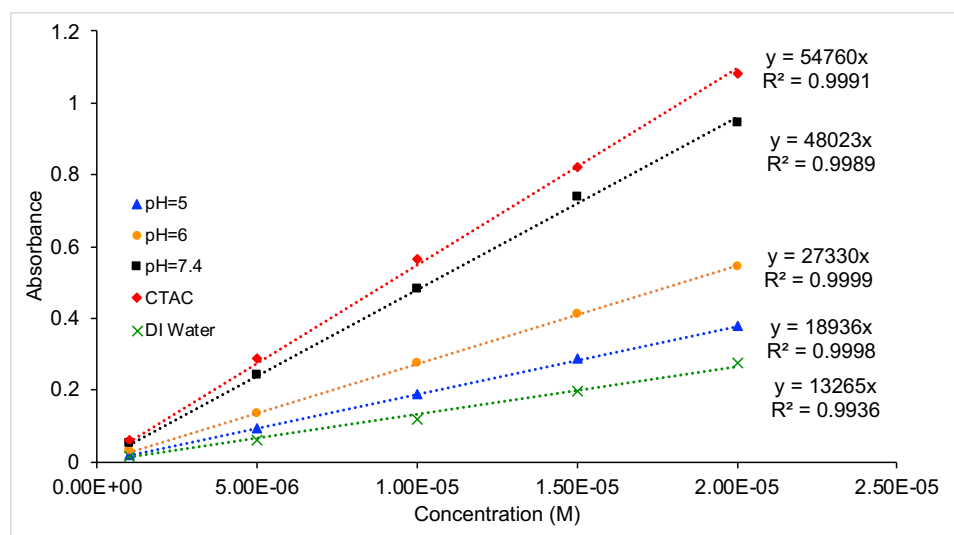
Figure A15. Fluorescein sodium salt calibration curve.
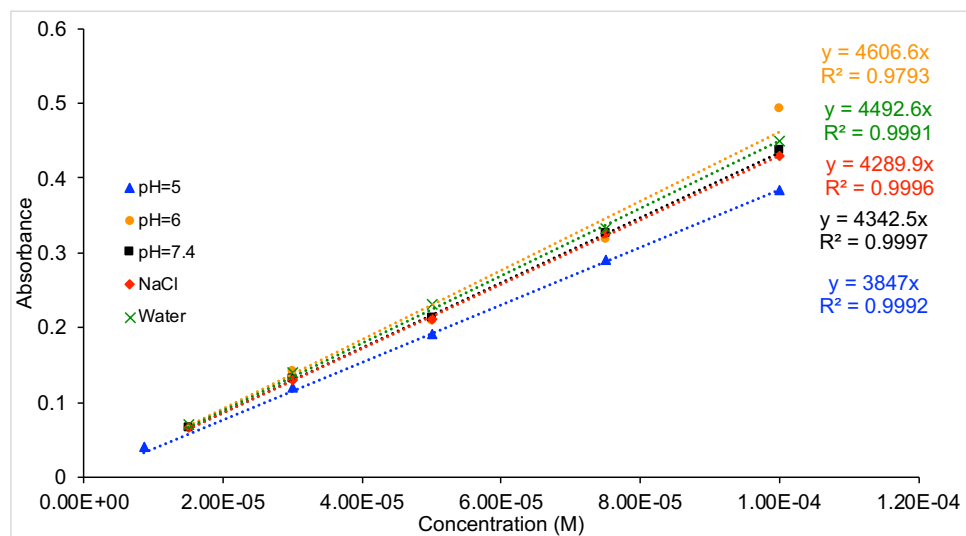
Figure A16. Diclofenac sodium salt calibration curve.
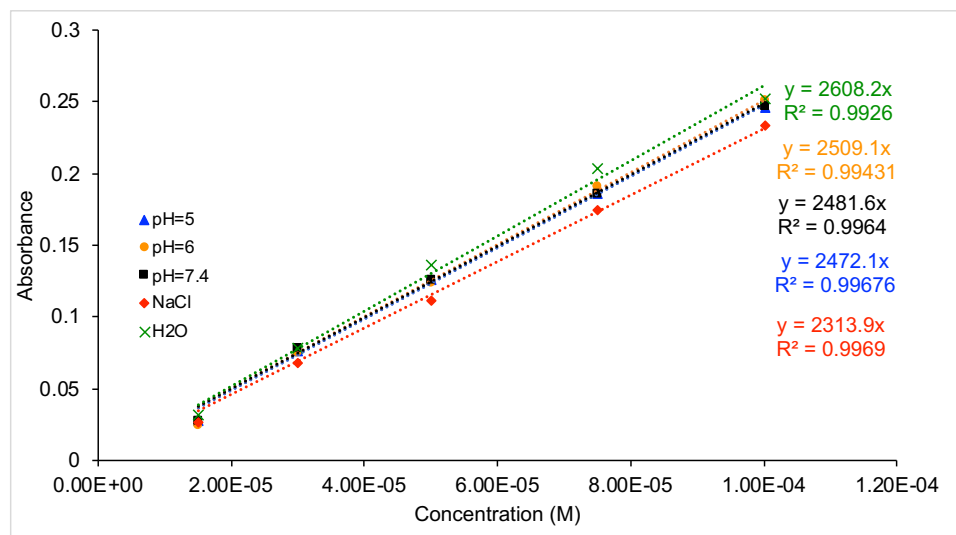
Figure A17. Tryptophan calibration curve.

7.2   Appendix B: Supporting Information for Chapter 3
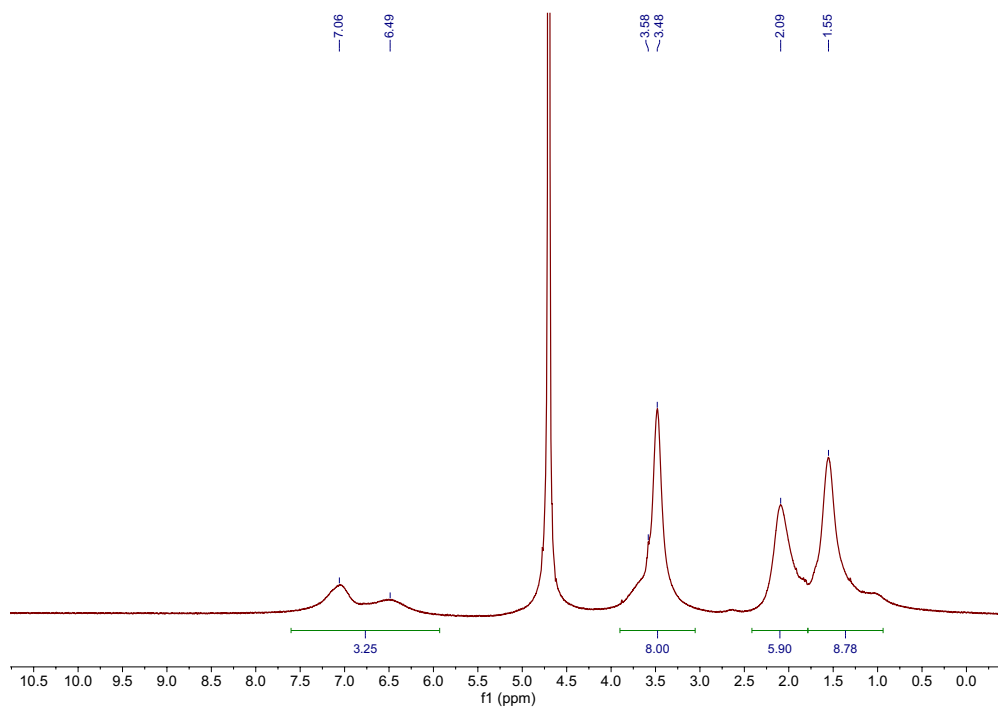
Figure B1. ^{1}H NMR spectrum of **P-Hp-P** polymer (400 MHz, D$_2$O).
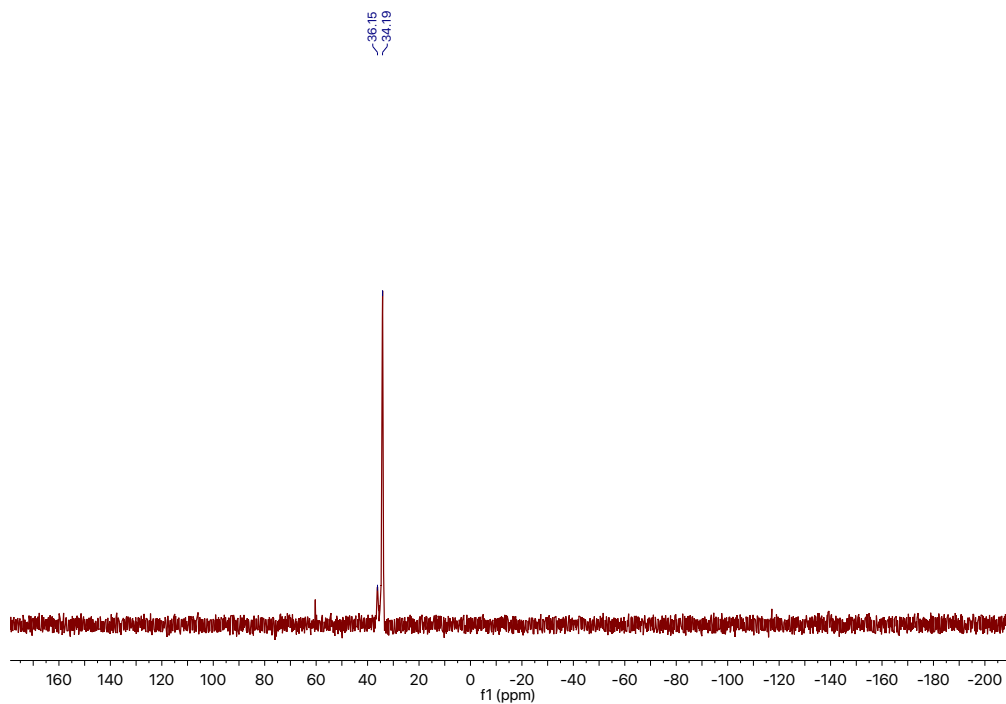
Figure B2. $^{31}P\{^{1}H\}$ NMR spectrum **P-Hp-P** polymer (161.8 MHz, D_2O).
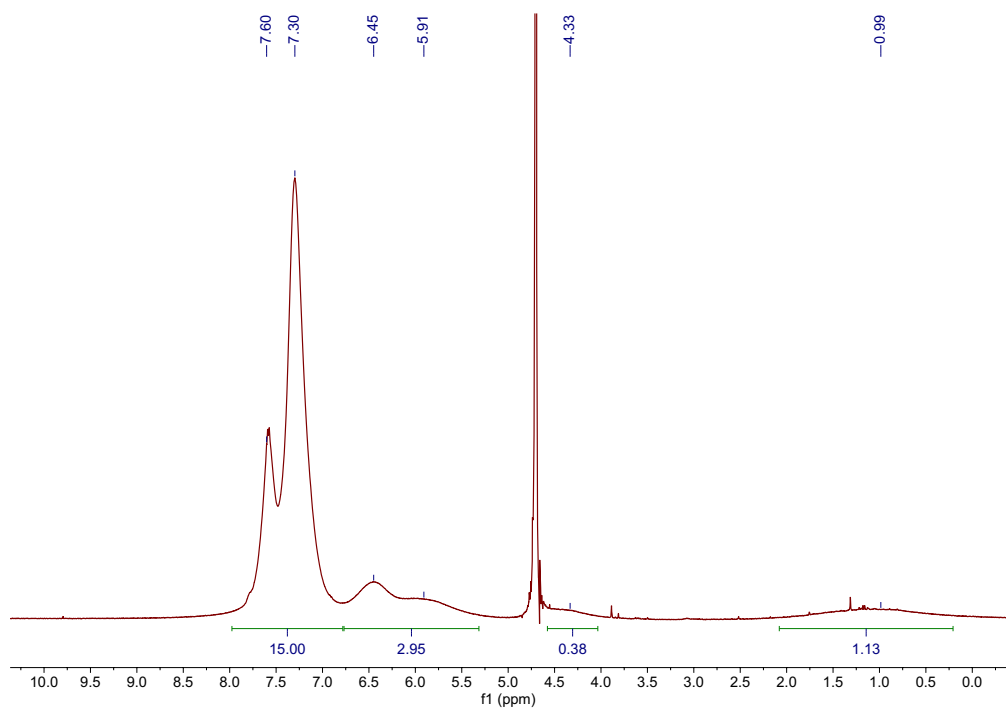
Figure B3. ^{1}H NMR spectrum of **P-Ph-P** polymer (400 MHz, D_2O).
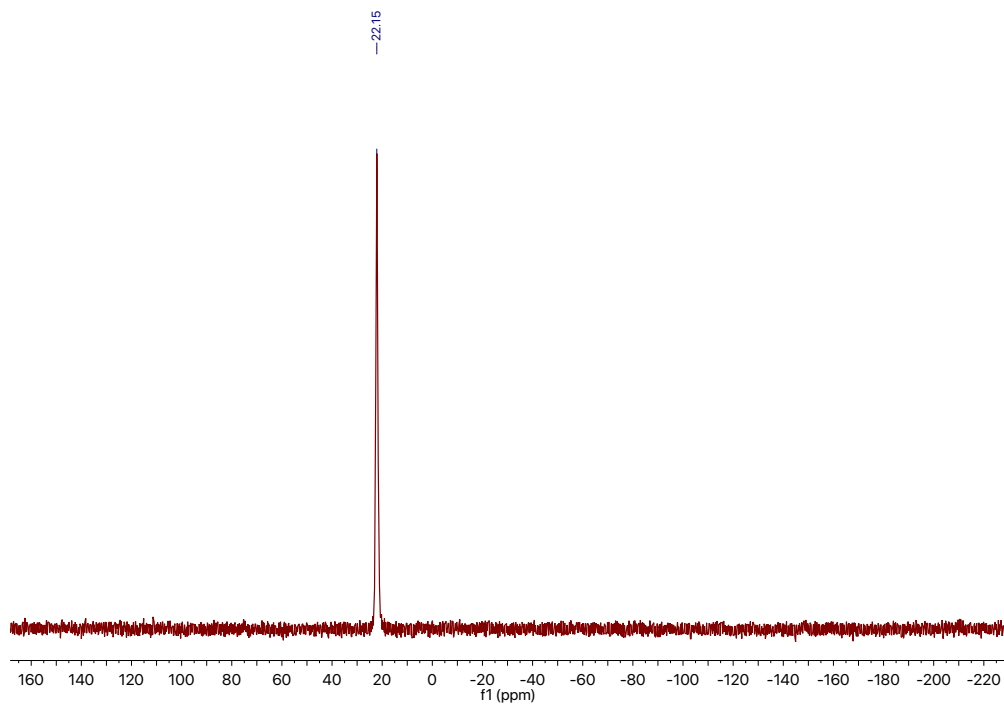
Figure B4. ^{31}P{^{1}H} NMR spectrum **P-Ph-P** polymer (161.8 MHz, D$_2$O).
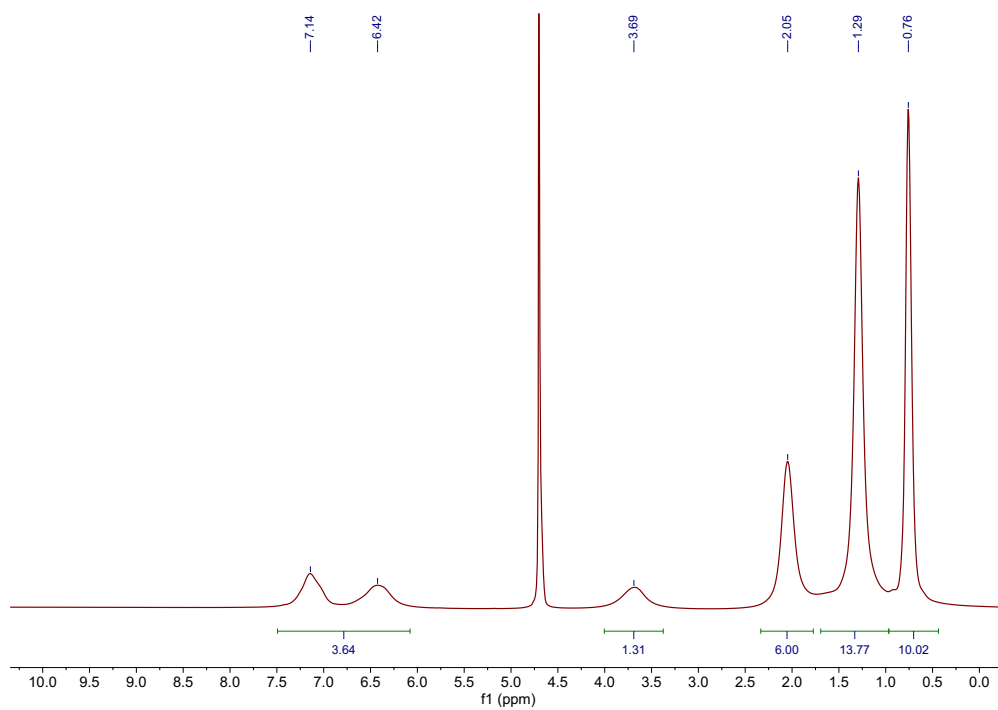
Figure B5. ^{1}H NMR spectrum of **P-Bu-P** polymer (400 MHz, D$_2$O).
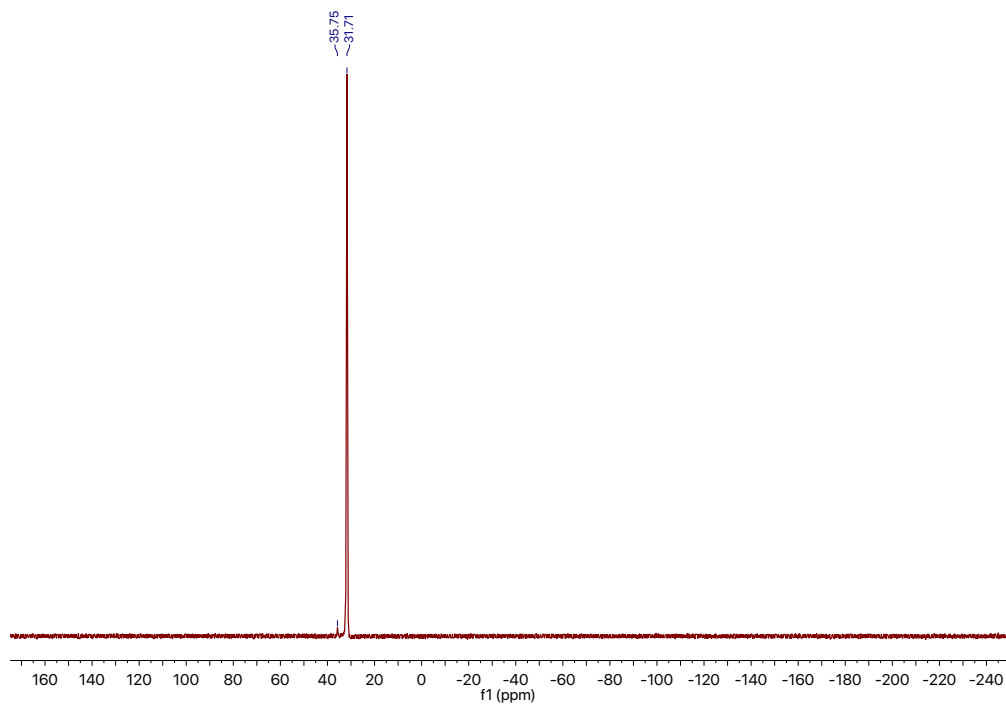
Figure B6. $^{31}P\{^{1}H\}$ NMR spectrum **P-Bu-P** polymer (161.8 MHz, D$_2$O).
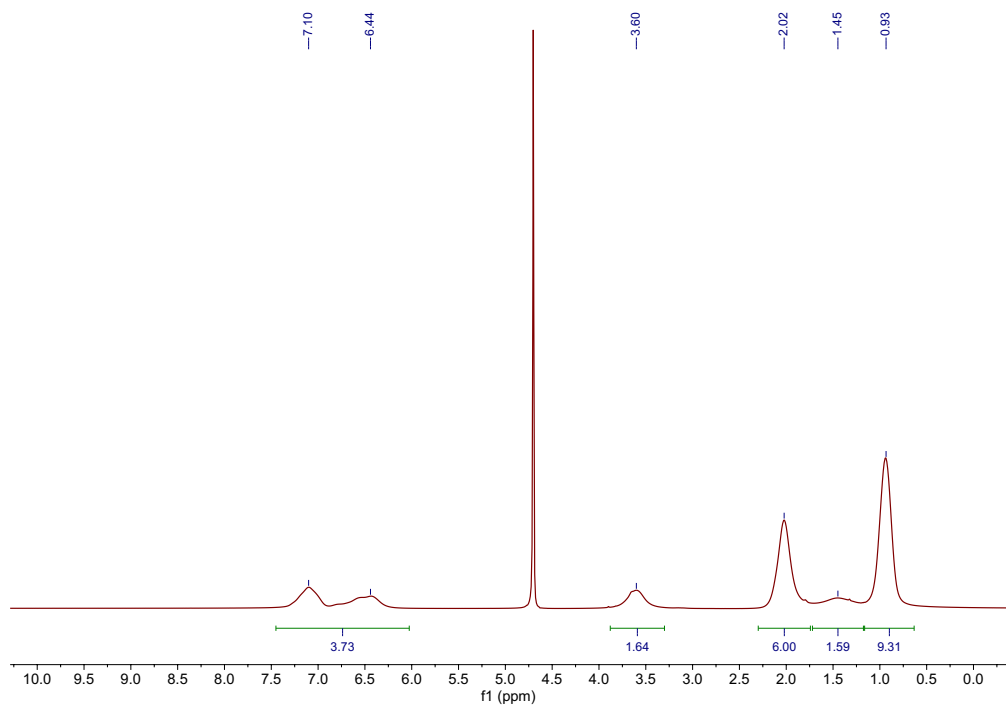
Figure B7. ^{1}H NMR spectrum of **P-Et-P** polymer (400 MHz, D$_2$O).
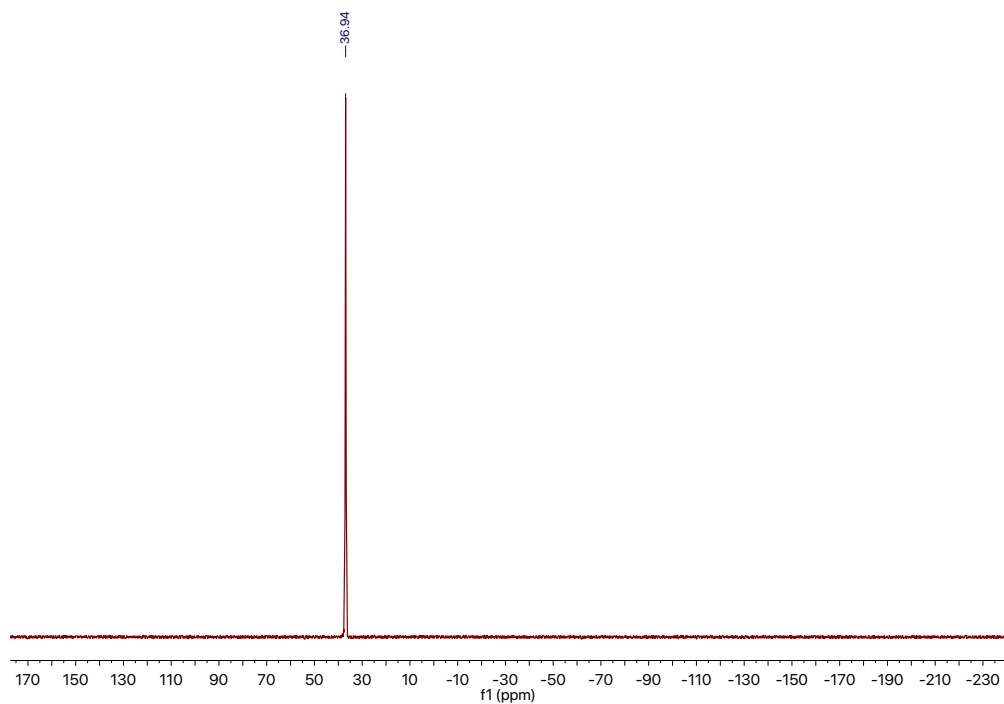
Figure B8. $^{31}P\{^1H\}$ NMR spectrum **P-Et-P** polymer (161.8 MHz, D$_2$O).
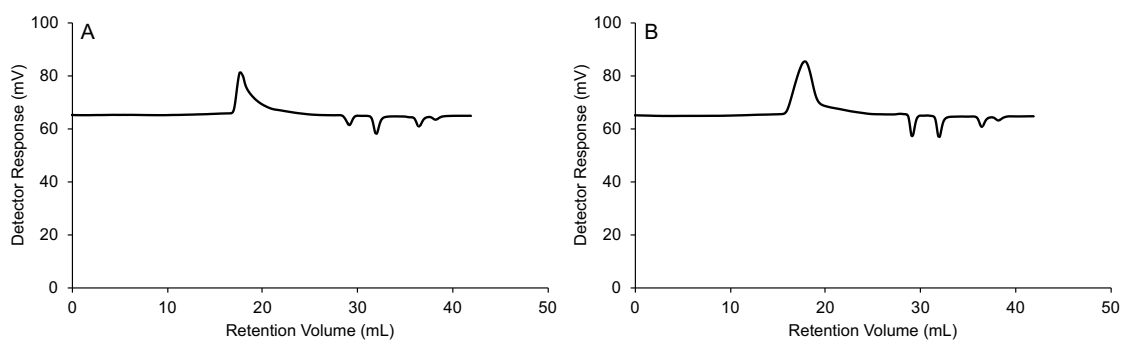
Figure B9. Size exclusion chromatograms for A) **P-Ph-P** and B) **P-Bu-P**.
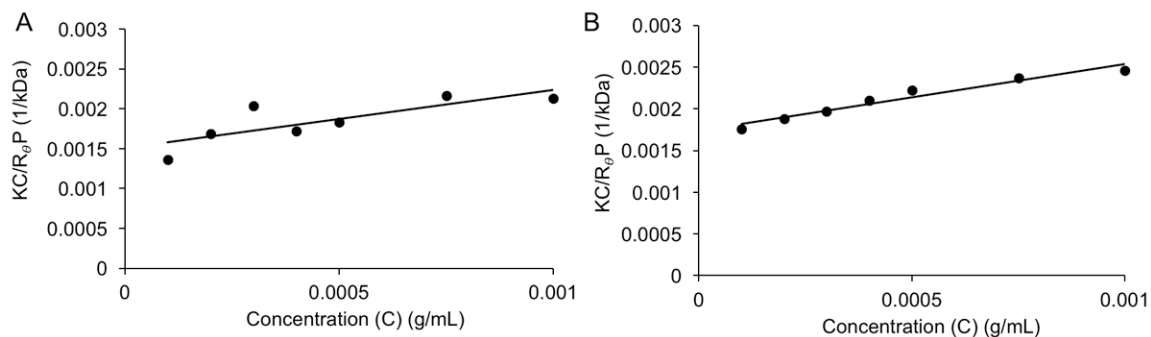
Figure B10. Light scattering Debye plot for A) **P-Hp-P**; B) **P-Et-P**.
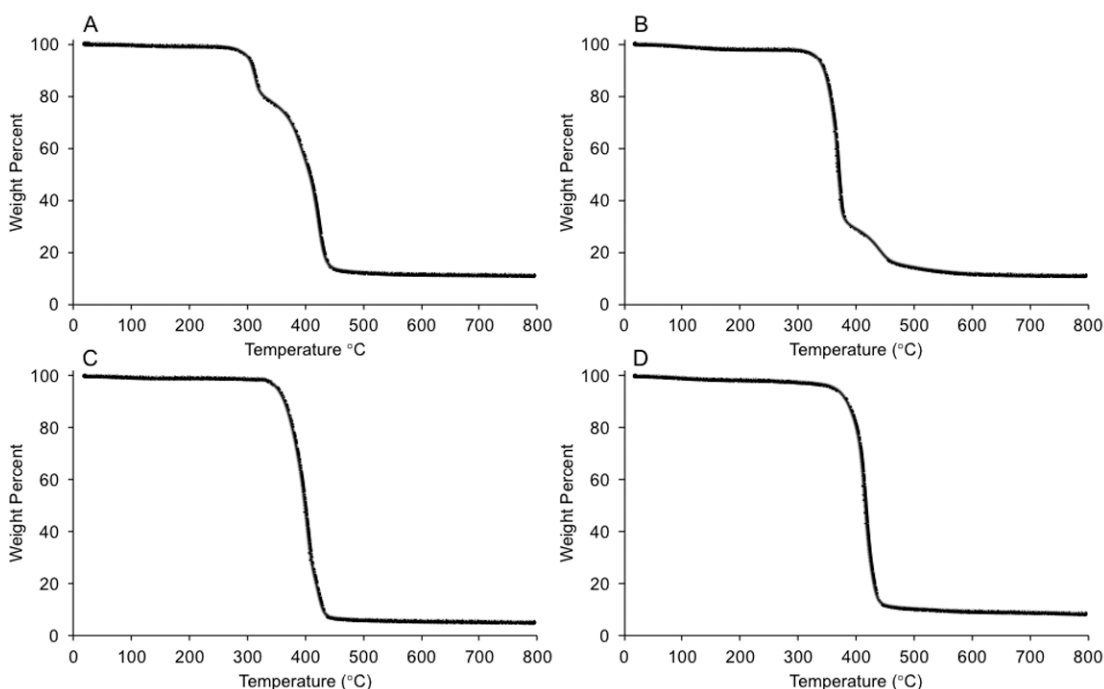
Figure B11. Thermogravimetric analysis of A) **P-Hp-P** (T_o = 290 °C); B) **P-Ph-P** (T_o = 325 °C); C) **P-Bu-P** (T_o = 344 °C); D) **P-Et-P** (T_o = 330 °C). The two-step decomposition for **P-Hp-P** and **P-Ph-P** is hypothesized to be either Hoffman elimination or reverse Menschutkin (nucleophilic) degradation which can been seen in related ammonium systems.[49]
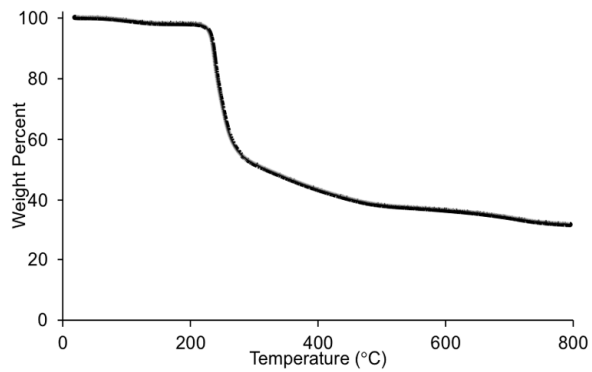
Figure B12. Thermogravimetric analysis of **HA** (T_o = 220 °C).
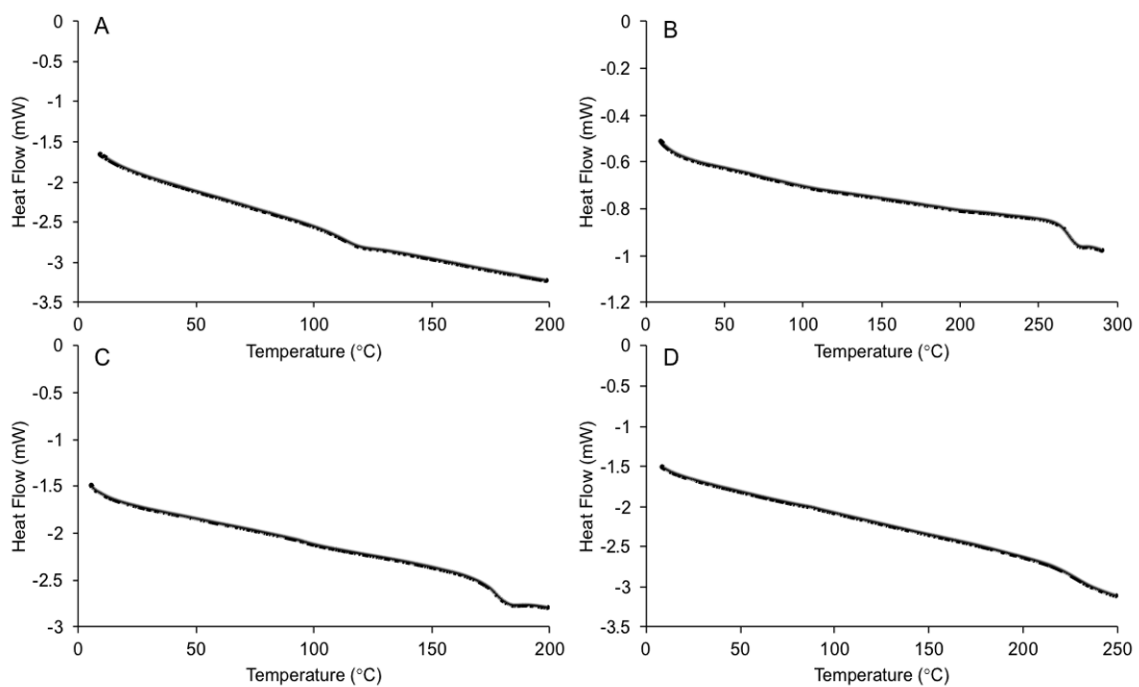
Figure B13. Differential scanning calorimetry thermogram of A) **P-Hp-P**; B) **P-Ph-P**; C) **P-Bu-P**; D) **P-Et-P**.
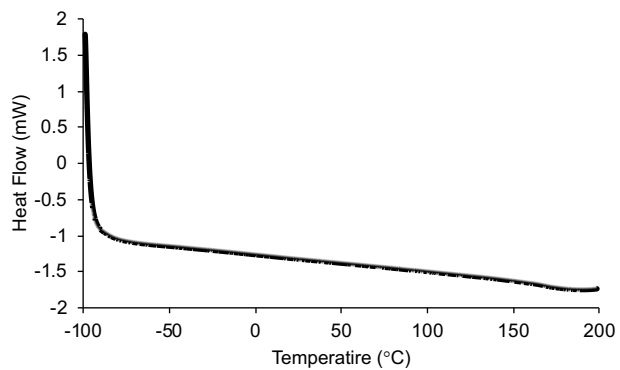
Figure B14. Differential scanning calorimetry thermogram of **HA**.
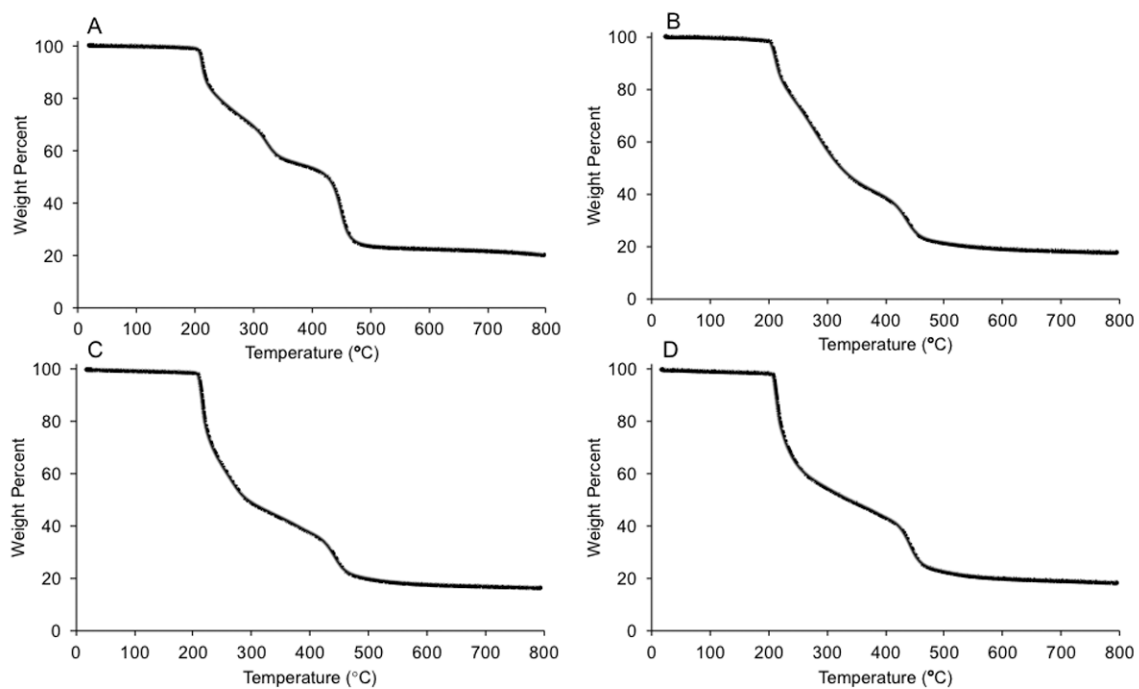
Figure B15. Thermogravimetric analyses of lyophilized networks: A) **P-Hp-P-HA**; B) **P-Ph-P-HA**; C) **P-Bu-P-HA**; D) **P-Et-P-HA**.
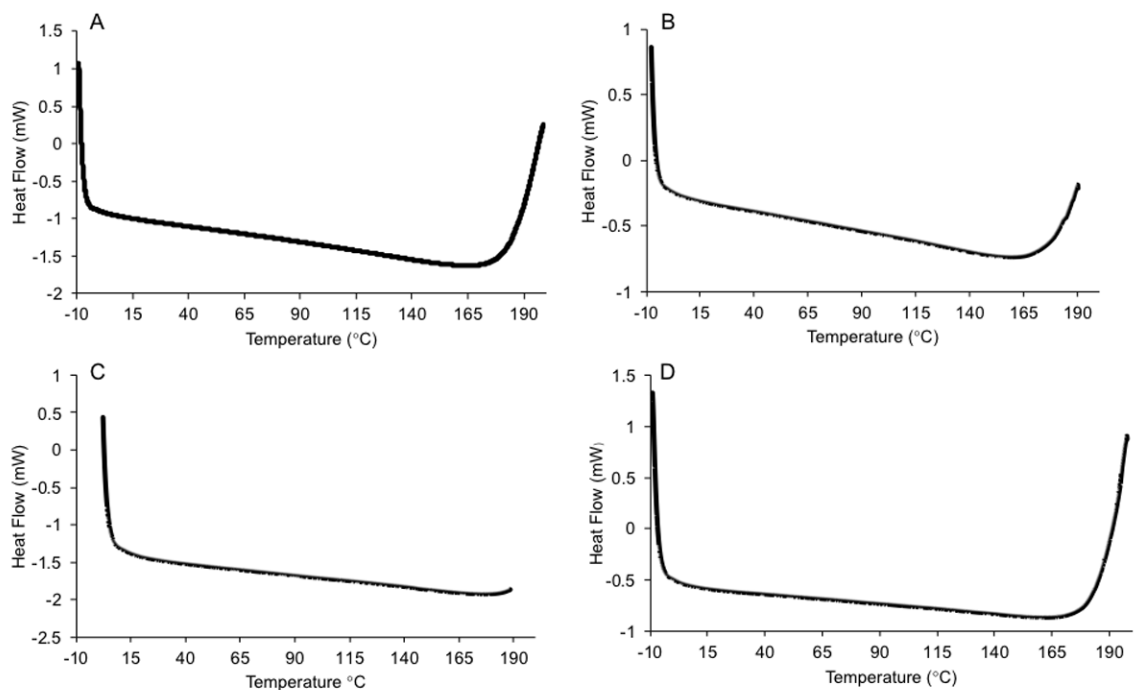
Figure B16. Differential scanning calorimetry thermograms of A) **P-Hp-P**; B) **P-Ph-P**; C) **P-Bu-P**; D) **P-Et-P**.
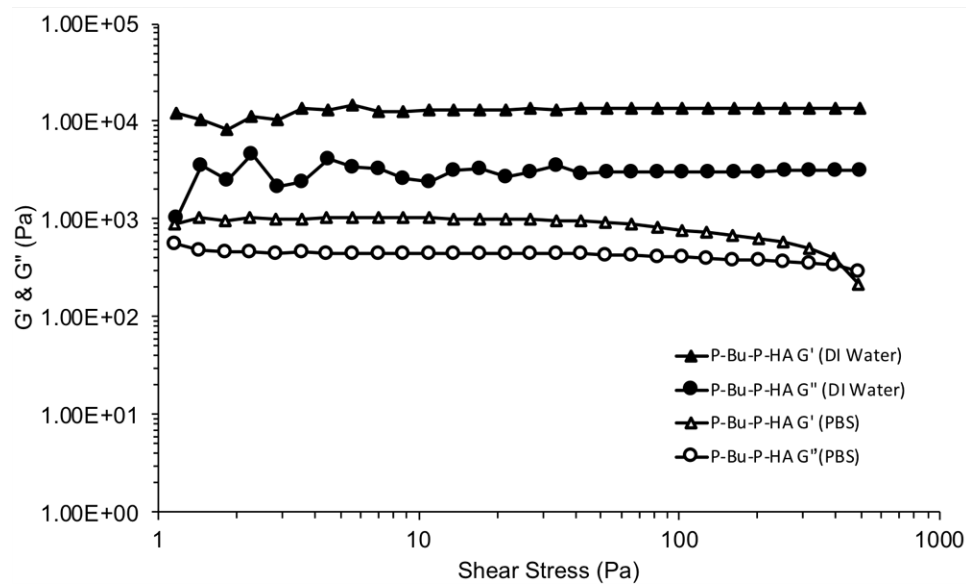
Figure B17. G' and G" for **P-Bu-P-HA**, measured using small amplitude oscillatory shear at different shear stress amplitudes at a constant angular frequency of 1 rad/s.
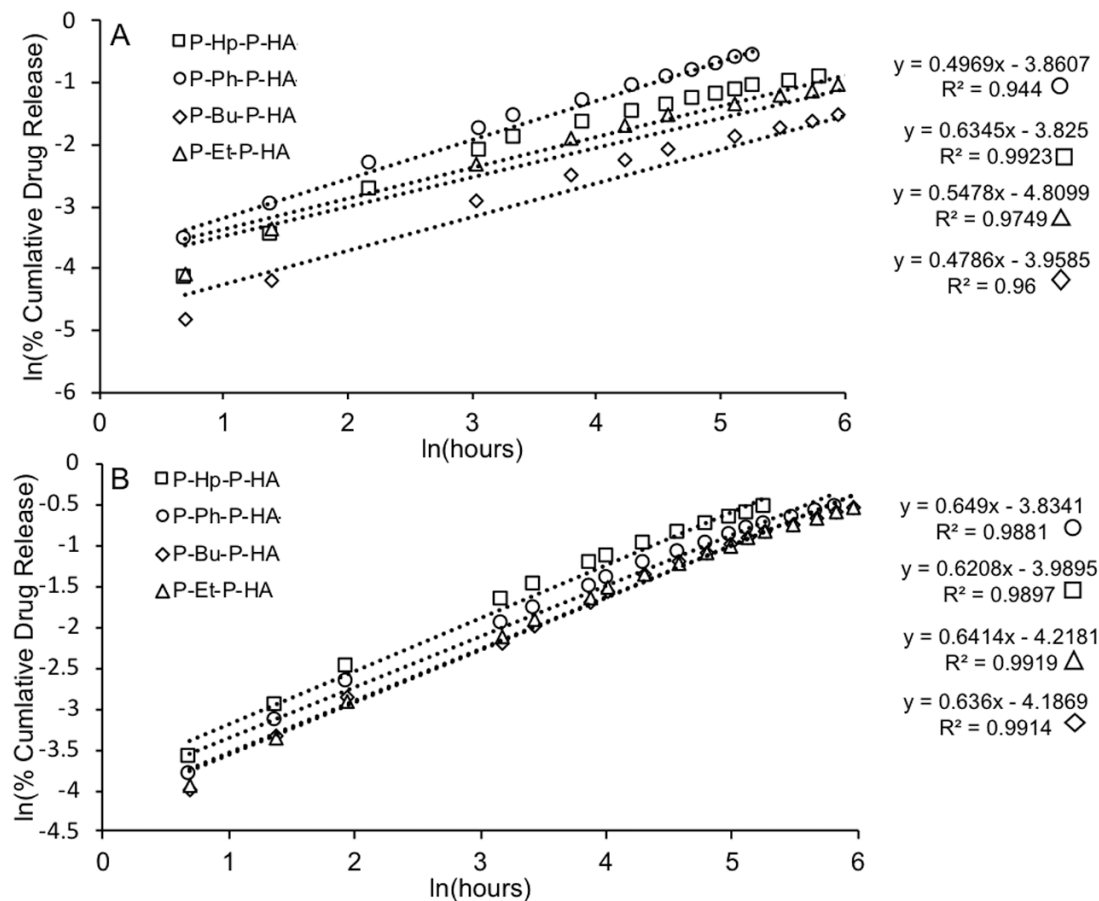
Figure B18. Fitting to the linearized version of the Korsmeyer-Peppas equation: $\ln(M_t/M_\infty)$ versus $\ln(t)$ up to $M_t/M_\infty = 0.6$ for the release of A) fluorescein and B) diclofenac from the PEC networks in PBS at 37 °C. The slopes of the graphs (indicated from the equations y = mx +b provided above) correspond to the diffusional exponent n. Note that the release of ATP was not fitted due to its rapid release and consequent absence of sufficient data points for $M_t/M_\infty < 0.6$.

7.3   Appendix C: Supporting Information for Chapter 4
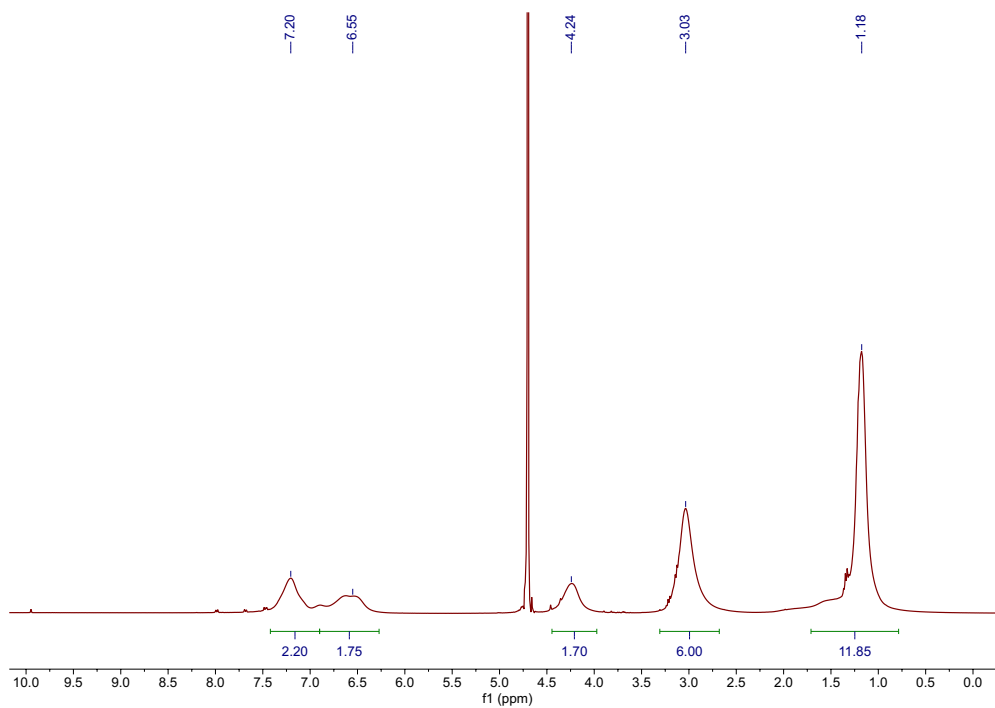
Figure C1. ^{1}H NMR spectrum of **P-Et-N** polymer (400 MHz, D$_2$O).
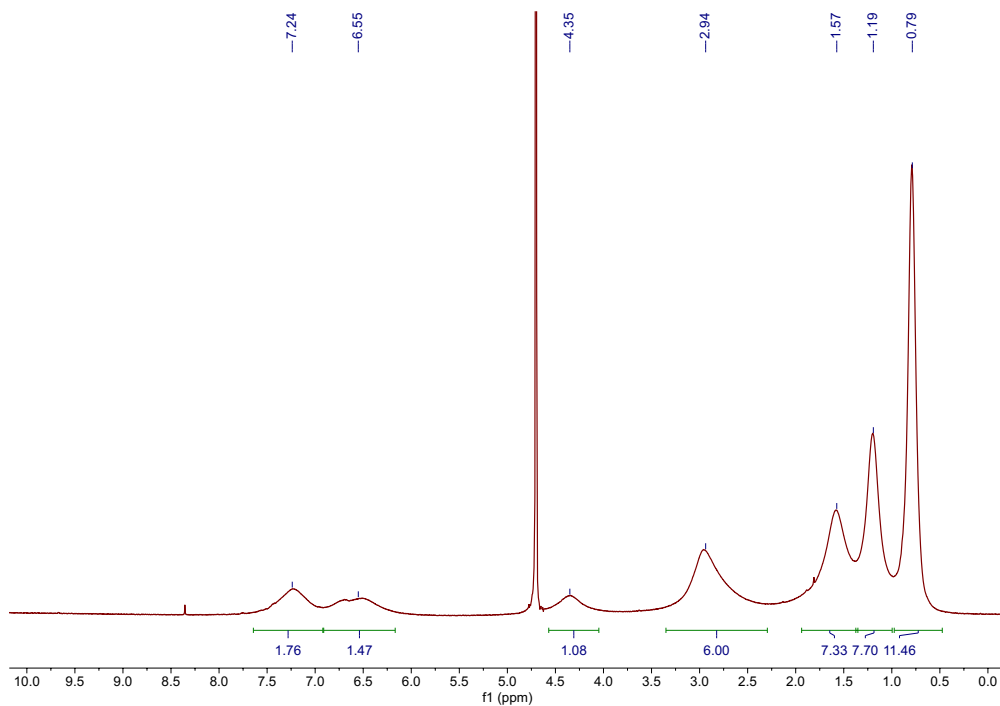
Figure C2. ^{1}H NMR spectrum of **P-Bu-N** polymer (400 MHz, D$_2$O).
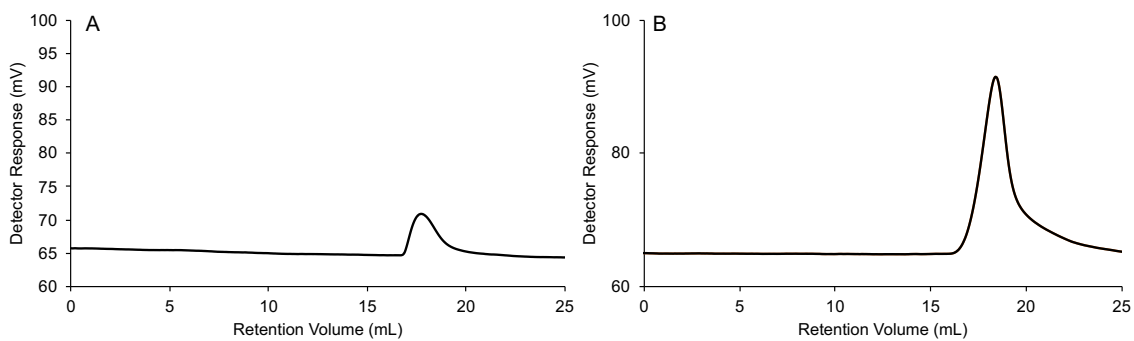
Figure C3. Size exclusion chromatograms for A) **P-Et-N** and B) **P-Bu-N**.
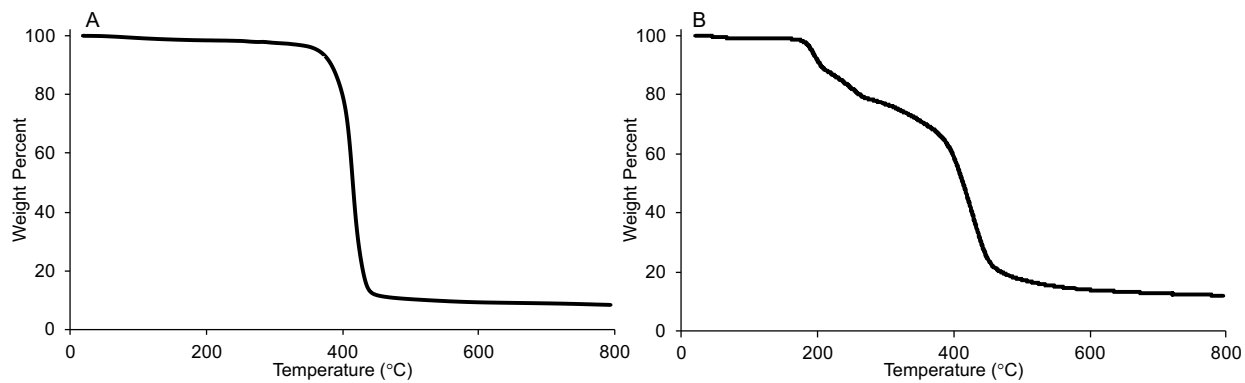
Figure C4. Thermogravimetric analysis of A) **P-Et-P** and B) **P-Et-N**.
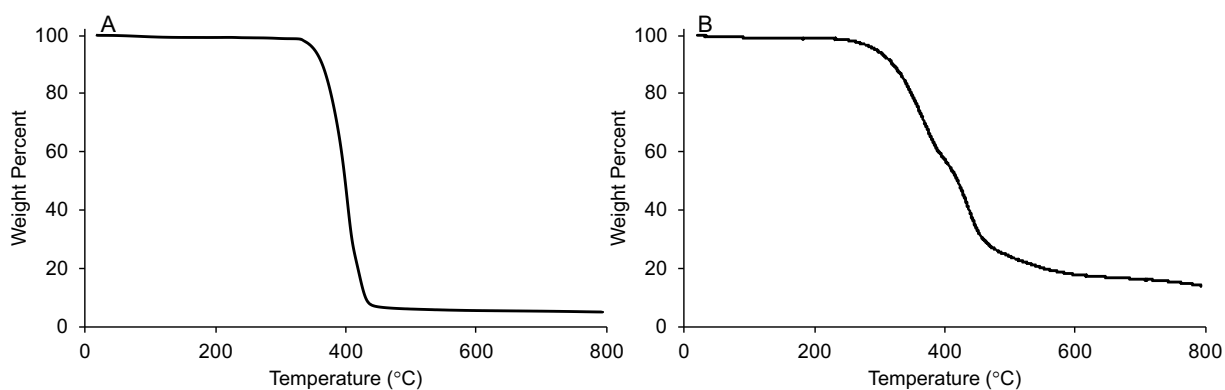
Figure C5. Thermogravimetric analysis of A) **P-Bu-P** and B) **P-Bu-N**.
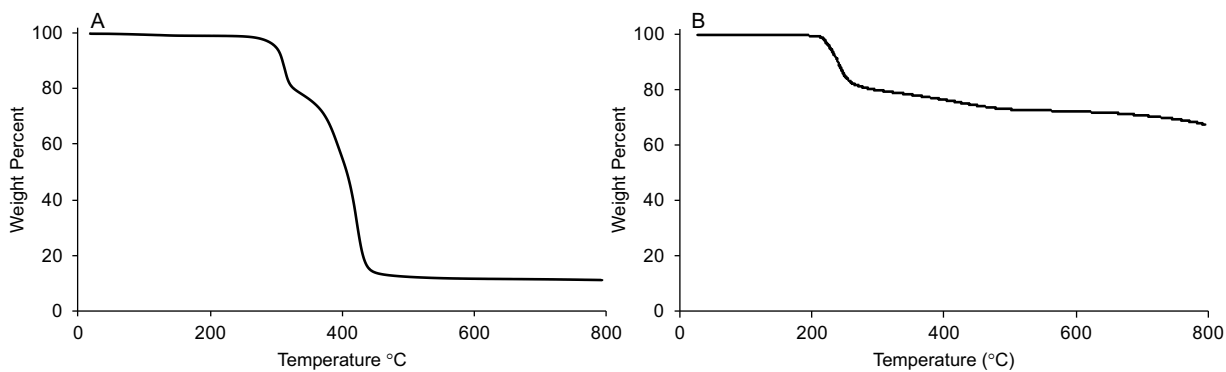
Figure C6. Thermogravimetric analysis of A) **P-Hp-P** and B) **SA**.
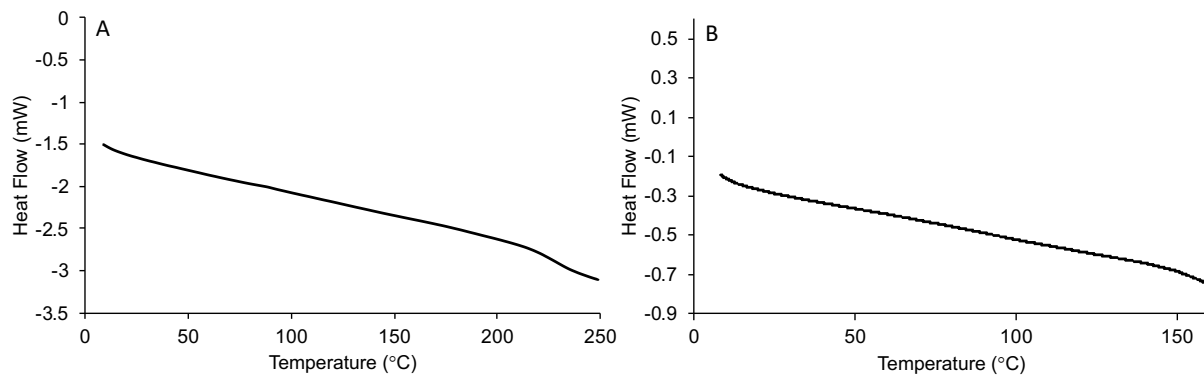
Figure C7. Differential scanning calorimetry thermogram of A) **P-Et-P** and B) **P-Et-N**.
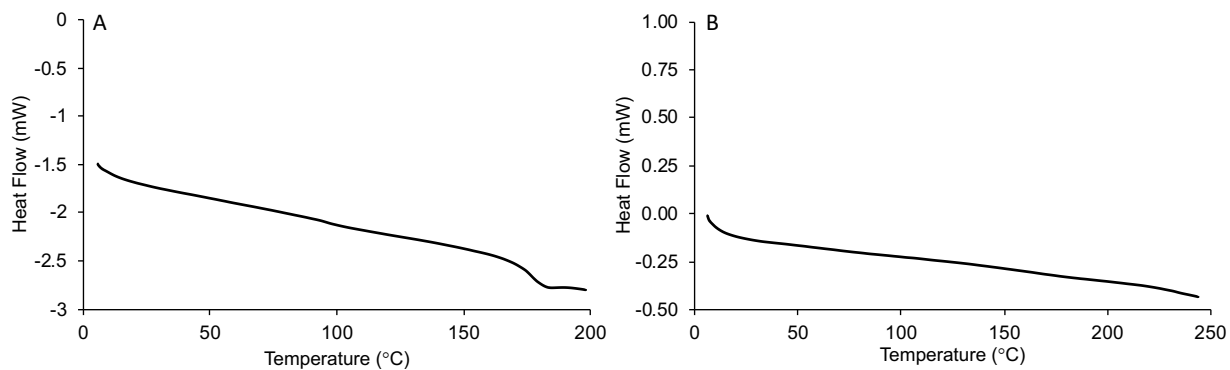
Figure C8. Differential scanning calorimetry thermogram of A) **P-Bu-P** and B) **P-Bu-N**.
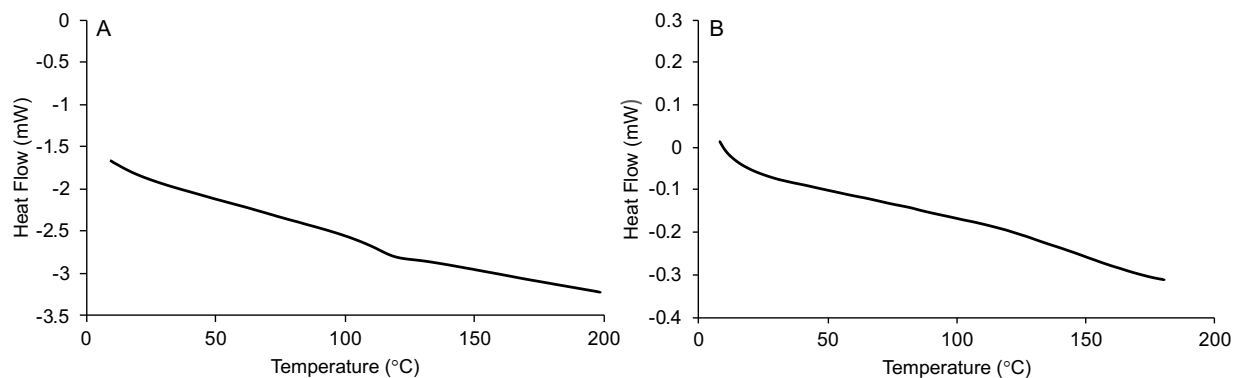
Figure C9. Differential scanning calorimetry thermogram of A) **P-Hp-P** and B) **SA**.
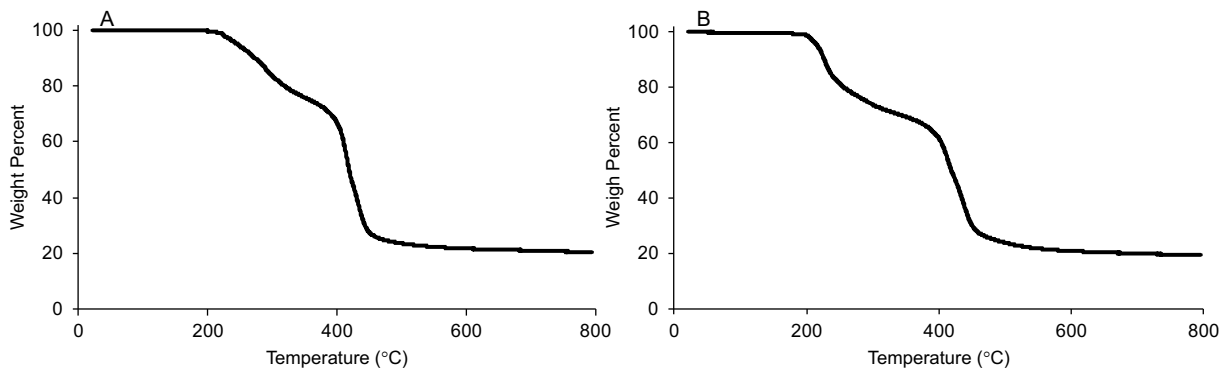
Figure C10. Thermogravimetric analysis of A) **P-Et-P-Alg** and B) **P-Et-N-Alg**.
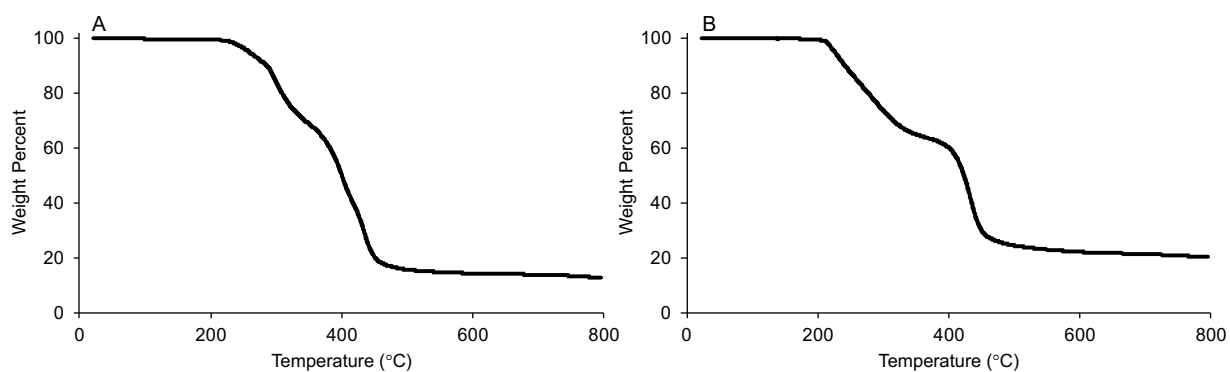
Figure C11. Thermogravimetric analysis of A) **P-Bu-P-Alg** and B) **P-Bu-N-Alg**.
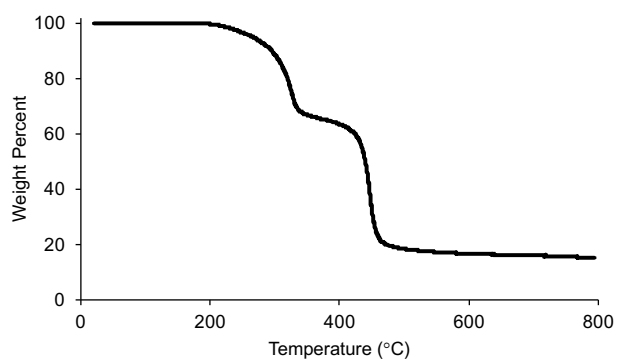
Figure C12. Thermogravimetric analysis of **P-Hp-P-Alg**.
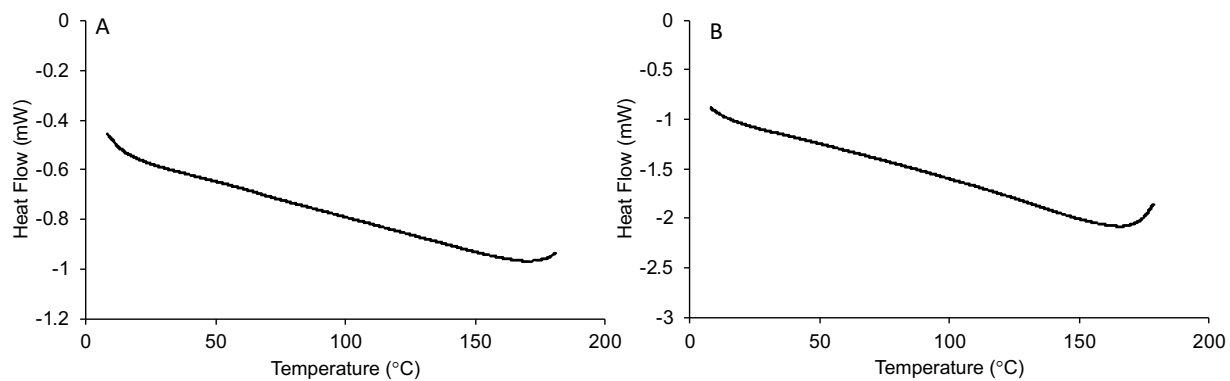
Figure C13. Differential scanning calorimetry thermogram of A) **P-Et-P-Alg** and B) **P-Et-N-Alg**.
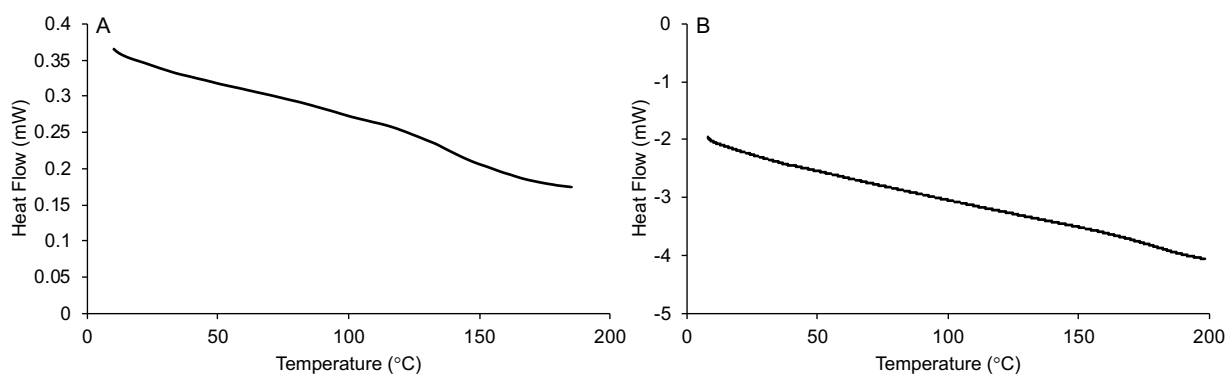
Figure C14. Differential scanning calorimetry thermogram of A) **P-Bu-P-Alg** and B) **P-Bu-N-Alg**.
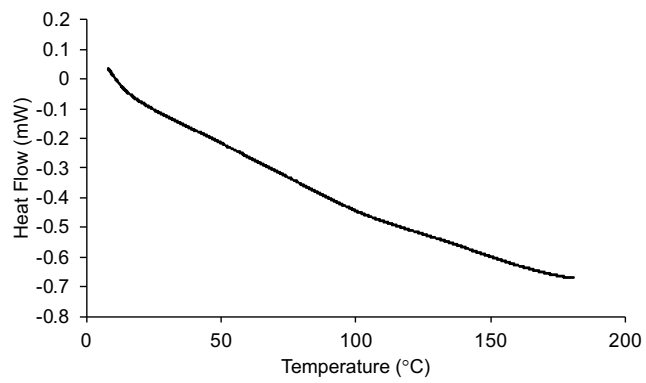
Figure C15. Differential scanning calorimetry thermogram of **P-Hp-P-Alg**.
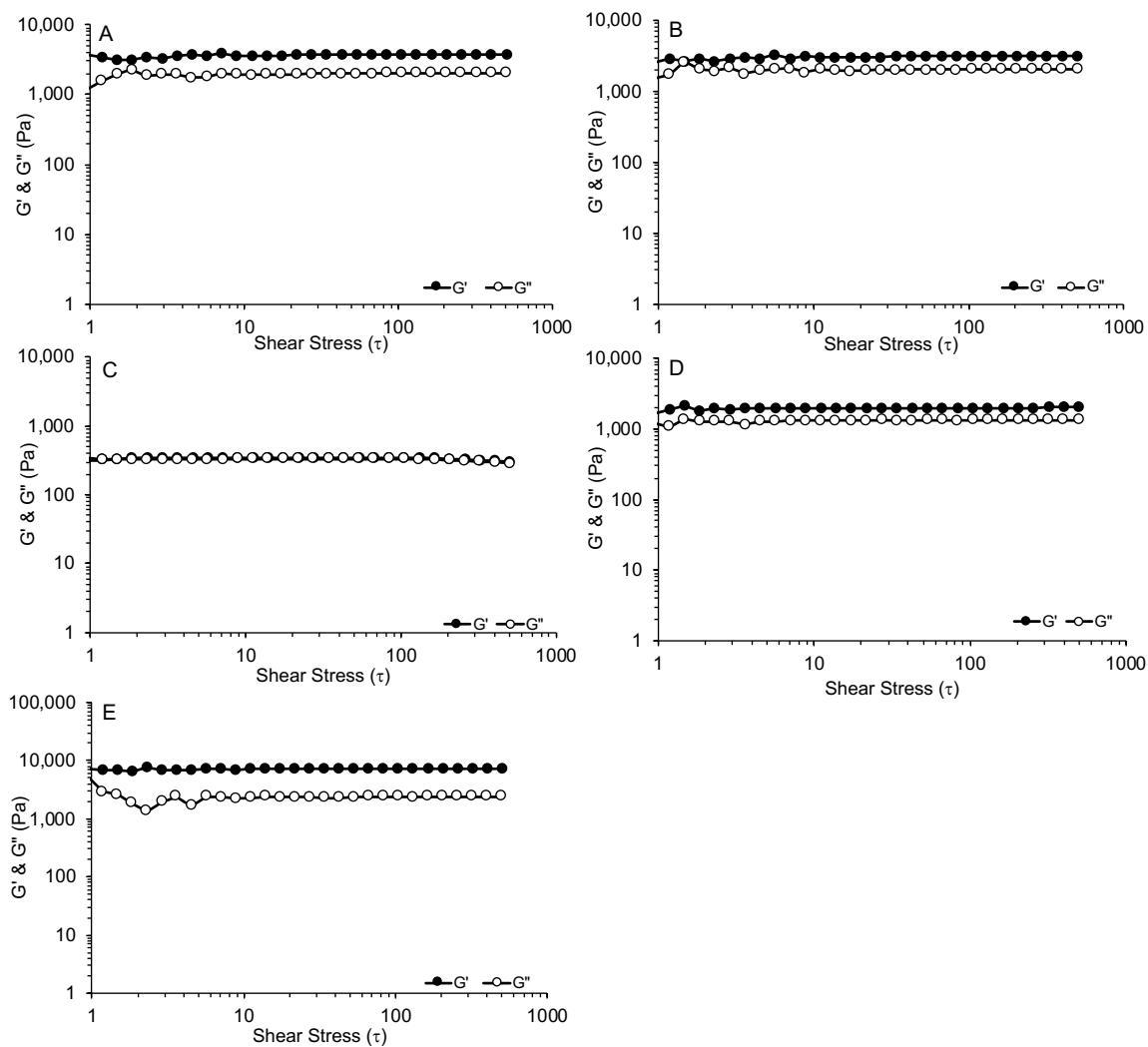
Figure C16. G' and G'' for A) **P-Et-P-Alg**, B) **P-Et-N-Alg**, C) **P-Bu-P-Alg**, D) **P-Bu-N-Alg**, E) **P-Hp-P-Alg** measured using small amplitude oscillatory shear at different shear stress amplitudes at a constant angular frequency of 1 rad/s.
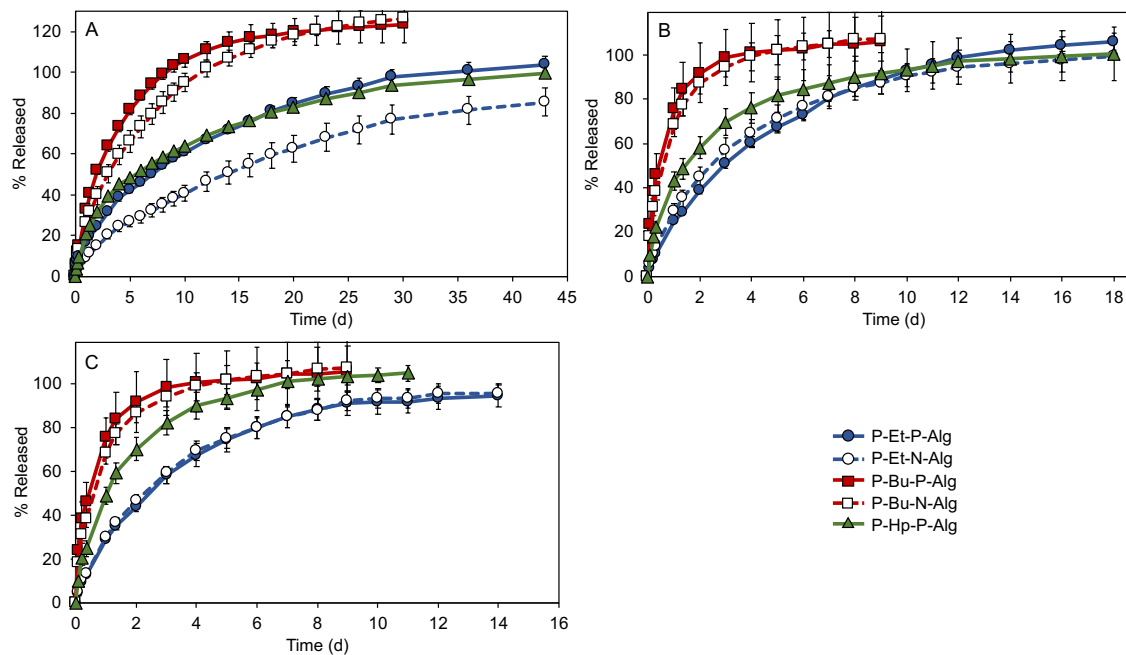
Figure C17. Release curves of A) fluorescein sodium salt, B) etodolac sodium salt, C) methotrexate disodium salt. Error bars correspond to the standard deviations (N = 3).
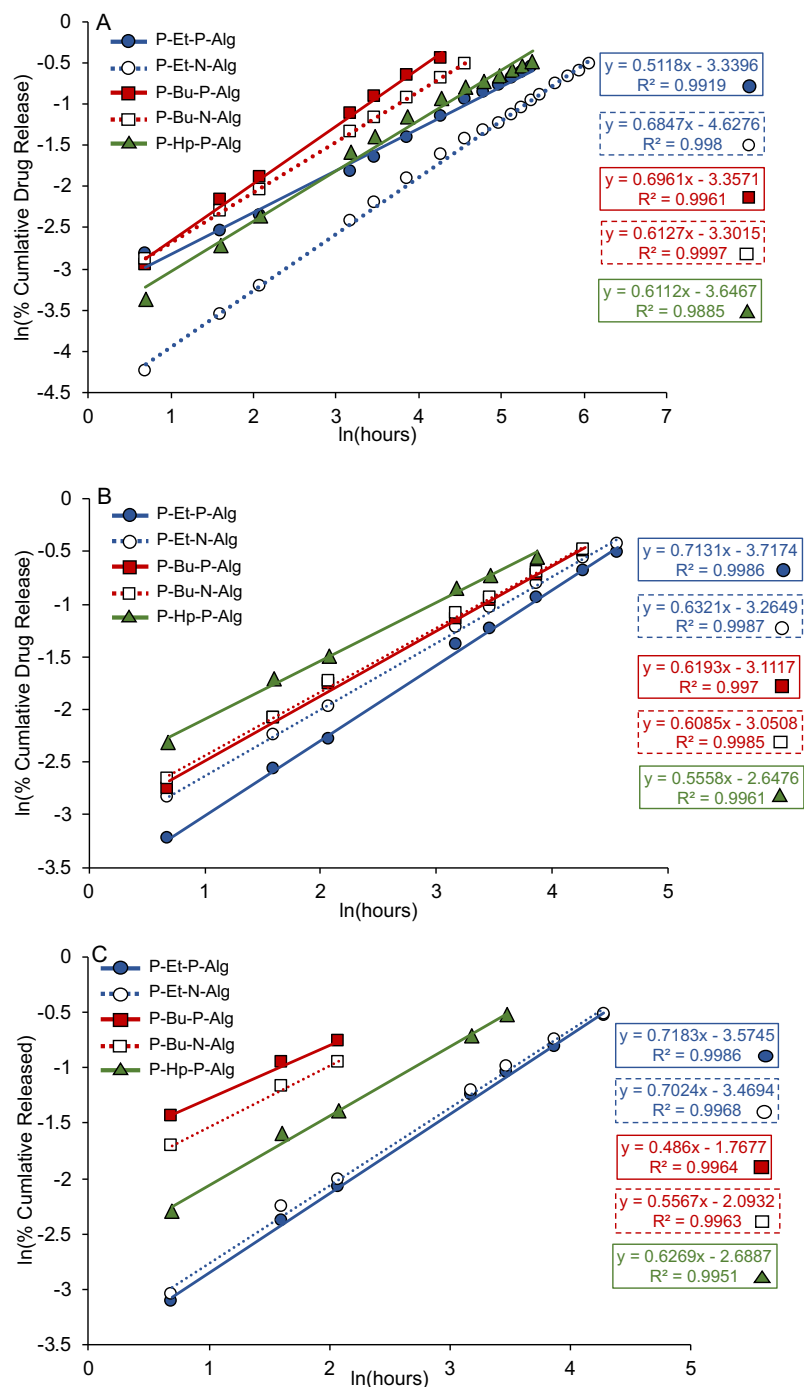
Figure C18. Fitting to the linearized version of the Korsmeyer-Peppas equation: $\ln(M_t/M_\infty)$ versus $\ln(t)$ up to $M_t/M_\infty = 0.6$ for the release of A) fluorescein, B) etodolac and C) methotrexate from the PEC networks in PBS at 37 °C. The slopes of the graphs (indicated from the equations y = mx +b provided above) correspond to the diffusional exponent *n*.
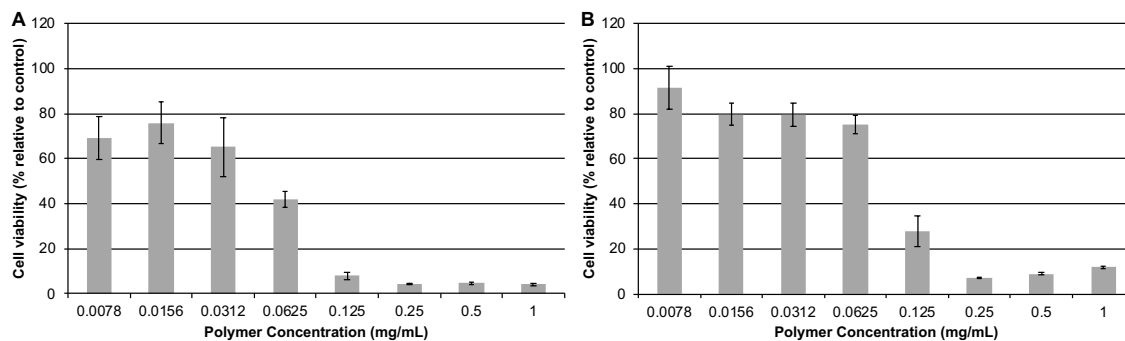
Figure C19. In vitro cytotoxicity of A) **P-Et-N** and B) **P-Bu-N** as measured by MTT assays following 24 h incubations with C2C12 mouse myoblast cells. Data represent the mean and standard deviation of six replicates per concentration.
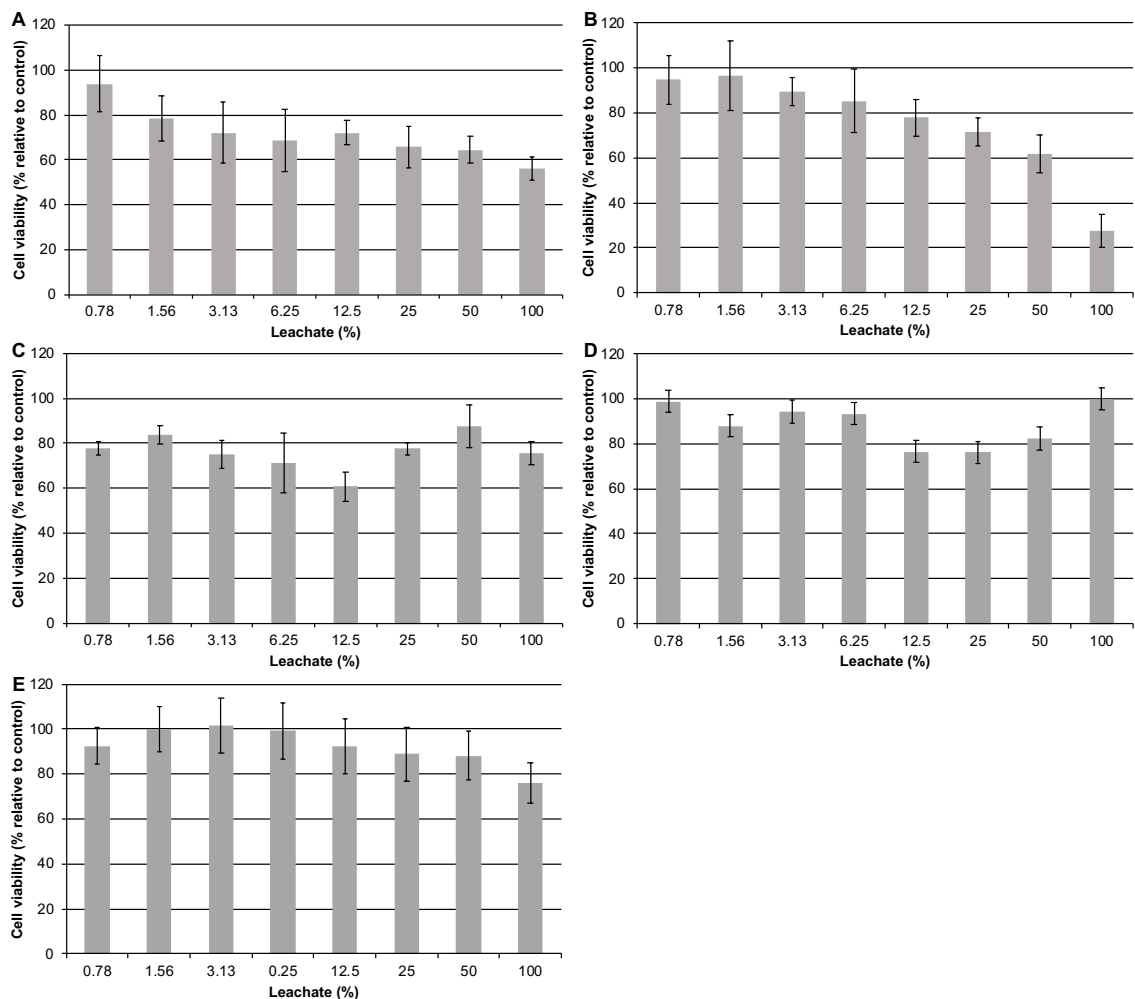
Figure C20. In vitro cytotoxicity of A) **P-Et-P-Alg**; B) **P-Et-N-Alg**; C) **P-Bu-P-Alg**; D**) P-Bu-N-Alg** and E) **P-Hp-P-Alg** as measured by MTT assays following 24 h incubations with C2C12 mouse myoblast cells. Data represent the mean and standard deviation of six replicates per concentration.
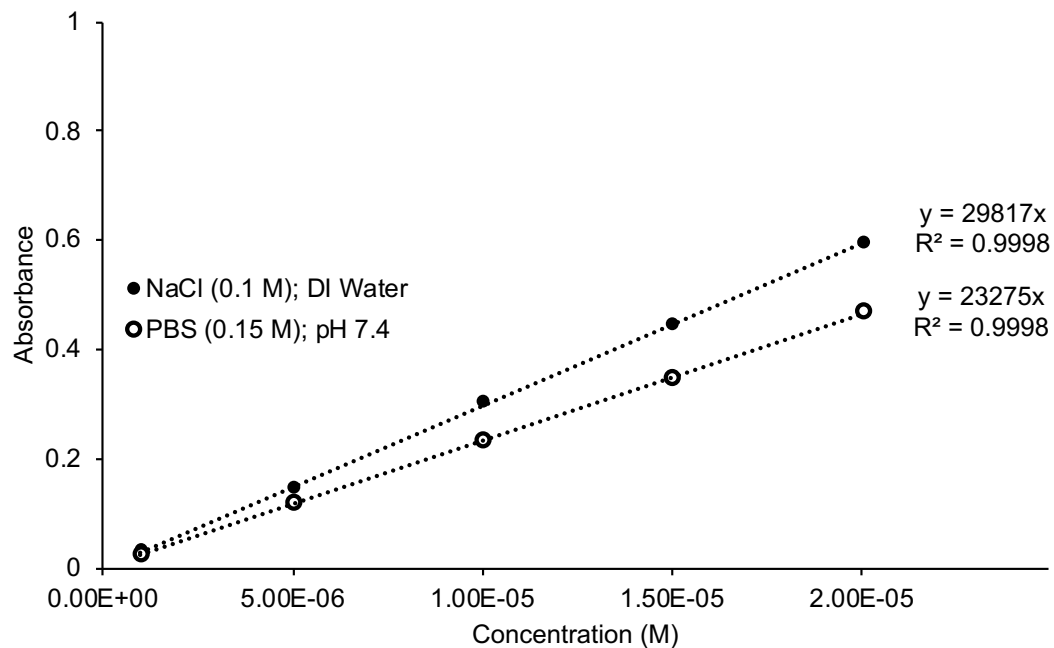
Figure C21. Calibration curve of fluorescein sodium salt.
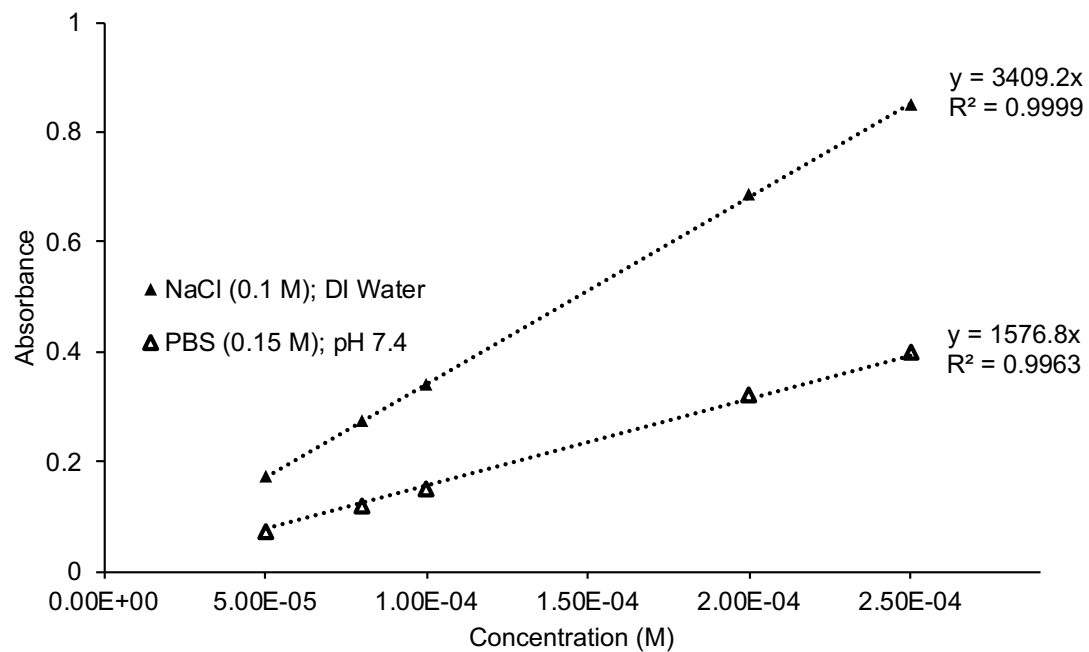
Figure C22. Calibration curve of etodolac sodium salt.
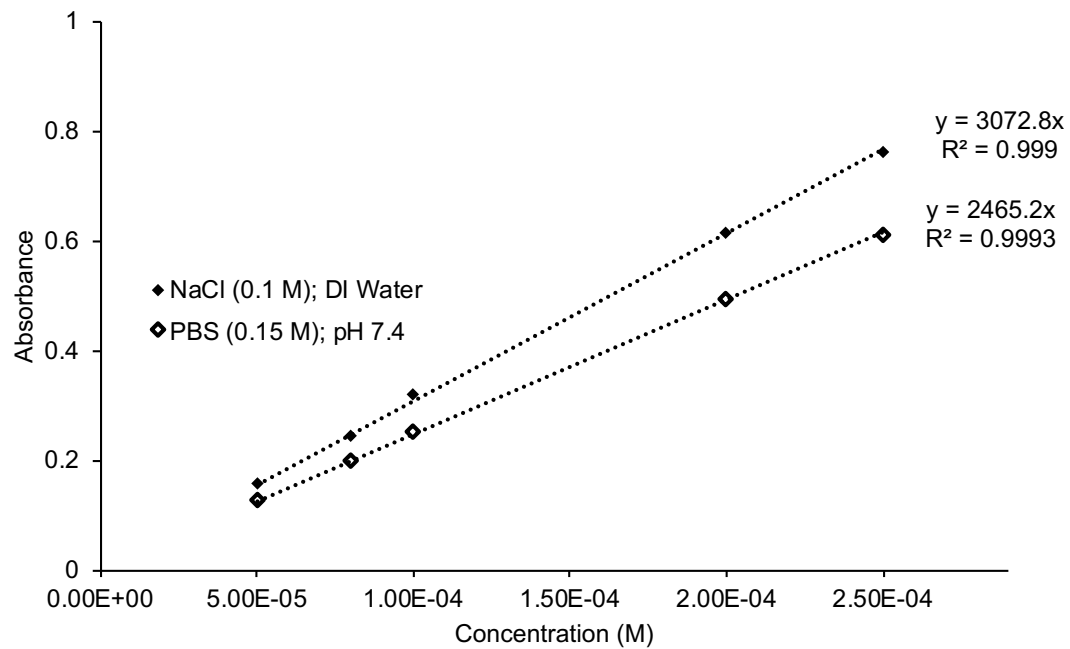
Figure 23. Calibration curve of methotrexate sodium salt.

7.4 Appendix D: Supporting Information for Chapter 5
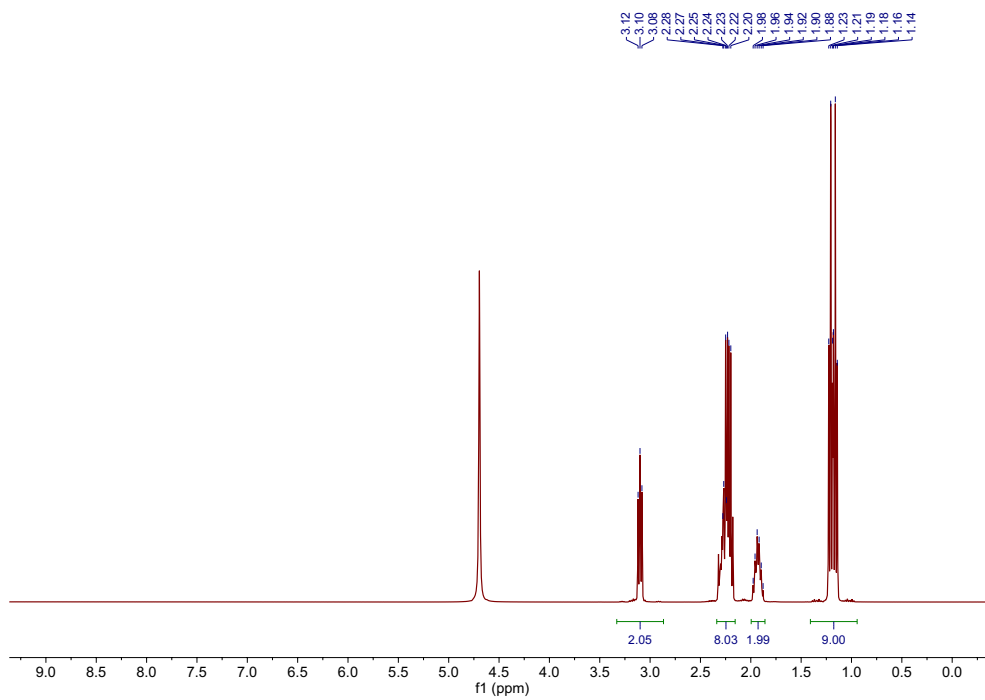
Figure D1. ^{1}H NMR spectrum of **EtP** (400 MHz, D_2O)
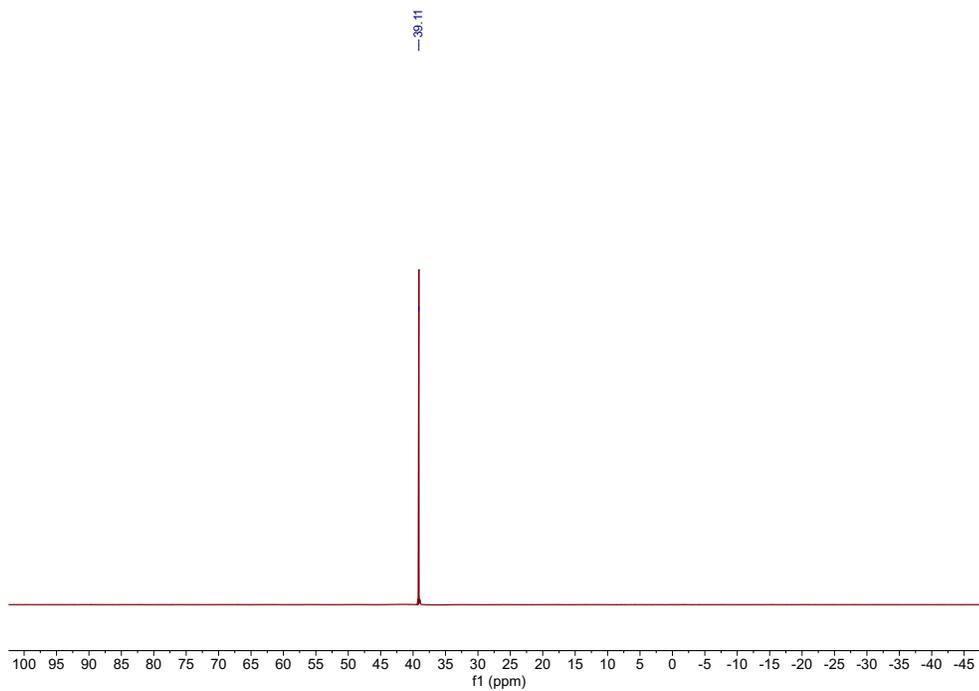
Figure D2. $^{31}P\{^1H\}$ NMR spectrum of **EtP** (161.82 MHz, D_2O).
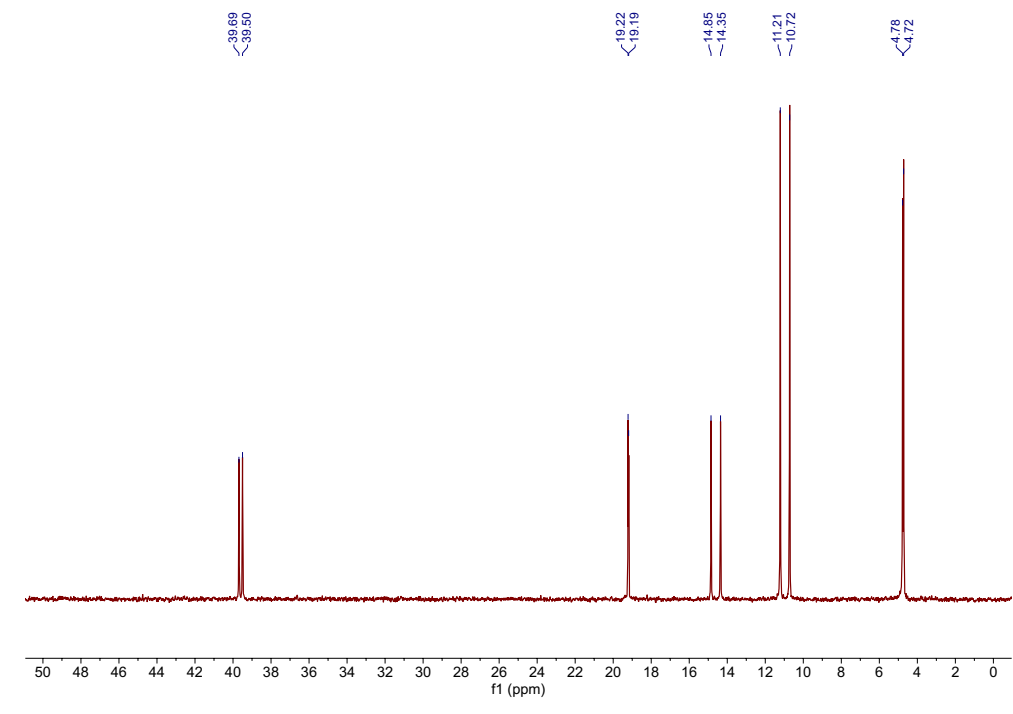
Figure D3. $^{13}C\{^1H\}$ NMR spectrum of **EtP** (100.5 MHz, D_2O).
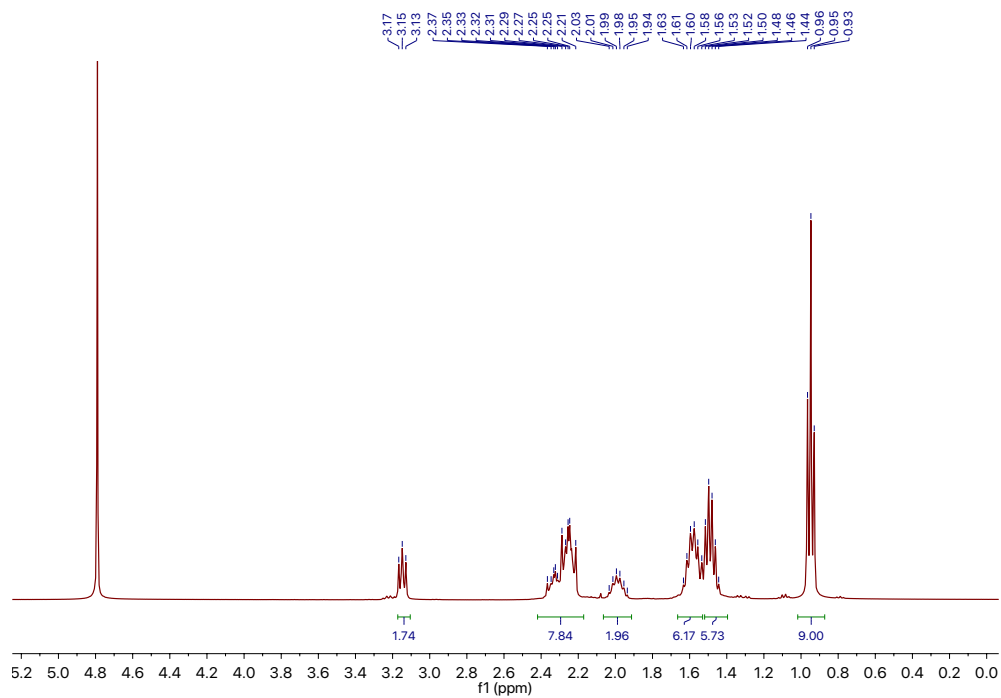
Figure D4. ^{1}H NMR spectrum of **BuP** (400 MHz, D$_2$O).
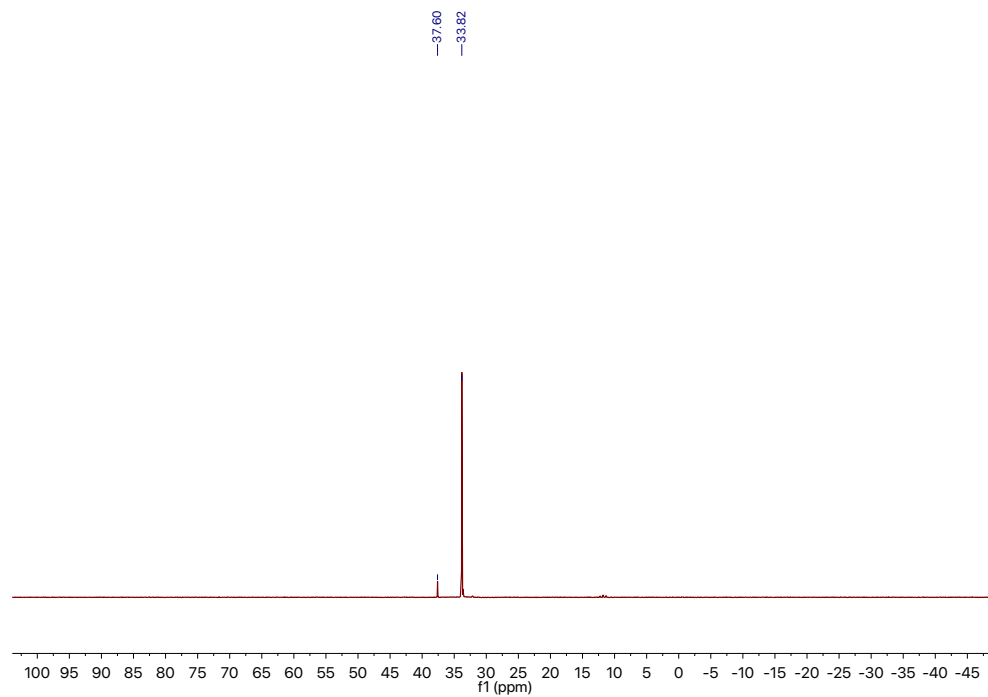
Figure D5. ^{31}P{^{1}H} NMR spectrum **BuP** (161.8 MHz, D$_2$O).
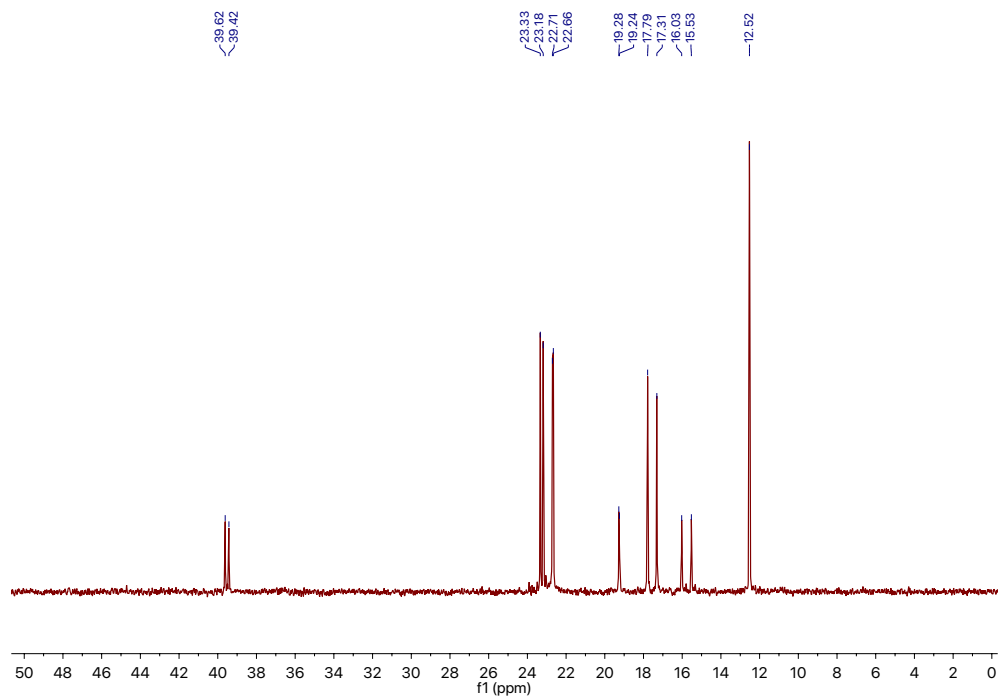
Figure D6. $^{13}C\{^1H\}$ NMR spectrum **BuP** (100.5 MHz, D$_2$O).
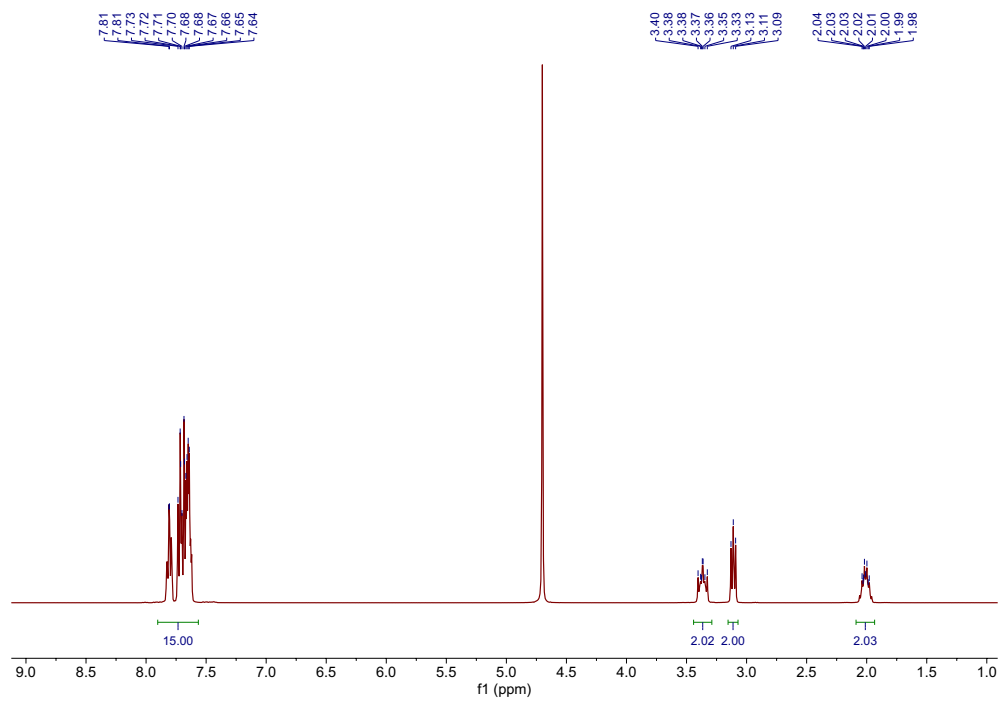
Figure D7. ^1H NMR spectrum of **PhP** (400 MHz, D$_2$O).
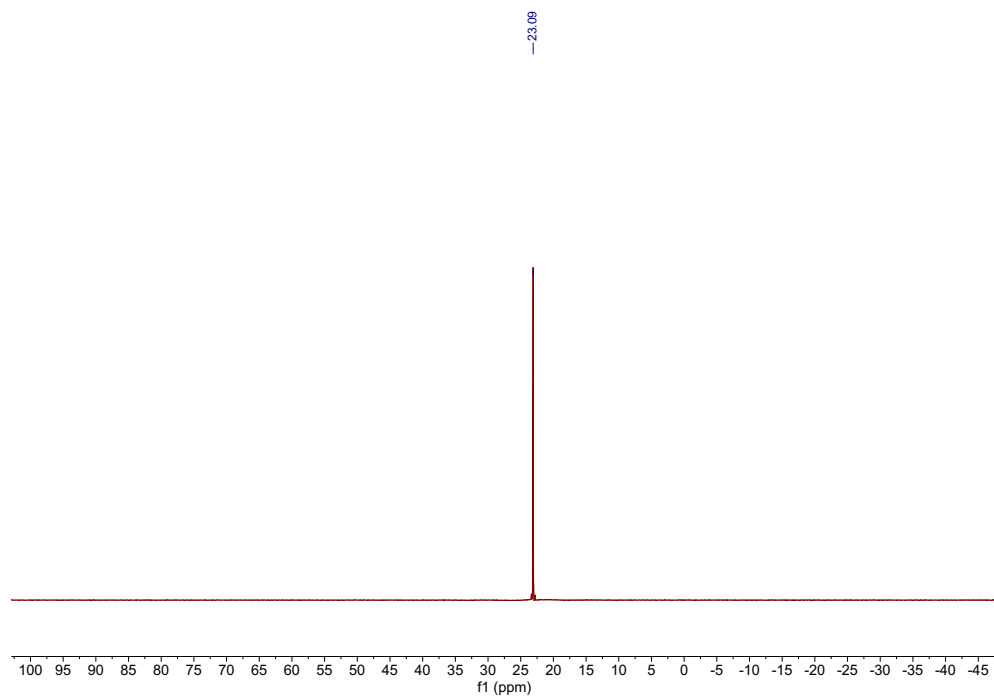
Figure D8. ^{31}P{^{1}H} NMR spectrum **Ph-P** (161.8 MHz, D$_2$O).
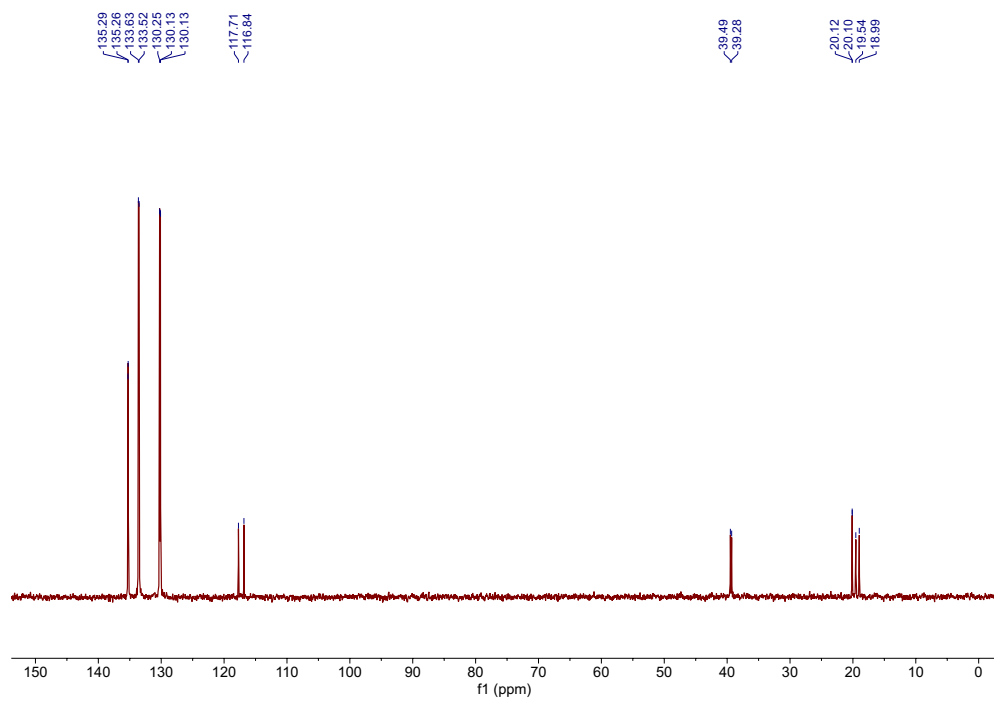
Figure D9. ^{13}C{^{1}H} NMR spectrum **PhP** (100.5 MHz, D$_2$O).
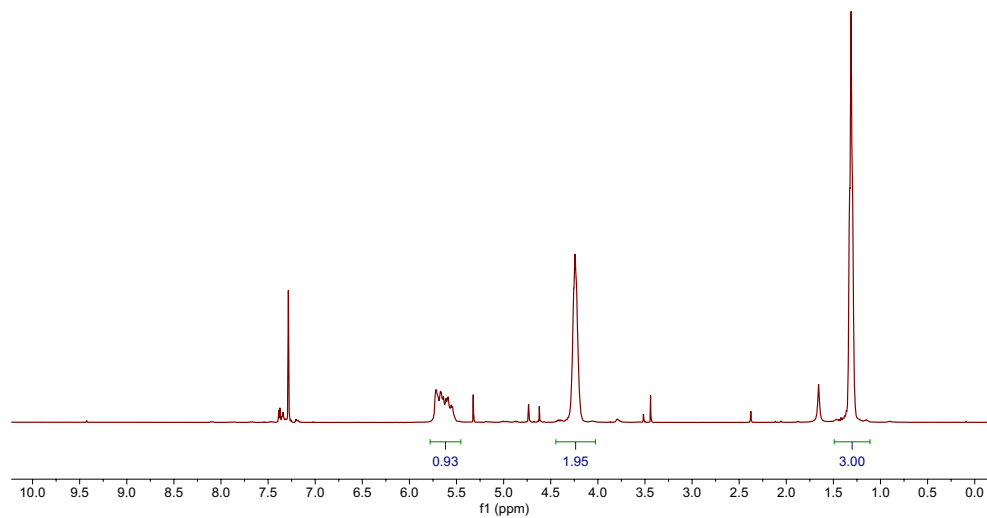
Figure D10. ^{1}H NMR spectrum of **PEtG** (400 MHz, CDCl$_3$).
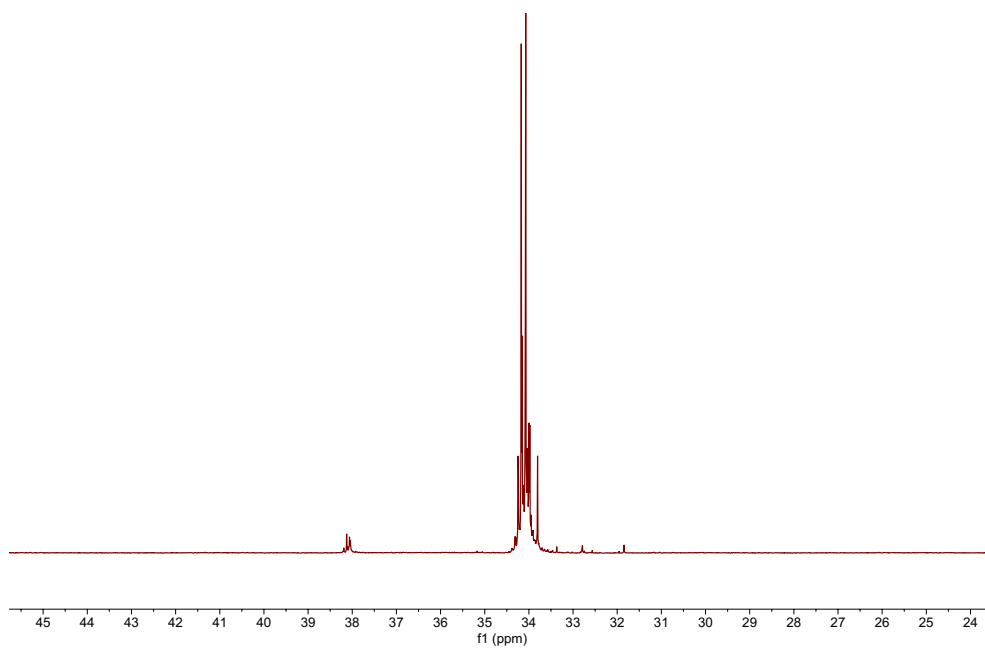
Figure D11. $^{31}P\{^{1}H\}$ NMR spectrum of the attempted addition of **BuP** to **PEtG** in the presence of 2 stoichiometric equivalents of triethylamine at 70 °C over 5 days (161.8 MHz, CD_3CN).
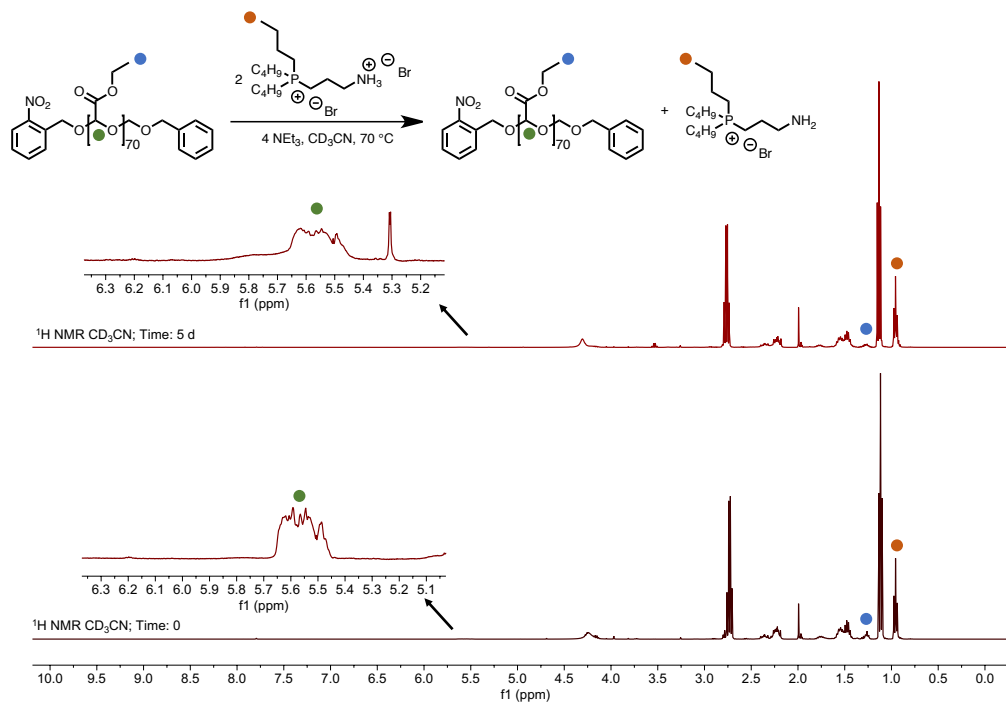
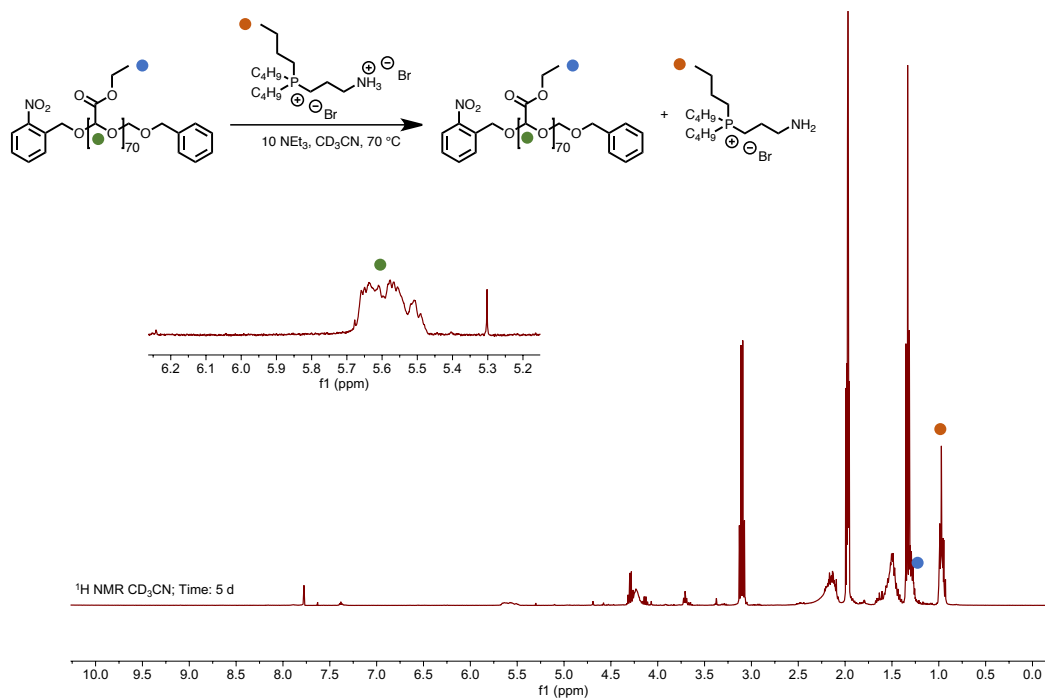**Figure D12.** ¹H NMR spectrum NMR spectrum of the attempted addition of 2 stoichiometric equivalents of **BuP** to **PEtG** in the presence of 4 stoichiometric equivalents of triethylamine at 70 °C over 5 days (400 MHz, CD₃CN).
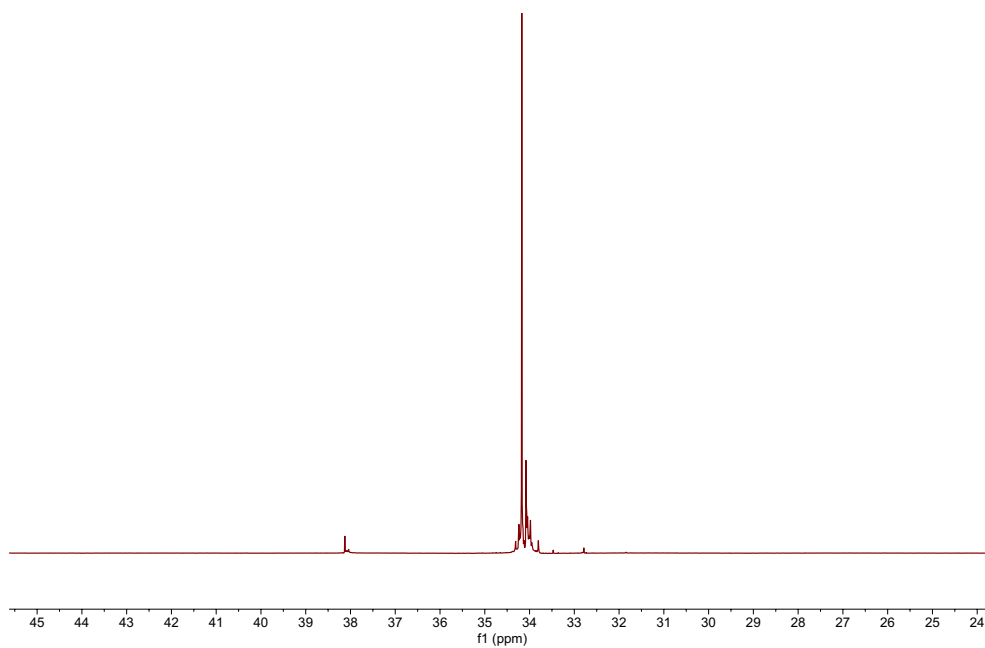
Figure D13. ^{31}P{^{1}H} NMR spectrum of the attempted addition of 2 stoichiometric equivalents of **BuP** to **PEtG** in the presence of 4 stoichiometric equivalents of triethylamine at 70 °C over 5 days (161.8 MHz, CD$_3$CN).
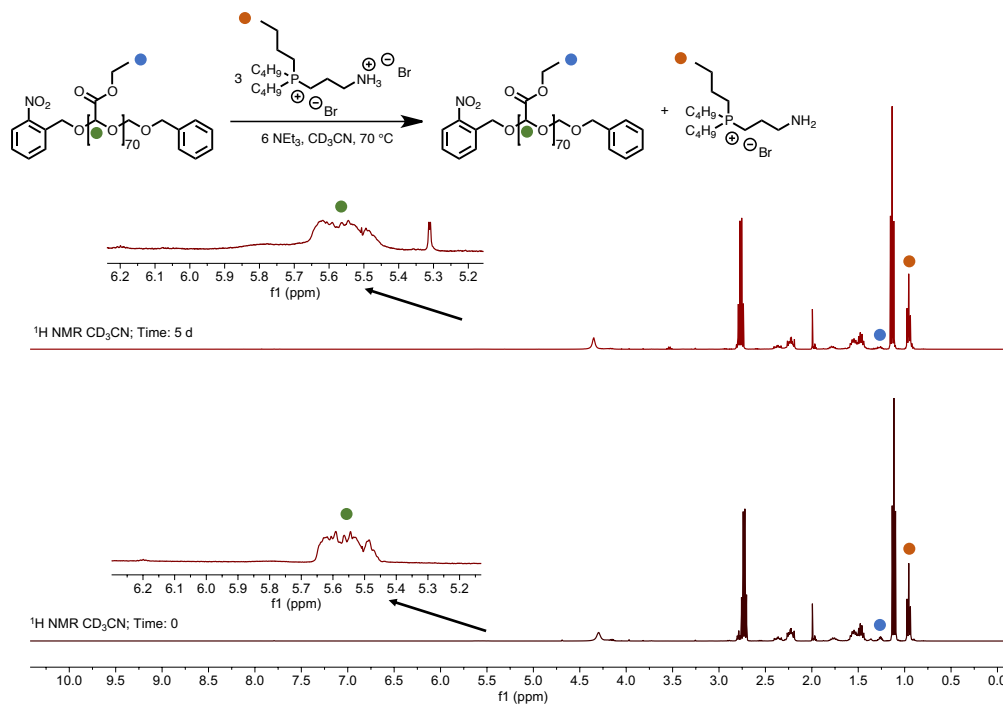
Figure D14. ¹H NMR spectrum of the attempted addition of 3 stoichiometric equivalents of **BuP** to **PEtG** in the presence of 6 stoichiometric equivalents of triethylamine at 70 °C over 5 days (400 MHz, CD₃CN).
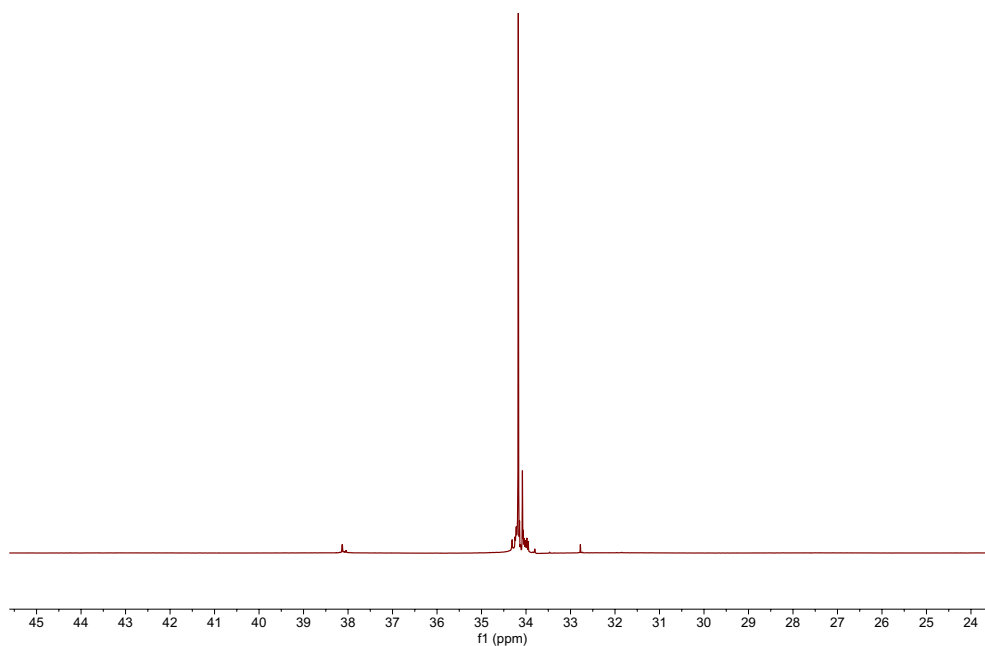
Figure D15. $^{31}P\{^1H\}$ NMR spectrum of the attempted addition of 3 stoichiometric equivalents of **BuP** to **PEtG** in the presence of 6 stoichiometric equivalents of triethylamine at 70 °C over 5 days (161.8 MHz, CD₃CN).

Figure D16. ¹H NMR spectrum of the attempted addition of 1 stoichiometric equivalents of **BuP** to **PEtG** in the presence of 10 stoichiometric equivalents of triethylamine at 70 °C over 5 days (400 MHz, CD₃CN).
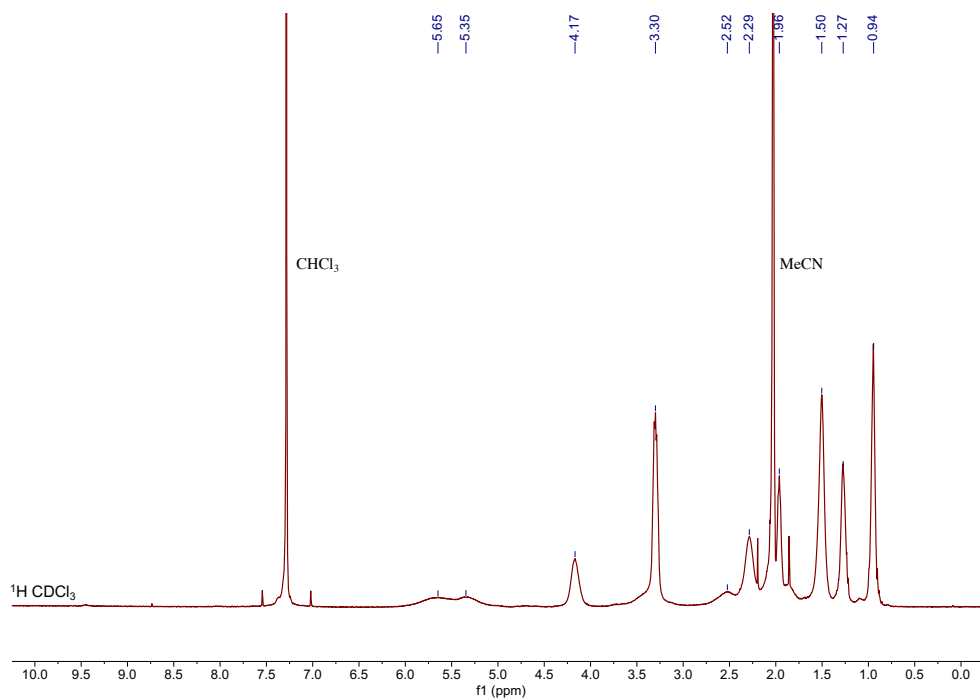
Figure D17. ¹H NMR spectrum of **PGAm$_{BuP}$** (400 MHz, CDCl$_3$).
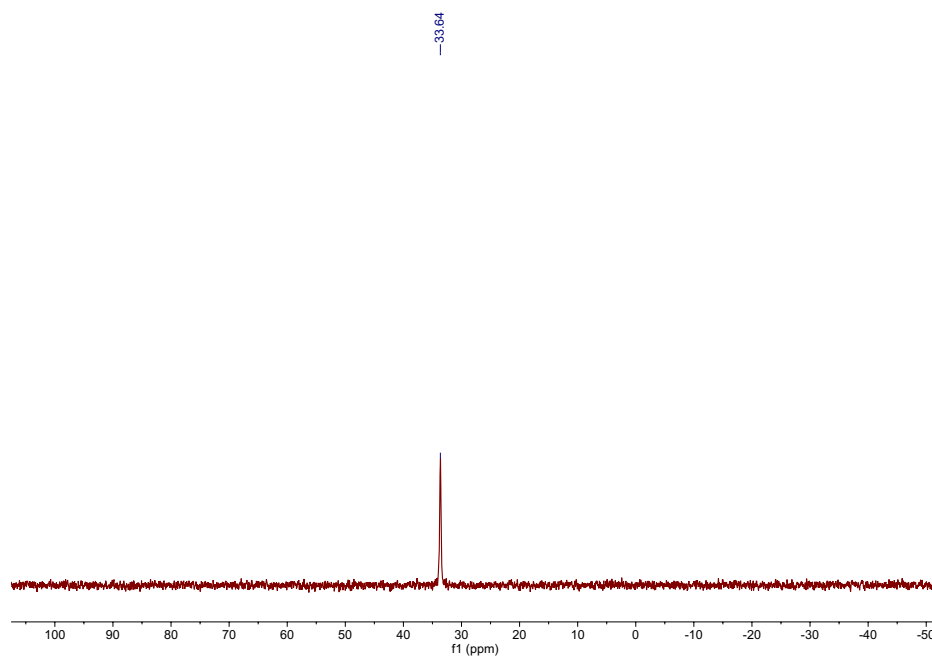
Figure D18. ³¹P{¹H} NMR spectrum **PGAm$_{BuP}$** (161.8 MHz, CDCl$_3$).
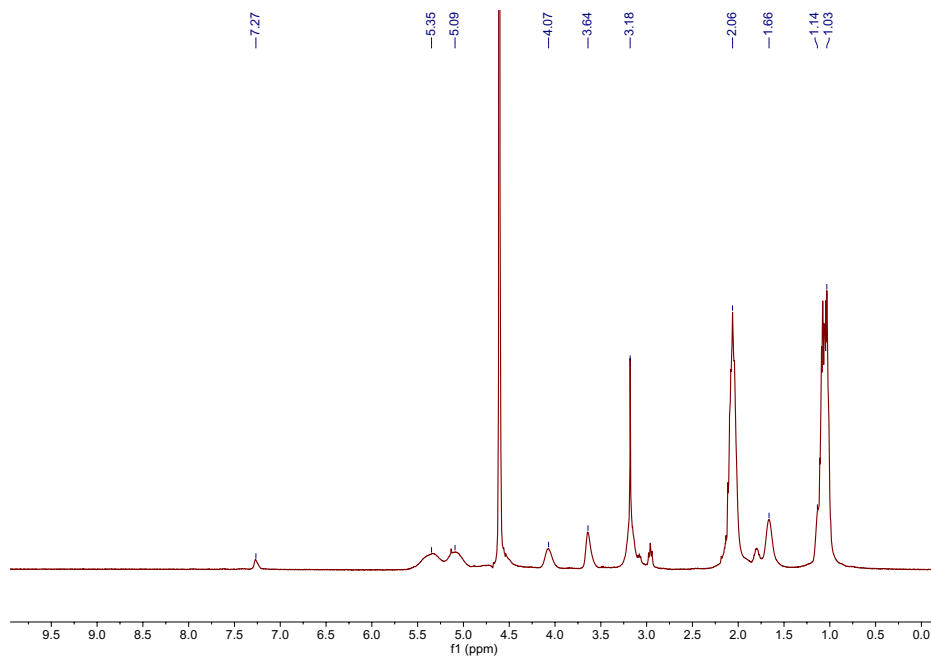
Figure D19. ¹H NMR spectrum of **PGAm$_{EtP}$** (400 MHz, D$_2$O).
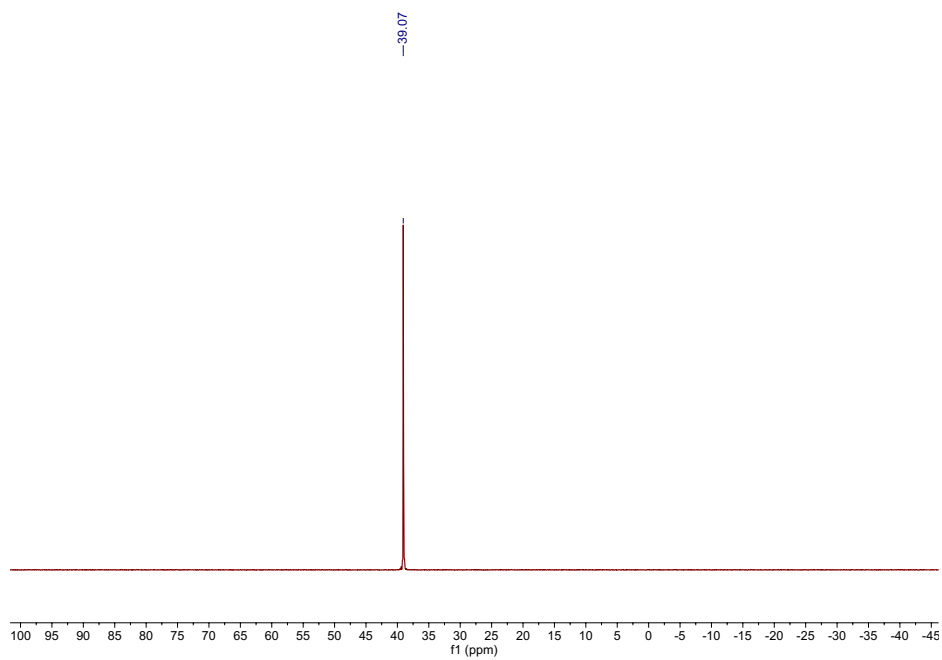
Figure D20. ³¹P{¹H} NMR spectrum **PGAm$_{EtP}$** (161.8 MHz, D$_2$O).
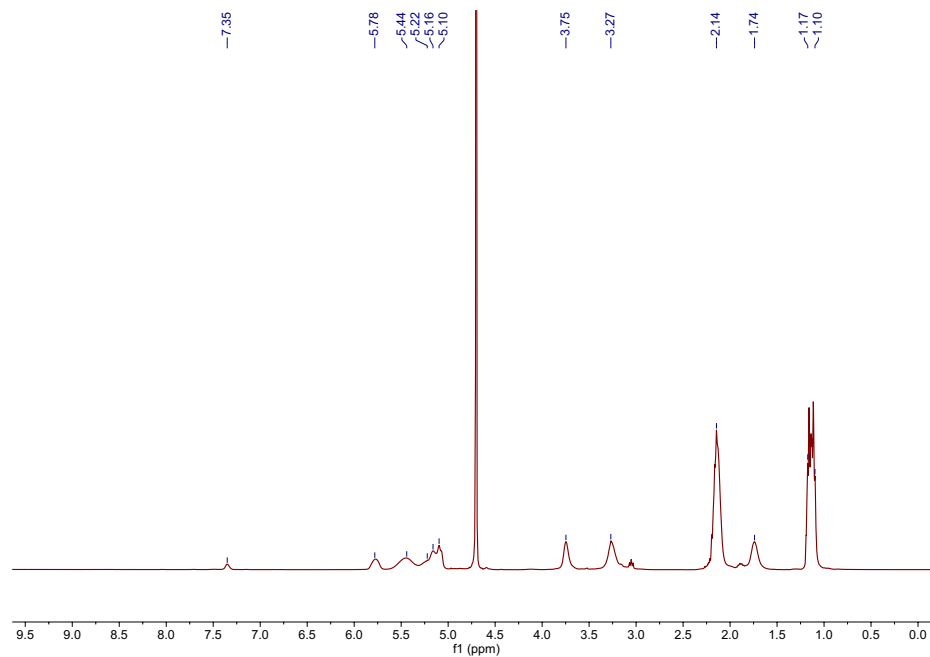
Figure D21. ¹H NMR spectrum of **PGAm_EtP-AllylAm** (400 MHz, D₂O).
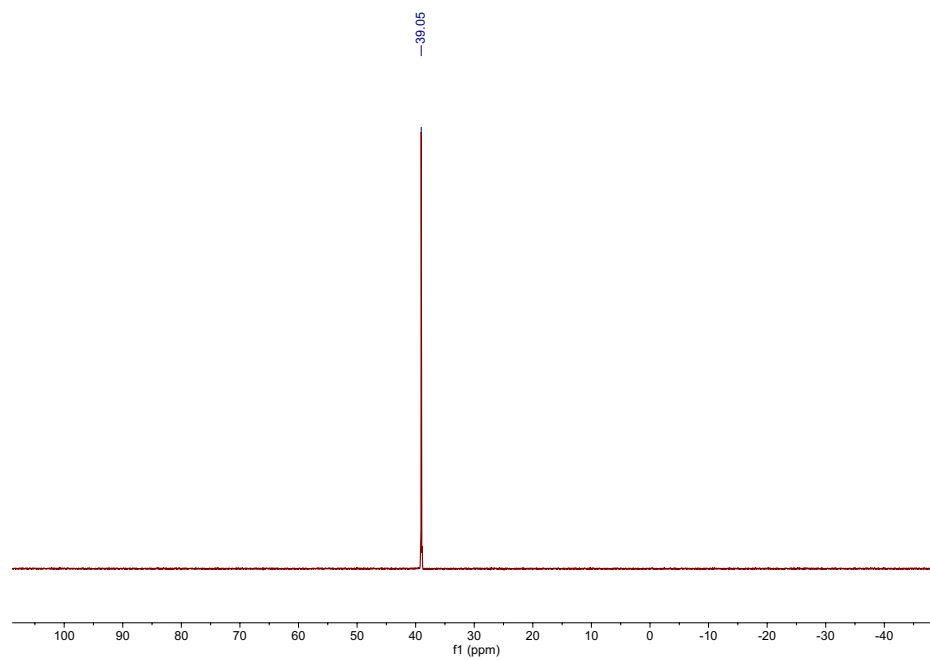
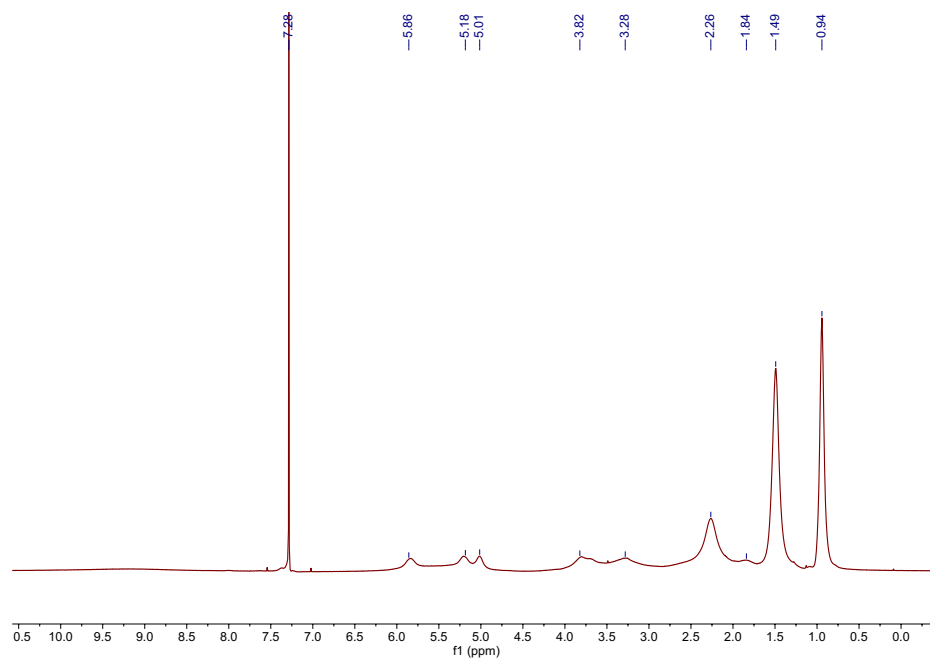**Figure D22.** ³¹P{¹H} NMR spectrum **PGAm_EtP-AllylAm** (161.8 MHz, D₂O).

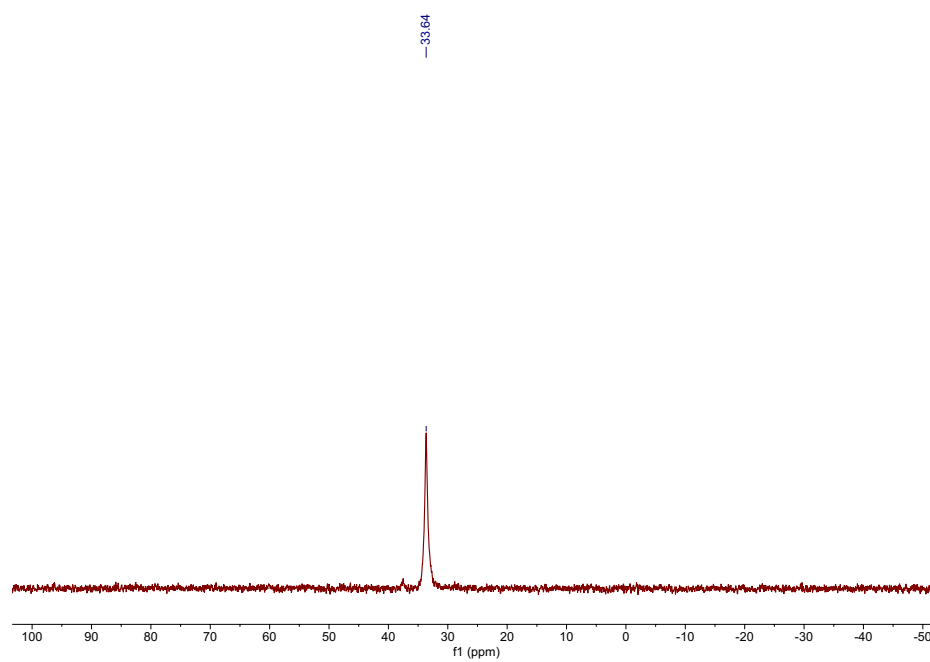**Figure D23**. ^{1}H NMR spectrum of **PGAm$_{BuP-AllylAm}$** (400 MHz, CDCl$_3$).

Figure D24. ^{31}P{^{1}H} NMR spectrum of **PGAm$_{BuP-AllylAm}$** (400 MHz, CDCl$_3$).

7.5 Appendix E: Permission to use Copyrighted Material

7.5.1 Permission to use Figure 1-6

Dear Dr. Harrison,

Your permission requested is granted and there is no fee for this reuse. In your planned reuse, you must cite the ACS article as the source, add this direct link **https://pubs.acs.org/doi/10.1021/bm900373c**, and include a notice to readers that further permissions related to the material excerpted should be directed to the ACS.

If you need further assistance, please let me know.

Sincerely,
Keith Pearl
ACS Publications Support
Customer Services & Information
Website: https://help.acs.org/

Incident Information:

Incident #:	3170497
Date Created:	2019-12-02T20:16:26
Priority:	3
Customer:	Tristan David Harrison
Title:	RightsLink
Description:	Hi,

I would like to get permission to use the abstract figure in my thesis/dissertation introduction to help show the importance of ultracentrifugation packing.

https://pubs.acs.org/doi/10.1021/bm900373c

Thanks

7.5.2 Permission to use Figure 1-9

ELSEVIER LICENSE
TERMS AND CONDITIONS
Dec 16, 2019

This Agreement between Western University -- Tristan Harrison ("You") and Elsevier ("Elsevier") consists of your license details and the terms and conditions provided by Elsevier and Copyright Clearance Center.

License Number	4720801006138
License date	Dec 02, 2019
Licensed Content Publisher	Elsevier
Licensed Content Publication	Journal of Controlled Release
Licensed Content Title	Controlled release strategy designed for intravitreal protein delivery to the retina
Licensed Content Author	Vianney Delplace,Arturo Ortin-Martinez,En Leh S. Tsai,Alan N. Amin,Valerie Wallace,Molly S. Shoichet
Licensed Content Date	Jan 10, 2019
Licensed Content Volume	293
Licensed Content Issue	n/a

Licensed Content Pages	11
Start Page	10
End Page	20
Type of Use	reuse in a thesis/dissertation
Portion	figures/tables/illustrations
Number of figures/tables/illustrations	1
Format	electronic
Are you the author of this Elsevier article?	No
Will you be translating?	No
Title	Tristan Harrison Thesis
Institution name	Western University
Expected presentation date	Jan 2020
Portions	I waould like to use figure 1a for my thesis introduction.
Requestor Location	Western University 1151 Richmond St London, ON N6A 3K7 Canada Attn: Western University
Publisher Tax ID	GB 494 6272 12

7.5.3   Permission to use Figure 5-2

JOHN WILEY AND SONS LICENSE
TERMS AND CONDITIONS

Dec 16, 2019

_____

_____

This Agreement between Western University -- Tristan Harrison ("You") and John Wiley and Sons ("John Wiley and Sons") consists of your license details and the terms and conditions provided by John Wiley and Sons and Copyright Clearance Center.

License Number	4727760469474

License date	Dec 14, 2019
Licensed Content Publisher	John Wiley and Sons
Licensed Content Publication	Angewandte Chemie International Edition
Licensed Content Title	Reversibly Switching the Function of a Surface between Attacking and Defending against Bacteria
Licensed Content Author	Zhiqiang Cao, Luo Mi, Jose Mendiola, et al
Licensed Content Date	Dec 30, 2011
Licensed Content Volume	51
Licensed Content Issue	11
Licensed Content Pages	4
Type of use	Dissertation/Thesis
Requestor type	University/Academic
Format	Electronic
Portion	Figure/table
Number of figures/tables	1
Original Wiley figure/table number(s)	I would like to use figure 1 in my thesis introduction
Will you be translating?	No
Title of your thesis / dissertation	Tristan Harrison Thesis
Expected completion date	Jan 2020
Expected size (number of pages)	1
Requestor Location	Western University 1151 Richmond St London, ON N6A 3K7 Canada Attn: Western University
Publisher Tax ID	EU826007151

Total   0.00 CAD

7.5.4   Permission to Reproduce Chapter 2

Rights retained by authors

When the author accepts the exclusive licence to publish for a journal article, he/she retains certain rights that may be exercised without reference to the Royal Society of Chemistry.

Reproduce/republish portions of the article (including the abstract).

Photocopy the article and distribute such photocopies and distribute copies of the PDF of the article for personal or professional use only (the Royal Society of Chemistry makes this PDF available to the corresponding author of the article upon publication. Any such copies should not be offered for sale. Persons who receive or access the PDF mentioned above must be notified that this may not be made available further or distributed.).

Adapt the article and reproduce adaptations of the article for any purpose other than the commercial exploitation of a work similar to the original.

Reproduce, perform, transmit and otherwise communicate the article to the public in spoken presentations (including those that are accompanied by visual material such as slides, overheads and computer projections).

The author(s) must submit a written request to the Royal Society of Chemistry for any use other than those specified above.

All cases of republication/reproduction must be accompanied by an acknowledgement of first publication of the work by the Royal Society of Chemistry, the wording of which depends on the journal in which the article was published originally. The acknowledgement should also include a hyperlink to the article on the Royal Society of Chemistry website.

The author also has some rights concerning the deposition of the whole article.

7.5.5　Permission to Reproduce Chapter 3

Curriculum Vitae

Name: Tristan D. Harrison

Post-secondary Western University
Education and   London, Ontario, Canada
Degrees: 2011-2015 B.Sc.

Honours and   Province of Ontario Graduate Scholarship
Awards: 2018-2019

        Poster Prize, 100th Canadian Chemistry Conference and Exhibition
        2017

Related Work   Graduate Teaching Assistant
Experience   Western University
        2015-2019

        Graduate Research Assistant
        Western University
        2015-2019

Publications:

6. **Harrison, T. D.**; Salmon, A. J.; De Bruyn, J. R.; Ragogna, P. J.; Gillies, E. R. Phosphonium vs. Ammonium Polyion Complex Networks with Alginate – Which is better for the Delivery of Ionic Cargo? *Submitted*.

5. **Harrison, T. D.**; Yunyaeva, O.; Borecki, A.; Hopkins, C. C.; De Bruyn, J. R.; Ragogna, P. J.; Gillies, E. R. Phosphonium Polyelectrolyte Complexes for the Encapsulation and Slow Release of Ionic Cargo. *Biomacromolecules*, **2020**, *21*, 152–162.

4. **Harrison, T. D.**; Ragogna, P. J.; Gillies, E. R. *Chem. Commun.* **2018**, *54*, 11164–11167.

3. Cuthbert, T. J.; Hisey, B.; **Harrison, T. D.**; Trant, J. F.; Gillies, E. R.; Ragogna, P. J. *Angew. Chem., Int. Ed.* **2018**, 57, 12707–12710.

2. Guterman, R.; **Harrison, T. D.**; Gillies, E. R.; Ragogna, P. J. *Polym. Chem.* **2017**, 8, 3425–3430.

1. Cuthbert, T. J.; **Harrison, T. D.**; Ragogna, P. J.; Gillies, E. R. *J. Mater. Chem. B.* **2016**, 4, 4872–4883.

Conference Presentations

8. **Harrison, T. D.**; Salmon, A. J.; Ragogna, P. J.; Gillies, E. R. "Phosphonium vs. Ammonium Ionic Networks – A comparison Study for the Delivery of Biologically Relevant Molecules. 102nd Canadian Chemistry Conference and Exhibition, Quebec City, Quebec. June 3 – 7, 2019. Poster Presentation.

7. **Harrison, T. D.**; Yunyaeva, O.; Borecki, A.; de Bruyn, J. R.; Ragogna, P. J.; Gillies, E. R. "Phosphonium Containing Polyelectrolyte Complexes for the Delivery of Ionic Cargo" 102nd Canadian Chemistry Conference and Exhibition, Quebec City, Quebec. June 3 – 7, 2019. Oral Presentation.

6. **Harrison, T. D.**; Gillies, E. R.; Ragogna, P. J. "Phosphonium Hydrogels for the release of Ionic Cargo" 34th Meeting of the Canadian Biomaterials Society, Victoria, British Columbia. May 16 – 19, 2018. Oral Presentation.

5. **Harrison, T. D.**; Gillies, E. R.; Ragogna, P. J. "The Utility of Phosphorus in Polymer Networks" 50th Inorganic Discussion Weekend, Toronto, Ontario. November 3 – 5, 2017. Oral Presentation.

4. **Harrison, T. D.**; Ragogna, P. J.; Gillies, E. R. "Phosphonium Containing Polymers for Controlled Drug Delivery" 100th Canadian Chemistry Conference and Exhibition, Toronto, Ontario. May 28 – June 1, 2017. Poster Presentation.

3. **Harrison, T. D.**; Hisey, B.; Gillies, E. R.; Ragogna P. J. "Phosphorus in Polymers: Offering Control" Fallona Interdisciplinary Showcase, London, Ontario. January 16, 2017. Poster Presentation.

2. **Harrison, T. D.**; Hisey, B.; Gillies, E. R. "Design and Synthesis of Functional Polymeric Materials and Biomaterials" Research Showcase for Industry, London, Ontario. April 7, 2016. Poster Presentation.

1. **Harrison, T. D.**; Cuthbert, T. J.; Gillies, E. R.; Ragogna P. J. "Phosphonium Polymers and their Antibacterial Applications" Southern Ontario Undergraduate Student Chemistry Conference, Mississauga, Ontario, March 21, 2015. Oral Presentation.